

**DOCTORAL THESIS**

# Unravelling the Mechanisms of Energetics-Induced Fast-to-Slow Phenotypic Shift in Creatine-Deficient Mice

Romain Bernasconi

TALLINN UNIVERSITY OF TECHNOLOGY  
DOCTORAL THESIS  
87/2025

**Unravelling the Mechanisms of  
Energetics-Induced Fast-to-Slow  
Phenotypic Shift in Creatine-Deficient  
Mice**

ROMAIN BERNASCONI



TALLINN UNIVERSITY OF TECHNOLOGY

School of Science

Department of Cybernetics

This dissertation was accepted for the defence of the degree of Doctor of Philosophy in Biomedicine on 29/10/2025.

**Supervisor:**

Dr. Rikke Birkedal Nielsen  
Laboratory of Systems Biology  
Tallinn University of Technology  
Tallinn, Estonia

**Co-supervisor:**

Professor Marko Vendelin  
Laboratory of Systems Biology  
Tallinn University of Technology  
Tallinn, Estonia

**Opponents:**

Associate Professor Rasmus Kjøbsted  
Department of Nutrition, Exercise and Sports  
University of Copenhagen  
Copenhagen, Denmark

Professor Allen Kaasik  
Department of Pharmacology  
University of Tartu  
Tartu, Estonia

**Defence of the thesis:** 03/12/2025, Tallinn

**Declaration:**

Hereby I declare that this doctoral thesis, my original investigation and achievement, submitted for the doctoral degree at Tallinn University of Technology has not been submitted for doctoral or equivalent academic degree.

Romain Bernasconi



European Union  
European Regional  
Development Fund



Investing  
in your future

-----  
signature

Copyright: Romain Bernasconi, 2025

ISSN 2585-6898 (publication)

ISBN 978-9916-80-411-7 (publication)

ISSN 2585-6901 (PDF)

ISBN 978-9916-80-412-4 (PDF)

DOI <https://doi.org/10.23658/taltech.87/2025>

Printed by EVG Print

Bernasconi, R. (2025). *Unravelling the Mechanisms of Energetics-Induced Fast-to-Slow Phenotypic Shift in Creatine-Deficient Mice* [TalTech Press]. <https://doi.org/10.23658/taltech.87/2025>

TALLINNA TEHNIKAÜLIKOOL  
DOKTORITÖÖ  
87/2025

**Energeetikast indutseeritud kiire-aeglase  
fenotüübilise nihke mehhanismide uurimine  
kreatiipuudulikkusega hiirtel**

ROMAIN BERNASCONI





# Contents

Contents.....	5
List of publications .....	7
Author's contribution to the publications .....	8
Introduction .....	9
Abbreviations .....	11
1 Muscle energetics .....	13
1.1 ATP hydrolysis and main ATPases in skeletal muscle.....	13
1.2 Muscle metabolism .....	14
2 Muscle plasticity: phenotypes and phenotypic shift.....	16
2.1 Skeletal muscle phenotypes.....	16
2.2 Phenotypic shift .....	17
2.3 Signaling pathways involved in fast-to-slow phenotypic shift .....	18
2.3.1 The AMPK/PGC1 $\alpha$ axis .....	19
2.3.2 The Ca <sup>2+</sup> /CaM/CaMKIV/CREB/PGC1 $\alpha$ axis .....	22
2.3.3 The Ca <sup>2+</sup> /CaM/CaN/NFATc1/MEF2 axis .....	22
2.3.4 Other signaling pathways.....	23
3 The creatine kinase system.....	24
4 Consequences of defective CK system on skeletal muscle phenotype.....	26
4.1 Models of defective CK system .....	26
4.2 CK-deficient models .....	26
4.2 CrT-deficient and $\beta$ -GPA-treated models.....	27
4.4 GAMT KO and AGAT KO creatine-deficient models .....	29
5 What remains unknown? .....	31
Aims of the thesis.....	32
Methods.....	33
6 Results and discussion.....	34
6.1 Development of the IOC BIO gel software to analyse Western blot results.....	34
6.2 AMPK is more activated in slow muscle than in fast muscle .....	34
6.3 GAMT KO mice exhibit subtle changes in phenotype independently of AMPK activity .	36
6.4 AGAT KO mice exhibit a deep remodeling of their muscle phenotype in a muscle- dependent manner, associated with AMPK/PGC1 $\alpha$ axis .....	37
6.5 Does AMPK activation in AGAT KO gastrocnemius have an energetic origin? .....	39
6.6 Is AMPK signaling responsible for the AGAT KO phenotypic shift? .....	39
6.7 Energetics induces higher Ca <sup>2+</sup> release: a potential signaling for MHC shift in AGAT KO gastrocnemius .....	40
Conclusion.....	43
References .....	44
Acknowledgements.....	68
Abstract.....	69

Lühikokkuvõte.....	70
Publication I .....	71
Publication II .....	83
Publication III .....	99
Publication IV .....	101
Publication V .....	103
Publication VI .....	125
Curriculum vitae.....	127
Elulookirjeldus.....	129

## List of publications

The list of author's publications, on the basis of which the thesis has been prepared:

- I Kütt, J; Margus, G; Kask, L; Rätsepso, T; Soodla, K; **Bernasconi, R**; Birkedal, R; Järv, P; Laasmaa, M; Vendelin, M (2023). Simple analysis of gel images with IOCBIO Gel. BMC Biology, DOI: 10.1186/s12915-023-01734-8.
- II **Bernasconi, R**; Soodla, K; Sirp, A; Zovo, K; Kuhtinskaja, M; Lukk, T; Vendelin, M; Birkedal, R (2024). Higher AMPK activation in mouse oxidative compared to glycolytic muscle does not correlate with LKB1 or CaMKK $\beta$  expression. Am J Physiol - Endocrinology and Metabolism, DOI: 10.1152/ajpendo.00261.2024.
- III (Manuscript) **Bernasconi, R**; Soodla, K; Samuli, M; Rätsepso, T; Vendelin, M; Birkedal, R. Similar levels of phosphorylated AMPK in skeletal muscles from creatine deficient guanidino-acetate methyltransferase knockout (GAMT KO) and wildtype mice.
- IV (Manuscript) **Bernasconi, R**; Soodla, K; Samuli, M; Rätsepso, T; Vendelin, M; Birkedal, R. Creatine deficient AGAT KO mice exhibit stronger remodeling of glycolytic than oxidative muscles through ER $\alpha$ -LKB1-AMPK-PGC1 $\alpha$  signaling.
- V Branovets, J\*; Laasmaa, M\*; Stolova, J; Shen, X; Rätsepso, T; **Bernasconi, R**; Soodla, K; Balodis, MJ; Grahv, C; Hendrikson, E; Louch, W; Birkedal, R; Vendelin, M (2025). Life-long creatine deficiency leads to augmented sarcoplasmic reticulum calcium release but not heart failure. Am J Physiol – Heart Circ Physiol, DOI: 10.1152/ajpheart.00106.2025.
- VI (Manuscript) Di Gallo, M; Delivry, L; Pereira, D; Jauliac, E; Macaux, G; Guilbert, T; Denis, RGP; Backer, S; Saintpierre, M; Adoux, L; **Bernasconi, R**; Laasmaa, M; Birkedal, R; Vendelin, M; Dos Santos, M; Wojtaszewski, JFP; Foretz, M; Viollet, B; Maire, P; Sotiropoulos, A; Launay, T\*; Britto, FA\*. SIX1-dependent myofiber typology and metabolism controls muscle hypertrophy.

\*Equal contribution

## **Author's contribution to the publications**

Contribution to the papers in this thesis are:

- I The author contributed to testing and giving feedback regarding the user interface of the IOC BIO Gel software. The author also contributed to the writing of few paragraphs in the manuscript.
- II The author conceptualized (with Birkedal, R), performed, and analysed all the experiments (with Soodla, K, who did 50 % of the measurements and analyses). The author prepared the figures and wrote the first draft of the manuscript.
- III The author conceptualized (with Birkedal, R), performed, and analysed all experiments (with Soodla, K, who did 50 % of the measurements and analyses). The co-authors Samuli, M, and Rätsepso, T are optimizing the Western blotting of MHC isoforms. The author prepared the figures and wrote the first draft of the manuscript.
- IV The author conceptualized (with Birkedal, R), performed, and analysed all experiments (with Soodla, K, who did 50 % of the measurements and analyses). The co-authors Samuli, M, and Rätsepso, T are optimizing the Western blotting of MHC isoforms. The author prepared the figures and wrote the first draft of the manuscript.
- V The author performed and analysed western blot experiments of LKB1/AMPK signalling pathway.
- VI The author performed and analysed the Ca<sup>2+</sup> transients in C2C12 myotubes treated with 2DG. The author participated in writing the method section and discussed his results.

## Introduction

Skeletal muscle accounts for 40-50% of the human body weight and is the organ of movement. The muscle contraction generates the movement, and this phenomenon is fueled by ATP hydrolysis. To ensure its function, skeletal muscle needs to match its energy production with energy demand. Within a muscle, each fiber exhibits distinct metabolic and contractile characteristics that enable it to perform specific functions. Slow fibers, such as type I, base their ATP production on oxidative metabolism. Mixed fibers, such as type IIa, produce ATP through both oxidative and glycolytic metabolism. Finally, fast fibers such as type IIX and IIB rely primarily on glycolytic metabolism. Slow and mixed fibers produce less strength but are more enduring, as their rate of ATP consumption is moderate and their metabolism can sustain this consumption over time. Consequently, enduring muscles such as the soleus (SOL) are predominantly composed of slow fibers. In contrast, fast fibers can produce more strength, but their endurance is limited, as their rate of ATP consumption is too high to be sustained by glycolysis over an extended period. Therefore, muscles with a burst activity, such as the gastrocnemius (GAST), are mainly composed of fast fibers.

The fiber composition determines the phenotype. SOL muscle can be considered as a slow phenotype, mainly composed of type I and IIa, whereas GAST can be considered as a fast phenotype, essentially composed of type IIX and IIB. As a plastic tissue, skeletal muscle can adapt its phenotype in response to various stimuli. For example, endurance training induces a fast-to-slow phenotypic shift, whereas inactivity will favor expression of the fast phenotype. The phenotypic shift is driven by several signaling pathways, among which, AMP-activated protein kinase (AMPK) has been highlighted as an important player. Upon a rise in ADP or AMP concentration, AMPK is acutely activated to stimulate metabolism and match the increasing energy demand, especially in fast muscles, which are more prone to developing energetic debt upon exercise. However, long-term AMPK activity promotes atrophy and fast-to-slow phenotypic shift.

The creatine kinase (CK) system is an essential contributor to muscle energetics. CK catalyzes a bidirectional reaction: it can regenerate ATP from ADP using phosphocreatine (PCr) as a phosphate source, or conversely, use ATP to phosphorylate creatine (Cr) and form PCr. CK is an essential ATP buffering system that maintains an adequate ATP concentration near ATPases. Its enzymatic activity is extremely rapid, and the high concentrations of PCr in muscle enable it to rapidly compensate for sudden ATP depletion during muscle contraction.

Several models have been developed to evaluate the importance of the CK system in muscle function, either by knocking out the expression of CK, disturbing its activity, or suppressing the endogenous Cr biosynthesis. Overall, disturbing the CK system has been shown to affect energetics (ATP concentration), induce muscle atrophy, and a fast-to-slow phenotypic shift, associated with higher AMPK activity. However, energetics and muscle consequences vary considerably depending on the experimental model employed. Absence of Cr seems to induce a more severe phenotype than the absence of CK. Nevertheless, mice deficient in Guanidinoacetate N-methyltransferase (GAMT KO) and L-Arginine: Glycine amidinotransferase (AGAT KO), which both lack endogenous Cr biosynthesis, exhibit different degrees of severity in muscle atrophy and metabolic shift. Moreover, muscles respond differently to Cr deficiency, with the fast GAST muscle being more severely affected than the slow SOL muscle. The exact effect of Cr deficiency on

muscle phenotype remains unclear, and the signaling pathways responsible for those changes need to be further investigated in both GAMT KO and AGAT KO mice.

In this thesis, I have investigated the consequences of Cr deficiency on muscle atrophy and phenotype, using both GAMT KO and AGAT KO mice. I have also investigated the activation of AMPK in both fast and slow muscles from GAMT KO and AGAT KO mice. Furthermore, I have highlighted a muscle-dependent activation of AMPK. Based on our findings, I have reviewed the potential impact of AMPK activity on muscle phenotypic shift. Finally, we provided additional data suggesting an alternative mechanism of energetics-induced fast-to-slow phenotypic shift.

## Abbreviations

2DG	2-Deoxy-D-glucose
$\beta$ -GPA	Beta-guanidopropionic acid
ACC	Acetyl-CoA carboxylase
AGAT	L-Arginine: Glycine amidinotransferase
AICAR	5-aminoimidazole-4-carboxamide-1- $\beta$ -4-ribofuranoside
AK	Adenylate kinase
AMPK	AMP-activated protein kinase
Arg	Arginine
B-CK	Brain creatine kinase
CaM	Calmodulin
CaMKIV	Calcium/calmodulin-dependent protein kinase IV
CaMKK $\beta$	Calcium/calmodulin-dependent protein kinase kinase 2
CaN	Calcineurin
CK	Creatine kinase
Cr	Creatine
CREB	cAMP Response Element Binding protein
CrT	Creatine transporter
EDL	Extensor digitorum longus
ER $\alpha$	Estrogen receptor alpha
FADH <sub>2</sub>	Flavin adenine dinucleotide
FOXO3a	Forkhead box protein O3a
GAA	Guanidinoacetic acid
GAMT	Guanidinoacetate N-methyltransferase
GAST	Gastrocnemius
Gly	Glycine
GS	Glycogen synthase
HDAC4	Histone deacetylase 4
HPLC/MS	High-Performance Liquid Chromatography / Mass Spectrometry
LDH	Lactate dehydrogenase
LKB1	Liver kinase B1
MaFbx	Atrogin-1
M-CK	Cytosolic creatine kinase
MEF2	Myocyte enhancer factor-2
MHC	Myosin heavy chain
Mi <sub>s</sub> -CK	Sarcomeric mitochondrial creatine kinase
mTOR	Mammalian Target of Rapamycin
mtTFA	Mitochondrial transcription factor A
MuRF1	Muscle RING finger 1
MyoD	Myoblast determination protein 1

NFATc1	Nuclear Factor of activated T-cells c1
NMR	Nuclear Magnetic Resonance
p38	p38 mitogen-activated protein kinase
PCr	phosphocreatine
PGC1 $\alpha$	Peroxisome proliferator-activated receptor gamma coactivator 1-alpha
PLA	Plantaris
Pi	Inorganic phosphate
RyR	Ryanodine receptors
Ser	Serine
SERCA	Sarco/Endoplasmic reticulum calcium ATPase
SIRT1	NAD <sup>+</sup> -dependent deacetylase sirtuin-1
SOL	Soleus
SR	Sarcoplasmic reticulum
STBD1	Starch-binding domain 1
Thr	Threonine
ULK1	Unc-51 like autophagy activating kinase 1
UPS	Ubiquitin-proteasome system
YY1	Ying Yang 1

Explanations of abbreviations used in the thesis.

# 1 Muscle energetics

Muscle is the predominant tissue type in the human body. Muscle tissues are involved in various physiological functions essential for human survival, particularly movement, blood circulation, and respiration. Skeletal muscles alone represent 40–50% of the total body weight and are specialized for movement. They also play a central role in the regulation of the whole-body metabolism and serve as the main protein reservoir.

Skeletal muscle is a tissue with a high and fluctuating energy demand due to muscle contraction. Cellular energy is supplied through ATP hydrolysis, necessitating the maintenance of stable ATP concentrations over time. This section examines the principal ATP-consuming and ATP-generating processes within skeletal muscle tissue.

## 1.1 ATP hydrolysis and main ATPases in skeletal muscle

Muscles are highly dependent on ATP hydrolysis. The ATP consists of an adenosine group bound by three phosphate groups. Hydrolytic cleavage of one phosphate group produces ADP and inorganic phosphate (Pi) ( $\text{ATP} + \text{H}_2\text{O} \rightarrow \text{ADP} + \text{Pi} + \text{H}^+$ ), releasing energy utilized in numerous biological processes. More rarely, ADP can also be hydrolyzed into AMP and Pi to produce energy ( $\text{ADP} + \text{H}_2\text{O} \rightarrow \text{AMP} + \text{Pi} + \text{H}^+$ ). Additionally, two ADP can also be converted into ATP + AMP by adenylate kinase (AK) activity (1).

ATP hydrolysis is fundamental for muscle contraction. Upon electrical activity,  $\text{Ca}^{2+}$  is released from the sarcoplasmic reticulum (SR) in the cytoplasm by Ryanodine Receptors (RyR). The resulting increase in cytoplasmic  $\text{Ca}^{2+}$  concentration leads to  $\text{Ca}^{2+}$  binding to troponin C, triggering a conformational shift in tropomyosin. This tropomyosin displacement exposes myosin-binding sites on actin filaments, enabling binding by myosin heavy chain (MHC) heads. Subsequently, MHC heads undergo a power stroke that generates force and causes filament sliding, resulting in muscle shortening. Following each power stroke, MHC heads require ATP binding and hydrolysis to detach from actin and reinitiate the cross-bridge cycle (2, 3). The speed of the MHC head cycle greatly determines the power generated and is highly dependent on its isoforms (4). The fast myosin heavy chain isoforms (IIX and IIB), have a faster cycle (faster activity) and therefore consume more ATP per second than the slow isoforms (I and IIa) (4, 5). The increased ATP consumption by MHC cross-bridges during contraction represents the primary driver of energetic fluctuations in skeletal muscle. Muscle relaxation requires the removal of cytoplasmic  $\text{Ca}^{2+}$ , which must be pumped back into the SR. This process is ensured by Sarco/Endoplasmic Reticulum Calcium ATPase (SERCA) pumps, which are major consumers of ATP. Indeed, SERCA pumps have been estimated to account for 40-50% of the ATP consumption at rest (6) and 30–40% during contraction (7). Other ionic pumps, such as  $\text{Na}^+/\text{K}^+$ , essential for regulating membrane potential, have been estimated to consume nearly 2% of total ATP during contraction (8). Consequently, muscle contraction represents the principal ATP-consuming process in skeletal muscle, and ATP depletion directly compromises muscular activity.

Protein synthesis represents another major energy-consuming process in skeletal muscle. Performed by ribosomes, translation has been estimated to consume four high-energy bonds ( $1 \text{ ATP} \rightarrow \text{ADP} \rightarrow \text{AMP} + 2 \text{ GTP} \rightarrow 2 \text{ GDP}$ ) to fix one single amino acid (aa) in prokaryotic cells (9, 10). Given that muscles express a significant number of large proteins, such as MHC (~1,959 aa) or Titin (~34,550 aa), muscular hypertrophy constitutes one of the most energetically demanding processes in skeletal muscle. Furthermore, some proteins require continuous replacement due to their relatively short half-lives.

In healthy adults, protein turnover is estimated to be ~300g per day. This turnover is higher following muscle activity, which significantly increases the protein damage (11). One of the main protein degradation systems in muscle is the ubiquitin proteasome system (UPS), whose activity is transiently increased after muscle activity (12, 13). The UPS is a selective degradation mechanism of misfolded proteins. Initially, target proteins must be tagged by a chain of polyubiquitin ( $\geq 4$  ubiquitins), where each ubiquitin binding requires the hydrolysis of one ATP (14, 15). This process is ensured by E3 ubiquitin ligases, of which the most common in skeletal muscle are Muscle RING Finger 1 (MuRF1) and Atrogin-1 (MaFbx). Following polyubiquitination, proteins are transported to the 26S proteasome for degradation. Proteasomal entry necessitates complete protein unfolding, consuming approximately one ATP molecule per three amino acids (15–17). Hence, protein synthesis and turnover represent a significant part of the ATP consumption at rest or post-exercise. However, those processes are negligible during intense muscle activity and are shut down for energy saving.

In summary, skeletal muscle physiology is fundamentally dependent on ATP hydrolysis. Whether supporting contraction, relaxation, repair, or growth, adequate ATP availability is essential for optimal muscle function.

## 1.2 Muscle metabolism

Cellular ATP pools are relatively small. Muscle tissue typically contains only 5–6 mmol/kg of wet weight or ~8mM concentrations of ATP (18, 19), which would suffice for only a few seconds of contraction, depending on exercise intensity. While the creatine kinase (CK) system serves as the primary ATP buffering mechanism in muscle, its capacity would extend activity by only a few additional seconds. Since muscle tissue rapidly consumes ATP, it must simultaneously regenerate it through ADP rephosphorylation. Muscle cells employ two metabolic pathways allowing ATP production. They differ by their speed of ATP production, their capacity (availability of their fuel), and their localization in the cell. Based on these pathways, three metabolic strategies can be distinguished: one purely anaerobic, one purely aerobic, and a mixed strategy.

Anaerobic glycolysis is the metabolic pathway of burst activities. It takes place in the cytosol and consists of ten steps, transforming one molecule of glucose into 2 ATP, 2 NADH, and 2 pyruvate, without the need for oxygen (20). Under anaerobic conditions, NADH and pyruvate serve as substrates for lactate dehydrogenase (LDH), which produces  $\text{NAD}^+$ , lactate, and  $\text{H}^+$ . The increased  $\text{NAD}^+$  availability is required to stimulate glycolytic flux, thereby enhancing ATP production. For its part, lactate can be reconverted into pyruvate or exit the muscle toward other organs such as the brain or liver (21, 22). During intense and sustained muscular exercise, overactivity of LDH will ultimately lead to  $\text{H}^+$  accumulation and acidosis. Anaerobic glycolysis operates at a very high rate, enabling immediate matching of ATP production to ATP demands, perfect for sustaining burst activities. However, the efficiency of this process is limited in time. The yield is poor, and the capacity is restricted by acidosis,  $\text{P}_i$  accumulation, and glucose availability, all contributing to inducing muscle fatigue (23–25).

In the presence of oxygen, muscle cells can employ a mixed strategy often referred to as aerobic glycolysis. The pyruvate and NADH produced from glycolysis can be taken up by mitochondria to give 30 more ATP. Pyruvate is converted into acetyl-CoA, which will be used in the Krebs cycle to produce GTP,  $\text{H}^+$ , NADH, and Flavin adenine dinucleotide ( $\text{FADH}_2$ ). Those metabolites will be further used by the oxidative phosphorylation system, where ATP synthase rephosphorylates ADP into ATP (26). Although further use of pyruvate

increases the ATP yield of the initial glycolysis, the mitochondrial processing is much longer, usually estimated to be ~2–3 times slower than glycolysis (27). Pyruvate oxidation following glycolysis is a mixed metabolic strategy employed either during contraction or at rest. Its use will greatly depend on the muscle activity.

The final metabolic strategy, commonly termed “oxidative metabolism,” occurs exclusively within mitochondria, requires oxygen, and is based on fatty-acid substrate. Fatty acids are taken up by mitochondria for  $\beta$ -oxidation (28).  $\beta$ -oxidation is a metabolic process that degrades the long chains of fatty acids into acetyl-CoA, NADH, and FADH<sub>2</sub>. Acetyl-CoA will be used in the Krebs cycle, as previously explained, whereas NADH, and FADH<sub>2</sub> will feed the electron transport chain to produce proton motive force (electrochemical gradient for H<sup>+</sup>). Proton motive force will ultimately be used by the ATP synthase to rephosphorylate ADP into ATP (26). For a fatty acid of sixteen carbon, such as palmitic acid, its metabolism will provide 106 ATP, which is the highest yield from all metabolic strategies. However, this system is slow, making it unable to follow sudden needs for ATP. Therefore, this strategy will be favored at rest or during low-intensity muscular activity (29).

Muscle metabolic strategies are used in different ways depending on the need for ATP. When the demand is sudden and high, anaerobic or mixed strategies will be preferentially used, while at rest or low intensity exercise, ATP will be produced mainly by oxidative metabolism. This specialization of metabolism makes it possible to cope with variations in ATP consumption. In the muscle, each fiber has a metabolic specialization that supports the energy consumption of its contractile properties. In the next section, I will introduce the different fiber types, their metabolic and contractile characteristics, and how a muscle can be specialized by changing its fiber composition.

## 2 Muscle plasticity: phenotypes and phenotypic shift

Skeletal muscle is a fascinating organ. Fascinating for its level of specialization and its capacity for adaptation, also called muscular plasticity. The specialization is what allows the scalene muscles to constantly hold your head up, while your quadriceps will inevitably tire when climbing a couple of floors. The plasticity, or capacity for adaptation, is what enables an ultramarathon runner to become a bodybuilder, and *vice versa*. These contrasting functional requirements necessitate different muscle phenotypes and distinct adaptive mechanisms. In this section, I will define the different muscle phenotypes and examine the signaling pathways that induce fast-to-slow phenotypic shift.

### 2.1 Skeletal muscle phenotypes

Skeletal muscles are composed of muscle fibers, which are long, polynucleated cells. Most of the space is occupied by contractile units (sarcomeres) arranged in series and in parallel, which shorten during contraction. It is in the sarcomeres that contractile proteins, myosin heavy chain (MHC), actin, and tropomyosin are located (30). Mammalian muscle fibers are classified into four main types, based on their MHC isoform composition (31, 32):

- **Type I:** known as the “slow-oxidative” or “slow-twitch” fiber. They are composed of MHC1, which has a slow rate of ATP use (4, 33), and base their metabolic strategy on oxidative ATP production (30).
- **Type IIa:** known as “mixed”, or “fast-oxidative”. They are composed of MHC2a, which has a moderate rate of ATP use (4, 33) and employs a mixed metabolic strategy (25, 34).
- **Type IIx:** known as “fast-glycolytic” or “fast-twitch” fiber. They are composed of MHC2X, which has a high rate of ATP use (4, 33), and are mostly based on anaerobic glycolysis strategy for ATP production (35).
- **Type IIB** (only in animals): the fastest fiber, also known as “fast-glycolytic” or “fast-twitch” fiber. They are composed of MHC2B, which has a very high rate of ATP use (4, 33), and are mostly based on anaerobic glycolysis strategy for ATP production (35).

Each fiber type exhibits specific excitation threshold, contractile and metabolic properties, which determine its size, strength, endurance, rate of ATP utilization and production (30, 36–40), all summarized in **Table 1**.

**Table 1.** Characteristics and physiological properties of the mammalian skeletal muscle fiber types.

Fiber type (relative size)	MHC isoform	Activation threshold	Metabolism	Strength/Endurance	ATP utilization rate	Suitable function
Type I 	MHC1	Low	Oxidative	Low/ Very high	Low	Posture Endurance
Type IIa 	MHC2a	Moderate	Mixed	Moderate/ Moderate	Moderate	Repeated moderate intensity
Type IIX 	MHC2X	High	Mainly Glycolytic	High/ Low	High	High intensity
Type IIB 	MHC2B	High	Glycolytic	Very high/ Very low	Very high	High intensity

This diversity in the mechanical and metabolic properties of fiber types enables for skeletal muscle specialization. Each muscle has a unique fiber composition, allowing it to fulfill its specific function. For example, in mice, a muscle such as the soleus (SOL) mainly performs postural activity, which implies constant low-intensity muscle work. Hence, SOL is mainly composed of type I and type IIa fibers, which are fatigue resistant and do not express type IIB (41, 42). Oppositely, the nearby muscle gastrocnemius (GAST), essentially undergoes a burst activity, which implies sudden, intense contraction, requiring significant force generation. GAST predominantly expresses type IIB and IIX, efficient in producing a lot of strength, but expresses poorly type IIa and I (41, 42).

Beyond this conventional classification, muscle also exhibits hybrid fibers (43). Commonly, hybrid fibers have a mixed expression of relatively close MHC isoforms regarding their molecular properties, such as hybrid I/IIa, IIa/IIX, and IIX/IIB. However, their proportion varies between the muscles and often depends on the location within the same muscle (43). For example, mouse SOL expresses around 17% of hybrid fibers, predominantly hybrid I/IIa, whereas GAST expresses 9% hybrids, preferentially IIX/IIB (43).

Although the variety of fiber composition is important between different skeletal muscles, the mouse SOL and GAST muscles represent the opposition of two very different phenotypes: a “fast” phenotype mainly composed of type IIX and IIB fibers, and a “slow” phenotype mainly composed of type I and IIa fibers.

## 2.2 Phenotypic shift

As previously established, muscle fiber composition dictates its physiological properties and, therefore, its capacity to ensure a specific function. However, the daily functioning of a marathon runner’s quadriceps obviously differs from that of a sedentary office worker. For the quadriceps to be able to run a race of 42.2 km, it must be specialized. To do so, the quadriceps will modify its fiber composition toward a “slower” phenotype. This process is one of the most important phenomena of muscle plasticity and is called phenotypic shift.

The phenotypic shift is mostly a linear process, where a fiber shifts to the near faster or slower type, usually crossing a hybrid state (43, 44). However, it is rare to observe a full spectrum shift of fiber from type IIB to type I or vice versa. Usually, fibers do not shift more than type I to IIX or IIB to IIa (31, 45). As shown in **Figure 1**, several factors can influence the muscle phenotype or induce a phenotypic shift (30, 31, 46). For example, a slow-to-fast phenotypic shift can be triggered by hormonal changes such as hyperthyroidism (31) (**Figure 1**). But one of the most powerful is undoubtedly the type of muscular activity. Generally speaking, any muscular activity of low or moderate intensity, sustained over time, will favor the slow phenotype. For example, nerve tonic activity (constant stimulation) or endurance training are known to maintain a slow phenotype or induce a shift from fast-to-slow (30, 44, 47) (**Figure 1**). In contrast, any muscular inactivity or brief activity of very high intensity will favor the fast phenotype. For example, nerve phasic activity (intermittent high frequency), high-speed training, or inactivity promotes maintenance of a fast phenotype or transition from slow-to-fast (30, 45, 47, 48) (**Figure 1**). The molecular consequences and signaling cascades vary depending on the stimuli. In the fast-to-slow phenotypic shift, two very important initial signals are known to trigger signaling pathways influencing the muscle phenotype: the Ca<sup>2+</sup> dynamics and the energetic stress.

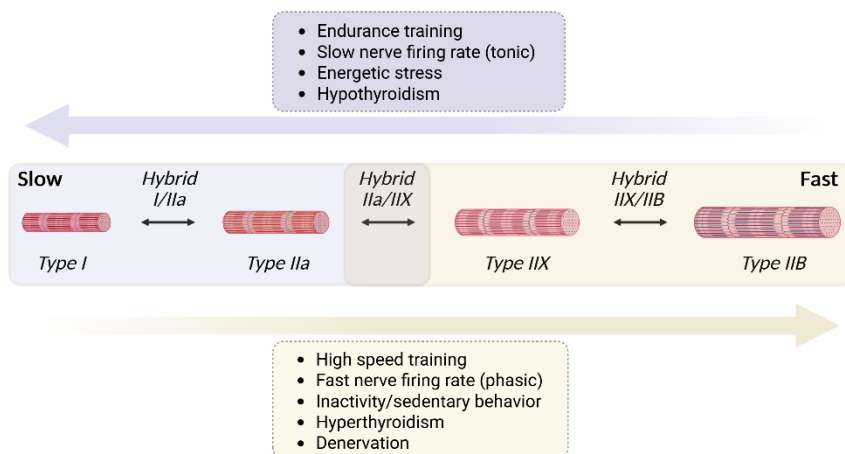


**Figure 1.** Factors influencing the muscle phenotype and the phenotypic shift. Endurance training, tonic nerve stimulation, energetic stress, and hypothyroidism promote the expression of the slow phenotype (Type I and IIa fibers). Strength training, phasic nerve stimulation, inactivity, sedentary behavior, hyperthyroidism, and denervation promote the expression of the fast phenotype (Type IIX and IIB fibers). Created in <https://BioRender.com>.

### 2.3 Signaling pathways involved in fast-to-slow phenotypic shift

Multiple signaling pathways are known to directly or indirectly regulate the phenotype. While some specifically promote the slow or the fast phenotype, others are common, having different effects depending on the nature of stimuli. And sometimes the suppression of one is sufficient to promote the opposite phenotype (30, 31, 49). In this PhD thesis, I will focus on the signaling that induces a fast-to-slow phenotypic shift.

Muscle undergoing a fast-to-slow phenotypic shift is characterized by an increase in the type I and/or IIa expression concomitant with a decrease in the type IIX and/or IIB

expression. The muscle appears more reddish due to a higher myoglobin concentration, and becomes metabolically more oxidative (50, 51). Mitochondrial density increases as well as fatty-acid use (51), and the muscle shows higher endurance performance (52). If the stimuli do not trigger hypertrophy, these metabolic changes can be accompanied by a decrease in the maximal strength and a physiologic reduction of the fiber size, characteristic of the slower fibers (see relative fiber size **Table 1**).

All of those metabolic and contractile changes are driven by the activation of specific signaling pathways. Three major signaling pathways inducing fast-to-slow phenotypic shift have been identified so far:

- The energetically derived signal AMP-activated protein kinase (AMPK) / Peroxisome proliferator-activated receptor gamma coactivator 1-alpha (PGC1 $\alpha$ ) axis.
- The nerve-derived signal Ca<sup>2+</sup> / Calmodulin (CaM) / calcium-calmodulin-dependent protein kinase IV (CaMKIV) / cAMP Response Element-Binding protein (CREB)/ PGC1 $\alpha$  axis.
- The nerve-derived signal Ca<sup>2+</sup> / CaM / Calcineurin (CaN) / Nuclear Factor of Activated T-cells (NFAT) / Myocyte Enhancer Factor 2 (MEF2) axis.

In the following sections, we will detail these three pathways, all summarized in **Figure 2**.

### 2.3.1 The AMPK/PGC1 $\alpha$ axis

#### **AMPK:**

The study of the AMP-activated protein kinase (AMPK) regulation occupied a large part of my Ph.D. and will constitute an important part of the discussion of this thesis. Therefore, I will first delve deeper into the regulation of this protein in skeletal muscle.

AMPK is a ubiquitous serine/threonine protein kinase known as the master regulator of metabolism (53). It is composed of a heterotrimeric complex: one catalytic  $\alpha$  subunit, one regulatory  $\beta$  subunit, and one  $\gamma$  subunit. Each subunit can occur as multiple isoforms ( $\alpha 1$ ,  $\alpha 2$ ,  $\beta 1$ ,  $\beta 2$ ,  $\gamma 1$ ,  $\gamma 2$ , and  $\gamma 3$ ), enabling the formation of twelve different  $\alpha\beta\gamma$  heterotrimer combinations (54). The most common isoforms in skeletal muscle are  $\alpha 2\beta 2\gamma 1$ ,  $\alpha 1\beta 2\gamma 1$ , and  $\alpha 2\beta 2\gamma 3$  (mostly in fast muscle) (55). AMPK is an energetic sensor, activated by the rise of AMP and ADP concentration following ATP hydrolysis. Conversely, high ATP concentration will keep AMPK inactive by competing with AMP or ADP binding, and promotes its deactivation (56–60). AMPK activation is essentially triggered by AMP and/or ADP binding to the  $\gamma$  subunit, which induces changes in AMPK allosteric conformation, enabling its phosphorylation on Thr<sup>172</sup> by its main upstream kinase Liver Kinase B1 (LKB1) (59, 61, 62). In cultured cells, the AMPK activity correlates with the LKB1 expression (62), and several studies have shown that AMPK activity is highly dependent on LKB1 in muscle (61, 63–65).

Alternatively, AMPK can also be phosphorylated on Thr<sup>172</sup> independently of AMP or ADP by calcium/calmodulin-dependent protein kinase kinase 2 (CaMKK $\beta$ ) (66–70). CaMKK $\beta$  is activated by calmodulin (CaM) following an increase in Ca<sup>2+</sup> concentration. Despite CaMKK $\beta$  being an upstream kinase of AMPK *in vitro* (66, 71, 72), its role in muscle is controversial. Indeed, CaMKK $\beta$  is poorly expressed in muscle (68, 72, 73), and the direct effect of CaMKK $\beta$  phosphorylation of AMPK following Ca<sup>2+</sup> signaling in muscle has been suggested, but never proven (63, 67, 68, 74). In agreement with a recent publication (73), we have shown that CaMKK $\beta$  does not phosphorylate AMPK in muscle (72). These results are described in **Publication II** and will be discussed in this thesis.

AMPK regulation has also been suggested to be isoform-dependent. AMPK $\alpha$ 1 enzymatic activity has been reported to be more sensitive to Ca<sup>2+</sup> signalling in muscle (63, 67), however, *in vitro* studies show that CaMKK $\beta$  is more prone to phosphorylate AMPK $\alpha$ 2 (59, 72). LKB1 is also more likely to interact with AMPK $\alpha$ 2 (61). Interestingly, isoform distribution also varies between muscle phenotypes, where AMPK $\alpha$ 2 represents ~90% of all AMPK in fast muscle and ~70% in slow muscles, the rest being occupied by AMPK $\alpha$ 1 (55). In insect cells, or other organs such as the liver, the sensitivity to AMP binding and the rate of allosteric activation seem to be higher for AMPK $\alpha$ 2 isoform (75), suggesting AMPK $\alpha$ 2 as a better option to sense sudden energetic variation that fast muscles undergo.

Acute AMPK activation can be viewed as a rebalancing mechanism whose objective is to compensate for an ATP drop by increasing the uptake and utilization of metabolic substrates. AMPK activity increases the cellular uptake of glucose and fatty acids by promoting the translocation of GLUT4 and CD36 transporters to the cell membrane (76–78). Moreover, it enhances the oxidation of fatty acids through its inhibition of acetyl-CoA carboxylase (ACC) (79, 80), making AMPK a primary target to fight metabolic diseases. AMPK activity is particularly linked to glucose metabolism, especially AMPK $\alpha$ 2, which can inhibit glycogen synthase (GS) to favor glycolysis (81, 82). Glucose deprivation has been shown to induce activation of AMPK by LKB1 independently of AMP/ADP levels (83), whereas glycogen binding to the  $\beta$  subunit inhibits its activity even in AMP presence (84). Hence, AMPK is an energetic sensor that promotes substrate metabolism to restore energetic equilibrium while also being directly regulated by glucose availability.

To restore energetic balance, AMPK will also act as an inhibitor of ATP-consuming processes such as protein synthesis, i.e. anabolism. Acute treatment with AMPK activator 5-aminoimidazole-4-carboxamide-1- $\beta$ -D-ribofuranoside (AICAR) inhibits protein synthesis, by indirectly inhibiting mammalian Target of Rapamycin (mTOR) (85–89). In contrast, AMPK activation promotes catabolism, increasing the degradation of organelles and proteins. AMPK induce catabolism is mediated through autophagy, ubiquitin-proteasome system (UPS), or specific mitophagy, where AMPK directly phosphorylates Unc-51 like autophagy activating kinase 1 (ULK1) and Forkhead box protein O3a (FOXO3a) (90–97). The acute activation of these degradative systems enables the recycling of cellular components that can be reused in metabolism. Additionally, AMPK may regulate lysosomal degradation of specific substrates such as glycophagy (degrade glycogen) or macrolipophagy (degrade triglycerides) (98). Particularly for glycophagy, as AMPK can phosphorylate starch-binding domain 1 (STBD1) in muscle, which is responsible for the transport of glycogen to the phagosome (99, 100). In summary, AMPK activation promotes catabolism by substrate metabolism and protein degradation, and acts as an inhibitor of protein synthesis.

Beyond transient activation, long-term AMPK activity has deeper consequences on muscle tissue. Long-term activity was shown to inhibit muscle hypertrophy, particularly through AMPK $\alpha$ 1 (101–105), and to promote muscle atrophy in C2C12 muscle myotubes (96, 106, 107). Although acute AMPK inhibits protein synthesis and promotes protein degradation, whether chronic AMPK activity induces skeletal muscle atrophy remains controversial (108). Chronic AMPK activation is also well known to promote mitochondrial biogenesis, thereby increasing oxidative capacity (109–114). Furthermore, AMPK activity was shown to influence the expression of MHC toward slower isoforms (115–117), but this effect remains unclear (109, 112, 118, 119). Indeed, the suppression of various AMPK subunits has no consequences on the MHC composition (112, 118, 119). In contrast, long-term AICAR treatments on C2C12 myotubes and rodent muscles have

shown some subtle changes in MHC composition (115, 117, 120). One study showed that suppression of AMPK $\alpha$ 2 upon an endurance training program reduces the shift from IIB to IIX and IIa (116). Furthermore, AMPK suppression has been shown to prevent the MHC shift toward a slower phenotype in C2C12 cells following arginine and procyanidin B2 treatments (121, 122). Therefore, while AMPK-induced mitochondrial biogenesis is well established, its capacity to promote MHC shifts toward slower isoforms remains to be confirmed. However, both mitochondrial biogenesis and expression of slow MHC isoforms are driven by the same transcription factor: Peroxisome proliferator-activated receptor gamma coactivator 1-alpha (PGC1 $\alpha$ ).

### ***AMPK/PGC1 $\alpha$ axis:***

AMPK directly and indirectly interacts with PGC1 $\alpha$ . AMPK directly phosphorylates PGC1 $\alpha$  at Thr<sup>177</sup> and Ser<sup>538</sup>, which increases its nuclear localization and leads to PGC1 $\alpha$  binding its own promoter, thereby enhancing PGC1 $\alpha$  expression (123). In addition, AMPK increases NAD<sup>+</sup>-dependent deacetylase sirtuin-1 (SIRT1) activity, which deacetylates PGC1 $\alpha$  and greatly increases its transcriptional activity (124–126). PGC1 $\alpha$  activity promotes the transcription of nuclear mitochondrial genes coding for COX4, ATP synthase, and mitochondrial Transcription Factor A (mtTFA), a key activator of mitochondrial DNA transcription and replication (127–129). Hence, increasing PGC1 $\alpha$  expression and activity promotes mitochondrial biogenesis and the development of oxidative metabolism in muscle.

PGC1 $\alpha$  overexpression is also known to shift the MHC composition from fast isoforms IIB and IIX to slow isoforms IIa and I (130–135). PGC1 $\alpha$  can interact with myocyte enhancer factor-2 (MEF2) (136–138), which is the main transcription factor binding the slow fibers gene promoters (139–141). MEF2 belongs to the myogenic regulatory factor (MRF) family, which also includes myoblast determination protein 1 (MyoD). These factors work concurrently to shape muscle phenotype. MyoD is highly expressed in fast fibers (142), and its upregulation increases the proportion of type IIB-IIX fibers in mouse muscle (143). Conversely, MyoD KO mice exhibit a shift of fast fibers towards a slower phenotype (142, 144). While MEF2 expression seems even between fast and slow fibers (145), increasing its activity or expression promotes the expression of slow fibers (145). In skeletal muscle, MyoD appears naturally more active, and its constant inhibition (146), or high and sustained MEF2 activity, may be required for expression of the slow phenotype (147, 148).

PGC1 $\alpha$  gene promoter can be bound by MEF2 itself, thereby increasing PGC1 $\alpha$  expression, whereas PGC1 $\alpha$  interaction with MEF2 is associated with an increased transcription of slow fibers gene (136–138, 149, 150). Therefore, PGC1 $\alpha$  overexpression promotes the shift and maintenance of the slow phenotype through its interaction with MEF2 and by increasing mitochondrial biogenesis.

In summary, the energetic-derived activation of the AMPK/PGC1 $\alpha$  axis is a signaling pathway able to induce a fast-to-slow phenotypic shift, by modifying the metabolism toward oxidative and MHC expression toward slow isoforms. PGC1 $\alpha$  is the central key transcription factor, whose expression and activity are modulated directly by AMPK or indirectly through SIRT1. The signaling pathway is represented schematically in **Figure 2.A.**

### 2.3.2 The Ca<sup>2+</sup>/CaM/CaMKIV/CREB/PGC1α axis

Muscle phenotype is strongly determined by daily muscle activity (151). Upon electrical activity, Ca<sup>2+</sup> is released from the SR into the cytoplasm through RyRs to trigger contraction. This Ca<sup>2+</sup> is pumped back into the SR by SERCA pumps, inducing muscle relaxation. Ca<sup>2+</sup> transients are nerve-derived signals regulating contraction, whose frequency and amplitude also inform the tissue about muscular activity.

One important Ca<sup>2+</sup> sensing protein is Calmodulin (CaM). CaM consists of two lobes able to bind two Ca<sup>2+</sup> ions each. The rise of Ca<sup>2+</sup> concentration leads to saturation of the lobes, allowing CaM to interact with a multitude of downstream targets, including calcium/calmodulin-dependent protein IV (CaMKIV) or CaMKKβ (152, 153). The binding of CaM on CaMKIV induces its partial activation, allowing CaMKKβ (also an upstream kinase of AMPK) to phosphorylate on Thr<sup>196</sup>, making CaMKIV fully active (154–156). Active CaMKIV is known to localize in the nucleus and to phosphorylate cAMP Response Element-Binding protein (CREB) on Ser<sup>133</sup> in the brain and in muscle (149, 157–160). Once phosphorylated, CREB binds to the PGC1α promoter, increasing its transcription and expression, which promotes oxidative metabolism (149, 160, 161). However, while this mechanism is well established in the brain, it is important to note that CaMKIV and CaMKKβ are poorly expressed in skeletal muscle tissue (72, 73, 160, 162). Furthermore, muscle-based studies have overexpressed CaMKIV, which strongly diverges from physiological conditions.

Therefore, the Ca<sup>2+</sup>/CaM/CaMKIV/CREB/PGC1α axis has been suggested as a nerve-derived pathway that could induce a fast-to-slow phenotypic shift in muscle, especially linking Ca<sup>2+</sup> with mitochondrial biogenesis. However, the poor expression of CaMKIV and CaMKKβ in muscle suggests a minor importance in physiological conditions. This signaling pathway is represented schematically in **Figure 2.B**.

### 2.3.3 The Ca<sup>2+</sup>/CaM/CaN/NFATc1/MEF2 axis

Another nerve-derived pathway that mediates MHC shift in muscle is Ca<sup>2+</sup>/CaM/CaN/NFATc1/MEF2. Activated CaM can interact with Calcineurin (CaN) in the cytosol, with which it forms an active phosphatase complex (163). The primary target of the CaM/CaN complex is the dephosphorylation of Nuclear Factor of Activated T-cells (NFAT) family proteins (164).

In muscle, NFAT proteins are mainly cytosolic, but upon dephosphorylation by CaM/CaN complex, they relocate and accumulate in the nucleus (165–168). NFATc1 nuclear accumulation is notably known to interact with MEF2 and enhance its activity (139, 169), to inhibit MyoD (170), which increases the expression of slow MHC isoforms and reduces fast MHC isoform expression (167, 171–173).

NFATc1 nuclear accumulation is very dependent on muscle activity, especially long-term low-frequency stimulation (166–168, 172), which is characteristic of muscles with postural activity, such as SOL. Interestingly, NFATc1 has an activity-dependent circadian cycle, predominantly cytosolic during the resting period and predominantly nuclear during the active period in mice (174). Additionally, NFATc1 rapidly exits the nucleus upon cessation of activity (168). Moreover, inhibition of the CaN/NFATc1 signaling pathway has been shown to modify the MHC gene expression from the slow isoform toward the fast isoforms, highlighting its importance in the maintenance of a slow phenotype (168, 170, 172, 173, 175).

Hence, the  $\text{Ca}^{2+}$ /CaM/CaN/NFATc1/MEF2 pathway is an essential and dynamic nerve-derived signaling, able to modify the muscle phenotype from fast to slow if maintained activated over time. This signaling pathway is represented schematically in **Figure 2.C**.

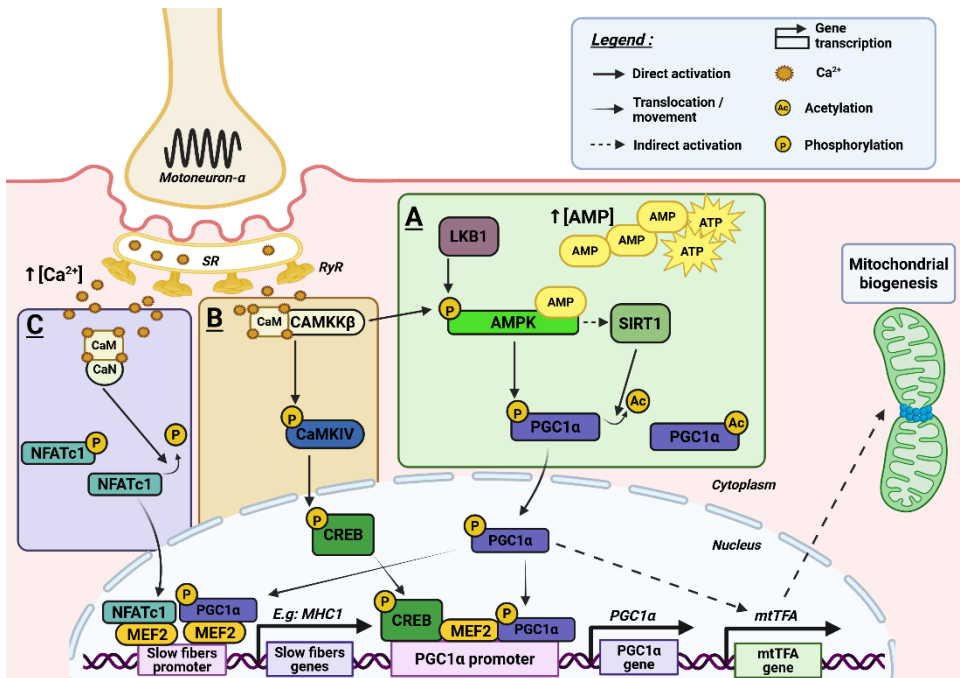


**Figure 2.** Molecular signaling pathways involved in fast-to-slow muscle phenotypic shift. **A.** AMP-activated protein kinase (AMPK) is phosphorylated by Liver Kinase B1 (LKB1) following the rise of ADP or AMP in the cytoplasm. AMPK activity induces the direct phosphorylation and indirect SIRT1 deacetylation of Peroxisome proliferator-activated receptor gamma coactivator 1-alpha (PGC1α). PGC1α nuclear translocation increases slow fiber genes, PGC1α expression, and promotes mitochondrial biogenesis. **B.** Cytoplasmic  $\text{Ca}^{2+}$  accumulation activates Calmodulin (CaM), inducing calcium-calmodulin-dependent protein kinase IV (CaMKIV) phosphorylation by calcium/calmodulin-dependent protein kinase 2 (CaMKKβ). CaMKIV phosphorylates cAMP Response Element-Binding protein (CREB), which will bind the PGC1α promoter. **C.** Cytoplasmic  $\text{Ca}^{2+}$  accumulation activates CaM and Calcineurin (CaN) complex, inducing Nuclear Factor of Activated T-cells cytoplasmic 1 (NFATc1) dephosphorylation and nuclear translocation. NFATc1 coactivates slow fiber gene expression with myocyte enhancer factor-2 (MEF2). Created in <https://BioRender.com>.

### 2.3.4 Other signaling pathways

The signaling pathways presented in **Figure 2** are the most extensively characterized mechanisms governing fast-to-slow phenotypic shift, and the most relevant for this PhD thesis. Nevertheless, additional regulatory pathways have been identified in the literature, such as p38 mitogen-activated protein kinase (p38) regulation of PGC1α (176, 177) or the mTOR/Yin Yang 1 (YY1)/PGC1α pathway (178, 179). For simplicity purposes, these supplementary pathways will not be discussed, allowing for focused examination of the primary mechanisms outlined above.

### 3 The creatine kinase system

As previously mentioned, matching ATP production with ATP need/demand is essential for muscle function. The sudden need for ATP induced by contraction requires an immediate buffering system. In muscle, this function is ensured by the creatine kinase (CK) system.

CK catalyzes the ADP rephosphorylation into ATP from phosphocreatine (PCr) and the reverse reaction using ATP to phosphorylate creatine (Cr) to PCr according to the following formula:  $\text{Cr} + \text{ATP} \leftrightarrow \text{PCr} + \text{ADP} + \text{H}^+$ . Through this reversible reaction, the CK system acts as an immediate ATP buffer near ATPases (180–182). In most muscles, the immediate maximal rate of CK system ATP synthesis is considered higher than both glycolysis and oxidative phosphorylation at their maximal capacity (181).

ATP production sites, such as mitochondria, are not always close to the ATP consumption sites. Although ATP diffuses naturally in the muscle cell, its diffusion is slowed down by the structural barriers (181–183). Furthermore, as diffusion depends on the concentration gradient, low physiological concentrations of ADP ( $\mu\text{M}$  range) will favor its accumulation near ATPases. This ADP accumulation near ATPases must be continuously rephosphorylated to maintain the phosphorylation potential. Consequently, CK has been hypothesized as an energy transport system for the phosphate group, especially because PCr concentration is higher and diffuses faster than ATP and ADP (181, 182). Therefore, the CK system facilitates the energy transport, allowing rapid transfer of high-energy phosphate bound across the cellular space and enabling faster diffusion with PCr, as illustrated in **Figure 3**.

Skeletal muscles mainly express the muscle-specific cytosolic CK (M-CK) isoform and the sarcomeric mitochondrial CK (Mi<sub>s</sub>-CK), which is located in the mitochondrial intermembrane space (181). However, other CK isoenzymes, such as brain-specific (B-CK) or mixed (MB-CK) exist and can be detected in oxidative muscles (184, 185) or transiently expressed during skeletal muscle development (181).

One of the key substrates of the CK system is creatine (Cr). Cr is a ubiquitous non-protein amino acid that can be absorbed through food or be endogenously synthesized in two steps (**Figure 3**). The first step occurs in the kidneys, where L-Arginine: Glycine amidinotransferase (AGAT) catalyzes the transfer of arginine (Arg) to glycine (Gly), to produce ornithine and guanidinoacetic acid (GAA). GAA is then transported to the liver, where it is methylated by Guanidinoacetate N-methyltransferase (GAMT) to produce Cr (186). Cr travels through the bloodstream and is taken up by organs through the creatine transporter (CrT; SLC6A8). While the brain can generate some Cr of its own by local concentration of AGAT and GAMT, skeletal muscles are dependent on Cr-uptake from the circulation (187–189).

To summarize, the CK system is an essential ATP buffering system in skeletal muscle. The high PCr concentration and the speed of ADP rephosphorylation by CK, make it the most dynamic energetic system in muscle, able to follow brief and significant drops in ATP concentration. Consequently, any disturbance of the CK system will compromise muscle energetics and function.

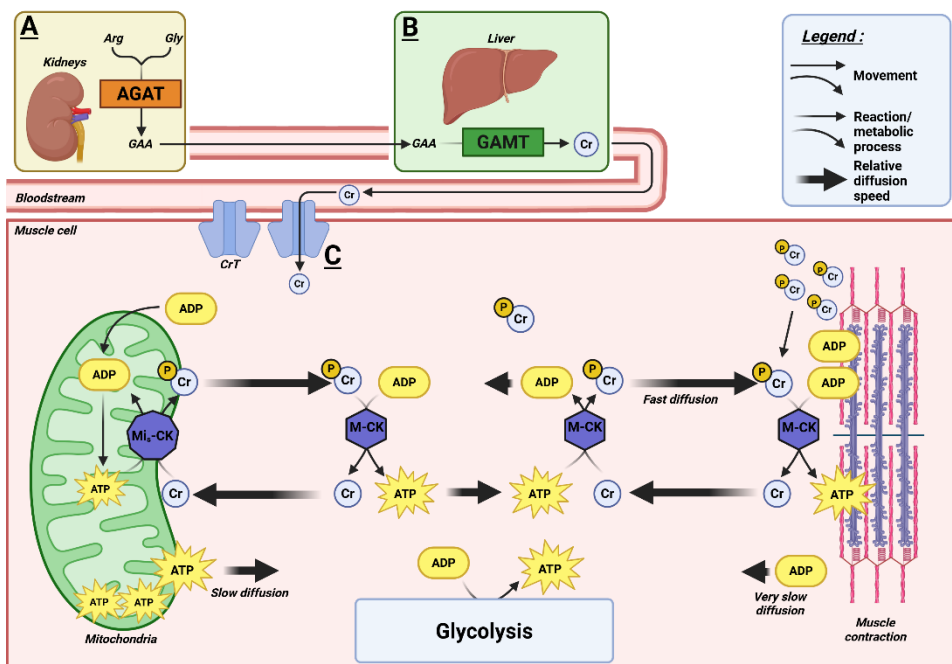


**Figure 3.** Creatine (Cr) biosynthesis and involvement in the creatine kinase (CK) system. **A.** In kidneys, L-Arginine: Glycine amidinotransferase (AGAT) catalyzes the transfer of arginine (Arg) to glycine (Gly), to produce guanidinoacetic acid (GAA). **B.** GAA travels to the liver, where Guanidinoacetate N-methyltransferase (GAMT) converts it into Cr. **C.** Cr enters the muscle fibers through the creatine transporter (CrT). One phosphate group of ATP produced in mitochondria or from glycolysis is transferred onto Cr by sarcomeric mitochondrial CK (Mi<sub>s</sub>-CK) or muscle-specific cytosolic CK (M-CK). This reaction produces ADP and phosphocreatine (PCr). Another M-CK will transfer the phosphate from PCr onto one ADP, giving ATP and Cr. This reversible reaction near ATPases, ATP production sites, and across the cytoplasm enables for the fast diffusion of phosphate groups, as PCr diffuses faster than ATP or ADP. PCr near ATPases acts as a phosphate reservoir, allowing the immediate rephosphorylation of ADP into ATP when contraction starts, which is essential to maintain local phosphorylation potential. Created in <https://BioRender.com>.

## 4 Consequences of defective CK system on skeletal muscle phenotype

Maintenance of energetic balance is essential for skeletal muscle physiology. Long-term disruption of the CK system chronically disturbs the energy transfer and regulation, potentially triggering muscle adaptation. As previously mentioned, contraction, protein synthesis, and AMPK activity (**Figure 2**) are all directly influenced by energetics and could ultimately lead to muscle weakness, atrophy, and a shift from fast-to-slow phenotype. In this section, I will provide a comprehensive literature review describing how CK system deficiency affects muscle energetics and phenotype.

### 4.1 Models of defective CK system

The CK system serves as the most important ATP buffering system in many organs, including the brain, Heart, and skeletal muscle. Given its physiological importance, numerous animal models have been developed to evaluate CK function under both physiological and pathological conditions. Disruption of the CK system can be achieved through two approaches: either inhibiting the CK enzyme or eliminating its substrate Cr. In skeletal muscle studies,  $Mi_s$ -CK KO, M-CK KO, and double KO  $Mi_s$ -CK/M-CK (CK KO) mice have been used to modulate CK activity, whereas treatment with beta-guanidinopropionic acid ( $\beta$ -GPA), CrT KO, GAMT KO, and AGAT KO mice have been used to modulate creatine levels.

### 4.2 CK-deficient models

Skeletal muscles mainly express M-CK and  $Mi_s$ -CK isoforms. Those isoform concentrations and activity vary between fiber types (190). M-CK expression is highest in type IIB and IIX fibers, intermediate in type IIa fibers, and lowest in type I fibers. This pattern is opposite to that of the mitochondrial isoform ( $Mi_s$ -CK), which also plays a structural role in mitochondria (191), and is therefore correlated to the mitochondrial density, being higher in type I fibers. However, the main difference between the muscle types lies in the total CK activity. Fast muscles exhibit substantially higher total CK activity than slow muscles, and this difference is predominantly attributed to M-CK activity (184, 192, 193). Therefore, a fast muscle such as GAST, quadriceps, or extensor digitorum longus (EDL) will be more dependent on CK activity than slow muscle, especially M-CK. In contrast, a slow muscle such as SOL will rely on both M-CK and  $Mi_s$ -CK isoforms (194, 195).

When looking at the literature, the knockout of  $Mi_s$ -CK alone has minor effects in both fast and slow muscles, all summarized in **Table 2**. Overall, muscles show no sign of atrophy but minor changes in metabolism, where slow muscles such as SOL increase activity of the glycolytic metabolism. Suppression of M-CK alone similarly does not significantly affect muscle energetics, as evidenced by unchanged PCr and ATP concentrations, although one study reported moderate AMPK activation (196). However, several studies reported an increase in the oxidative metabolism in fast muscle GAST. Lastly, models suppressing both  $Mi_s$ -CK and M-CK demonstrate more severe muscle effects, inducing muscle atrophy of both fast and slow muscles, shifting the metabolism slightly toward oxidative in fast muscles, and reducing the expression of fast fibers (**Table 2**).

Overall, studies showed that slow muscles exhibit greater dependence on Mi<sub>5</sub>-CK and undergo a compensatory shift toward glycolytic metabolism when this isoform is suppressed. Conversely, selective suppression of M-CK induces mitochondrial biogenesis, which increases total Mi<sub>5</sub>-CK levels and may contribute to the maintenance of PCr and ATP concentrations at rest (197, 198). Double KO produces more pronounced effects, impacting muscle mass, metabolism, and fast MHC isoform expression. However, the current literature remains limited in scope, and information regarding the signaling pathways involved and energetics is missing.

**Table 2.** Literature overview of the muscle consequences of CK-deficient models.

Model	BW	Muscle	Metabolite	Atrophy	Metabolism	MHC	Signaling	Ref
Mi <sub>5</sub> -CK KO		Quads		No	↑oxidative (subtle)		= PGC1α	(199)
Mi <sub>5</sub> -CK KO	=	SOL		No	↑glycolytic			(200)
Mi <sub>5</sub> -CK KO		GAST	= PCr = ATP					(201)
M-CK KO		GAST			↑oxidative ↑mito		= PGC1α +44% AMPK	(196)
M-CK KO		GAST, SOL			↑oxidative in GAST			(202)
M-CK KO		GAST, SOL			↑oxidative in GAST			(203)
M-CK KO		GAST	= PCr = ATP					(201)
M-CK KO		GAST	= PCr = ATP		↑oxidative			(204)
M-CK KO			= PCr = ATP		↑oxidative			(198)
CK KO		GAST			↑mito			(205)
CK KO	=	GAST, SOL		W/BW -39% SOL	↑oxidative ↓glycolytic in GAST	-11% IIB +200% IIX in GAST No IIX in SOL		(206)
CK KO	=	GAST, EDL, SOL		W/BW - 33% SOL -27% EDL	↑oxidative = glycolytic in GAST			(207)
CK KO		GAST	-24% PCr +10% ATP					(201)

The percentages were calculated by the author of this thesis and not by the authors of the articles. They are approximate (based on mean values) and only indicative. Creatine kinase (CK); Sarcomeric mitochondrial CK KO (Mi<sub>5</sub>-CK KO); Muscle-specific cytosolic CK KO (M-CK KO); Double KO Mi<sub>5</sub>-CK/M-CK (CK KO); Bodyweight (BW); Quadriceps (Quads); Gastrocnemius (GAST); Soleus (SOL); Extensor digitorum longus (EDL); Phosphocreatine (PCr); Weight (W); Mitochondria (mito); Myosin heavy chain (MHC); Peroxisome proliferator-activated receptor gamma coactivator 1-alpha (PGC1α); AMP-activated protein kinase (AMPK).

## 4.2 CrT-deficient and β-GPA-treated models

Other models directly impacting Cr concentration in muscle have been studied. β-GPA serves as a Cr analogue but demonstrates poor substrate efficiency, being utilized by CK at only 1% of the rate of Cr (208). Mice treated with β-GPA, significantly accumulate this analogue in the muscle, thereby reducing the efficiency of the CK system. β-GPA treatment substantially impairs muscle energetics, resulting in decreased PCr and ATP availability (**Table 3**). Muscle atrophy has been reported despite a lower impact on body weight. Interestingly, the fast muscle phenotype is significantly altered, resulting in a

metabolic and MHC shift toward a slow phenotype. Those phenotypic changes are associated with an upregulation in the energy-related axis AMPK/PGC1 $\alpha$  (**Table 3**), and one study demonstrated that oxidative metabolism adaptation is AMPK dependent (114). Additionally, several other studies have highlighted an increase in AMPK activity following  $\beta$ -GPA treatment (meta-analysis) (209).

Despite variability in experimental design (treatment duration ranging from 14 to 240 days and varying dosages) and the persistence of residual Cr levels, reduction in PCr levels by  $\beta$ -GPA treatment activates the AMPK pathway, induces muscle atrophy, and modifies the muscle phenotype.

Another, more radical model consists of suppressing the entry of Cr into the cell. Studies employing CrT KO mice have reported a significant reduction in Cr and ATP availability in muscle (210–213). CrT KO mice exhibit a severe reduction in their body weight, accompanied by a significant muscle atrophy (**Table 3**). This atrophy has been associated with an inhibition of protein synthesis, and higher expression of the E3 ligase F-box only protein 32 (MaFbx) (210), a central player in the UPS system. The muscle metabolism shifts massively toward oxidative in fast muscles, associated with PGC1 $\alpha$  overexpression (210). Additionally, one study reported a moderate change in MHC composition (210). Interestingly, one study carried out on rats exhibited no minor changes in muscle atrophy, consistent with no changes in protein synthesis signaling (214). However, this discrepancy may be explained by the retention of significant creatine levels in this model. The model used was slightly different than mice CrT KO, as the author induced a specific mutation (xY389C) on the CrT instead of a complete KO, which might have partly maintained the ability to uptake Cr.

Overall, affecting Cr concentration impacts muscle profoundly compared to CK-deficient models. All evidence points toward a fast-to-slow phenotypic shift in fast muscles lacking Cr. However,  $\beta$ -GPA-treated and CrT KO models still present Cr in their muscles and can endogenously synthesize it. The remaining creatine could mitigate the severity of their muscle phenotype.

**Table 3.** Literature overview of the muscle consequences of CrT-deficient and  $\beta$ -GPA-treated models.

Model	BW	Muscle	Metabolite	Atrophy	Metabolism	MHC	Signaling	Ref
$\beta$ -GPA	-12%	GAST	-67% PCr -17% ATP -30% Pi	-21% W -21% FS				(215)
$\beta$ -GPA (Meta-analysis)	-10%		-66% Cr -80% PCr -39% ATP		$\uparrow$ mito $\uparrow$ oxidative $\downarrow$ glycolytic	$\downarrow$ IIB $\uparrow$ Ila, I	$\uparrow$ AMPK	(209)
$\beta$ -GPA	=	GAST	-55% PCr -42% ATP -60% ATP/AMP (all worse in AMPK KD)		$\uparrow$ mito $\uparrow$ oxidative (all AMPK dependent)		+94% AMPK +200% PGC1 $\alpha$ +187% CaMKIV (all AMPK dependent)	(114)
$\beta$ -GPA (rats)	=	GAST				$\downarrow$ IIB $\uparrow$ IIX, Ila		(216)
$\beta$ -GPA		GAST		$\downarrow$ FS (IIB)	$\uparrow$ mito $\uparrow$ oxidative			(217)
$\beta$ -GPA		GAST, PLA	-80% Cr -90% PCr -43% ATP = Pi					(218)
CrT KO	-43%	EDL	-50% ATP	-71% FS	$\uparrow\uparrow$ mito	+25% IIX -16% IIB	+75% PGC1 $\alpha$ +200% MaFbx $\downarrow$ protein synthesis	(210)
CrT KO (rats)		Quads	-64% Cr	$\downarrow$ FS (subtle)			= MaFbx =protein synthesis	(214)
CrT KO	-49% BW, -31% BMI	EDL	-88% Cr	-41% FS	$\uparrow$ oxidative			(212)
CrT KO	-48%	GAST	-94% Cr	-50% FS				(211)
CrT KO	-36%	GAST	-75% ATP		$\uparrow$ oxidative			(213)

The percentages were calculated by the author of this thesis and not by the authors of the articles. They are approximate (based on mean values) and only indicative. Beta-guanidinopropionic acid ( $\beta$ -GPA); Creatine transporter KO (CrT KO); Bodyweight (BW); Body mass index (BMI); Quadriceps (Quads); Gastrocnemius (GAST); Plantaris (PLA); Extensor digitorum longus (EDL); Creatine (Cr); Phosphocreatine (PCr); Inorganic phosphate (Pi); Mitochondria (mito); Weight (W); Fiber size (FS); Myosin heavy chain (MHC); Peroxisome proliferator-activated receptor gamma coactivator 1-alpha (PGC1 $\alpha$ ); AMP-activated protein kinase (AMPK); Calcium-calmodulin-dependent protein IV (CaMKIV); F-box only protein 32 (MaFbx).

#### 4.4 GAMT KO and AGAT KO creatine-deficient models

Both GAMT KO and AGAT KO mice suppress one of the two key enzymes in Cr biosynthesis (**Figure 3**). As illustrated in **Table 4**, most of the studies show either a complete absence or a residual amount of Cr that mice ingested at a younger age via breast milk. One study showed that Cr remains in GAMT KO mice, but this could be attributed to coprophagia between WT and KO littermates (219). Both GAMT KO and AGAT KO mice exhibit reduced body weight, muscle atrophy, and increased oxidative metabolism. However, these changes appear more pronounced in AGAT KO mice (**Table 4**). Moreover, muscle consequences vary between the muscle types, with the fast muscle GAST exhibiting more severe atrophy and metabolic shift than SOL (220). This pattern is consistent with results observed in previous models (**Tables 2 and 3**),

where fast muscles appear to be more affected than slow muscles by CK system deficiency. In AGAT KO, results indicate a potential activation of the AMPK/PGC1 $\alpha$  pathway. Nevertheless, none of these studies specified the muscle fiber types examined.

**Table 4.** Literature overview of the muscle consequences of creatine-deficient GAMT KO and AGAT KO mice.

Model	BW	Muscle	Metabolite	Atrophy	Metabolism	MHC	Signaling	Ref
GAMT KO		GAST	-90% Cr ↑ PGAA	No				(221)
GAMT KO	-35%		↓ PCr ↑ PGAA	No				(219)
GAMT KO	-26%	GAST, SOL		W -34% GAST -29% SOL (minor when W/BW)	GAST ↑ oxidative = glycolytic SOL ↑ oxidative ↑ glycolytic (subtle)			(220)
GAMT KO			0 PCr ↑ PGAA					(222)
AGAT KO	-41%	GAST, SOL		W -76% GAST -37% SOL (W/BW no atrophy for SOL)	GAST ↑↑ oxidative ↓↓ glycolytic SOL ↑ oxidative = glycolytic			(220)
AGAT KO							+75% AMPK	(223)
AGAT KO					↑ oxidative		+60% PGC1 $\alpha$	(224)
AGAT KO	-30% BMI		0 Cr 0 GAA				+250% AMPK	(225)
AGAT KO			-97% Cr -99% PCr -47% ATP	-34% FS	↑ oxidative			(226)

The percentages were calculated by the author of this thesis and not by the authors of the articles. They are approximate (based on mean values) and only indicative. Guanidinoacetate N-methyltransferase KO (GAMT KO); L-Arginine: Glycine amidinotransferase KO (AGAT KO); Bodyweight (BW); Body mass index (BMI); Gastrocnemius (GAST); Plantaris (PLA); Extensor digitorum longus (EDL); Creatine (Cr); Phosphocreatine (PCr); Guanidinoacetic acid (GAA); Phospho-guanidinoacetic acid (PGAA); Weight (W); Weight/Bodyweight (W/BW); Fiber size (FS); Myosin heavy chain (MHC); Peroxisome proliferator-activated receptor gamma coactivator 1-alpha (PGC1 $\alpha$ ); AMP-activated protein kinase (AMPK).

## 5 What remains unknown?

Disturbing the CK system affects muscle tissue. However, a decrease in the Cr concentration has more severe consequences than affecting one isoform of CK alone. Double CK KO (M-CK and Mi<sub>s</sub>-CK) exhibits more pronounced muscle consequences than M-CK KO or Mi<sub>s</sub>-CK KO alone, although remaining milder compared to all Cr-deficient models. One plausible explanation is that M-CK and Mi<sub>s</sub>-CK models target the muscle CK system exclusively, whereas Cr-deficiency affects the whole organism, including other organs such as the brain (227). Indeed, several models lacking Cr demonstrate cognitive and motor dysfunction (214, 228, 229), which could induce more systemic effects influencing the muscle phenotype.

Overall, studies of  $\beta$ -GPA-treated mice, CrT KO, GAMT KO, and AGAT KO converge toward a similar direction: reducing Cr availability impairs muscle energetics, induces atrophy, and a fast-to-slow phenotypic shift associated with an overactivation of the AMPK/PGC1 $\alpha$  pathway in fast muscles (**Tables 3 and 4**). As previously introduced, the AMPK activity affects protein synthesis and promotes catabolic pathways, which could lead to muscle atrophy under chronic activation conditions. Furthermore, long-term AMPK activation promotes mitochondrial biogenesis through PGC1 $\alpha$  and potentially induces a shift in MHC composition (**Figure 2**). The chronic activity of AMPK in Cr-deficient models could explain all phenotypic changes observed. However, several pieces of the puzzle are missing from GAMT KO and AGAT KO mice. First, information on the MHC composition is unavailable for both models. Second, the signaling is puzzling in AGAT KO. Studies reported AMPK activation (223, 225), whereas others show higher PGC1 $\alpha$  expression (224), which together could be a responsible signaling for phenotypic adaptations. Third, atrophy and phenotypic adaptation seem to be more pronounced in fast than slow muscle in AGAT KO mice (220), thereby the signaling might also be muscle-dependent. Finally, comprehensive signaling pathway analysis is lacking for GAMT KO mice, which, despite complete creatine deficiency, exhibit milder phenotypic consequences compared to AGAT KO mice (220) or CrT KO. Therefore, **this thesis aims** to determine the muscle phenotype, atrophy, and signaling in fast and slow muscles from Cr-deficient AGAT KO and GAMT KO mice.

As previously established, AMPK activation could serve as the initial trigger for the signaling cascade in Cr-deficient muscle. AMPK activation resulting from disturbance of energetics in Cr-deficient mice is a logical consequence. However, muscle consequences in Cr-deficient mice seem to be different according to the muscle phenotype. AMPK regulation is complex, and as mentioned before, its activation does not always need the presence of AMP or ADP (66–70, 83). This is especially true for the Ca<sup>2+</sup>-related upstream kinase CaMKK $\beta$ . Given that fast and slow muscles diverge in their metabolic stability (230–233), but also in their daily Ca<sup>2+</sup> release (151, 234), we speculated that basal AMPK activity and regulation may differ according to the muscle phenotype. Looking into the literature, we were surprised to see that this question has never been addressed. To better understand the link between AMPK activity and muscle phenotype, **this thesis also aims** to delve deeper into the activation of AMPK between the muscle phenotypes.

Lastly, Ca<sup>2+</sup>-related signals are well known to induce profound changes in muscle phenotype (**Figure 2**). Direct links between energetics and Ca<sup>2+</sup> signaling have been poorly explored in skeletal muscle physiology. Based on new findings (235), and through experiments in collaboration with Dr. Florian Britto (Institut Cochin, Paris, France), **this thesis aims** to test several aspects of a new potential regulatory mechanism for fast-to-slow phenotypic shift by energetics.

## **Aims of the thesis**

- To compare the activation of the AMPK pathway in fast muscles (GAST and EDL) and slow muscles (SOL and Heart) in WT mice.
- To determine the state of atrophy, phenotype, and AMPK signaling of the gastrocnemius (GAST) and soleus (SOL) muscles in GAMT KO.
- To determine the state of atrophy, phenotype, and AMPK signaling of the gastrocnemius (GAST) and soleus (SOL) muscles in AGAT KO mice.
- To test several aspects of a new potential mechanism by which energetic stress triggers higher  $\text{Ca}^{2+}$ /NFAT signaling and induces fast-to-slow phenotypic shift.

## Methods

Detailed information can be found in the methods section of each publication. As a part of this thesis, I used the following methods:

- Western blot, **all Publications**.
- Muscle transversal slices immunostaining, **Publication III, IV, and VI**.
- Cellular fractionation was used to separate cytosolic, mitochondrial and nuclear fraction, **Publication IV**.
- Rat CaMKK $\beta$  (calcium/calmodulin-dependent protein kinase kinase 2) and mutant AMPK $\alpha$ 2 (AMP-activated protein kinase  $\alpha$ 2) K45R recombinant proteins were produced in E.Coli and purified with HisTrap FF affinity chromatography, **Publication II**.
- *In vitro* and homogenate CaMKK $\beta$  phosphorylation of mutant AMPK $\alpha$ 2 K45R, **Publication II**.
- AGAT (L-Arginine: Glycine amidinotransferase) KO mice, **Publication IV, and V**.
- GAMT (Guanidinoacetate N-methyltransferase) KO mice, **Publication III**.
- C2C12 cell culture, **Publication VI**.
- HPLC/MS of ATP, ADP, and AMP from muscle samples, **Publication II**.
- Record and analysis of Ca<sup>2+</sup> transients, **Publication VI**.

## 6 Results and discussion

### 6.1 Development of the IOCBIO gel software to analyse Western blot results

As one of the methodological parts of this thesis, we developed a gel analysis software called IOCBIO gel to analyse our Western blot results (236). During its development, I contributed to testing and providing feedback on the user interface design (**Publication I**). The primary objective of developing IOCBIO gel was to provide in our laboratory a FAIR (Findable, Accessible, Interoperable, and Reusable) method for Western blot analysis. In its current form, IOCBIO gel is an easy-to-use, reliable, and user-friendly software that centralizes data into a database. This software enables rapid correction of each measurement with immediate database updates.

### 6.2 AMPK is more activated in slow muscle than in fast muscle

To determine AMPK activation, we measured the total form of AMPK (T-AMPK) and the phosphorylated form on Thr<sup>172</sup> (p-AMPK), whose ratio p-AMPK/T-AMPK determines the level of AMPK activation. However, the p-AMPK signal alone is physiologically more relevant in the case of lower total AMPK expression. Indeed, in terms of signaling, the most important factor is the absolute amount of phosphorylated AMPK, because it is catalytically active. The ratio is relevant when the total level of AMPK does not vary significantly.

Including different muscles such as gastrocnemius, extensor digitorum longus (EDL), soleus, and Heart, we showed that AMPK was naturally more activated (ratio and phosphorylation) in slow muscles (SOL and Heart) than in fast muscles (GAST and EDL). In **Publication II**, we showed that on average, Heart and SOL AMPK activation (ratio) was ~5X higher than in GAST and EDL (**Publication II**; Figure 3). This first result was surprising. Indeed, previous work showed that SOL and Heart exhibit remarkable metabolic stability during increases in workload, whereas in the GAST, the levels of ADP and Pi increase significantly during exercise (230–233). Hence, why would AMPK (energetic sensor) be more activated in an energetically stable muscle?

To understand the origin of these differences, we measured the expression of the upstream kinases of AMPK. First LKB1, whose phosphorylation of AMPK is dependent on AMP binding (59, 61, 62), and then CaMKK $\beta$ , which phosphorylates AMPK following a rise in Ca<sup>2+</sup> concentration independently of AMP (66–70). Apart from higher LKB1 expression in the Heart compared to the GAST, we observed no consistent phenotypic pattern in LKB1 expression (**Publication II**; Figure 7). As LKB1 expression was shown to correlate with AMPK activation in cultured cells (62), we performed the same statistical analysis and found no correlation across the different muscle tissues (**Publication II**; Supplementary Figure S3). We subsequently attempted to measure ATP, ADP, and AMP in the different muscle types using perchloric acid extraction and High-Performance Liquid Chromatography / Mass Spectrometry (HPLC/MS) analysis. Unfortunately, in our hands, there was a degradation of ATP leading to unphysiologically high concentrations of ADP. Considering that the samples are diluted upon perchloric acid extraction and neutralization, the AMP concentrations would be below the limit of quantification of the available equipment. Therefore, we did not proceed further with these experiments. However, one study calculated the overall concentrations of ADP and AMP from Nuclear Magnetic Resonance (NMR) and HPLC measurements and found no difference between the mouse soleus and

EDL using three different mouse strains (237). Merging these data with the results on the expression of LKB1 suggests that differences in AMPK activation between the muscle phenotypes likely do not arise from global differences in ATP, ADP, and AMP concentrations.

Given that SOL and Heart receive more daily electrical activity and therefore more continuous  $\text{Ca}^{2+}$  release (151), we hypothesized that CaMKK $\beta$  activity, which can phosphorylate AMPK independently of AMP (66–70), might be responsible for higher AMPK activation in slow muscles. However, this hypothesis turned out to be incorrect. First, we found that CaMKK $\beta$  is poorly expressed in skeletal muscle, but more in the Heart and even more in the brain (reference sample) (**Publication II**; Figure 9). Despite its low expression in skeletal muscles, we attempted to measure its basal activity using AMPK $\alpha$ 2 K45R mutant recombinant protein as a downstream target. AMPK $\alpha$ 2 K45R mutant is an ideal downstream target, as it is catalytically inactive and does not retro-inhibit CaMKK $\beta$  autonomous activity (71). We first produced mutant AMPK K45R and CaMKK $\beta$  recombinant proteins in E.Coli and conducted some preliminary tests *in vitro* and in brain homogenates. *In vitro* using recombinant CaMKK $\beta$  and in the brain homogenate with endogenous CaMKK $\beta$ , mutant AMPK K45R was phosphorylated following  $\text{Ca}^{2+}$  stimulation, and abolished when incubated with STO-609, a specific CaMKK $\beta$  inhibitor (**Publication II**; Supplementary Figure S6-S9). However, when performed in muscle homogenates, AMPK was not phosphorylated following  $\text{Ca}^{2+}$  stimulation in GAST, SOL, or Heart (**Publication II**; Figure 11). Therefore, we concluded that CaMKK $\beta$  is not involved in AMPK activation in muscle tissues, which corroborates a recent study (73). However, the mechanism underlying higher AMPK activation in slow muscle remains enigmatic.

We suggest that this AMPK activity is differently compartmentalized between the muscle types and is not related to an overall energetic deficit. Indeed, basal ADP levels are similar between fast and slow muscles, but energetic compartmentalization has already been demonstrated in cardiomyocytes (238–241), as well as AMPK pools (242–245). For example, AK activity, which converts two ADP into ATP + AMP is also known to be compartmentalized (241, 246), and its local activity could influence local activation of AMPK. In line with this concept, AMPK pools are differently activated upon energetic stress. In MEFs and HEK 293 cells, AMPK activity is increased specifically in the lysosome, cytosol, and endoplasmic reticulum but not the nucleus or mitochondria upon glucose starvation (242, 243). However, the mitochondrial pools are specifically activated following a significant increase in AMP concentration in cells and muscle (244). Overall, AMPK appears to be more readily activated in lysosomes and cytosol compared to other compartments (243–245). Nevertheless, acute stimulation is not exactly basal activity. It has been reported several times that AMPK pools are important to induce specific mitophagy and coordinate mitochondrial dynamics (93, 244, 247, 248). On this line, basal AMPK activation in slow muscles, which are very oxidative, could also participate in mitochondrial dynamics independently of global energetics.

In conclusion, we found that AMPK is naturally more activated in slow than in fast muscles. This differential activation could not be explained by a higher expression of LKB1 or activity of CaMKK $\beta$ . We suggest that AMPK activity might be compartmentalized. This result also suggests that higher AMPK activity might not only be a cause but also a consequence of a fast-to-slow phenotypic shift. On this point, few studies have shown that AMPK dephosphorylation occurs upon forced inactivity in slow muscle SOL (249–255). This dephosphorylation of AMPK was associated with a decline in oxidative metabolism and slow fiber type (250, 253), suggesting that chronic AMPK activation could be physiologically required to maintain a slow oxidative phenotype.

### 6.3 GAMT KO mice exhibit subtle changes in phenotype independently of AMPK activity

The main aim of this study was to better understand the muscle consequences of a complete absence of Cr using GAMT KO and AGAT KO mice, which both lack endogenous Cr biosynthesis. However, these models show differences in severity (220). We first investigated the muscle fiber size, MHC composition, and AMPK activity in muscles from GAMT KO mice in **Publication III**.

We started with the measurement of AMPK activation. Although our results in **Publication II** suggest that its regulation might be more complex than we previously thought, its activity remains closely related to energetics and ATP/AMP ratio. In all Cr deficient models, a drop in PCr and ATP availability occurs (**Table 2 and 3**), and should be, at least partly, responsible for AMPK activation.

In GAMT KO mice, we found no differences in AMPK activation in both GAST and SOL muscle compared to WT littermates (**Publication III**; Figure 1). These results were surprising because they would mean that, despite a total lack of Cr, GAMT KO did not experience changes in ATP/AMP ratio, suggesting a compensatory mechanism in energetics. One possible explanation would be the accumulation of phospho-GAA (PGAA) in GAMT KO muscle. PGAA can be used by CK as a Cr analogue and has been shown to partly compensate for the loss of Cr in muscle (222). A significant accumulation of PGAA in the muscle and plasma of GAMT KO mice has been extensively reported (219, 228, 229, 256, 257) (**Table 4**), and some show an equivalent concentration as Cr in WT (222). Although CK utilization of GAA is ~100 times slower than Cr (222), its accumulation might compensate for the lack of Cr, at least at rest. Therefore, ATP level may decline faster than in WT only during muscle activity, which would explain a similar basal level of p-AMPK (**Publication III**; Figure 1).

GAMT KO muscles previously demonstrated subtle metabolic changes toward oxidative metabolism (220). As MHC composition often follows the changes in metabolism, we measured the state of MHC composition in GAST and SOL of GAMT KO mice. Following peer review feedback after submission of **Publication III**, we discovered that using a standard Western blot protocol was not optimal for the quantification of MHC isoforms. The myosin heavy chain migrates very slowly, and most of the extracted myosin remained outside the gel during electrophoresis. Therefore, the MHC composition results obtained from the Western Blot for GAMT KO and AGAT KO mice are preliminary results, being indicative of the relative MHC isoform composition.

Based on our preliminary results, the MHC composition remains unchanged in GAMT KO mice, except for a modest increase in MHC1 expression in GAMT KO gastrocnemius (**Publication II**; Figure 2). This increase in MHC1 expression could corroborate the higher oxidative metabolism in GAMT KO gastrocnemius (220). Furthermore, this subtle phenotypic shift appears to be independent of basal AMPK activity, although the magnitude of the AMPK response in exercising GAMT KO mice remains to be elucidated.

Finally, we investigated the state of muscle atrophy in GAMT KO gastrocnemius, which has been inconsistently reported in the literature (**Table 4**). As previously shown (220), we found that both GAST and SOL weights were reduced in GAMT KO mice, with a more pronounced reduction in GAST than SOL (**Publication III**; Table 1). To characterize this atrophy, we immunostained transversal slices of GAST muscle with an anti-Laminin antibody. By distinguishing individual fibers, we found no differences in the number of fibers between GAMT KO and WT gastrocnemius (**Publication III**; Figure 3). However,

we found a significant reduction in the fiber size, resulting in a reduction of the whole muscle cross-sectional area (**Publication III**; Figure 3). These findings confirm that GAMT KO muscles are atrophied. Given that we did not examine additional targets, the exact mechanisms underlying this atrophy remain unclear. We can already conclude that the muscle did not undergo apoptosis, as indicated by the similar number of fibers (**Publication III**; Figure 3). However, the fiber size could have been reduced by a higher activity of autophagy or UPS, and inhibition of protein synthesis, but all independently of AMPK. Alternatively, Cr deficiency at a younger age may affect muscle growth. Indeed, Cr supplementation in C2C12 cultures was shown to significantly increase the myotube size by stimulation of the protein synthesis pathway (258, 259). Moreover, this effect is accompanied by an increase in fast MHC expression, overexpression of MyoD, and a decrease in MEF2 expression (258, 259). As Cr influences muscle hypertrophy, we could speculate that its absence at a younger age may influence the muscle growth and the MHC composition observed at adulthood.

To summarize, the GAMT KO mice, which are lacking Cr, exhibit muscle atrophy and subtle changes in GAST phenotype. Those muscle consequences appear to be independent of AMPK activation, suggesting an energetic equilibrium in GAMT KO muscles. Energetics of the GAMT KO muscle may be buffered at rest by the use of the PGAA as a Cr analogue. Further studies will be necessary to understand how GAMT KO really compensates for the lack of Cr and prevents AMPK activation.

#### **6.4 AGAT KO mice exhibit a deep remodeling of their muscle phenotype in a muscle-dependent manner, associated with AMPK/PGC1 $\alpha$ axis**

One of the aims of this study was to investigate the signaling and muscle consequences in AGAT KO mice. By suppressing the first step of creatine biosynthesis, AGAT KO mice do not synthesize Cr nor GAA (225), which may exacerbate the muscle consequences compared to GAMT KO. Therefore, we investigated the muscle phenotype of AGAT KO mice in **Publication IV**.

Following the same approach used for GAMT KO mice, we began by measuring AMPK activation in AGAT KO muscles, which exhibit significantly reduced ATP concentrations (226). In agreement with previous studies (223, 225), we found that AMPK was more activated in AGAT KO skeletal muscle (**Publication IV**; Figure 3.D and G). However, we also found that AMPK activation was muscle-dependent, being significantly increased in AGAT KO gastrocnemius but not SOL. In AGAT KO gastrocnemius, AMPK activation was  $\sim 8.5X$  and phosphorylation  $\sim 9X$  higher than in WT. This higher activation was associated with a higher LKB1 expression (**Publication III**; Figure 3.C), which is the main ATP/AMP ratio-dependent upstream kinase of AMPK (59, 61, 62). Considering our results on the basal AMPK activation between the different phenotypes (72) (**Publication II**), we separated the different cell fractions of AGAT KO gastrocnemius to determine in which subcellular location this activation takes place (**Publication IV**; Figure 4). We found that AMPK phosphorylation increased specifically in the cytosol of AGAT KO gastrocnemius (**Publication IV**; Figure 4.D). Cytosol is the fraction where contractile proteins sit, and where AMPK pools are the most sensitive to energetic stress (243–245). Hence, data suggest that AGAT KO gastrocnemius undergoes an energy-related overactivation of AMPK.

Compared to WT littermates, AGAT KO mice exhibit a lower body weight of about  $\sim 50\%$  and lower muscle weights, as shown in Table 3 and Figure 1.A (**Publication IV**). Fast muscle GAST weight was extremely low, about  $-83\%$  compared to WT, and  $-41\%$  for the

slow muscle SOL. This difference is even more pronounced when normalized by BMI (**Publication IV**; Table 3). Using the same immunostaining protocol as applied to GAMT KO mice in **Publication III**, we analysed muscle slices of GAST and SOL from AGAT KO mice. We found that both GAST and SOL fiber size were reduced in AGAT KO mice, but the reduction was much more severe in fast muscle GAST (**Publication IV**; Figure 1). Moreover, GAST atrophy, but not SOL atrophy, can also be explained by a smaller number of fibers, suggesting cell apoptosis. This atrophy was associated with a higher activity of the UPS system, highlighted by a higher total ubiquitinated proteins (**Publication III**; Figure 6.C and F). We also observed an overexpression of Histone Deacetylase 4 (HDAC4), which is well known to promote muscle atrophy (260–264), specifically in AGAT KO gastrocnemius (**Publication III**; Figure 6.A). Enhanced AMPK activity may also contribute to AGAT KO atrophy. In particular, AMPK $\alpha$ 1, which is overexpressed in AGAT KO gastrocnemius (**Publication IV**; Figure 3.H) and has been shown to limit muscle hypertrophy (101–105). However, higher AMPK $\alpha$ 1 expression might simply reflect the phenotypic shift, as oxidative muscle naturally expresses more AMPK $\alpha$ 1 (72) (**Publication II**; Figure 5). Moreover, although experiencing a milder effect, SOL is also atrophied in AGAT KO mice but does not exhibit higher AMPK activity. Therefore, the role of AMPK in AGAT KO gastrocnemius atrophy remains unclear and could be a combination of both AMPK activity and another consequence of Cr deficiency.

Beyond the atrophy, the gastrocnemius muscle phenotype was profoundly altered in AGAT KO mice. Previous work reported a major metabolic shift toward oxidative metabolism in GAST but not in SOL (220). Following the same dynamics, our preliminary data show that AGAT KO gastrocnemius, but not SOL, massively remodeled its MHC composition (**Publication IV**; Figure 2). Fast isoform MHC IIB was poorly expressed, whereas the slower isoforms MHC IIa and I were overexpressed. These results are supported by immunostained sections of AGAT KO gastrocnemius probed with anti-MHCIIa and anti-MHCI antibodies, which revealed that this change is extensive and is visible in terms of fiber composition (**Publication IV**; Figure 2.A). Furthermore, we observed a potential predominance of hybrid fibers, whose staining is fainter but remains visible. Finally, it is worth noting that MHC composition changes may occur in a sex-dependent manner, with AGAT KO females showing a greater MHC shift compared to males. The AMPK/PGC1 $\alpha$  axis is the most potent signaling pathway driving the metabolic and MHC shift in AGAT KO mice (114, 210, 224). Concomitant with AMPK activation, PGC1 $\alpha$  was overexpressed in AGAT KO gastrocnemius (**Publication IV**; Figure 3.E), which, based on the literature, suggests the AMPK/PGC1 $\alpha$  axis as the responsible pathway for the phenotypic adaptation in AGAT KO.

Overall, the data are consistent with a coherent adaptive response. AGAT KO fast muscle GAST, lacking both Cr and GAA, cannot provide enough ATP for its burst activity and the high ATP consumption of its MHCIIIB. Due to its poor yield and metabolic limitations, glycolytic metabolism is chronically overtaken without CK system assistance. ATP/AMP ratios are chronically altered, increasing AMPK activity and PGC1 $\alpha$  expression. The fiber composition shifts toward a slower profile, expressing economical MHC isoforms, more mitochondria, and highly oxidative to increase the yield of ATP production. However, despite the phenotypic shift observed being rather logical in a chronic energy-deprived context, the direct involvement of AMPK in the phenotypic shift of AGAT KO gastrocnemius remains debatable. Furthermore, distinguishing between AMPK activation resulting from the phenotypic change itself, versus that caused by the energy deficit associated with Cr deficiency, remains an unresolved question.

## 6.5 Does AMPK activation in AGAT KO gastrocnemius have an energetic origin?

Although the increase in AMPK activation in AGAT KO gastrocnemius might partly result from a phenotypic consequence (**Publication II**), AGAT KO gastrocnemius exhibits many signs of energetic deficit that should lead to AMPK activation: lower ATP concentration (226), elevated LKB1 expression, an increase of GLUT4 and p-ACC (223, 225), and a specific AMPK cytosolic activity (**Publication IV**; Figure 4). Nevertheless, we have demonstrated that AMPK is naturally more activated in slow oxidative muscles (**Publication II**). When comparing statistically, p-AMPK of AGAT KO gastrocnemius remains 3.6X higher than WT soleus (§§§;  $p < 0.001$ ) (**Publication IV**; Figure 3.D). Considering that WT soleus is inherently a “slower muscle” than the AGAT KO gastrocnemius, AMPK overactivation must, at least partly, have an energetic origin.

In **Publication V**, we showed that AGAT KO Heart, which is an oxidative muscle, also had a higher AMPK activity compared to WT (**Publication V**; Figure 6.D-F), again suggesting causes beyond purely phenotypic effects. However, in contrast with the GAST muscle, higher AMPK activation was not associated with an increase in LKB1 expression in AGAT KO Heart (**Publication V**; Figure 6.C). This result is intriguing, as it suggests that Cr deficiency induces muscle-specific adaptations in AMPK upstream kinases expression. If overexpression of LKB1 participates in AMPK overactivation in AGAT KO gastrocnemius, that could suggest that an alternative upstream kinase participates in AMPK activation in AGAT KO Heart. This could potentially be CaMKK $\beta$ , which is more expressed in the Heart than skeletal muscle, although we were unable to detect its activity in WT (**Publication II**). Alternatively, LKB1 expression may already be sufficient in the Heart to phosphorylate AMPK, whereas it is not the case for GAST. This is also supported by their expression being different in WT mice (**Publication II**; Figure 7). This difference in LKB1 expression also raises questions regarding the potential systemic effects in Cr deficient mice. Indeed, in adipocytes, LKB1 expression was shown to be dependent on Estrogen Receptor  $\alpha$  (ER $\alpha$ ) and sex hormones (265–267). In AGAT KO gastrocnemius specifically, we found a higher expression of ER $\alpha$  (**Publication IV**; Figure 3.A). Hence, it remains unclear whether higher ER $\alpha$  and LKB1 expression are a cause or a necessary consequence of higher AMPK activation in AGAT KO gastrocnemius.

Considering all available evidence, we propose that AMPK overactivation in AGAT KO gastrocnemius may have three origins: a phenotypic origin whose function requires clarification, a potential systemic origin, and an energetic origin that could influence the muscle phenotype.

## 6.6 Is AMPK signaling responsible for the AGAT KO phenotypic shift?

AMPK activation has been widely described to induce mitochondrial biogenesis (109–114), but its involvement in MHC shift is controversial (109, 112, 118, 119). Indeed, studies on various AMPK KO/KD models have reported no changes in the MHC composition (118, 119, 268). However, many studies have demonstrated a direct impact of AMPK activity on PGC1 $\alpha$  expression and mitochondrial content (109–111, 116, 118, 268, 269). Previous work using an AMPK $\alpha$ 2 KD model combined with  $\beta$ -GPA treatment showed that PGC1 $\alpha$  expression and mitochondrial biogenesis induced by CK system disturbance are an AMPK-dependent phenomenon (114). Nevertheless, it should be noted that AGAT KO mice exhibited subtle changes in MHC1 expression (**Publication III**; Figure 2) and increased oxidative metabolism (220), without AMPK activation (**Publication III**; Figure 1). However,

as previously mentioned, AMPK activation upon muscle activity could be greater in GAMT KO mice, which explains those phenotypic changes. Given the substantial evidence in the literature, metabolic adaptation in AGAT KO gastrocnemius should also be AMPK-dependent. However, we still lack definitive evidence regarding MHC composition changes.

In collaboration with Dr. Florian Britto (Institut Cochin, Paris, France), **Publication VI** provides additional insights into the role of AMPK in phenotypic adaptation. Plantaris (PLA) muscle from muscle-specific double AMPK $\alpha$ 1/ $\alpha$ 2 KO mice was subjected to overload training through tenotomy of other hindlimb muscles (SOL and GAST). This overload technique is known to induce a moderate fast-to-slow phenotypic shift by increasing the daily muscle activity. The fiber type shift induced by overload was similar with or without AMPK, whereas the shift in oxidative capacity was abolished (**Publication VI**; Figure 6.A and D). This finding again underscores the importance of AMPK in metabolic adaptations while seriously questioning its role in MHC shift.

Nevertheless, we still observed a higher expression of PGC1 $\alpha$  in the GAST of AGAT KO mice. Normally, PGC1 $\alpha$  is poorly expressed in fast muscle, and its transgenic expression induces a fast-to-slow phenotypic shift (130, 133, 135, 270). PGC1 $\alpha$  regulation is complex. It can be deacetylated, methylated, or phosphorylated by many kinases, which increase its half-life or activity (271). Consequently, the transcriptional activity and gene subset activated by PGC1 $\alpha$  vary according to the upstream signal (271). It has been proposed that AMPK/PGC1 $\alpha$  interaction may only lead to activation of a gene subset related to metabolism, such as GLUT4 and mitochondrial biogenesis, but potentially not the MHC composition (271). PGC1 $\alpha$  nuclear accumulation during exercise or AIRCAR treatment has been suggested as the main mechanism for mitochondrial biogenesis by increasing mtTFA expression (117, 123, 272–275). However, one study highlighted that PGC1 $\alpha$  and mtTFA colocalize in the cytosol and accumulate in subsarcolemmal mitochondrial fractions in an AMPK-dependent manner (276). This direct mechanism could explain the crucial role of AMPK in mitochondrial adaptation without AMPK-activated PGC1 $\alpha$  accumulating in the nucleus and potentially interacting with MEF2. Another possibility is that a threshold concentration of PGC1 $\alpha$  may be required to induce MHC adaptations. Indeed, many studies mentioning a change in MHC composition overexpressed PGC1 $\alpha$  (130, 133, 135), and fast-to-slow phenotypic shift are almost invariably associated with an increase in PGC1 $\alpha$  expression. Therefore, we could suggest a localization or concentration-dependent interaction of PGC1 $\alpha$  with other downstream targets. Along this line, chronic AMPK activation increases PGC1 $\alpha$  expression (123) and may contribute to conditioning the tissue for MHC shift, but is maybe not the key signaling to trigger contractile adaptations.

Therefore, AMPK activation in AGAT KO likely mediates the observed metabolic adaptations. However, it remains unclear whether AMPK overactivation is involved in the MHC shift of AGAT KO gastrocnemius. Consequently, AGAT KO gastrocnemius potentially undergoes an alternative signaling pathway able to shift its MHC composition.

## **6.7 Energetics induces higher Ca<sup>2+</sup> release: a potential signaling for MHC shift in AGAT KO gastrocnemius**

As mentioned in the literature review, Ca<sup>2+</sup>-related signaling is a strong determinant of muscle phenotype, particularly through the Ca<sup>2+</sup>/CaM/CaN/NFATc1/MEF2 pathway (**Figure 2**). Interestingly, we found that NFATc1 expression in the AGAT KO gastrocnemius cytosol was 3X higher than in WT littermates (**Publication IV**; Figure 5.A and B). Following

Ca<sup>2+</sup> signaling, dephosphorylated NFATc1 is known to translocate into the nucleus to interact with MEF2. However, we did not find NFATc1 nuclear accumulation (**Publication III**; Figure 5.C). NFATc1 exhibits a circadian cycle (activity-dependent), predominantly cytosolic during the day (resting period) and predominantly nuclear during the night (active period) in mice (174). Since mice were taken during the day, this timing may have contributed to our results. Nevertheless, NFATc1 overexpression was accompanied by an increase in CaMKK $\beta$  expression in the AGAT KO gastrocnemius specifically (**Publication IV**; Supplementary Figure S1). Both are Ca<sup>2+</sup> related proteins and downstream of CaM (**Figure 2**), suggesting a potential chronic excess of Ca<sup>2+</sup> in AGAT KO gastrocnemius. These results raised many questions regarding why and how AGAT KO gastrocnemius might experience an excess in Ca<sup>2+</sup>, and whether this excess could be responsible for the phenotypic shift.

As highlighted in the literature review, Ca<sup>2+</sup> dynamics, particularly SERCA function, represent a substantial component of total ATP hydrolysis in muscle (6, 7). Based on this observation, we wondered whether Cr-deficiency would affect SERCA performance and lead to Ca<sup>2+</sup> accumulation in the cytoplasm. In **Publication V**, Ca<sup>2+</sup> transients from isolated AGAT KO cardiomyocytes were analyzed. AGAT KO cardiomyocytes exhibited similar SERCA performances to WT, as indicated by comparable Ca<sup>2+</sup> concentration decay rates (**Publication V**; Figure 1.F). However, the peak amplitude, rise rate, and duration were increased in AGAT KO cardiomyocytes (**Publication V**; Figure 1.A-E), which means that Ca<sup>2+</sup> release by RyRs was higher in quantity, faster, and lasted longer at high concentration in the cytoplasm. The SR content in Ca<sup>2+</sup> was also slightly increased in AGAT KO cardiomyocytes (**Publication V**; Figure 4.B). Collectively, these results indicate that Cr-deficiency enhanced Ca<sup>2+</sup> release by RyR, but did not affect SERCA performances in cardiomyocytes. In other words, affecting energetics increases the Ca<sup>2+</sup> release by RyR in cardiac tissue. Nevertheless, the Heart remains different than a gastrocnemius, both in the metabolic aspect and the excitation-contraction coupling. Therefore, we wanted to test whether the same phenomenon could be observed in fast glycolytic muscle tissue.

To further investigate this mechanism in a fast glycolytic muscle tissue, we cultured C2C12 muscle myotubes on glass coverslips in collaboration with Dr. Florian Britto (Institut Cochin, Paris, France). C2C12 myotubes were electrically stimulated with or without 2-Deoxy-D-glucose (2DG), a glycolysis inhibitor, and Ca<sup>2+</sup> transients were recorded. Interestingly, the same phenomenon was observed in C2C12 myotubes treated with 2DG, where RyR Ca<sup>2+</sup> release was higher under energetically compromised conditions (**Publication VI**; Figure 5.F). Consistent with our findings in AGAT KO cardiomyocytes, SERCA performance was maintained in 2DG-treated C2C12 myotubes (**Publication VI**; Figure 5.H). The mechanism underlying increased RyR Ca<sup>2+</sup> release remains enigmatic, particularly given that RyR opening probability is higher with ATP binding compared to AMP or ADP (277). Therefore, RyR opening may be modulated either through protein kinase phosphorylation or via an alternative, yet unknown mechanism. To summarize, similarly to AGAT KO cardiomyocytes, affecting energetics did not decrease SERCA performance but increase Ca<sup>2+</sup> release by RyR in glycolytic muscle tissue.

Our collaborators extended this investigation by treating mice subjected to overload with 2DG. They found a disparate increase in NFATc2 expression (**Publication VI**; Figure 5.E). But more importantly, 2DG treatment enhanced the fast-to-slow phenotypic shift induced by overload (**Publication VI**; Figure 5.C). These findings suggest that energetics participate in the MHC shift, but independently of AMPK (**Publication VI**; Figure 6.D),

although they did not test the effect of 2DG treatment on muscle AMPK KO mice in overload. Nevertheless, an increase in NFAT expression suggests that  $\text{Ca}^{2+}$  dynamics may be altered by energetics, and we provided evidence that it increases the RyR  $\text{Ca}^{2+}$  release. However, further studies are required to understand the mechanism and its exact contribution to fast-to-slow phenotypic shift.

Thus, affecting energetics seems to induce an increase in RyR  $\text{Ca}^{2+}$  release. The mechanism by which RyR opening is modulated by energetics remains unknown. Whether this higher  $\text{Ca}^{2+}$  release can influence the  $\text{Ca}^{2+}$ /CaM/CaN/NFATc1/MEF2 pathway and muscle phenotype needs further investigation. The involvement of such a mechanism in the phenotypic shift of AGAT KO gastrocnemius is speculative. Nevertheless, **Figure 4** provides a comprehensive overview of the potential mechanisms underlying the fast-to-slow phenotypic shift in AGAT KO gastrocnemius.

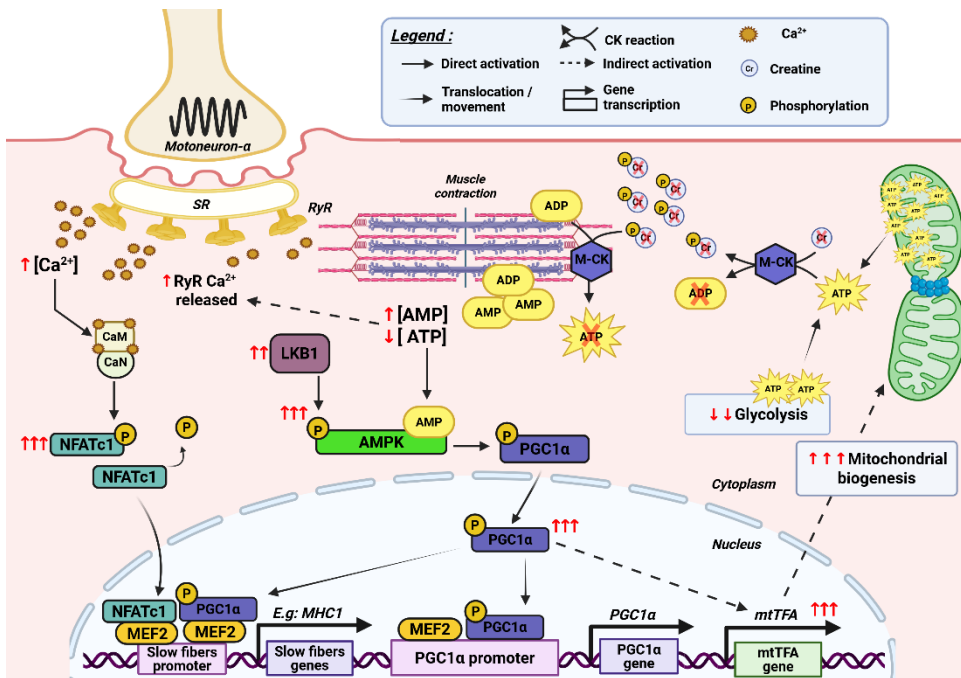


**Figure 4.** Theoretical proposal of the signaling pathways involved in the fast-to-slow phenotypic shift of AGAT KO gastrocnemius. Red arrows and crosses indicate the known effects of AGAT KO Cr-deficiency presented in this thesis. AGAT KO induced a total loss of creatine (Cr) in skeletal muscle, which disturbs the creatine kinase (CK) system. Fast muscle gastrocnemius, mainly composed of fast fibers IIB and IIX overconsume ATP, and cannot be buffered by CKs in AGAT KO mice. AMP and ADP levels rise in the cytoplasm and chronically activate AMP-activated protein kinase (AMPK). AMPK higher phosphorylation is ensured by increased Liver Kinase B1 (LKB1) expression. AMPK activity promotes activation and overexpression of Peroxisome proliferator-activated receptor gamma coactivator 1-alpha (PGC1α). PGC1α overexpression promotes mitochondrial biogenesis, increasing oxidative capacities and expression of slow fiber genes. Upon muscular activity, the average cytoplasmic  $\text{Ca}^{2+}$  concentration increases through energy-induced higher  $\text{Ca}^{2+}$  release by ryanodine receptors (RyRs). Calmodulin (CaM) / Calcineurin (CaN) complex is activated. Nuclear Factor of Activated T-cells cytoplasmic 1 (NFATc1) is dephosphorylated and translocates to the nucleus. NFATc1 interacts with Myocyte enhancer factor-2 (MEF2) to promote slow fiber genes expression. Created in <https://BioRender.com>.

## Conclusion

- Basal AMPK activity is higher in slow than fast muscles, and this is not due to higher CaMKK $\beta$  activity.
- GAMT KO creatine-deficient mice exhibited subtle changes in GAST muscle mass and phenotype independently of AMPK activity. The use of GAA at rest could prevent phenotypic adaptations.
- AGAT KO creatine-deficient mice, lacking Cr and GAA, showed a severe atrophy and fast-to-slow phenotypic shift in fast muscle GAST. Those changes are associated with a GAST-specific activation of LKB1/p-AMPK/PGC1 $\alpha$  pathway. However, the direct influence of AMPK activity to change MHC composition remains questionable.
- Affecting energetics increases RyR Ca<sup>2+</sup> release in AGAT KO cardiomyocytes and C2C12 myotubes. Through NFAT signaling, this could constitute an alternative mechanism linking energetics, Ca<sup>2+</sup> signaling, and fast-to-slow phenotypic shift.

## References

1. **Fujisawa K.** Regulation of Adenine Nucleotide Metabolism by Adenylate Kinase Isozymes: Physiological Roles and Diseases. *International Journal of Molecular Sciences* 24: 5561, 2023. doi: 10.3390/ijms24065561.
2. **Kawai M, Candau R.** Muscle Contraction and Supplying ATP to Muscle Cells. In: *Exercise Physiology: from a Cellular to an Integrative Approach*. IOS Press, p. 3–25.
3. **Stehle R, Solzin J, Iorga B, Poggesi C.** Insights into the kinetics of Ca<sup>2+</sup>-regulated contraction and relaxation from myofibril studies. *Pflugers Arch - Eur J Physiol* 458: 337–357, 2009. doi: 10.1007/s00424-008-0630-2.
4. **He Z-H, Bottinelli R, Pellegrino MA, Ferenczi MA, Reggiani C.** ATP Consumption and Efficiency of Human Single Muscle Fibers with Different Myosin Isoform Composition. *Biophysical Journal* 79: 945–961, 2000. doi: 10.1016/S0006-3495(00)76349-1.
5. **Han Y-S, Geiger PC, Cody MJ, Macken RL, Sieck GC.** ATP consumption rate per cross bridge depends on myosin heavy chain isoform. *Journal of Applied Physiology* 94: 2188–2196, 2003. doi: 10.1152/jappphysiol.00618.2002.
6. **Smith IC, Bombardier E, Vigna C, Tupling AR.** ATP Consumption by Sarcoplasmic Reticulum Ca<sup>2+</sup> Pumps Accounts for 40–50% of Resting Metabolic Rate in Mouse Fast and Slow Twitch Skeletal Muscle. *PLOS ONE* 8: e68924, 2013. doi: 10.1371/journal.pone.0068924.
7. **Barclay CJ, Woledge RC, Curtin NA.** Energy turnover for Ca<sup>2+</sup> cycling in skeletal muscle. *J Muscle Res Cell Motil* 28: 259–274, 2007. doi: 10.1007/s10974-007-9116-7.
8. **Clausen T.** Quantification of Na<sup>+</sup>,K<sup>+</sup> pumps and their transport rate in skeletal muscle: Functional significance. *Journal of General Physiology* 142: 327–345, 2013. doi: 10.1085/jgp.201310980.
9. **Mrnjavac N, Martin WF.** GTP before ATP: The energy currency at the origin of genes. *Biochimica et Biophysica Acta (BBA) - Bioenergetics* 1866: 149514, 2025. doi: 10.1016/j.bbabi.2024.149514.
10. **Stouthamer AH.** A theoretical study on the amount of ATP required for synthesis of microbial cell material. *Antonie van Leeuwenhoek* 39: 545–565, 1973. doi: 10.1007/BF02578899.
11. **Poortmans JR, Carpentier A, Pereira-Lancha LO, Lancha A.** Protein turnover, amino acid requirements and recommendations for athletes and active populations. *Braz J Med Biol Res* 45: 875–890, 2012. doi: 10.1590/S0100-879X2012007500096.
12. **Cunha TF, Moreira JBN, Paixão NA, Campos JC, Monteiro AWA, Bacurau AVN, Bueno CR, Ferreira JCB, Brum PC.** Aerobic exercise training upregulates skeletal muscle calpain and ubiquitin-proteasome systems in healthy mice. *Journal of Applied Physiology* 112: 1839–1846, 2012. doi: 10.1152/jappphysiol.00346.2011.
13. **Stefanetti RJ, Lamon S, Wallace M, Vendelbo MH, Russell AP, Vissing K.** Regulation of ubiquitin proteasome pathway molecular markers in response to endurance and resistance exercise and training. *Pflugers Arch - Eur J Physiol* 467: 1523–1537, 2015. doi: 10.1007/s00424-014-1587-y.

14. **Finley D.** Recognition and Processing of Ubiquitin-Protein Conjugates by the Proteasome. *Annu Rev Biochem* 78: 477–513, 2009. doi: 10.1146/annurev.biochem.78.081507.101607.
15. **Lecker SH, Goldberg AL, Mitch WE.** Protein Degradation by the Ubiquitin-Proteasome Pathway in Normal and Disease States. *Journal of the American Society of Nephrology* 17: 1807, 2006. doi: 10.1681/ASN.2006010083.
16. **Beckwith R, Estrin E, Worden EJ, Martin A.** Reconstitution of the 26S proteasome reveals functional asymmetries in its AAA+ unfoldase. *Nat Struct Mol Biol* 20: 1164–1172, 2013. doi: 10.1038/nsmb.2659.
17. **Goldberg AL.** Protein degradation and protection against misfolded or damaged proteins. *Nature* 426: 895–899, 2003. doi: 10.1038/nature02263.
18. **Sundberg CW, Fitts RH.** Bioenergetic basis of skeletal muscle fatigue. *Curr Opin Physiol* 10: 118–127, 2019. doi: 10.1016/j.cophys.2019.05.004.
19. **Taylor DJ, Styles P, Matthews PM, Arnold DA, Gadian DG, Bore P, Radda GK.** Energetics of human muscle: Exercise-induced ATP depletion. *Magnetic Resonance in Med* 3: 44–54, 1986. doi: 10.1002/mrm.1910030107.
20. **Chandel NS.** Glycolysis. *Cold Spring Harb Perspect Biol* 13: a040535, 2021. doi: 10.1101/cshperspect.a040535.
21. **Cori CF.** The Glucose–Lactic Acid Cycle and Gluconeogenesis. In: *Current Topics in Cellular Regulation*, edited by Estabrook RW, Srere P. Academic Press, p. 377–387.
22. **Zhu X, Chen W, Pinho RA, Thirupathi A.** Lactate-induced metabolic signaling is the potential mechanism for reshaping the brain function - role of physical exercise. *Front Endocrinol* 16, 2025. doi: 10.3389/fendo.2025.1598419.
23. **Sutton JR, Jones NL, Toews CJ.** Effect of pH on Muscle Glycolysis during Exercise. *Clinical Science* 61: 331–338, 1981. doi: 10.1042/cs0610331.
24. **Westerblad H, Bruton JD, Lännergren J.** The effect of intracellular pH on contractile function of intact, single fibres of mouse muscle declines with increasing temperature. *The Journal of Physiology* 500: 193–204, 1997. doi: 10.1113/jphysiol.1997.sp022009.
25. **Westerblad H, Bruton JD, Katz A.** Skeletal muscle: Energy metabolism, fiber types, fatigue and adaptability. *Experimental Cell Research* 316: 3093–3099, 2010. doi: 10.1016/j.yexcr.2010.05.019.
26. **Slater EC.** Mechanism of Oxidative Phosphorylation. *Annual Review of Biochemistry* 46: 1015–1026, 1977. doi: 10.1146/annurev.bi.46.070177.005055.
27. **Kukurugya MA, Rosset S, Titov DV.** The Warburg Effect is the result of faster ATP production by glycolysis than respiration. *Proceedings of the National Academy of Sciences* 121: e2409509121, 2024. doi: 10.1073/pnas.2409509121.
28. **Watt MJ, Cheng Y.** Triglyceride metabolism in exercising muscle. *Biochimica et Biophysica Acta (BBA) - Molecular and Cell Biology of Lipids* 1862: 1250–1259, 2017. doi: 10.1016/j.bbalip.2017.06.015.
29. **Hargreaves M, Spriet LL.** *Exercise Metabolism*. Human Kinetics, 2006.

30. **Schiaffino S, Reggiani C.** Fiber Types in Mammalian Skeletal Muscles. *Physiological Reviews* 91: 1447–1531, 2011. doi: 10.1152/physrev.00031.2010.
31. **Blaauw B, Schiaffino S, Reggiani C.** Mechanisms Modulating Skeletal Muscle Phenotype. In: *Comprehensive Physiology*, edited by Terjung R. Wiley, p. 1645–1687.
32. **Scott W, Stevens J, Binder–Macleod SA.** Human Skeletal Muscle Fiber Type Classifications. *Physical Therapy* 81: 1810–1816, 2001. doi: 10.1093/ptj/81.11.1810.
33. **Han Y-S, Geiger PC, Cody MJ, Macken RL, Sieck GC.** ATP consumption rate per cross bridge depends on myosin heavy chain isoform. *Journal of Applied Physiology* 94: 2188–2196, 2003. doi: 10.1152/jappphysiol.00618.2002.
34. **Egan B, Zierath JR.** Exercise Metabolism and the Molecular Regulation of Skeletal Muscle Adaptation. *Cell Metabolism* 17: 162–184, 2013. doi: 10.1016/j.cmet.2012.12.012.
35. **Spamer C, Pette D.** Activity patterns of phosphofructokinase, glyceraldehydephosphate dehydrogenase, lactate dehydrogenase and malate dehydrogenase in microdissected fast and slow fibres from rabbit psoas and soleus muscle. *Histochemistry* 52: 201–206, 1977. doi: 10.1007/BF00495857.
36. **Goodman CA, Kotecki JA, Jacobs BL, Hornberger TA.** Muscle Fiber Type-Dependent Differences in the Regulation of Protein Synthesis. *PLOS ONE* 7: e37890, 2012. doi: 10.1371/journal.pone.0037890.
37. **He Z-H, Bottinelli R, Pellegrino MA, Ferenczi MA, Reggiani C.** ATP Consumption and Efficiency of Human Single Muscle Fibers with Different Myosin Isoform Composition. *Biophysical Journal* 79: 945–961, 2000. doi: 10.1016/S0006-3495(00)76349-1.
38. **Henneman E, Somjen G, Carpenter DO.** Functional significance of cell size in spinal motoneurons. *Journal of Neurophysiology* 28: 560–580, 1965. doi: 10.1152/jn.1965.28.3.560.
39. **Pette D, Staron RS.** Myosin isoforms, muscle fiber types, and transitions. *Microscopy Research and Technique* 50: 500–509, 2000. doi: 10.1002/1097-0029(20000915)50:6<500::AID-JEMT7>3.0.CO;2-7.
40. **Westerblad H, Bruton JD, Katz A.** Skeletal muscle: Energy metabolism, fiber types, fatigue and adaptability. *Experimental Cell Research* 316: 3093–3099, 2010. doi: 10.1016/j.yexcr.2010.05.019.
41. **Sawano S, Komiya Y, Ichitsubo R, Ohkawa Y, Nakamura M, Tatsumi R, Ikeuchi Y, Mizunoya W.** A One-Step Immunostaining Method to Visualize Rodent Muscle Fiber Type within a Single Specimen. *PLOS ONE* 11, 2016. doi: 10.1371/journal.pone.0166080.
42. **Campos VACRPGER.** SKELETAL MUSCLE FIBER TYPES IN C57BL6J MICE. *SKELETAL MUSCLE FIBER TYPES IN C57BL6J MICE* 21: 0–0, 2017.
43. **Medler S.** Mixing it up: the biological significance of hybrid skeletal muscle fibers. *Journal of Experimental Biology* 222: jeb200832, 2019. doi: 10.1242/jeb.200832.
44. **Termin A, Staron RS, Pette D.** Changes in myosin heavy chain isoforms during chronic low-frequency stimulation of rat fast hindlimb muscles. *European Journal of Biochemistry* 186: 749–754, 1989. doi: 10.1111/j.1432-1033.1989.tb15269.x.

45. **Ausoni S, Gorza L, Schiaffino S, Gundersen K, Lomo T.** Expression of myosin heavy chain isoforms in stimulated fast and slow rat muscles. *J Neurosci* 10: 153–160, 1990. doi: 10.1523/JNEUROSCI.10-01-00153.1990.
46. **Flück M, Hoppeler H.** Molecular basis of skeletal muscle plasticity-from gene to form and function. In: *Reviews of Physiology, Biochemistry and Pharmacology*. Springer, p. 159–216.
47. **Hoh JF.** Selective and non-selective reinnervation of fast-twitch and slow-twitch rat skeletal muscle. *The Journal of Physiology* 251: 791–801, 1975. doi: 10.1113/jphysiol.1975.sp011122.
48. **Hämäläinen N, Pette D.** Slow-to-fast transitions in myosin expression of rat soleus muscle by phasic high-frequency stimulation. *FEBS Letters* 399: 220–222, 1996. doi: 10.1016/S0014-5793(96)01325-7.
49. **Chang KC.** Key signalling factors and pathways in the molecular determination of skeletal muscle phenotype. *animal* 1: 681–698, 2007. doi: 10.1017/S1751731107702070.
50. **Neurohr JM, Paulson ET, Kinsey ST.** A higher mitochondrial content is associated with greater oxidative damage, oxidative defenses, protein synthesis and ATP turnover in resting skeletal muscle. *Journal of Experimental Biology* 224: jeb242462, 2021. doi: 10.1242/jeb.242462.
51. **Pereyra AS, Lin C-T, Sanchez DM, Laskin J, Spangenburg EE, Neuffer PD, Fisher–Wellman K, Ellis JM.** Skeletal muscle undergoes fiber type metabolic switch without myosin heavy chain switch in response to defective fatty acid oxidation. *Molecular Metabolism* 59: 101456, 2022. doi: 10.1016/j.molmet.2022.101456.
52. **Horowitz JF, Sidossis LS, Coyle EF.** High Efficiency of Type I Muscle Fibers Improves Performance. *Int J Sports Med* 15: 152–157, 1994. doi: 10.1055/s-2007-1021038.
53. **Towler Mhairi C., Hardie D. Grahame.** AMP-Activated Protein Kinase in Metabolic Control and Insulin Signaling. *Circulation Research* 100: 328–341, 2007. doi: 10.1161/01.RES.0000256090.42690.05.
54. **Ross FA, MacKintosh C, Hardie DG.** AMP-activated protein kinase: a cellular energy sensor that comes in 12 flavours. *The FEBS Journal* 283: 2987–3001, 2016. doi: 10.1111/febs.13698.
55. **Kjøbsted R, Hingst JR, Fentz J, Foretz M, Sanz M-N, Pehmøller C, Shum M, Marette A, Mounier R, Treebak JT, Wojtaszewski JFP, Viollet B, Lantier L.** AMPK in skeletal muscle function and metabolism. *FASEB J* 32: 1741–1777, 2018. doi: 10.1096/fj.201700442R.
56. **Gowans GJ, Hawley SA, Ross FA, Hardie DG.** AMP Is a True Physiological Regulator of AMP-Activated Protein Kinase by Both Allosteric Activation and Enhancing Net Phosphorylation. *Cell Metabolism* 18: 556–566, 2013. doi: 10.1016/j.cmet.2013.08.019.

57. **Hardie DG, Carling D, Gamblin SJ.** AMP-activated protein kinase: also regulated by ADP? *Trends in Biochemical Sciences* 36: 470–477, 2011. doi: 10.1016/j.tibs.2011.06.004.
58. **Pelosse M, Cottet-Rousselle C, Bidan CM, Dupont A, Gupta K, Berger I, Schlattner U.** Synthetic energy sensor AMPfret deciphers adenylate-dependent AMPK activation mechanism. *Nat Commun* 10: 1038, 2019. doi: 10.1038/s41467-019-08938-z.
59. **Suter M, Riek U, Tuerk R, Schlattner U, Wallimann T, Neumann D.** Dissecting the Role of 5'-AMP for Allosteric Stimulation, Activation, and Deactivation of AMP-activated Protein Kinase \*. *Journal of Biological Chemistry* 281: 32207–32216, 2006. doi: 10.1074/jbc.M606357200.
60. **Xiao B, Sanders MJ, Underwood E, Heath R, Mayer FV, Carmena D, Jing C, Walker PA, Eccleston JF, Haire LF, Saiu P, Howell SA, Aasland R, Martin SR, Carling D, Gamblin SJ.** Structure of mammalian AMPK and its regulation by ADP. *Nature* 472: 230–233, 2011. doi: 10.1038/nature09932.
61. **Sakamoto K, McCarthy A, Smith D, Green KA, Grahame Hardie D, Ashworth A, Alessi DR.** Deficiency of LKB1 in skeletal muscle prevents AMPK activation and glucose uptake during contraction. *EMBO J* 24: 1810–1820, 2005. doi: 10.1038/sj.emboj.7600667.
62. **Woods A, Johnstone SR, Dickerson K, Leiper FC, Fryer LGD, Neumann D, Schlattner U, Wallimann T, Carlson M, Carling D.** LKB1 Is the Upstream Kinase in the AMP-Activated Protein Kinase Cascade. *Current Biology* 13: 2004–2008, 2003. doi: 10.1016/j.cub.2003.10.031.
63. **Tanner CB, Madsen SR, Hallowell DM, Goring DMJ, Moore TM, Hardman SE, Heninger MR, Atwood DR, Thomson DM.** Mitochondrial and performance adaptations to exercise training in mice lacking skeletal muscle LKB1. *American Journal of Physiology-Endocrinology and Metabolism* 305: E1018–E1029, 2013. doi: 10.1152/ajpendo.00227.2013.
64. **McGee SL, Mustard KJ, Hardie DG, Baar K.** Normal hypertrophy accompanied by phosphorylation and activation of AMP-activated protein kinase  $\alpha$ 1 following overload in LKB1 knockout mice. *The Journal of Physiology* 586: 1731–1741, 2008. doi: 10.1113/jphysiol.2007.143685.
65. **Sakamoto K, Zarrinpashneh E, Budas GR, Pouleur A-C, Dutta A, Prescott AR, Vanoverschelde J-L, Ashworth A, Jovanović A, Alessi DR, Bertrand L.** Deficiency of LKB1 in heart prevents ischemia-mediated activation of AMPK $\alpha$ 2 but not AMPK $\alpha$ 1. *American Journal of Physiology-Endocrinology and Metabolism* 290: E780–E788, 2006. doi: 10.1152/ajpendo.00443.2005.
66. **Fujiwara Y, Kawaguchi Y, Fujimoto T, Kanayama N, Magari M, Tokumitsu H.** Differential AMP-activated Protein Kinase (AMPK) Recognition Mechanism of Ca<sup>2+</sup>/Calmodulin-dependent Protein Kinase Kinase Isoforms\*. *Journal of Biological Chemistry* 291: 13802–13808, 2016. doi: 10.1074/jbc.M116.727867.

67. **Jensen TE, Rose AJ, Hellsten Y, Wojtaszewski JFP, Richter EA.** Caffeine-induced Ca<sup>2+</sup> release increases AMPK-dependent glucose uptake in rodent soleus muscle. *American Journal of Physiology-Endocrinology and Metabolism* 293: E286–E292, 2007. doi: 10.1152/ajpendo.00693.2006.
68. **Jensen TE, Rose AJ, Jørgensen SB, Brandt N, Schjerling P, Wojtaszewski JFP, Richter EA.** Possible CaMKK-dependent regulation of AMPK phosphorylation and glucose uptake at the onset of mild tetanic skeletal muscle contraction. *American Journal of Physiology-Endocrinology and Metabolism* 292: E1308–E1317, 2007. doi: 10.1152/ajpendo.00456.2006.
69. **Woods A, Dickerson K, Heath R, Hong S-P, Momcilovic M, Johnstone SR, Carlson M, Carling D.** Ca<sup>2+</sup>/calmodulin-dependent protein kinase kinase- $\beta$  acts upstream of AMP-activated protein kinase in mammalian cells. *Cell Metabolism* 2: 21–33, 2005. doi: 10.1016/j.cmet.2005.06.005.
70. **Hawley SA, Pan DA, Mustard KJ, Ross L, Bain J, Edelman AM, Frenguelli BG, Hardie DG.** Calmodulin-dependent protein kinase kinase- $\beta$  is an alternative upstream kinase for AMP-activated protein kinase. *Cell Metabolism* 2: 9–19, 2005. doi: 10.1016/j.cmet.2005.05.009.
71. **Nakanishi A, Hatano N, Fujiwara Y, Sha'ri A, Takabatake S, Akano H, Kanayama N, Magari M, Nozaki N, Tokumitsu H.** AMP-activated protein kinase-mediated feedback phosphorylation controls the Ca<sup>2+</sup>/calmodulin (CaM) dependence of Ca<sup>2+</sup>/CaM-dependent protein kinase kinase  $\beta$ . *Journal of Biological Chemistry* 292: 19804–19813, 2017. doi: 10.1074/jbc.M117.805085.
72. **Bernasconi R, Soodla K, Sirp A, Zovo K, Kuhtinskaja M, Lukk T, Vendelin M, Birkedal R.** Higher AMPK activation in mouse oxidative compared with glycolytic muscle does not correlate with LKB1 or CaMKK $\beta$  expression. *American Journal of Physiology-Endocrinology and Metabolism* 328: E21–E33, 2025. doi: 10.1152/ajpendo.00261.2024.
73. **Negoita F, Addinsall AB, Hellberg K, Bringas CF, Hafen PS, Sermersheim TJ, Agerholm M, Lewis CTA, Ahwazi D, Ling NXY, Larsen JK, Deshmukh AS, Hossain MA, Oakhill JS, Ochala J, Brault JJ, Sankar U, Drewry DH, Scott JW, Witczak CA, Sakamoto K.** CaMKK2 is not involved in contraction-stimulated AMPK activation and glucose uptake in skeletal muscle. *Molecular Metabolism* 75: 101761, 2023. doi: 10.1016/j.molmet.2023.101761.
74. **Abbott MJ, Edelman AM, Turcotte LP.** CaMKK is an upstream signal of AMP-activated protein kinase in regulation of substrate metabolism in contracting skeletal muscle. *American Journal of Physiology-Regulatory, Integrative and Comparative Physiology* 297: R1724–R1732, 2009. doi: 10.1152/ajpregu.00179.2009.
75. **Smiles WJ, Ovens AJ, Oakhill JS, Kofler B.** The metabolic sensor AMPK: Twelve enzymes in one. *Molecular Metabolism* 90: 102042, 2024. doi: 10.1016/j.molmet.2024.102042.
76. **Habets DDJ, Coumans WA, Voshol PJ, den Boer MAM, Febbraio M, Bonen A, Glatz JFC, Luiken JJFP.** AMPK-mediated increase in myocardial long-chain fatty acid uptake critically depends on sarcolemmal CD36. *Biochem Biophys Res Commun* 355: 204–210, 2007. doi: 10.1016/j.bbrc.2007.01.141.

77. **Holmes BF, Kurth-Kraczek EJ, Winder WW.** Chronic activation of 5'-AMP-activated protein kinase increases GLUT-4, hexokinase, and glycogen in muscle. *Journal of Applied Physiology* 87: 1990–1995, 1999. doi: 10.1152/jappl.1999.87.5.1990.
78. **Kurth-Kraczek EJ, Hirshman MF, Goodyear LJ, Winder WW.** 5' AMP-activated protein kinase activation causes GLUT4 translocation in skeletal muscle. *Diabetes* 48: 1667–1671, 1999. doi: 10.2337/diabetes.48.8.1667.
79. **Dzamko N, Schertzer JD, Ryall JG, Steel R, Macaulay SL, Wee S, Chen Z-P, Michell BJ, Oakhill JS, Watt MJ, Jørgensen SB, Lynch GS, Kemp BE, Steinberg GR.** AMPK-independent pathways regulate skeletal muscle fatty acid oxidation. *The Journal of Physiology* 586: 5819–5831, 2008. doi: 10.1113/jphysiol.2008.159814.
80. **Park SH, Gammon SR, Knippers JD, Paulsen SR, Rubink DS, Winder WW.** Phosphorylation-activity relationships of AMPK and acetyl-CoA carboxylase in muscle. *Journal of Applied Physiology* 92: 2475–2482, 2002. doi: 10.1152/japplphysiol.00071.2002.
81. **Jørgensen SB, Nielsen JN, Birk JB, Olsen GS, Viollet B, Andreelli F, Schjerling P, Vaulont S, Hardie DG, Hansen BF, Richter EA, Wojtaszewski JFP.** The  $\alpha$ 2-5'AMP-Activated Protein Kinase Is a Site 2 Glycogen Synthase Kinase in Skeletal Muscle and Is Responsive to Glucose Loading. *Diabetes* 53: 3074–3081, 2004. doi: 10.2337/diabetes.53.12.3074.
82. **Halse R, Fryer LGD, McCormack JG, Carling D, Yeaman SJ.** Regulation of Glycogen Synthase by Glucose and Glycogen: A Possible Role for AMP-Activated Protein Kinase. *Diabetes* 52: 9–15, 2003. doi: 10.2337/diabetes.52.1.9.
83. **Zhang C-S, Hawley SA, Zong Y, Li M, Wang Z, Gray A, Ma T, Cui J, Feng J-W, Zhu M, Wu Y-Q, Li TY, Ye Z, Lin S-Y, Yin H, Piao H-L, Hardie DG, Lin S-C.** Fructose-1,6-bisphosphate and aldolase mediate glucose sensing by AMPK. *Nature* 548: 112–116, 2017. doi: 10.1038/nature23275.
84. **McBride A, Ghilagaber S, Nikolaev A, Hardie DG.** The Glycogen-Binding Domain on the AMPK  $\beta$  Subunit Allows the Kinase to Act as a Glycogen Sensor. *Cell Metabolism* 9: 23–34, 2009. doi: 10.1016/j.cmet.2008.11.008.
85. **Bolster DR, Crozier SJ, Kimball SR, Jefferson LS.** AMP-activated Protein Kinase Suppresses Protein Synthesis in Rat Skeletal Muscle through Down-regulated Mammalian Target of Rapamycin (mTOR) Signaling\*. *Journal of Biological Chemistry* 277: 23977–23980, 2002. doi: 10.1074/jbc.C200171200.
86. **Gwinn DM, Shackelford DB, Egan DF, Mihaylova MM, Mery A, Vasquez DS, Turk BE, Shaw RJ.** AMPK Phosphorylation of Raptor Mediates a Metabolic Checkpoint. *Molecular Cell* 30: 214–226, 2008. doi: 10.1016/j.molcel.2008.03.003.
87. **Inoki K, Zhu T, Guan K-L.** TSC2 Mediates Cellular Energy Response to Control Cell Growth and Survival. *Cell* 115: 577–590, 2003. doi: 10.1016/S0092-8674(03)00929-2.
88. **Saha AK, Xu XJ, Lawson E, Deoliveira R, Brandon AE, Kraegen EW, Ruderman NB.** Downregulation of AMPK Accompanies Leucine- and Glucose-Induced Increases in Protein Synthesis and Insulin Resistance in Rat Skeletal Muscle. *Diabetes* 59: 2426–2434, 2010. doi: 10.2337/db09-1870.

89. **Thomson DM, Fick CA, Gordon SE.** AMPK activation attenuates S6K1, 4E-BP1, and eEF2 signaling responses to high-frequency electrically stimulated skeletal muscle contractions. *Journal of Applied Physiology* 104: 625–632, 2008. doi: 10.1152/jappphysiol.00915.2007.
90. **Egan DF, Shackelford DB, Mihaylova MM, Gelino S, Kohnz RA, Mair W, Vasquez DS, Joshi A, Gwinn DM, Taylor R, Asara JM, Fitzpatrick J, Dillin A, Violette B, Kundu M, Hansen M, Shaw RJ.** Phosphorylation of ULK1 (hATG1) by AMP-Activated Protein Kinase Connects Energy Sensing to Mitophagy. *Science* 331: 456–461, 2011. doi: 10.1126/science.1196371.
91. **Gao J, Yu L, Wang Z, Wang R, Liu X.** Induction of mitophagy in C2C12 cells by electrical pulse stimulation involves increasing the level of the mitochondrial receptor FUNDC1 through the AMPK-ULK1 pathway. *Am J Transl Res* 12: 6879–6894, 2020.
92. **Greer EL, Oskoui PR, Banko MR, Maniar JM, Gygi MP, Gygi SP, Brunet A.** The Energy Sensor AMP-activated Protein Kinase Directly Regulates the Mammalian FOXO3 Transcription Factor \*. *Journal of Biological Chemistry* 282: 30107–30119, 2007. doi: 10.1074/jbc.M705325200.
93. **Laker RC, Drake JC, Wilson RJ, Lira VA, Lewellen BM, Ryall KA, Fisher CC, Zhang M, Saucerman JJ, Goodyear LJ, Kundu M, Yan Z.** Ampk phosphorylation of Ulk1 is required for targeting of mitochondria to lysosomes in exercise-induced mitophagy. *Nat Commun* 8: 548, 2017. doi: 10.1038/s41467-017-00520-9.
94. **Lee JW, Park S, Takahashi Y, Wang H-G.** The Association of AMPK with ULK1 Regulates Autophagy. *PLOS ONE* 5: e15394, 2010. doi: 10.1371/journal.pone.0015394.
95. **Longo M, Bishnu A, Risiglione P, Montava-Garriga L, Cuenco J, Sakamoto K, MacKintosh C, Ganley IG.** Opposing roles for AMPK in regulating distinct mitophagy pathways. *Molecular Cell* 84: 4350-4367.e9, 2024. doi: 10.1016/j.molcel.2024.10.025.
96. **NAKASHIMA K, YAKABE Y.** AMPK Activation Stimulates Myofibrillar Protein Degradation and Expression of Atrophy-Related Ubiquitin Ligases by Increasing FOXO Transcription Factors in C2C12 Myotubes. *Bioscience, Biotechnology, and Biochemistry* 71: 1650–1656, 2007. doi: 10.1271/bbb.70057.
97. **Sanchez AM, Csibi A, Raibon A, Cornille K, Gay S, Bernardi H, Candau R.** AMPK promotes skeletal muscle autophagy through activation of forkhead FoxO3a and interaction with Ulk1. *Journal of Cellular Biochemistry* 113: 695–710, 2012. doi: 10.1002/jcb.23399.
98. **He C.** Balancing nutrient and energy demand and supply via autophagy. *Current Biology* 32: R684–R696, 2022. doi: 10.1016/j.cub.2022.04.071.
99. **Koutsifeli P, Varma U, Daniels LJ, Annandale M, Li X, Neale JPH, Hayes S, Weeks KL, James S, Delbridge LMD, Mellor KM.** Glycogen-autophagy: Molecular machinery and cellular mechanisms of glycophagy. *Journal of Biological Chemistry* 298, 2022. doi: 10.1016/j.jbc.2022.102093.

100. **Ducommun S, Deak M, Zeigerer A, Göransson O, Seitz S, Collodet C, Madsen AB, Jensen TE, Viollet B, Foretz M, Gut P, Sumpton D, Sakamoto K.** Chemical genetic screen identifies Gapex-5/GAPVD1 and STBD1 as novel AMPK substrates. *Cellular Signalling* 57: 45–57, 2019. doi: 10.1016/j.cellsig.2019.02.001.
101. **Deng Z, Luo P, Lai W, Song T, Peng J, Wei H-K.** Myostatin inhibits eEF2K-eEF2 by regulating AMPK to suppress protein synthesis. *Biochemical and Biophysical Research Communications* 494: 278–284, 2017. doi: 10.1016/j.bbrc.2017.10.040.
102. **Lantier L, Mounier R, Leclerc J, Pende M, Foretz M, Viollet B.** Coordinated maintenance of muscle cell size control by AMP-activated protein kinase. *FASEB j* 24: 3555–3561, 2010. doi: 10.1096/fj.10-155994.
103. **Mounier R, Lantier L, Leclerc J, Sotiropoulos A, Pende M, Daegelen D, Sakamoto K, Foretz M, Viollet B.** Important role for AMPK $\alpha$ 1 in limiting skeletal muscle cell hypertrophy. *FASEB j* 23: 2264–2273, 2009. doi: 10.1096/fj.08-119057.
104. **Mounier R, Lantier L, Leclerc J, Sotiropoulos A, Foretz M, Viollet B.** Antagonistic control of muscle cell size by AMPK and mTORC1. *Cell Cycle* 10: 2640–2646, 2011. doi: 10.4161/cc.10.16.17102.
105. **Mu J, Barton ER, Birnbaum MJ.** Selective suppression of AMP-activated protein kinase in skeletal muscle: update on 'lazy mice.' *Biochemical Society Transactions* 31: 236–241, 2003. doi: 10.1042/bst0310236.
106. **Egawa T, Ohno Y, Goto A, Ikuta A, Suzuki M, Ohira T, Yokoyama S, Sugiura T, Ohira Y, Yoshioka T, Goto K.** AICAR-induced activation of AMPK negatively regulates myotube hypertrophy through the HSP72-mediated pathway in C2C12 skeletal muscle cells. *American Journal of Physiology-Endocrinology and Metabolism* 306: E344–E354, 2014. doi: 10.1152/ajpendo.00495.2013.
107. **Kang MJ, Moon JW, Lee JO, Kim JH, Jung EJ, Kim SJ, Oh JY, Wu SW, Lee PR, Park SH, Kim HS.** Metformin induces muscle atrophy by transcriptional regulation of myostatin via HDAC6 and FoxO3a. *Journal of Cachexia, Sarcopenia and Muscle* 13: 605–620, 2022. doi: 10.1002/jcsm.12833.
108. **Thomson DM.** The Role of AMPK in the Regulation of Skeletal Muscle Size, Hypertrophy, and Regeneration. *International Journal of Molecular Sciences* 19: 3125, 2018. doi: 10.3390/ijms19103125.
109. **Garcia-Roves PM, Osler ME, Holmström MH, Zierath JR.** Gain-of-function R225Q Mutation in AMP-activated Protein Kinase  $\gamma$ 3 Subunit Increases Mitochondrial Biogenesis in Glycolytic Skeletal Muscle \*. *Journal of Biological Chemistry* 283: 35724–35734, 2008. doi: 10.1074/jbc.M805078200.
110. **Jørgensen SB, Wojtaszewski JFP, Viollet B, Andreelli F, Birk JB, Hellsten Y, Schjerling P, Vaulont S, Neufer PD, Richter EA, Pilegaard H.** Effects of  $\alpha$ -AMPK knockout on exercise-induced gene activation in mouse skeletal muscle. *The FASEB Journal* 19: 1146–1148, 2005. doi: 10.1096/fj.04-3144fje.

111. **Lantier L, Fentz J, Mounier R, Leclerc J, Treebak JT, Pehmøller C, Sanz N, Sakakibara I, Saint-Amand E, Rimbaud S, Maire P, Marette A, Ventura-Clapier R, Ferry A, Wojtaszewski JFP, Foretz M, Viollet B.** AMPK controls exercise endurance, mitochondrial oxidative capacity, and skeletal muscle integrity. *The FASEB Journal* 28: 3211–3224, 2014. doi: 10.1096/fj.14-250449.
112. **O’Neill HM, Maarbjerg SJ, Crane JD, Jeppesen J, Jørgensen SB, Schertzer JD, Shyroka O, Kiens B, van Denderen BJ, Tarnopolsky MA, Kemp BE, Richter EA, Steinberg GR.** AMP-activated protein kinase (AMPK)  $\beta$ 1 $\beta$ 2 muscle null mice reveal an essential role for AMPK in maintaining mitochondrial content and glucose uptake during exercise. *Proceedings of the National Academy of Sciences* 108: 16092–16097, 2011. doi: 10.1073/pnas.1105062108.
113. **Winder WW, Holmes BF, Rubink DS, Jensen EB, Chen M, Holloszy JO.** Activation of AMP-activated protein kinase increases mitochondrial enzymes in skeletal muscle. *Journal of Applied Physiology* 88: 2219–2226, 2000. doi: 10.1152/jappl.2000.88.6.2219.
114. **Zong H, Ren JM, Young LH, Pypaert M, Mu J, Birnbaum MJ, Shulman GI.** AMP kinase is required for mitochondrial biogenesis in skeletal muscle in response to chronic energy deprivation. *Proceedings of the National Academy of Sciences* 99: 15983–15987, 2002. doi: 10.1073/pnas.252625599.
115. **Hou Y, Su L, Zhao Y, Liu C, Yao D, Zhang M, Zhao L, Jin Y.** Effect of chronic AICAR treatment on muscle fiber composition and enzyme activity in skeletal muscle of rats. *Journal of Applied Animal Research* 49: 89–96, 2021. doi: 10.1080/09712119.2021.1889563.
116. **Röckl KSC, Hirshman MF, Brandauer J, Fujii N, Witters LA, Goodyear LJ.** Skeletal Muscle Adaptation to Exercise Training : AMP-Activated Protein Kinase Mediates Muscle Fiber Type Shift. *Diabetes* 56: 2062–2069, 2007. doi: 10.2337/db07-0255.
117. **Suwa M, Nakano H, Kumagai S.** Effects of chronic AICAR treatment on fiber composition, enzyme activity, UCP3, and PGC-1 in rat muscles. *Journal of Applied Physiology* 95: 960–968, 2003. doi: 10.1152/jappphysiol.00349.2003.
118. **Miura S, Kai Y, Tadaishi M, Tokutake Y, Sakamoto K, Bruce CR, Febbraio MA, Kita K, Chohnan S, Ezaki O.** Marked phenotypic differences of endurance performance and exercise-induced oxygen consumption between AMPK and LKB1 deficiency in mouse skeletal muscle: changes occurring in the diaphragm. *American Journal of Physiology-Endocrinology and Metabolism* 305: E213–E229, 2013. doi: 10.1152/ajpendo.00114.2013.
119. **Rhein P, Desjardins EM, Rong P, Ahwazi D, Bonhoure N, Stolte J, Santos MD, Ovens AJ, Ehrlich AM, Sanchez Garcia JL, Ouyang Q, Yabut JM, Kjolby M, Membrez M, Jessen N, Oakhill JS, Treebak JT, Maire P, Scott JW, Sanders MJ, Descombes P, Chen S, Steinberg GR, Sakamoto K.** Compound- and fiber type-selective requirement of AMPK $\gamma$ 3 for insulin-independent glucose uptake in skeletal muscle. *Molecular Metabolism* 51: 101228, 2021. doi: 10.1016/j.molmet.2021.101228.

120. **Yang X, Xue P, Liu Z, Li W, Li C, Chen Z.** SESN2 prevents the slow-to-fast myofiber shift in denervated atrophy via AMPK/PGC-1 $\alpha$  pathway. *Cellular & Molecular Biology Letters* 27: 66, 2022. doi: 10.1186/s11658-022-00367-z.
121. **Chen X, Guo Y, Jia G, Liu G, Zhao H, Huang Z.** Arginine promotes skeletal muscle fiber type transformation from fast-twitch to slow-twitch via Sirt1/AMPK pathway. *The Journal of Nutritional Biochemistry* 61: 155–162, 2018. doi: 10.1016/j.jnutbio.2018.08.007.
122. **Xu M, Chen X, Huang Z, Chen D, Chen H, Luo Y, Zheng P, He J, Yu J, Yu B.** Procyanidin B2 Promotes Skeletal Slow-Twitch Myofiber Gene Expression through the AMPK Signaling Pathway in C2C12 Myotubes. *J Agric Food Chem* 68: 1306–1314, 2020. doi: 10.1021/acs.jafc.9b07489.
123. **Jager S, Handschin C, St.-Pierre J, Spiegelman BM.** AMP-activated protein kinase (AMPK) action in skeletal muscle via direct phosphorylation of PGC-1. *Proceedings of the National Academy of Sciences* 104: 12017–12022, 2007. doi: 10.1073/pnas.0705070104.
124. **Cantó C, Gerhart-Hines Z, Feige JN, Lagouge M, Noriega L, Milne JC, Elliott PJ, Puigserver P, Auwerx J.** AMPK regulates energy expenditure by modulating NAD<sup>+</sup> metabolism and SIRT1 activity. *Nature* 458: 1056–1060, 2009. doi: 10.1038/nature07813.
125. **Gerhart-Hines Z, Rodgers JT, Bare O, Lerin C, Kim S, Mostoslavsky R, Alt FW, Wu Z, Puigserver P.** Metabolic control of muscle mitochondrial function and fatty acid oxidation through SIRT1/PGC-1 $\alpha$ . *The EMBO Journal* 26: 1913–1923, 2007. doi: 10.1038/sj.emboj.7601633.
126. **Gurd BJ.** Deacetylation of PGC-1 $\alpha$  by SIRT1: importance for skeletal muscle function and exercise-induced mitochondrial biogenesis. *Appl Physiol Nutr Metab* 36: 589–597, 2011. doi: 10.1139/h11-070.
127. **Hock MB, Kralli A.** Transcriptional Control of Mitochondrial Biogenesis and Function. *Annu Rev Physiol* 71: 177–203, 2009. doi: 10.1146/annurev.physiol.010908.163119.
128. **Virbasius JV, Scarpulla RC.** Activation of the human mitochondrial transcription factor A gene by nuclear respiratory factors: a potential regulatory link between nuclear and mitochondrial gene expression in organelle biogenesis. *Proceedings of the National Academy of Sciences* 91: 1309–1313, 1994. doi: 10.1073/pnas.91.4.1309.
129. **Wu Z, Puigserver P, Andersson U, Zhang C, Adelmant G, Mootha V, Troy A, Cinti S, Lowell B, Scarpulla RC, Spiegelman BM.** Mechanisms Controlling Mitochondrial Biogenesis and Respiration through the Thermogenic Coactivator PGC-1. *Cell* 98: 115–124, 1999. doi: 10.1016/S0092-8674(00)80611-X.
130. **Lin J, Wu H, Tarr PT, Zhang C-Y, Wu Z, Boss O, Michael LF, Puigserver P, Isotani E, Olson EN, Lowell BB, Bassel-Duby R, Spiegelman BM.** Transcriptional co-activator PGC-1 $\alpha$  drives the formation of slow-twitch muscle fibres. *Nature* 418: 797–801, 2002. doi: 10.1038/nature00904.

131. **Mortensen OH, Frandsen L, Schjerling P, Nishimura E, Grunnet N.** PGC-1 $\alpha$  and PGC-1 $\beta$  have both similar and distinct effects on myofiber switching toward an oxidative phenotype. *American Journal of Physiology-Endocrinology and Metabolism* 291: E807–E816, 2006. doi: 10.1152/ajpendo.00591.2005.
132. **Schuler M, Ali F, Chambon C, Duteil D, Bornert J-M, Tardivel A, Desvergne B, Wahli W, Chambon P, Metzger D.** PGC1 $\alpha$  expression is controlled in skeletal muscles by PPAR $\beta$ , whose ablation results in fiber-type switching, obesity, and type 2 diabetes. *Cell Metabolism* 4: 407–414, 2006. doi: 10.1016/j.cmet.2006.10.003.
133. **Ying F, Zhang L, Bu G, Xiong Y, Zuo B.** Muscle fiber-type conversion in the transgenic pigs with overexpression of PGC1 $\alpha$  gene in muscle. *Biochemical and Biophysical Research Communications* 480: 669–674, 2016. doi: 10.1016/j.bbrc.2016.10.113.
134. **Zechner C, Lai L, Zechner JF, Geng T, Yan Z, Rumsey JW, Collia D, Chen Z, Wozniak DF, Leone TC, Kelly DP.** Total Skeletal Muscle PGC-1 Deficiency Uncouples Mitochondrial Derangements from Fiber Type Determination and Insulin Sensitivity. *Cell Metabolism* 12: 633–642, 2010. doi: 10.1016/j.cmet.2010.11.008.
135. **Zhang L, Zhou Y, Wu W, Hou L, Chen H, Zuo B, Xiong Y, Yang J.** Skeletal Muscle-Specific Overexpression of PGC-1 $\alpha$  Induces Fiber-Type Conversion through Enhanced Mitochondrial Respiration and Fatty Acid Oxidation in Mice and Pigs. *Int J Biol Sci* 13: 1152–1162, 2017. doi: 10.7150/ijbs.20132.
136. **McGee SL, Hargreaves M.** AMPK-mediated regulation of transcription in skeletal muscle. *Clinical Science* 118: 507–518, 2010. doi: 10.1042/CS20090533.
137. **Cohen TJ, Choi M-C, Kapur M, Lira VA, Yan Z, Yao T-P.** HDAC4 Regulates Muscle Fiber Type-Specific Gene Expression Programs. *Mol Cells* 38: 343–348, 2015. doi: 10.14348/molcells.2015.2278.
138. **Lin J, Wu H, Tarr PT, Zhang C-Y, Wu Z, Boss O, Michael LF, Puigserver P, Isotani E, Olson EN, Lowell BB, Bassel-Duby R, Spiegelman BM.** Transcriptional co-activator PGC-1 $\alpha$  drives the formation of slow-twitch muscle fibres. *Nature* 418: 797–801, 2002. doi: 10.1038/nature00904.
139. **Wu H, Rothermel B, Kanatous S.** Activation of MEF2 by muscle activity is mediated through a calcineurin-dependent pathway. *The EMBO Journal* 20: 6414–6423, 2001. doi: 10.1093/emboj/20.22.6414.
140. **Wu H, J.Naya F, A.McKinsey T.** MEF2 responds to multiple calcium-regulated signals in the control of skeletal muscle fiber type. *The EMBO Journal* 19: 1963–1973, 2000. doi: 10.1093/emboj/19.9.1963.
141. **Potthoff MJ, Wu H, Arnold MA, Shelton JM, Backs J, McAnally J, Richardson JA, Bassel-Duby R, Olson EN.** Histone deacetylase degradation and MEF2 activation promote the formation of slow-twitch myofibers. *J Clin Invest* 117: 2459–2467, 2007. doi: 10.1172/JCI31960.
142. **Hughes SM, Koishi K, Rudnicki M, Maggs AM.** MyoD protein is differentially accumulated in fast and slow skeletal muscle fibres and required for normal fibre type balance in rodents. *Mechanisms of Development* 61: 151–163, 1997. doi: 10.1016/S0925-4773(96)00631-4.

143. **Hennebry A, Berry C, Siriatt V, O'Callaghan P, Chau L, Watson T, Sharma M, Kambadur R.** Myostatin regulates fiber-type composition of skeletal muscle by regulating MEF2 and MyoD gene expression. *American Journal of Physiology-Cell Physiology* 296: C525–C534, 2009. doi: 10.1152/ajpcell.00259.2007.
144. **Macharia R, Otto A, Valasek P, Patel K.** Neuromuscular junction morphology, fiber-type proportions, and satellite-cell proliferation rates are altered in MyoD<sup>-/-</sup> mice. *Muscle & Nerve* 42: 38–52, 2010. doi: 10.1002/mus.21637.
145. **Potthoff MJ, Wu H, Arnold MA, Shelton JM, Backs J, McAnally J, Richardson JA, Bassel-Duby R, Olson EN.** Histone deacetylase degradation and MEF2 activation promote the formation of slow-twitch myofibers. *J Clin Invest* 117: 2459–2467, 2007. doi: 10.1172/JCI31960.
146. **Ekmark M, Rana ZA, Stewart G, Hardie DG, Gundersen K.** De-phosphorylation of MyoD is linking nerve-evoked activity to fast myosin heavy chain expression in rodent adult skeletal muscle. *The Journal of Physiology* 584: 637–650, 2007. doi: 10.1113/jphysiol.2007.141457.
147. **Taylor MV, Hughes SM.** Mef2 and the skeletal muscle differentiation program. *Seminars in Cell & Developmental Biology* 72: 33–44, 2017. doi: 10.1016/j.semcd.2017.11.020.
148. **Tsuji R, Hayashi T, Takahashi S, Asakura A, Fujita R.** The multifaceted role of MyoD in adult skeletal muscle: homeostasis, regeneration, and diseases. *American Journal of Physiology-Cell Physiology* 329: C200–C212, 2025. doi: 10.1152/ajpcell.00334.2025.
149. **Handschin C, Rhee J, Lin J, Tarr PT, Spiegelman BM.** An autoregulatory loop controls peroxisome proliferator-activated receptor  $\gamma$  coactivator 1 $\alpha$  expression in muscle. *Proceedings of the National Academy of Sciences* 100: 7111–7116, 2003. doi: 10.1073/pnas.1232352100.
150. **Moore ML, Park EA, McMillin JB.** Upstream Stimulatory Factor Represses the Induction of Carnitine Palmitoyltransferase-1 $\beta$  Expression by PGC-1\*. *Journal of Biological Chemistry* 278: 17263–17268, 2003. doi: 10.1074/jbc.M210486200.
151. **Hodgson JA, Roy RR, Higuchi N, Monti RJ, Zhong H, Grossman E, Edgerton VR.** Does daily activity level determine muscle phenotype? *Journal of Experimental Biology* 208: 3761–3770, 2005. doi: 10.1242/jeb.01825.
152. **Marcelo KL, Means AR, York B.** The Ca<sup>2+</sup>/Calmodulin/CaMKK2 Axis: Nature's Metabolic CaMshaft. *Trends in Endocrinology & Metabolism* 27: 706–718, 2016. doi: 10.1016/j.tem.2016.06.001.
153. **Soderling TR, Stull JT.** Structure and Regulation of Calcium/Calmodulin-Dependent Protein Kinases. *Chem Rev* 101: 2341–2352, 2001. doi: 10.1021/cr0002386.
154. **Anderson KA, Means RL, Huang Q-H, Kemp BE, Goldstein EG, Selbert MA, Edelman AM, Fremeau RT, Means AR.** Components of a Calmodulin-dependent Protein Kinase Cascade: MOLECULAR CLONING, FUNCTIONAL CHARACTERIZATION AND CELLULAR LOCALIZATION OF Ca<sup>2+</sup>/CALMODULIN-DEPENDENT PROTEIN KINASE  $\beta$  \*. *Journal of Biological Chemistry* 273: 31880–31889, 1998. doi: 10.1074/jbc.273.48.31880.

155. **Tokumitsu H, Enslen H, Soderling TR.** Characterization of a Ca<sup>2+</sup>/Calmodulin-dependent Protein Kinase Cascade: MOLECULAR CLONING AND EXPRESSION OF CALCIUM/CALMODULIN-DEPENDENT PROTEIN KINASE KINASE (\*). *Journal of Biological Chemistry* 270: 19320–19324, 1995. doi: 10.1074/jbc.270.33.19320.
156. **Tokumitsu H, Hatano N, Inuzuka H, Yokokura S, Nozaki N, Kobayashi R.** Mechanism of the Generation of Autonomous Activity of Ca<sup>2+</sup>/Calmodulin-dependent Protein Kinase IV\*. *Journal of Biological Chemistry* 279: 40296–40302, 2004. doi: 10.1074/jbc.M406534200.
157. **Bito H, Deisseroth K, Tsien RW.** CREB Phosphorylation and Dephosphorylation: A Ca<sup>2+</sup>- and Stimulus Duration–Dependent Switch for Hippocampal Gene Expression. *Cell* 87: 1203–1214, 1996. doi: 10.1016/S0092-8674(00)81816-4.
158. **Sun P, Enslen H, Myung PS, Maurer RA.** Differential activation of CREB by Ca<sup>2+</sup>/calmodulin-dependent protein kinases type II and type IV involves phosphorylation of a site that negatively regulates activity. *Genes Dev* 8: 2527–2539, 1994. doi: 10.1101/gad.8.21.2527.
159. **Sun P, Lou L, Maurer RA.** Regulation of Activating Transcription Factor-1 and the cAMP Response Element-binding Protein by Ca<sup>2+</sup>/Calmodulin-dependent Protein Kinases Type I, II, and IV (\*). *Journal of Biological Chemistry* 271: 3066–3073, 1996. doi: 10.1074/jbc.271.6.3066.
160. **Wu H, Kanatous SB, Thurmond FA, Gallardo T, Isotani E, Bassel-Duby R, Williams RS.** Regulation of Mitochondrial Biogenesis in Skeletal Muscle by CaMK. *Science* 296: 349–352, 2002. doi: 10.1126/science.1071163.
161. **Guerfali I, Manissolle C, Durieux A-C, Bonnefoy R, Bartegi A, Freyssenet D.** Calcineurin A and CaMKIV transactivate PGC-1 $\alpha$  promoter, but differentially regulate cytochrome c promoter in rat skeletal muscle. *Pflugers Arch - Eur J Physiol* 454: 297–305, 2007. doi: 10.1007/s00424-007-0206-6.
162. **Akimoto T, Ribar TJ, Williams RS, Yan Z.** Skeletal muscle adaptation in response to voluntary running in Ca<sup>2+</sup>/calmodulin-dependent protein kinase IV-deficient mice. *American Journal of Physiology-Cell Physiology* 287: C1311–C1319, 2004. doi: 10.1152/ajpcell.00248.2004.
163. **Creamer TP.** Calcineurin. *Cell Communication and Signaling* 18: 137, 2020. doi: 10.1186/s12964-020-00636-4.
164. **Rao A, Luo C, Hogan PG.** TRANSCRIPTION FACTORS OF THE NFAT FAMILY: Regulation and Function. *Annual Review of Immunology* 15: 707–747, 1997. doi: 10.1146/annurev.immunol.15.1.707.
165. **Delling U, Tureckova J, Lim HW, De Windt LJ, Rotwein P, Molkentin JD.** A Calcineurin-NFATc3-Dependent Pathway Regulates Skeletal Muscle Differentiation and Slow Myosin Heavy-Chain Expression. *Molecular and Cellular Biology* 20: 6600–6611, 2000. doi: 10.1128/MCB.20.17.6600-6611.2000.
166. **Kubis H-P, Hanke N, Scheibe RJ, Meissner JD, Gros G.** Ca<sup>2+</sup> transients activate calcineurin/NFATc1 and initiate fast-to-slow transformation in a primary skeletal muscle culture. *American Journal of Physiology-Cell Physiology* 285: C56–C63, 2003. doi: 10.1152/ajpcell.00377.2002.

167. **Martins KJB, St-Louis M, Murdoch GK, MacLean IM, McDonald P, Dixon WT, Putman CT, Michel RN.** Nitric oxide synthase inhibition prevents activity-induced calcineurin–NFATc1 signalling and fast-to-slow skeletal muscle fibre type conversions. *The Journal of Physiology* 590: 1427–1442, 2012. doi: 10.1113/jphysiol.2011.223370.
168. **Tothova J, Blaauw B, Pallafacchina G, Rudolf R, Argentini C, Reggiani C, Schiaffino S.** NFATc1 nucleocytoplasmic shuttling is controlled by nerve activity in skeletal muscle. *Journal of Cell Science* 119: 1604–1611, 2006. doi: 10.1242/jcs.02875.
169. **Swoap SJ, Hunter RB, Stevenson EJ, Felton HM, Kansagra NV, Lang JM, Esser KA, Kandarian SC.** The calcineurin-NFAT pathway and muscle fiber-type gene expression. *American Journal of Physiology-Cell Physiology* 279: C915–C924, 2000. doi: 10.1152/ajpcell.2000.279.4.C915.
170. **Ehlers ML, Celona B, Black BL.** NFATc1 Controls Skeletal Muscle Fiber Type and Is a Negative Regulator of MyoD Activity. *Cell Reports* 8: 1639–1648, 2014. doi: 10.1016/j.celrep.2014.08.035.
171. **Calabria E, Ciciliot S, Moretti I, Garcia M, Picard A, Dyar KA, Pallafacchina G, Tothova J, Schiaffino S, Murgia M.** NFAT isoforms control activity-dependent muscle fiber type specification. *Proceedings of the National Academy of Sciences* 106: 13335–13340, 2009. doi: 10.1073/pnas.0812911106.
172. **McCullagh KJA, Calabria E, Pallafacchina G, Ciciliot S, Serrano AL, Argentini C, Kalhovde JM, Lømo T, Schiaffino S.** NFAT is a nerve activity sensor in skeletal muscle and controls activity-dependent myosin switching. *PNAS* 101: 10590–10595, 2004. doi: 10.1073/pnas.0308035101.
173. **Shin J, Nunomiya A, Gonda K, Nagatomi R.** Specification of skeletal muscle fiber-type is determined by the calcineurin/NFATc1 signaling pathway during muscle regeneration. *Biochemical and Biophysical Research Communications* 659: 20–28, 2023. doi: 10.1016/j.bbrc.2023.03.032.
174. **Dyar KA, Ciciliot S, Tagliazucchi GM, Pallafacchina G, Tothova J, Argentini C, Agatea L, Abraham R, Ahdesmäki M, Forcato M, Biciato S, Schiaffino S, Blaauw B.** The calcineurin-NFAT pathway controls activity-dependent circadian gene expression in slow skeletal muscle. *Molecular Metabolism* 4: 823–833, 2015. doi: 10.1016/j.molmet.2015.09.004.
175. **Kim J-M, Kim HK, Cho HJ, Moon S-A, Kim Y, Hong JY, Lee SH, Kim K, Koh J-M.** Extracellular C1qbp inhibits myogenesis by suppressing NFATc1. *Sci Rep* 14: 15678, 2024. doi: 10.1038/s41598-024-66549-1.
176. **Akimoto T, Pohnert SC, Li P, Zhang M, Gumbs C, Rosenberg PB, Williams RS, Yan Z.** Exercise Stimulates *Pgc-1 $\alpha$*  Transcription in Skeletal Muscle through Activation of the p38 MAPK Pathway\*. *Journal of Biological Chemistry* 280: 19587–19593, 2005. doi: 10.1074/jbc.M408862200.
177. **Song P, Zhao J, Li F, Zhao X, Feng J, Su Y, Wang B, Zhao J.** Vitamin A regulates mitochondrial biogenesis and function through p38 MAPK-PGC-1 $\alpha$  signaling pathway and alters the muscle fiber composition of sheep. *J Animal Sci Biotechnol* 15: 18, 2024. doi: 10.1186/s40104-023-00968-4.

178. **Cunningham JT, Rodgers JT, Arlow DH, Vazquez F, Mootha VK, Puigserver P.** mTOR controls mitochondrial oxidative function through a YY1–PGC-1 $\alpha$  transcriptional complex. *Nature* 450: 736–740, 2007. doi: 10.1038/nature06322.
179. **Ji K, Zheng J, Lv J, Xu J, Ji X, Luo Y-B, Li W, Zhao Y, Yan C.** Skeletal muscle increases FGF21 expression in mitochondrial disorders to compensate for energy metabolic insufficiency by activating the mTOR–YY1–PGC1 $\alpha$  pathway. *Free Radical Biology and Medicine* 84: 161–170, 2015. doi: 10.1016/j.freeradbiomed.2015.03.020.
180. **Piquereau J, Veksler V, Novotova M, Ventura-Clapier R.** Energetic Interactions Between Subcellular Organelles in Striated Muscles. *Frontiers in Cell and Developmental Biology* 8: 1077, 2020. doi: 10.3389/fcell.2020.581045.
181. **Wallimann T, Wyss M, Brdiczka D, Nicolay K, Eppenberger HM.** Intracellular compartmentation, structure and function of creatine kinase isoenzymes in tissues with high and fluctuating energy demands: the “phosphocreatine circuit” for cellular energy homeostasis. *Biochem J* 281: 21–40, 1992.
182. **Wallimann T, Tokarska-Schlattner M, Schlattner U.** The creatine kinase system and pleiotropic effects of creatine. *Amino Acids* 40: 1271–1296, 2011. doi: 10.1007/s00726-011-0877-3.
183. **Birkedal R, Laasmaa M, Branovets J, Vendelin M.** Ontogeny of cardiomyocytes: ultrastructure optimization to meet the demand for tight communication in excitation–contraction coupling and energy transfer. *Philosophical Transactions of the Royal Society B: Biological Sciences* 377: 20210321, 2022. doi: 10.1098/rstb.2021.0321.
184. **Yamashita K, Yoshioka T.** Profiles of creatine kinase isoenzyme compositions in single muscle fibres of different types. *J Muscle Res Cell Motil* 12: 37–44, 1991. doi: 10.1007/BF01781172.
185. **Apple FS, Billadello JJ.** Expression of creative kinase M and B mRNAs in treadmill trained rat skeletal muscle. *Life Sciences* 55: 585–592, 1994. doi: 10.1016/0024-3205(94)00484-6.
186. **Bonilla DA, Kreider RB, Stout JR, Forero DA, Kerksick CM, Roberts MD, Rawson ES.** Metabolic Basis of Creatine in Health and Disease: A Bioinformatics-Assisted Review. *Nutrients* 13: 1238, 2021. doi: 10.3390/nu13041238.
187. **Baker SA, Gajera CR, Wawro AM, Corces MR, Montine TJ.** GATM and GAMT synthesize creatine locally throughout the mammalian body and within oligodendrocytes of the brain. *Brain Research* 1770: 147627, 2021. doi: 10.1016/j.brainres.2021.147627.
188. **Braissant O, Henry H, Béard E, Uldry J.** Creatine deficiency syndromes and the importance of creatine synthesis in the brain. *Amino Acids* 40: 1315–1324, 2011. doi: 10.1007/s00726-011-0852-z.
189. **Wyss M, Kaddurah-Daouk R.** Creatine and Creatinine Metabolism. *Physiological Reviews* 80: 1107–1213, 2000. doi: 10.1152/physrev.2000.80.3.1107.

190. **Yamashita K, Yoshioka T.** Profiles of creatine kinase isoenzyme compositions in single muscle fibres of different types. *J Muscle Res Cell Motil* 12: 37–44, 1991. doi: 10.1007/BF01781172.
191. **Schlattner U, Tokarska-Schlattner M, Wallimann T.** Mitochondrial creatine kinase in human health and disease. *Biochimica et Biophysica Acta (BBA) - Molecular Basis of Disease* 1762: 164–180, 2006. doi: 10.1016/j.bbadis.2005.09.004.
192. **Ventura-Clapier R, Kuznetsov A, Veksler V, Boehm E, Anflous K.** Functional coupling of creatine kinases in muscles: Species and tissue specificity. *Mol Cell Biochem* 184: 231–247, 1998. doi: 10.1023/A:1006840508139.
193. **Veksler VI, Kuznetsov AV, Anflous K, Mateo P, Deursen J van, Wieringa B, Ventura-Clapier R.** Muscle Creatine Kinase-deficient Mice: II. CARDIAC AND SKELETAL MUSCLES EXHIBIT TISSUE-SPECIFIC ADAPTATION OF THE MITOCHONDRIAL FUNCTION (\*). *Journal of Biological Chemistry* 270: 19921–19929, 1995. doi: 10.1074/jbc.270.34.19921.
194. **Ventura-Clapier R, Kuznetsov A, Veksler V, Boehm E, Anflous K.** Functional coupling of creatine kinases in muscles: species and tissue specificity. *MolCell Biochem* 184: 231–247, 1998.
195. **Veksler VI, Kuznetsov AV, Anflous K, Mateo P, van Deursen J, Wieringa B, Ventura-Clapier R.** Muscle creatine kinase-deficient mice. II. Cardiac and skeletal muscles exhibit tissue-specific adaptation of the mitochondrial function. *JBiolChem* 270: 19921–19929, 1995.
196. **Vaarmann A, Fortin D, Veksler V, Momken I, Ventura-Clapier R, Garnier A.** Mitochondrial biogenesis in fast skeletal muscle of CK deficient mice. *Biochimica et Biophysica Acta (BBA) - Bioenergetics* 1777: 39–47, 2008. doi: 10.1016/j.bbabi.2007.11.003.
197. **Roman BB, Meyer RA, Wiseman RW.** Phosphocreatine kinetics at the onset of contractions in skeletal muscle of MM creatine kinase knockout mice. *American Journal of Physiology-Cell Physiology* 283: C1776–C1783, 2002. doi: 10.1152/ajpcell.00210.2002.
198. **van Deursen J, Heerschap A, Oerlemans F, Rultenbeek W, Jap P, ter Laak H, Wieringa B.** Skeletal muscles of mice deficient in muscle creatine kinase lack burst activity. *Cell* 74: 621–631, 1993. doi: 10.1016/0092-8674(93)90510-W.
199. **Niel R, Le Moyec L, Launay T, Mille-Hamard L, Triba MN, Maciejak O, Billat VL, Momken I.** Physical performance level in sarcomeric mitochondria creatine kinase knockout mouse model throughout ageing. *Experimental Gerontology* 146: 111246, 2021. doi: 10.1016/j.exger.2021.111246.
200. **Boehm E.** Maintained Coupling of Oxidative Phosphorylation to Creatine Kinase Activity in Sarcomeric Mitochondrial Creatine Kinase-deficient Mice. *Journal of Molecular and Cellular Cardiology* 30: 901–912, 1998. doi: 10.1006/jmcc.1998.0692.

201. **Steeghs K, Benders A, Oerlemans F, de Haan A, Heerschap A, Ruitenbeek W, Jost C, van Deursen J, Perryman B, Pette D, Brückwilder M, Koudijs J, Jap P, Veerkamp J, Wieringa B.** Altered Ca<sup>2+</sup> Responses in Muscles with Combined Mitochondrial and Cytosolic Creatine Kinase Deficiencies. *Cell* 89: 93–103, 1997. doi: 10.1016/S0092-8674(00)80186-5.
202. **de Groof AJC, Smeets B, Groot Koerkamp MJA, Mul AN, Janssen EEW, Tabak HF, Wieringa B.** Changes in mRNA expression profile underlie phenotypic adaptations in creatine kinase-deficient muscles. *FEBS Letters* 506: 73–78, 2001. doi: 10.1016/S0014-5793(01)02879-4.
203. **de Groof AJC, Oerlemans FTJJ, Jost CR, Wieringa B.** Changes in glycolytic network and mitochondrial design in creatine kinase-deficient muscles. *Muscle & Nerve* 24: 1188–1196, 2001. doi: 10.1002/mus.1131.
204. **van Deursen J, Ruitenbeek W, Heerschap A, Jap P, ter Laak H, Wieringa B.** Creatine kinase (CK) in skeletal muscle energy metabolism: a study of mouse mutants with graded reduction in muscle CK expression. *Proceedings of the National Academy of Sciences* 91: 9091–9095, 1994. doi: 10.1073/pnas.91.19.9091.
205. **Novotová M, Pavlovičová M, Veksler VI, Ventura-Clapier R, Zahradník I.** Ultrastructural remodeling of fast skeletal muscle fibers induced by invalidation of creatine kinase. *American Journal of Physiology-Cell Physiology* 291: C1279–C1285, 2006. doi: 10.1152/ajpcell.00114.2006.
206. **Momken I, Lechêne P, Koulmann N, Fortin D, Mateo P, Doan BT, Hoerter J, Bigard X, Veksler V, Ventura-Clapier R.** Impaired voluntary running capacity of creatine kinase-deficient mice. *The Journal of Physiology* 565: 951–964, 2005. doi: 10.1113/jphysiol.2005.086397.
207. **Kaasik A, Veksler V, Boehm E, Novotova M, Ventura-Clapier R.** From energy store to energy flux: a study in creatine kinase deficient fast skeletal muscle. *The FASEB Journal* 17: 708–710, 2003. doi: 10.1096/fj.02-0684fj.
208. **Chevli R, Fitch CD.**  $\beta$ -Guanidinopropionate and phosphorylated  $\beta$ -guanidinopropionate as substrates for creatine kinase. *Biochemical Medicine* 21: 162–167, 1979. doi: 10.1016/0006-2944(79)90068-1.
209. **Oudman I, Clark JF, Brewster LM.** The Effect of the Creatine Analogue Beta-guanidinopropionic Acid on Energy Metabolism: A Systematic Review. *PLOS ONE* 8: e52879, 2013. doi: 10.1371/journal.pone.0052879.
210. **Pertici I, D'Angelo D, Vecellio Reane D, Reconditi M, Morotti I, Putignano E, Napoli D, Rastelli G, Gherardi G, De Mario A, Rizzuto R, Boncompagni S, Baroncelli L, Linari M, Caremani M, Raffaello A.** Creatine transporter (SLC6A8) knockout mice exhibit reduced muscle performance, disrupted mitochondrial Ca<sup>2+</sup> homeostasis, and severe muscle atrophy. *Cell Death Dis* 16: 99, 2025. doi: 10.1038/s41419-025-07381-x.
211. **Wawro AM, Gajera CR, Baker SA, Nirschl JJ, Vogel H, Montine TJ.** Creatine transport and pathological changes in creatine transporter deficient mice. *Journal of Inherited Metabolic Disease* 44: 939–948, 2021. doi: 10.1002/jimd.12358.

212. **Stockebrand M, Sasani A, Das D, Hornig S, Hermans-Borgmeyer I, Lake HA, Isbrandt D, Lygate CA, Heerschap A, Neu A, Choe C-U.** A Mouse Model of Creatine Transporter Deficiency Reveals Impaired Motor Function and Muscle Energy Metabolism [Online]. *Frontiers in Physiology* 9, 2018. <https://www.frontiersin.org/article/10.3389/fphys.2018.00773> [19 Jan. 2022].
213. **Perna MK, Kokenge AN, Miles KN, Udobi KC, Clark JF, Pyne-Geithman GJ, Khuchua Z, Skelton MR.** Creatine transporter deficiency leads to increased whole body and cellular metabolism. *Amino Acids* 48: 2057–2065, 2016. doi: 10.1007/s00726-016-2291-3.
214. **Duran-Trio L, Fernandes-Pires G, Grosse J, Soro-Arnaiz I, Roux-Petronelli C, Binz P-A, De Bock K, Cudalbu C, Sandi C, Braissant O.** Creatine transporter-deficient rat model shows motor dysfunction, cerebellar alterations, and muscle creatine deficiency without muscle atrophy. *Journal of Inherited Metabolic Disease* 45: 278–291, 2022. doi: 10.1002/jimd.12470.
215. **Ross TT, Overton JD, Houmard KF, Kinsey ST.**  $\beta$ -GPA treatment leads to elevated basal metabolic rate and enhanced hypoxic exercise tolerance in mice. *Physiological Reports* 5: e13192, 2017. doi: 10.14814/phy2.13192.
216. **Adams GR, Bodell PW, Baldwin KM.** Running performance and cardiovascular capacity are not impaired in creatine-depleted rats. *Journal of Applied Physiology* 79: 1002–1007, 1995. doi: 10.1152/jappl.1995.79.3.1002.
217. **van Deursen J, Jap P, Heerschap A, ter Laak H, Ruitenbeek W, Wieringa B.** Effects of the creatine analogue  $\beta$ -guanidinopropionic acid on skeletal muscles of mice deficient in muscle creatine kinase. *Biochimica et Biophysica Acta (BBA) - Bioenergetics* 1185: 327–335, 1994. doi: 10.1016/0005-2728(94)90248-8.
218. **Shoubridge EA, Radda GK.** A gated  $^{31}\text{P}$  NMR study of tetanic contraction in rat muscle depleted of phosphocreatine. *American Journal of Physiology-Cell Physiology* 252: C532–C542, 1987. doi: 10.1152/ajpcell.1987.252.5.C532.
219. **Schmidt A, Marescau B, Boehm EA, Renema WKJ, Peco R, Das A, Steinfeld R, Chan S, Wallis J, Davidoff M, Ullrich K, Waldschütz R, Heerschap A, De Deyn PP, Neubauer S, Isbrandt D.** Severely altered guanidino compound levels, disturbed body weight homeostasis and impaired fertility in a mouse model of guanidinoacetate N-methyltransferase (GAMT) deficiency. *Human Molecular Genetics* 13: 905–921, 2004. doi: 10.1093/hmg/ddh112.
220. **Barsunova K, Vendelin M, Birkedal R.** Marker enzyme activities in hindleg from creatine-deficient AGAT and GAMT KO mice – differences between models, muscles, and sexes. *Sci Rep* 10: 7956, 2020. doi: 10.1038/s41598-020-64740-8.
221. **Kan HE, Buse-Pot TE, Peco R, Isbrandt D, Heerschap A, de Haan A.** Lower force and impaired performance during high-intensity electrical stimulation in skeletal muscle of GAMT-deficient knockout mice. *American Journal of Physiology-Cell Physiology* 289: C113–C119, 2005. doi: 10.1152/ajpcell.00040.2005.
222. **Kan HE, Jan Renema WK, Isbrandt D, Heerschap A.** Phosphorylated guanidinoacetate partly compensates for the lack of phosphocreatine in skeletal muscle of mice lacking guanidinoacetate methyltransferase. *The Journal of Physiology* 560: 219–229, 2004. doi: 10.1113/jphysiol.2004.067926.

223. **Faller KME, Atzler D, McAndrew DJ, Zervou S, Whittington HJ, Simon JN, Aksentijevic D, Ten Hove M, Choe C-U, Isbrandt D, Casadei B, Schneider JE, Neubauer S, Lygate CA.** Impaired cardiac contractile function in arginine:glycine amidinotransferase knockout mice devoid of creatine is rescued by homoarginine but not creatine. *Cardiovasc Res* 114: 417–430, 2018. doi: 10.1093/cvr/cvx242.
224. **Stockebrand M, Nejad AS, Neu A, Kharbanda KK, Sauter K, Schillemeit S, Isbrandt D, Choe C.** Transcriptomic and metabolic analyses reveal salvage pathways in creatine-deficient AGAT<sup>-/-</sup> mice. *Amino Acids* 48: 2025–2039, 2016. doi: 10.1007/s00726-016-2202-7.
225. **Choe C, Nabuurs C, Stockebrand MC, Neu A, Nunes P, Morellini F, Sauter K, Schillemeit S, Hermans-Borgmeyer I, Marescau B, Heerschap A, Isbrandt D.** l-arginine:glycine amidinotransferase deficiency protects from metabolic syndrome. *Human Molecular Genetics* 22: 110–123, 2013. doi: 10.1093/hmg/ddt407.
226. **Nabuurs CI, Choe CU, Veltien A, Kan HE, Loon LJC van, Rodenburg RJT, Matschke J, Wieringa B, Kemp GJ, Isbrandt D, Heerschap A.** Disturbed energy metabolism and muscular dystrophy caused by pure creatine deficiency are reversible by creatine intake. *The Journal of Physiology* 591: 571–592, 2013. doi: 10.1113/jphysiol.2012.241760.
227. **Béard E, Braissant O.** Synthesis and transport of creatine in the CNS: importance for cerebral functions. *Journal of Neurochemistry* 115: 297–313, 2010. doi: 10.1111/j.1471-4159.2010.06935.x.
228. **Torremans A, Marescau B, Possemiers I, Van Dam D, D’Hooge R, Isbrandt D, De Deyn PP.** Biochemical and behavioural phenotyping of a mouse model for GAMT deficiency. *Journal of the Neurological Sciences* 231: 49–55, 2005. doi: 10.1016/j.jns.2004.12.014.
229. **Iqbal F, Hoeger H, Lubec G, Bodamer O.** Biochemical and behavioral phenotype of AGAT and GAMT deficient mice following long-term Creatine monohydrate supplementation. *Metab Brain Dis* 32: 1951–1961, 2017. doi: 10.1007/s11011-017-0092-3.
230. **Allen PS, Matheson GO, Zhu G, Gheorgiu D, Dunlop RS, Falconer T, Stanley C, Hochachka PW.** Simultaneous 31P MRS of the soleus and gastrocnemius in Sherpas during graded calf muscle exercise. *American Journal of Physiology-Regulatory, Integrative and Comparative Physiology* 273: R999–R1007, 1997. doi: 10.1152/ajpregu.1997.273.3.R999.
231. **Hochachka PW, McClelland GB.** Cellular Metabolic Homeostasis During Large-Scale Change in Atp Turnover Rates in Muscles. *Journal of Experimental Biology* 200: 381–386, 1997. doi: 10.1242/jeb.200.2.381.
232. **Kushmerick MJ, Meyer RA, Brown TR.** Regulation of oxygen consumption in fast- and slow-twitch muscle. *American Journal of Physiology-Cell Physiology* 263: C598–C606, 1992. doi: 10.1152/ajpcell.1992.263.3.C598.

233. **Katz LA, Swain JA, Portman MA, Balaban RS.** Relation between phosphate metabolites and oxygen consumption of heart in vivo. *American Journal of Physiology-Heart and Circulatory Physiology* 256: H265–H274, 1989. doi: 10.1152/ajpheart.1989.256.1.H265.
234. **Pette D, Vrbová G.** What does chronic electrical stimulation teach us about muscle plasticity? *Muscle & Nerve* 22: 666–677, 1999. doi: 10.1002/(SICI)1097-4598(199906)22:6<666::AID-MUS3>3.0.CO;2-Z.
235. **Branovets J, Laasmaa M, Stolova J, Shen X, Rätsepso T, Bernasconi R, Soodla K, Balodis MJ, Grahv C, Hendrikson E, Louch WE, Birkedal R, Vendelin M.** Lifelong creatine deficiency leads to augmented sarcoplasmic reticulum calcium release but not heart failure. *American Journal of Physiology-Heart and Circulatory Physiology* 329: H471–H489, 2025. doi: 10.1152/ajpheart.00106.2025.
236. **Kütt J, Margus G, Kask L, Rätsepso T, Soodla K, Bernasconi R, Birkedal R, Järv P, Laasmaa M, Vendelin M.** Simple analysis of gel images with IOCBIO Gel. *BMC Biol* 21: 225, 2023. doi: 10.1186/s12915-023-01734-8.
237. **Overton JD, Adams GS, McCall RD, Kinsey ST.** High energy phosphate concentrations and AMPK phosphorylation in skeletal muscle from mice with inherited differences in hypoxic exercise tolerance. *Comparative Biochemistry and Physiology Part A: Molecular & Integrative Physiology* 152: 478–485, 2009. doi: 10.1016/j.cbpa.2008.11.019.
238. **Illaste A, Laasmaa M, Peterson P, Vendelin M.** Analysis of Molecular Movement Reveals Latticelike Obstructions to Diffusion in Heart Muscle Cells. *Biophysical Journal* 102: 739–748, 2012. doi: 10.1016/j.bpj.2012.01.012.
239. **Jepihhina N, Beraud N, Sepp M, Birkedal R, Vendelin M.** Permeabilized Rat Cardiomyocyte Response Demonstrates Intracellular Origin of Diffusion Obstacles. *Biophysical Journal* 101: 2112–2121, 2011. doi: 10.1016/j.bpj.2011.09.025.
240. **Sepp M, Vendelin M, Vija H, Birkedal R.** ADP Compartmentation Analysis Reveals Coupling between Pyruvate Kinase and ATPases in Heart Muscle. *Biophysical Journal* 98: 2785–2793, 2010. doi: 10.1016/j.bpj.2010.03.025.
241. **Birkedal R, Branovets J, Vendelin M.** Compartmentalization in cardiomyocytes modulates creatine kinase and adenylate kinase activities. *FEBS Letters* 598: 2623–2640, 2024. doi: 10.1002/1873-3468.14994.
242. **Miyamoto T, Rho E, Sample V, Akano H, Magari M, Ueno T, Gorshkov K, Chen M, Tokumitsu H, Zhang J, Inoue T.** Compartmentalized AMPK Signaling Illuminated by Genetically Encoded Molecular Sensors and Actuators. *Cell Reports* 11: 657–670, 2015. doi: 10.1016/j.celrep.2015.03.057.
243. **Zong Y, Zhang C-S, Li M, Wang W, Wang Z, Hawley SA, Ma T, Feng J-W, Tian X, Qi Q, Wu Y-Q, Zhang C, Ye Z, Lin S-Y, Piao H-L, Hardie DG, Lin S-C.** Hierarchical activation of compartmentalized pools of AMPK depends on severity of nutrient or energy stress. *Cell Res* 29: 460–473, 2019. doi: 10.1038/s41422-019-0163-6.

244. **Drake JC, Wilson RJ, Laker RC, Guan Y, Spaulding HR, Nichenko AS, Shen W, Shang H, Dorn MV, Huang K, Zhang M, Bandara AB, Brisendine MH, Kashatus JA, Sharma PR, Young A, Gautam J, Cao R, Wallrabe H, Chang PA, Wong M, Desjardins EM, Hawley SA, Christ GJ, Kashatus DF, Miller CL, Wolf MJ, Periasamy A, Steinberg GR, Hardie DG, Yan Z.** Mitochondria-localized AMPK responds to local energetics and contributes to exercise and energetic stress-induced mitophagy. *PNAS* 118, 2021. doi: 10.1073/pnas.2025932118.
245. **Schmitt DL, Curtis SD, Lyons AC, Zhang J, Chen M, He CY, Mehta S, Shaw RJ, Zhang J.** Spatial regulation of AMPK signaling revealed by a sensitive kinase activity reporter. *Nat Commun* 13: 3856, 2022. doi: 10.1038/s41467-022-31190-x.
246. **Branovets J, Soodla K, Vendelin M, Birkedal R.** Rat and mouse cardiomyocytes show subtle differences in creatine kinase expression and compartmentalization. *PLOS ONE* 18: e0294718, 2023. doi: 10.1371/journal.pone.0294718.
247. **Trefts E, Shaw RJ.** AMPK: restoring metabolic homeostasis over space and time. *Molecular Cell* 81: 3677–3690, 2021. doi: 10.1016/j.molcel.2021.08.015.
248. **Seabright AP, Fine NHF, Barlow JP, Lord SO, Musa I, Gray A, Bryant JA, Banzhaf M, Lavery GG, Hardie DG, Hodson DJ, Philp A, Lai Y-C.** AMPK activation induces mitophagy and promotes mitochondrial fission while activating TBK1 in a PINK1-Parkin independent manner. *The FASEB Journal* 34: 6284–6301, 2020. doi: 10.1096/fj.201903051R.
249. **Vilchinskaya NA, Mirzoev TM, Lomonosova YN, Kozlovskaya IB, Shenkman BS.** Human muscle signaling responses to 3-day head-out dry immersion. *J Musculoskelet Neuronal Interact* 15: 286–293, 2015.
250. **Vilchinskaya NA, Mochalova EP, Nemirovskaya TL, Mirzoev TM, Turtikova OV, Shenkman BS.** Rapid decline in MyHC I( $\beta$ ) mRNA expression in rat soleus during hindlimb unloading is associated with AMPK dephosphorylation. *The Journal of Physiology* 595: 7123–7134, 2017. doi: 10.1113/JP275184.
251. **Chibalin AV, Benziene B, Zakyranova GF, Kravtsova VV, Krivoi II.** Early endplate remodeling and skeletal muscle signaling events following rat hindlimb suspension. *Journal of Cellular Physiology* 233: 6329–6336, 2018. doi: 10.1002/jcp.26594.
252. **Egawa T, Ohno Y, Goto A, Yokoyama S, Hayashi T, Goto K.** AMPK Mediates Muscle Mass Change But Not the Transition of Myosin Heavy Chain Isoforms during Unloading and Reloading of Skeletal Muscles in Mice. *International Journal of Molecular Sciences* 19: 2954, 2018. doi: 10.3390/ijms19102954.
253. **Kostovski E, Boon H, Hjeltnes N, Lundell LS, Ahlsén M, Chibalin AV, Krook A, Iversen PO, Widegren U.** Altered content of AMP-activated protein kinase isoforms in skeletal muscle from spinal cord injured subjects. *American Journal of Physiology-Endocrinology and Metabolism* 305: E1071–E1080, 2013. doi: 10.1152/ajpendo.00132.2013.
254. **Tyganov SA, Mochalova EP, Belova SP, Sharlo KA, Rozhkov SV, Vilchinskaya NA, Paramonova II, Mirzoev TM, Shenkman BS.** Effects of Plantar Mechanical Stimulation on Anabolic and Catabolic Signaling in Rat Postural Muscle Under Short-Term Simulated Gravitational Unloading. *Front Physiol* 10, 2019. doi: 10.3389/fphys.2019.01252.

255. **Belova SP, Vilchinskaya NA, Mochalova EP, Mirzoev TM, Nemirovskaya TL, Shenkman BS.** Elevated p70S6K phosphorylation in rat soleus muscle during the early stage of unloading: Causes and consequences. *Archives of Biochemistry and Biophysics* 674: 108105, 2019. doi: 10.1016/j.abb.2019.108105.
256. **Khoja S, Lambert J, Nitzahn M, Eliav A, Zhang Y, Tamboline M, Le CT, Nasser E, Li Y, Patel P, Zhuravka I, Lueptow LM, Tkachyova I, Xu S, Nissim I, Schulze A, Lipshutz GS.** Gene therapy for guanidinoacetate methyltransferase deficiency restores cerebral and myocardial creatine while resolving behavioral abnormalities. *Molecular Therapy Methods & Clinical Development* 25: 278–296, 2022. doi: 10.1016/j.omtm.2022.03.015.
257. **Sasani A, Hornig S, Grzybowski R, Cordts K, Hanff E, Tsikas D, Böger R, Gerloff C, Isbrandt D, Neu A, Schwedhelm E, Choe C.** Muscle phenotype of AGAT- and GAMT-deficient mice after simvastatin exposure. *Amino Acids* 52: 73–85, 2020. doi: 10.1007/s00726-019-02812-4.
258. **Louis M, Van Beneden R, Dehoux M, Thissen JP, Francaux M.** Creatine increases IGF-I and myogenic regulatory factor mRNA in C2C12 cells. *FEBS Letters* 557: 243–247, 2004. doi: 10.1016/S0014-5793(03)01504-7.
259. **Deldicque L, Theisen D, Bertrand L, Hespel P, Hue L, Francaux M.** Creatine enhances differentiation of myogenic C2C12 cells by activating both p38 and Akt/PKB pathways. *American Journal of Physiology-Cell Physiology* 293: C1263–C1271, 2007. doi: 10.1152/ajpcell.00162.2007.
260. **Choi M-C, Cohen TJ, Barrientos T, Wang B, Li M, Simmons BJ, Yang JS, Cox GA, Zhao Y, Yao T-P.** A Direct HDAC4-MAP Kinase Crosstalk Activates Muscle Atrophy Program. *Molecular Cell* 47: 122–132, 2012. doi: 10.1016/j.molcel.2012.04.025.
261. **Liang D, Wang D, Zheng X, Xiang H, Liu S, Yu C, Tian J, Ma J, Niu Y.** Aerobic plus resistance exercise attenuates skeletal muscle atrophy induced by dexamethasone through the HDAC4/FoxO3a pathway. *Cellular Signalling* 127: 111581, 2025. doi: 10.1016/j.cellsig.2024.111581.
262. **Liu Y, Zhou T, Wang Q, Fu R, Zhang Z, Chen N, Li Z, Gao G, Peng S, Yang D.** m6A demethylase ALKBH5 drives denervation-induced muscle atrophy by targeting HDAC4 to activate FoxO3 signalling. *Journal of Cachexia, Sarcopenia and Muscle* 13: 1210–1223, 2022. doi: 10.1002/jcsm.12929.
263. **Ma W, Cai Y, Shen Y, Chen X, Zhang L, Ji Y, Chen Z, Zhu J, Yang X, Sun H.** HDAC4 Knockdown Alleviates Denervation-Induced Muscle Atrophy by Inhibiting Myogenin-Dependent AtroGene Activation. *Front Cell Neurosci* 15: 663384, 2021. doi: 10.3389/fncel.2021.663384.
264. **Pigna E, Renzini A, Greco E, Simonazzi E, Fulle S, Mancinelli R, Moresi V, Adamo S.** HDAC4 preserves skeletal muscle structure following long-term denervation by mediating distinct cellular responses. *Skeletal Muscle* 8: 6, 2018. doi: 10.1186/s13395-018-0153-2.
265. **McInnes KJ, Brown KA, Hunger NI, Simpson ER.** Regulation of LKB1 expression by sex hormones in adipocytes. *Int J Obes* 36: 982–985, 2012. doi: 10.1038/ijo.2011.172.

266. **Kim SA, Lee KY, Kim J-R, Choi HC.** Estrogenic compound attenuates angiotensin II-induced vascular smooth muscle cell proliferation through interaction between LKB1 and estrogen receptor  $\alpha$ . *Journal of Pharmacological Sciences* 132: 78–85, 2016. doi: 10.1016/j.jphs.2016.09.001.
267. **Nath-Sain S, Marignani PA.** LKB1 Catalytic Activity Contributes to Estrogen Receptor  $\alpha$  Signaling. *Mol Biol Cell* 20: 2785–2795, 2009. doi: 10.1091/mbc.E08-11-1138.
268. **Kido K, Egawa T, Fujiyoshi H, Suzuki H, Kawanaka K, Hayashi T.** AMPK is indispensable for overload-induced muscle glucose uptake and glycogenesis but dispensable for inducing hypertrophy in mice. *The FASEB Journal* 35: e21459, 2021. doi: 10.1096/fj.202002164R.
269. **Fentz J, Kjøbsted R, Kristensen CM, Hingst JR, Birk JB, Gudiksen A, Foretz M, Schjerling P, Viollet B, Pilegaard H, Wojtaszewski JFP.** AMPK $\alpha$  is essential for acute exercise-induced gene responses but not for exercise training-induced adaptations in mouse skeletal muscle. *American Journal of Physiology-Endocrinology and Metabolism* 309: E900–E914, 2015. doi: 10.1152/ajpendo.00157.2015.
270. **Selsby JT, Morine KJ, Pendrak K, Barton ER, Sweeney HL.** Rescue of Dystrophic Skeletal Muscle by PGC-1 $\alpha$  Involves a Fast to Slow Fiber Type Shift in the mdx Mouse. *PLOS ONE* 7: e30063, 2012. doi: 10.1371/journal.pone.0030063.
271. **Handschin C, Spiegelman BM.** Peroxisome Proliferator-Activated Receptor  $\gamma$  Coactivator 1 Coactivators, Energy Homeostasis, and Metabolism. *Endocrine Reviews* 27: 728–735, 2006. doi: 10.1210/er.2006-0037.
272. **Little JP, Safdar A, Cermak N, Tarnopolsky MA, Gibala MJ.** Acute endurance exercise increases the nuclear abundance of PGC-1 $\alpha$  in trained human skeletal muscle. *American Journal of Physiology-Regulatory, Integrative and Comparative Physiology* 298: R912–R917, 2010. doi: 10.1152/ajpregu.00409.2009.
273. **Vainshtein A, Tryon LD, Pauly M, Hood DA.** Role of PGC-1 $\alpha$  during acute exercise-induced autophagy and mitophagy in skeletal muscle. *American Journal of Physiology-Cell Physiology* 308: C710–C719, 2015. doi: 10.1152/ajpcell.00380.2014.
274. **Popov DV, Bachinin AV, Lysenko EA, Miller TF, Vinogradova OL.** Exercise-induced expression of peroxisome proliferator-activated receptor  $\gamma$  coactivator-1 $\alpha$  isoforms in skeletal muscle of endurance-trained males. *J Physiol Sci* 64: 317–323, 2014. doi: 10.1007/s12576-014-0321-z.
275. **Collu-Marchese M, Shuen M, Pauly M, Saleem A, Hood DA.** The regulation of mitochondrial transcription factor A (Tfam) expression during skeletal muscle cell differentiation. *Biosci Rep* 35: e00221, 2015. doi: 10.1042/BSR20150073.
276. **Smith BK, Mukai K, Lally JS, Maher AC, Gurd BJ, Heigenhauser GJF, Spriet LL, Holloway GP.** AMP-activated protein kinase is required for exercise-induced peroxisome proliferator-activated receptor  $\gamma$  co-activator 1 $\alpha$  translocation to subsarcolemmal mitochondria in skeletal muscle. *J Physiol* 591: 1551–1561, 2013. doi: 10.1113/jphysiol.2012.245944.
277. **Laver DR, Lenz GKE, Lamb GD.** Regulation of the calcium release channel from rabbit skeletal muscle by the nucleotides ATP, AMP, IMP and adenosine. *The Journal of Physiology* 537: 763–778, 2001. doi: 10.1111/j.1469-7793.2001.00763.x.

## Acknowledgements

This work was performed in the Laboratory of Systems Biology at the Institute of Cybernetics, Tallinn University of Technology (TalTech). The grammar and syntax of this thesis have been refined with assistance from the AI tool Claude.

First, I would like to express my sincere gratitude to my main supervisor, Rikke Birkedal. Thank you for guiding me through this remarkable yet challenging journey that is the doctoral experience. Your compassion, patience, and expertise have provided me with invaluable support throughout. Above all, thank you for the intellectual freedom and trust you have granted me over these four years.

I extend my deepest appreciation to my co-supervisor and head of the laboratory, Marko Vendelin. Thank you for providing me with the opportunity to work in your laboratory. I am grateful for your numerous insights and critiques—sometimes quite direct—that have fostered my growth both as a researcher and as an individual.

To K  rol Soodla, who made significant contributions to the work presented in this thesis: thank you for your dedication, motivation, and commitment through both successes and setbacks. I wish you all the best in your own PhD journey.

Many thanks to my other colleagues and collaborators who have contributed to this work and helped shape me as a researcher, with special recognition for Florian Britto, Martin Laasmaa, and Alex Sirp.

I would also like to thank my wife and family for their unwavering support throughout the highs and lows of my PhD journey.

This work was funded by the Estonian Research Council (PRG1127). In this regard, I would like to extend my heartfelt thanks to the Estonian nation and its people for welcoming me and supporting my research.

## Abstract

### Unravelling the mechanisms of energetics-induced fast-to-slow phenotypic shift in creatine-deficient mice

Skeletal muscle is the most predominant tissue in the human body and serves as the organ of movement. To sustain its function, a muscle specializes by expressing unique fiber compositions that define its phenotype. A slow phenotype consists primarily of type I and IIa fibers that are metabolically oxidative, exhibit lower force production, but demonstrate fatigue resistance. Conversely, a fast phenotype is predominantly composed of type IIx and IIb fibers that are metabolically glycolytic, generate greater force, but are more prone to fatigue. ATP hydrolysis is essential for muscle function, particularly contraction, and its concentration must remain stable. Muscle fiber metabolic specialization matches the myosin heavy chain (MHC) isoform ATP consumption, ensuring adequate energy provision. When an energetic imbalance occurs, elevated AMP and ADP levels activate the energetic sensor AMP-activated protein kinase (AMPK). While acute AMPK activation restores energetic equilibrium by stimulating metabolism, chronic AMPK activity has been associated with atrophy and fast-to-slow phenotypic shift.

Muscle tissue possesses an ATP buffering system known as the creatine kinase (CK) system. The CK enzyme catalyzes ADP rephosphorylation to ATP using phosphocreatine (PCr) and the reverse reaction, phosphorylating creatine (Cr) to PCr using ATP. The high rate of CK activity and elevated PCr concentrations in muscle enable rapid compensation for sudden ATP depletion during contraction. Disruption of the CK system induces muscle atrophy and fast-to-slow phenotypic shifts associated with AMPK activation. However, the energetics and muscle-dependent consequences of mice lacking endogenous Cr biosynthesis remain poorly understood. Cr biosynthesis can be suppressed by knockout Guanidinoacetate N-methyltransferase (GAMT KO) or L-Arginine: Glycine amidinotransferase (AGAT KO).

Using Western blot and immunostaining techniques, we investigated the muscle phenotype, atrophy, and AMPK activation in fast muscle gastrocnemius (GAST) and slow muscle soleus (SOL) of both GAMT KO and AGAT KO mice. We also evaluate the basal activation of AMPK and its upstream kinases expression between fast and slow muscles. Additionally, we examined the effects of energetic deprivation on  $Ca^{2+}$  dynamics in stimulated C2C12 myotubes and measured  $Ca^{2+}$ -related proteins in AGAT KO mice.

In this study, we provide evidence that basal AMPK activity is higher in slow compared to fast muscle. We suggest that AMPK activity may be compartmentalized, with activation being influenced by local rather than global energetics. Cr-deficient mice GAMT KO and AGAT KO exhibited radically different muscle phenotypes. GAMT KO mice showed subtle changes in fast muscle (GAST) mass and phenotype independently of AMPK activity. In contrast, AGAT KO showed a severe atrophy and fast-to-slow phenotypic shift in GAST associated with high AMPK activity. We speculated whether the use of GAA as a Cr substitute in GAMT KO may prevent AMPK activation and phenotypic adaptations. Based on our results and new findings by collaborators (Dr. Florian Britto, Institut Cochin, Paris, France), we discussed the potential involvement of AMPK in the phenotypic shift. Finally, we showed that energetic deprivation enhances the  $Ca^{2+}$  release by ryanodine receptors and theorized a new potential mechanism of energetics-induced fast-to-slow phenotypic shift.

## Lühikokkuvõte

### Energeetikast indutseeritud kiire-aeglase fenotüübilise nihke mehhanismide uurimine kreatiini puudulikkusega hiirtel

Skeletilihaskude moodustab inimese organismis suurima koe ja tagab keha liikumisvõime. Lihase spetsialiseerub oma funktsiooni säilitamiseks, ekspresseerides unikaalseid kiutüüpide kombinatsioone, mis määravad selle fenotüübi. Aeglane fenotüüp koosneb peamiselt I ja IIa tüüpi kiududest, mis on metaboolselt oksüdatiivsed, toodavad väiksemat jõudu, kuid on väsimuskindlad. Vastupidiselt sellele koosneb kiire fenotüüp valdavalt IIx ja IIb tüüpi kiududest, mis on metaboolselt glükolüütilised, genereerivad suuremat jõudu, kuid on vastuvõtlikumad väsimusele. ATP hüdrolyüs on lihase funktsioneerimiseks, eeskätt kontraktsiooniks, hädavajalik ning selle kontsentratsioon peab püsima stabiilsena. Lihaskiudude metaboolne spetsialiseerumine on kooskõlas müosiini raske ahela (MHC) isoformide ATP tarbimisega, tagades piisava energiavarustuse. Energeetilise tasakaalutuse tekkimisel aktiveerivad tõusnud AMP- ja ADP-tasemed energetilise sensori – AMP-aktiveeritud proteiinkinaasi (AMPK). Akuutne AMPK aktivatsioon taastab energetilise tasakaalu, stimuleerides ainevahetust, kuid krooniline AMPK aktiivsus on seotud atroofia ja kiire-aeglase fenotüübilise muutusega.

Lihaskoes toimib ATP-puhversüsteem, mida tuntakse kreatiinkinaasi (CK) süsteemina. CK ensüüm katalüüsib ADP refosforüülimist ATP-ks, kasutades fosfokreatiini (PCr), ning vastupidist reaktsiooni – kreatiini (Cr) fosforüülimist PCr-ks ATP abil. CK kõrge aktiivsus ja lihastes leiduvad suurenenud PCr kontsentratsioonid võimaldavad kiiret ATP languse kompenseerimist kontraktsiooni ajal. CK-süsteemi häirumine põhjustab lihasatroofiat ning kiire-aeglase fenotüübilisi muutusi, mis on seotud AMPK aktivatsiooniga. Siiski on endogeense Cr biosünteesi puudumise energetika ja lihasspetsiifilised tagajärjed hiirtel endiselt halvasti mõistetud. Cr biosünteesi saab pärssida kas guanidinoatsetaadi N-metüültransferaasi (GAMT KO) või L-arginiini: glütsiini amidinotransferaasi (AGAT KO) geenide väljalülitamisega.

Western blot'i ja immunovärvimise meetodite abil uurisime lihasfenotüüpi, atroofiat ja AMPK aktivatsiooni nii kiiretes kaksik-sääremarjalihastes (GAST) kui ka aeglastes lestlihastes (SOL) GAMT KO ja AGAT KO hiirtel. Lisaks hindasime AMPK basaalses aktivatsiooni ja selle ülesvoolu kinaaside ekspressiooni erinevust kiirete ja aeglaste lihaste vahel. Samuti uurisime energetilise defitsiidi mõju  $Ca^{2+}$  dünaamikale stimuleeritud C2C12 müototubulites ning mõõtsime  $Ca^{2+}$ -ga seotud valkude taset AGAT KO hiirtel.

Käesolevas uuringus esitame tõendid, et AMPK baasaktiivsus on aeglastes lihases kõrgem kui kiiretes lihases. Pakume välja, et AMPK aktiivsus võib olla kompartmentaliseeritud, kusjuures aktivatsiooni mõjutavad pigem lokaalsed kui globaalsed energetilised tingimused. Kreatiini puudulikkud hiired (GAMT KO ja AGAT KO) näitasid radikaalselt erinevaid lihasfenotüüpe. GAMT KO hiirtel esinesid kiiretes lihases (GAST) ainult väikesed muutused massis ja fenotüübis, mis toimusid sõltumatult AMPK aktiivsusest. Seevastu AGAT KO hiirtel täheldati rasket atroofiat ja kiire-aeglase fenotüübilist muutust GAST-is, mis oli seotud kõrge AMPK aktiivsusega. Oletasime, et guanidinoatsetaadi (GAA) kasutamine kreatiini asendajana GAMT KO hiirtel võib takistada AMPK aktivatsiooni ja fenotüübilisi kohandumisi. Meie tulemuste ja uute koostööpartnerite (Dr Florian Britto, Institut Cochin, Pariis, Prantsusmaa) leidude põhjal arutame AMPK võimalikku rolli fenotüübilises nihkes. Lõpuks näitasime, et energetiline defitsiit võimendab  $Ca^{2+}$  vabanemist rüanodiinireseptorite kaudu ning pakkusime välja uue potentsiaalse mehhanismi, mis vahendab energetikast tingitud kiire-aeglase fenotüübilist muutust.

## Publication I

Kütt, J; Margus, G; Kask, L; Rätsepso, T; Soodla, K; **Bernasconi, R**; Birkedal, R; Järv, P; Laasmaa, M; Vendelin, M.

**Simple analysis of gel images with IOCBIO Gel.**

BMC Biology, Oct 2023, DOI: 10.1186/s12915-023-01734-8.



SOFTWARE

Open Access

# Simple analysis of gel images with IOCBIO Gel



Jaak Kütt<sup>1</sup>, Georg Margus<sup>1</sup>, Lauri Kask<sup>1</sup>, Triinu Rätsepso<sup>1</sup>, Kärol Soodla<sup>1</sup>, Romain Bernasconi<sup>1</sup>, Rikke Birkedal<sup>1</sup>, Prit Järv<sup>2</sup>, Martin Laasmaa<sup>1</sup> and Marko Vendelin<sup>1\*</sup> 

## Abstract

**Background** Current solutions for the analysis of Western Blot images lack either transparency and reproducibility or can be tedious to use if one has to ensure the reproducibility of the analysis.

**Results** Here, we present an open-source gel image analysis program, IOCBIO Gel. It is designed to simplify image analysis and link the analysis results with the metadata describing the measurements. The software runs on all major desktop operating systems. It allows one to use it in either a single-researcher environment with local storage of the data or in a multiple-researcher environment using a central database to facilitate data sharing within the research team and beyond. By recording the original image and all operations performed on it, such as image cropping, subtraction of background, sample lane selection, and integration boundaries, the software ensures the reproducibility of the analysis and simplifies making corrections at any stage of the research. The analysis results are available either through direct access to the database used to store it or through the export of the relevant data.

**Conclusions** The software is not only limited to Western Blot image analysis and can be used to analyze images obtained as a part of many other widely used biochemical techniques such as isoelectric focusing. By recording the original data and all the analysis steps, the program improves reproducibility in the analysis and contributes to the implementation of FAIR principles in the related fields.

**Keywords** Data analysis, Reproducibility, FAIR, Western blotting, Southern blotting, Isoelectric focusing

## Background

When faced with the task of analyzing Western Blot [1] membrane images, in our experience, researchers usually use either proprietary software solutions built by imaging hardware manufacturers or the open-source ImageJ Gels plugin [2]. Unfortunately, these choices have significant shortcomings. As argued below, the major shortcoming

of both software choices is related to the reproducibility of the analysis.

Proprietary software can be a convenient solution. However, such software is frequently linked with specific hardware and the data analysis can usually be reproduced only using the same software package. This limits the ability to reproduce the analysis to the users having the same hardware platform for imaging. If, in the proprietary software, advanced algorithms have been used for background subtraction or data processing, those algorithms are usually not described in a way that other researchers could take the same images and obtain the same results. In addition, the workflow with the image processing and data selection steps is usually not available in a documented format that can be used

\*Correspondence:

Marko Vendelin  
markov@sysbio.ioc.ee

<sup>1</sup> Laboratory of Systems Biology, Department of Cybernetics, Tallinn University of Technology, Tallinn, Estonia

<sup>2</sup> Applied Artificial Intelligence Group, Department of Software Science, Tallinn University of Technology, Akadeemia 21, Tallinn 12618, Estonia



© The Author(s) 2023. **Open Access** This article is licensed under a Creative Commons Attribution 4.0 International License, which permits use, sharing, adaptation, distribution and reproduction in any medium or format, as long as you give appropriate credit to the original author(s) and the source, provide a link to the Creative Commons licence, and indicate if changes were made. The images or other third party material in this article are included in the article's Creative Commons licence, unless indicated otherwise in a credit line to the material. If material is not included in the article's Creative Commons licence and your intended use is not permitted by statutory regulation or exceeds the permitted use, you will need to obtain permission directly from the copyright holder. To view a copy of this licence, visit <http://creativecommons.org/licenses/by/4.0/>. The Creative Commons Public Domain Dedication waiver (<http://creativecommons.org/publicdomain/zero/1.0/>) applies to the data made available in this article, unless otherwise stated in a credit line to the data.

by other tools except the original software. As a result, the proprietary software for gel analysis often seems like a “black box,” and the users have to contend with the hope that the analyses are done correctly [3, 4].

As an alternative to proprietary software packages, researchers can use the free, open-source ImageJ Gels plugin [2]. The open-source solution means that, in principle, researchers have full control over the image processing and analysis steps, allowing one to fully document the analysis and make it reproducible by others. However, in practice, it is very labor-intensive to document all the analysis steps properly. Namely, one has to fully describe the overall image background subtraction, lanes selection, and integration of image intensities corresponding to each lane with the corresponding baseline selection. As a result, to our knowledge, anyone rarely does this documentation, and this leads to a reduction of the analysis reproducibility. An additional obstacle occurred, when some steps in the analysis had to be redone. For example, if the lane selection had to be adjusted, the user would have to repeat all the analysis steps and find and update the data in a spreadsheet or database before repeating all the statistical analyses. In our experience, this approach was time-consuming and prone to human errors.

A similar problem is encountered in many other popular biochemical techniques that lead to a relation between the sample and its signal, as in Western Blot. This is the case for all gel electrophoresis experiments, where each sample is allocated a well, and the applied electrical field pulls the sample through the gel, forming a lane. Within each lane, molecules within the sample are separated by charge and size. This technique is used in, for example, Western blotting (protein separation by size), Southern blotting (DNA separation by size), Northern blotting (RNA separation by size), and isoelectric focusing (separation by isoelectric point). Considering the popularity of these techniques, the inability to analyze the data in a reproducible manner contributes to the overall reproducibility crisis in science [5].

To address the shortcomings of the current solution, we designed a new open-source software for image analysis applicable for Western blot and similar techniques. During the design, the following aims were addressed. The software should be easy to use on the leading PC platforms. The software should facilitate the implementation of FAIR (findability, accessibility, interoperability, and reusability) principles [6]. In particular, the software should record all analysis steps by keeping the user selections in a form to retrace and correct them. In addition, the software should be able to store data centrally to facilitate efficient collaboration between researchers, link

obtained data to the samples, and export the results for sharing.

In line with the popular ImageJ Gels plugin naming, our software was named IOCBIO Gel and the image analysis as well as sample description is using the term *gel* to describe the physical object that is analyzed. Note that this is not always correct as in the case of Western Blot, where images are obtained from a membrane after the transfer from a gel. However, for simplicity, the term *gel* was used in the user interface and the general description below regardless of the specific experimental protocol and corresponding sample.

### Implementation

The developed software, IOCBIO Gel, is written in Python and uses Qt for the graphical user interface. This choice was based on the following. Qt has support for all the major desktop platforms allowing us to target researchers irrespective of their choice of operating system. Python was selected as it is one of the most popular programming languages, which simplifies maintenance and reviewing of the software, reduces the learning curve for new contributors, and allows to benefit from the large selection of scientific libraries in Python. In particular, we used scikit-image [7] for image processing and PyQt-Graph for plotting.

When selecting a solution to access original and analyzed data, we targeted the scenarios where the researcher uses the software either as a stand-alone solution on a PC or shares the data within the working group. For original data and gel images, we provided support for loading them either from a selected folder on the PC or from the central image database provided by OMERO [8]. Through the selected folder, we targeted users that keep their images locally or shared via local network file systems. While OMERO is designed for the central storage of microscopy data, we found it very useful for gel images allowing users to access those centrally. For analysis results and keeping the records regarding all analysis steps, we connect to a database through the SQLAlchemy library [9]. This library provides uniform access to local and central databases. As a result, we can keep analysis data locally using SQLite or centrally in PostgreSQL. To work with the analysis results, users can either export the results into a spreadsheet or directly fetch the data from the database.

The database layout has been designed to simplify the usage of the software in an environment where a central database is used to keep experimental results from different types of experiments, such as when a central laboratory database is shared by multiple primary analysis tools [10, 11] and management systems [12–15]. For that, we isolated the data stored by the software using PostgreSQL

schema—named collection of tables and views. To provide the link between sample analysis results, the software generates a table allowing users to enter the sample ID for each gel lane. This table can be further constrained by the user using applicable database software to link the entered sample ID with the table describing the sample.

The software was developed in an open manner through a publicly accessible software repository allowing the users to give direct feedback to the developers regarding the encountered issues and feature requests. The application is released under an open-source license, GPLv3.

## Results and discussion

### User interface

When designing the user interface, we had several aims. First, we aimed to reflect the connections between the physical sample, its location in the gel lane, gel images, and analysis results. That way, the users obtain not just the intensities of the peaks but also the data that links their sample to the protein content of interest or some other similar readout. The expectation is that the obtained data can be immediately analyzed using statistical programs. Second, we prioritized streamlining the operations that are frequent by making them accessible first.

The overall user interface (Fig. 1) consists of a single window, which is partitioned into the main action area, the application action type selection on the left (*selector*), accompanied by the toolbar (top) and status bar (bottom). To facilitate sharing the data within a research group and to avoid accidental analysis alteration, the application runs in *Viewing* mode by default. In this mode, the user can browse through projects and look at the images and their analysis steps without changing any data. To alter the analysis or enter new data, the user has to switch to *Editing* mode.

### Workflow

The overall workflow scheme is shown in Fig. 2 and includes entering metadata in addition to the analysis of the images, as described below.

As one of the first steps in analyzing the experiments, the user has to define the context. First, the user defines the types of measurements performed on a physical gel. For example, this could be the detection of a protein of interest using a specific antibody, overall protein content determination using staining, etc. Next, experiments on gels are usually a part of a larger project. Here, the user can handle project information in two ways. When using the same database for multiple projects, for example, in a central laboratory database or keeping all user's experiments together, we recommend defining projects in the

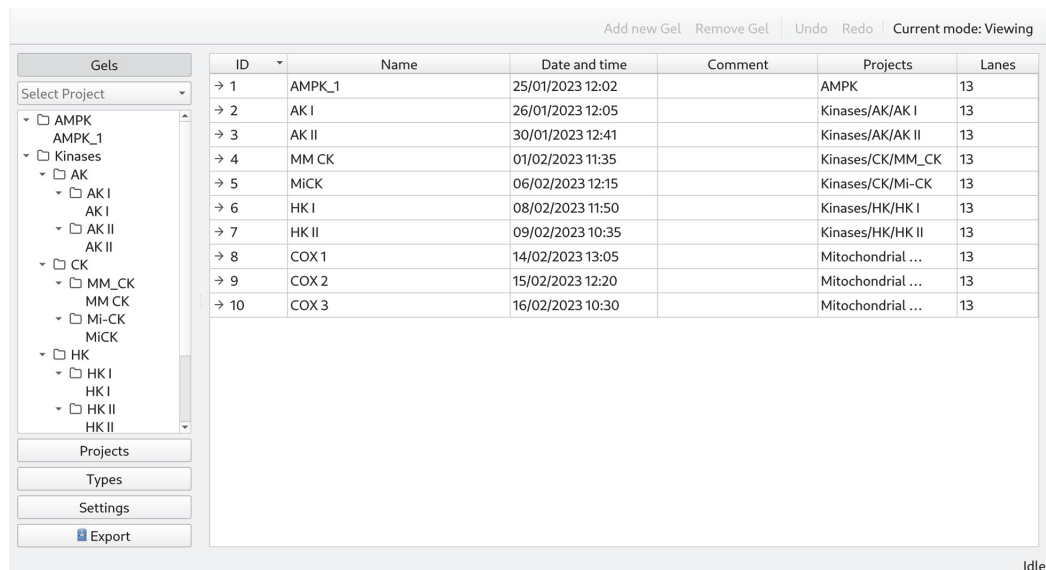


**Fig. 1** User interface of IOC BIO Gel. The application runs with a single window, which is partitioned to the main action area, application action type selection on the left (*selector*), the toolbar (top), and the status bar (bottom). The screenshot shows the default view after the start of the application

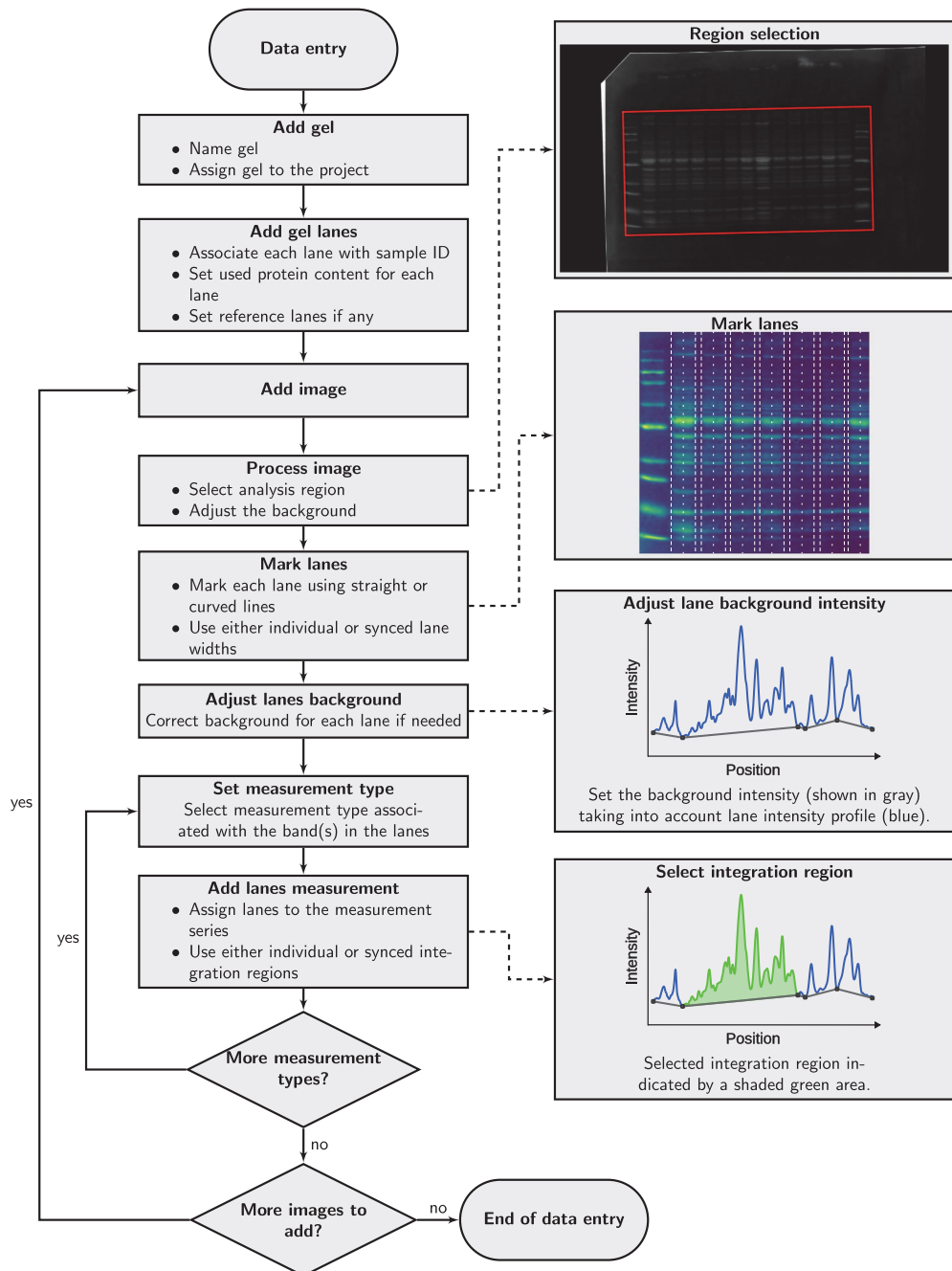


**Fig. 2** Gel image analysis workflow shown for new gel data entry. Steps include metadata entry at the beginning of the workflow, addition of images, processing them, assigning regions to lanes and performing measurements. Insets, linked with the main workflow scheme with the dashed arrows, illustrate different phases of the data entry

software. Similar to file systems, the projects can form a hierarchy allowing users to partition the measurements within one project into sub-projects. In the central database, we found it advantageous to position projects under each user's meta-project, making it easier for users to analyze and review their work. As an alternative to the definition of a project, the user can also use separate databases, with each database covering one project only. However, having separate databases would require users to redefine measurement types in each database again, making it inconvenient to switch between the projects.

With the context of the experiment defined, users can start entering the data related to a gel. Users can link a gel to one or multiple projects, as they see fit. Each physical gel is a container of samples that are allocated in gel lanes. As the next step in the analysis, the user is expected to describe each lane and relate it to the samples through their sample ID and the amount of protein in the sample. Some samples on a gel can be assigned as reference samples. This is used to compare samples between different gels, in which case the user relates measurements from the samples to a reference sample present in all these gels.

After the gel is described, the user can insert the images of that gel. In Western blotting, we usually take multiple images of the same membrane. Some are done on the full membrane, such as Ponceau staining, and some on the parts of a membrane, such as after cutting it into smaller subsections for labeling with different antibodies. All the images from the same membrane should be defined together. With a gel image added, it is analyzed by opening it in the application. Image analysis is done by selecting a gel on the image, subtracting the background, manually positioning the gel lanes on the image, and adjusting the baseline for each lane. With the lanes identified on the image and the baseline set, the user must link a measurement type to the image. With the measurement type linked or added to the image, the user can select a section of the intensity curve that is integrated to determine analysis results. Each image could have multiple measurements allowing users to analyze different intensity peaks separately. In addition, each measurement can be marked either as successful or not. Image analysis steps are demonstrated in Fig. 2.

While image analysis is performed manually, we have found that it does not take much time. The application supports different background subtraction algorithms, including rolling ball, that is rather effective for such cases as Ponceau staining. Lanes can be straight or curved, with the same width throughout the gel or individually adjusted. All these options allow users to find the best way to analyze their data in a way that fits their specific experiment. As all steps are recorded, it is easy to come back at any stage of the analysis and adjust it, for

example, change the width of the lane, intensity baseline, or section on the intensity curve that is integrated.

### Data analysis

Users can obtain the analysis results in either *raw* or *normalized* form. Here, the *raw* measurement data would contain an integrated intensity corresponding to a selected area of the measurement. This integrated intensity is not normalized. To take into account the amount of loaded sample in a lane, the user would have to divide the intensity by the protein content as a part of the further statistical analysis. As an alternative, *normalized* measurement values are available. Those values are obtained from the raw measurement values by relating these measurements to the measurements on the reference lanes. For that, the average reference measurement value is found by calculating the average for all reference samples on the image  $r$ , taking into account their protein content:

$$r = \frac{1}{R} \sum_{i=1}^R \frac{v_i}{m_i}, \quad (1)$$

where  $R$  is the number of successful reference samples in the image (could be just one),  $v$  and  $m$  correspond to the measurement value and protein content of the lane, respectively, and  $i$  corresponds to an index of the reference lanes that are marked as successful measurements. As soon as the reference value  $r$  is known (Eq. 1), the *normalized* measurement value  $w$  for each lane  $j$  would be

$$w_j = \frac{1}{r} \frac{v_j}{m_j}. \quad (2)$$

To get the measurement values  $v$  for each lane, the application first applies image cropping and background subtraction. All further analysis is performed on the background-subtracted image. Each lane is marked as a two-dimensional object on the image. As protein separation is expected to be according to the molecular weight, the vertical direction of the image, we first integrate the image intensity of the lane along its width. The result of this integration is shown to the user as a lane intensity profile graph which is intensity as a function of the image's vertical coordinate (Fig. 2 inset with lane intensity profile). This approach allows users to select curved lanes and preserves lane region selection if the lane has been moved. As a limitation, it does not allow to select lanes that would be horizontal at any of its segments. Next, the user can adjust the background reference for each lane separately. This is needed when the image background subtraction cannot fully take into account the heterogeneity of the background. At the last stage, after the user has selected integration bounds in the vertical

direction, the measurement value for the lane is found by integration of the difference between the lane intensity and background.

### Database structure and data export

The database schema layout is designed to ensure data consistency and flexibility in relations between gels and projects. For users, the data access was simplified through three views: a list of projects with their full path, a list of reference measurements for all gels, and a list of normalized values for all measurements. By using relationships between the tables and these views, it is easy to fetch the data from the database directly using SQL to limit the fetched records. Example SQL statements for fetching the data are given in the software repository and are referred to in the user manual. As some statistical analysis programs or data analysis frameworks, such as R, allow to import data from the databases directly, it is possible to use the provided SQL statements in the statistical analysis.

As an alternative to fetching the data from the database, users can export all data or data from a specific project to a spreadsheet. The spreadsheet will contain the same information as in the database and will be structured to simplify data analysis using statistical software. Depending on whether relative or absolute values are of interest, users can analyze raw data or normalized measurements. Note that the raw data does not have normalization to the protein content and has to be normalized by users. This is in contrast to the normalized measurements sheet, where protein content was taken into account.

### Validation

To test the software, we compared the estimation of expression levels and protein content performed by IOCBIO Gel and ImageJ Gels plugin, an established solution in the field. For testing, we used images acquired as a part of our earlier study [16] and asked three users to analyze the same images using both software solutions (Fig. 3). The used images are available as an additional file (see Additional file 1). Users obtained results that were similar to each other regardless of the software used. As illustrated in the example on Fig. 3A and B, estimates were mainly influenced by the complexity of determining the band border. For cases, where the bands were relatively well separated, as in the middle section of gel membrane in Fig. 3A, the spread of estimations was very small (Fig. 3B). In contrast, for bands close to the ladder with the signal of the ladder interfering with the band, the estimates had a larger deviation (Fig. 3B).

According to our tests, IOCBIO Gel and ImageJ Gels plugin resulted in very close estimates of the expression or protein content. As shown in Fig. 3C, when

plotted against each other, estimates by the different software solutions were located next to the equality line. Pearson's product-moment correlation between the estimates was statistically significant for all types of measurements ( $p < 0.001$ ) with  $r$  values of 0.99 (95% CI [0.98, 0.99]) for GAPDH, 0.99 (95% CI [0.99, 1.0]) for LTCC, and 0.89 (95% CI [0.85, 0.92]) for the Ponceau staining. The smaller correlation  $r$  for Ponceau staining was caused by curved lanes on the gel membranes and usage of larger regions when analyzing by IOCBIO Gel than in ImageJ Gels plugin, as done by Users 1 and 2. Such analysis of larger lane region was possible in IOCBIO Gel as it supports curved lanes. When done using the same regions of the images by the both software solutions, as done by User 3, the correlation  $r$  for Ponceau staining was 0.96 (95% CI [0.92, 0.98]).

In sum, as shown by the analysis, the estimation of the expression and protein content was the same in IOCBIO Gel and ImageJ Gels plugin.

### Reproducibility

In terms of reproducibility, there are two aspects that we addressed.

First, as IOCBIO Gel keeps all analysis steps in its database automatically, the analysis is reproducible in the sense that one can always open the old analysis and obtain the same result. This is in contrast to ImageJ Gels plugin where, as already explained in introduction, to our knowledge, users rarely record all the steps in such a detail that others could reproduce exactly the same results. So, as a result, there will be always some variability induced by the lack of analysis steps information.

Second, as a part of the reproducibility analysis, we wanted to test whether there was a difference in the variability of the results when the analysis was done by different users and compare that to the variability for ImageJ Gels plugin. For that, to quantify the variability, we used the standard deviation of the normalized estimated expression or protein content (data from Fig. 3). An example variability analysis for the image in Fig. 3A is shown in Fig. 4A. As shown in Fig. 4A, the variability depends on the lane with the more difficult lanes showing larger deviation in results obtained by the users. This was the same for the both software solutions. According to our analysis of all the recordings used (Fig. 4B), there are no statistically significant differences in variability between ImageJ Gels and IOCBIO Gel when users are asked to analyze the data for the first time. Thus, in variability of the results obtained by different users, IOCBIO Gel matches the established solution.

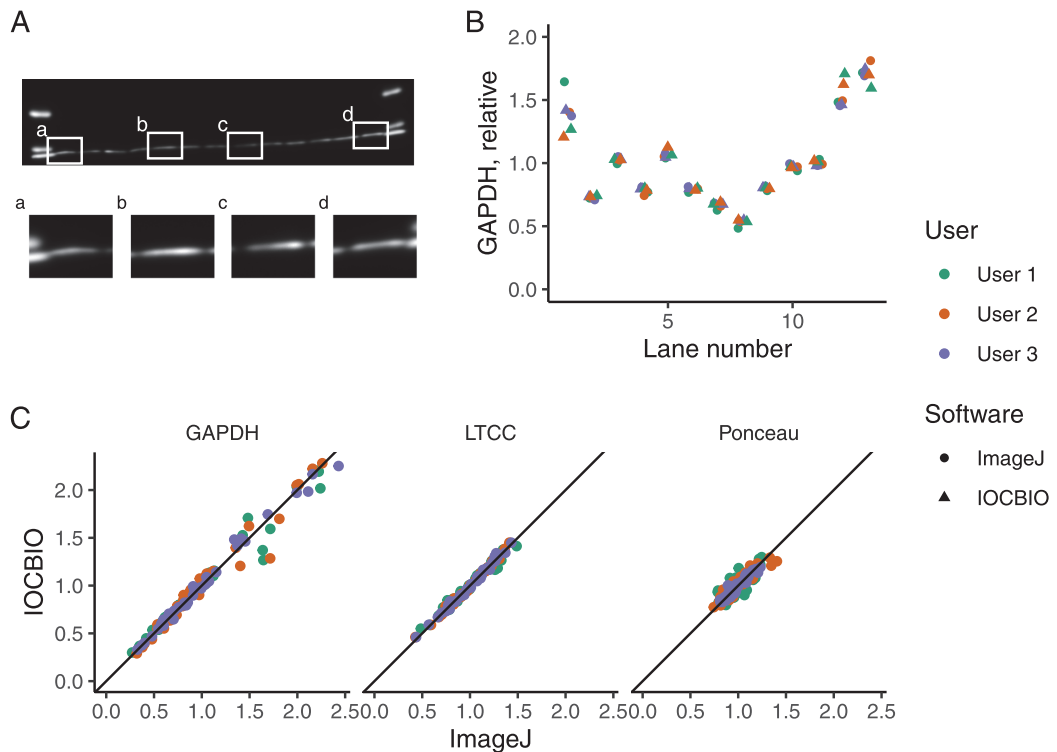


**Fig. 3** Comparison of analysis by IOC BIO Gel and ImageJ Gel plugin. **A** A representative example of a Western blot membrane labeled with primary and secondary antibodies to assess GAPDH expression (image acquired as a part of [16]). Insets a–d illustrate bands that are either easy to analyze due to clear separation between the lanes (b, c) and that are more complicated due to overlap with the ladder on the left (a) or on the right (d). **B** Results of the expression estimation performed by three users using either IOC BIO Gel or ImageJ Gels plugin to analyze the image shown in A. Notice the very small spread of the estimations in the most of the lanes and the larger spread on the first (shown in inset a of A) and the two last lanes (inset d in A corresponds to the last lane). **C** Expression of GAPDH, L-type calcium channel (LTCC), and estimation of protein loading using the Ponceau staining performed by IOC BIO Gel and ImageJ Gels plugin done on three separate membranes and by three different users (analyzed images acquired as a part of [16]). For comparison, the diagonal line corresponding to the equality in estimation is shown in black. Each dot on the plots corresponds to two estimations performed by specific user (shown by color) for the same lane on a gel using IOC BIO Gel (y-axis) and ImageJ Gels plugin (x-axis). Notice that the dots are distributed along the diagonal line with only small, occasional deviations. This demonstrates that the estimations by both software solutions are the same

### Comparison with available open-source software

In our lab, we started by using the ImageJ Gels plugin [2] for Western blotting analysis. It was relatively easy to use, and it did a good job when we had a few images to analyze. However, as we got more and more experiments to analyze, the rigidity of the plugin and the manual insertion of the values from the signal intensity measurements into our database became too time-consuming. In IOC BIO Gel, the measurements do not have to be re-typed, as the data are exported to either a spreadsheet or, in our case, to our database.

When comparing IOC BIO Gel with ImageJ Gels plugin, there is a major difference in the way how the

results are handled. ImageJ Gels plugin analyzes the results in the image-by-image manner. Thus, if one wants to relate the protein(s) of interest measurements to loading controls, the results have to be combined by the user from separate spreadsheets exported by ImageJ. To link that result to some sample ID, these spreadsheets would have to be tagged with the sample IDs as well. In IOC BIO Gel, sample information on the physical gel lane is entered separately and automatically linked to all measurements produced by the program. As a result, following the example above, it is trivial to relate the protein(s) of interest measurements

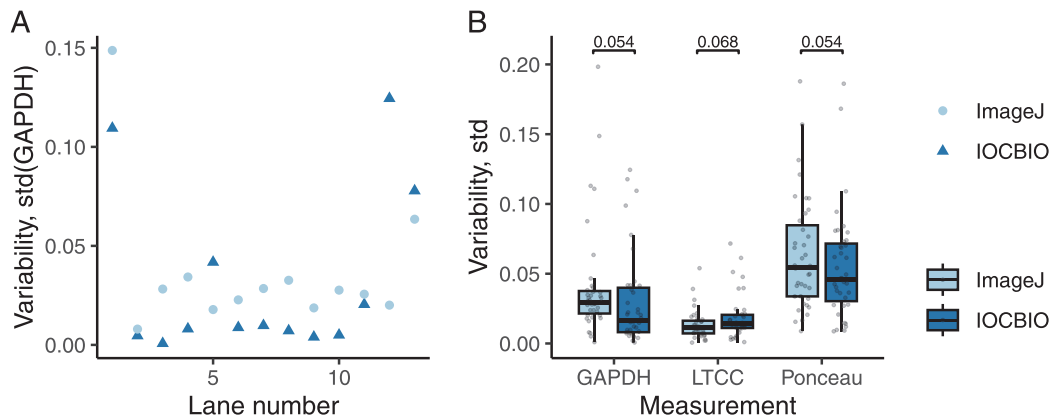


**Fig. 4** Variability of the analysis by IOC BIO Gel and ImageJ Gel plugin. Variability was estimated as the standard deviation between analysis results performed by different users. **A** Using the image from Fig. 3A, the variability was found for each gel lane when users were either using IOC BIO Gel or ImageJ Gels plugin. **B** Summary of variability estimates for all the gel membrane images that were used to estimate either GAPDH, LTCC, or protein content via Ponceau staining. The variability was found to be not statistically significantly different for the two software solutions (paired *t*-test results shown in the plot, number of compared pairs was  $n = 117$  for each case)

to loading controls by combining data from different images of the same sample probe at the statistical analysis stage.

The other major difference between IOC BIO Gel and other open-source solutions is in the way data are organized. Namely, all measurements related to a scientific study can be grouped together into a project, and it is simple to analyze data either by pulling it directly from the database or by exporting the whole project into a spreadsheet. This functionality is absent in ImageJ and has to be implemented by users through their data processing and organization separately.

IOC BIO Gel offers a fast way to re-analyze a dataset in the case when some correction is needed, such as changes in background subtraction or lane selection. Using the ImageJ Gels plugin, the user has to not only repeat the analysis, but all the new values have to be re-typed into our database or spreadsheets. With IOC BIO Gel, the data are re-analyzed, and the measurement values are updated in the database without the need for re-typing anything. The new data are quickly fetched using the same SQL statement as before. Thus, whereas ImageJ Gels works just fine if you have a few images to analyze, IOC BIO Gel is faster and more foolproof to use with small as well as large datasets. Taking into account that IOC BIO Gel tracks all the steps done while analyzing the gel, it ensures the reproducibility of the analysis at the same time.

Thus, through the automated link between measurements and metadata, IOC BIO Gel leads to a faster workflow that is less prone to human error and allows all data

to be stored in the same location. In addition, research laboratories are often joined by people for a short period, by students, post-docs, or even short-term interns. The use of a IOC BIO Gel with its central storage makes it possible to drastically limit the loss of data while offering the possibility of correcting the analysis, even after a person has left the laboratory.

#### Availability

In addition to the availability in source code form, the software is distributed as a prepared self-containing archive for MS Windows. For Linux and Mac OS, the software is distributed through the PyPi Python software repository. For installation instructions, see instructions at <https://iocbio.gitlab.io/gel>.

#### Future directions

One of the expected development directions would involve support for other database backends and image sources. The current selection was based on the expertise of our team and its use in our work environment. This includes the use of SQLite and PostgreSQL databases. However, support for the other databases is simple to add if it is supported by SQLAlchemy and if there is an interest. Other image sources can be envisioned as well, and their support will also be demand-driven.

Another line of further development is related to publishing the data. We plan to implement two separate export options for either targeting collaboration or assistance in the journal review process. As the application collects images and metadata describing gels,

it should be possible to export the data subset into an archive. Such an archive would be possible to send or distribute online, allowing others to examine and review the gel analysis steps used in the study together with the original gel images. In addition to the archive, we plan to implement report generation for assisting journals with the review of Western Blot and similar images. Many journals request authors to provide labeled Western blot images that would allow the journal to review the analysis steps. We plan to implement the generation of such labeled images that would tag the lanes and the used regions allowing users to provide the labeled images together with the original ones for journals to review.

Other further development will be planned based on the bottom-up approach, driven by the feedback of the users.

## Conclusions

We have developed IOCBIO Gel software that simplifies analysis and metadata entry related to analyzing Western Blot images. The software is not limited to Western blots and can be used to analyze any experimental data leading to a similar representation, i.e., the relationship between the image intensity and the sample. The software allows researchers to enter the data, make all the required image adjustment steps, and select areas of interest. All analysis steps and selections can be adjusted later and reviewed with ease. As a result of the analysis, the overall intensities are given and are associated with the samples in a simple way to incorporate into further statistical analysis.

The developed software addresses major shortcomings in analyzing specific but commonly used experimental protocols and ensures data analysis reproducibility used in these protocols.

## Methods

### Analysis of images

Images representing GAPDH and LTCC expression as well as protein content estimation using Ponceau staining taken from earlier measurements performed for [16]. From the dataset in that study, three membrane images were selected randomly and analyzed by three users. Each user selected the way for analysis as they commonly do, without any specific instructions. For comparison of results between ImageJ Gels plugin and IOCBIO Gel, estimated intensities for a lane were normalized by average intensity of all lanes obtained for that image by user using specific software. Thus, average intensities were found for each image/user/software combination. ImageJ Gels plugin was used as described in [17].

## Statistics

If not stated otherwise, statistics are reported using means  $\pm$  SD.  $p < 0.05$  was considered statistically significant. Differences between estimations performed by IOCBIO Gel and ImageJ Gels plugin were analyzed using paired samples  $t$ -test. Statistical analysis was performed in R [18].

## Supplementary Information

The online version contains supplementary material available at <https://doi.org/10.1186/s12915-023-01734-8>.

**Additional file 1.** Gel membrane images used for testing the software. Description of the data: Compressed archive contains images acquired from the same gel membrane either with Ponceau staining or after labeling with antibodies (GAPDH or LTCC). Name of each file in the archive contains the gel numbering and corresponding signal descriptor.

## Availability and requirements

Project name: IOCBIO Gel  
 Project home page: <https://iocbio.gitlab.io/gel>  
 Operating system(s): Linux, MacOS, Windows, others  
 Programming language: Python  
 Other requirements: Availability of Qt and SQLAlchemy on the platform, installed automatically  
 License: GNU GPLv3  
 Any restrictions to use by non-academics: as specified by the license

## Authors' contributions

JK, GM, and LK implemented the first version of the software; JK, ML, and MV revised the software and implemented the missing functionality; TR, KS, RB1 (Romain Bernasconi), and RB2 (Rikke Birkedal) tested the software; TR, KS, and RB1 benchmarked the software; RB2 wrote the software manual; PJ, ML, and MV supervised the project; MV and ML conceived the study; MV drafted the manuscript; ML and RB2 revised the manuscript. All authors read and approved the final manuscript.

## Funding

This work was supported by the Estonian Research Council (PRG1127).

## Availability of data and materials

All data generated or analyzed during this study are included in this published article and its supplementary information files.

## Declarations

### Ethics approval and consent to participate

Not applicable.

### Consent for publication

Not applicable.

### Competing interests

The authors declare that they have no competing interests.

Received: 17 April 2023 Accepted: 12 October 2023

Published online: 20 October 2023

## References

1. Kurien BT, Scofield RH. Western blotting. *Methods*. 2006;38:283–93.

2. Schneider CA, Rasband WS, Eliceiri KW. NIH Image to ImageJ: 25 years of image analysis. *Nat Methods*. 2012;9:671–5.
3. Morin A, Urban J, Adams PD, Foster I, Sali A, Baker D, et al. Shining light into black boxes. *Science*. 2012;336:159–60.
4. Morin A, Urban J, Sliz P. A quick guide to software licensing for the scientist-programmer. *PLoS Comput Biol*. 2012;8:e1002598.
5. Schooler JW. Metascience could rescue the ‘replication crisis.’ *Nat News*. 2014;515:9.
6. Wilkinson MD, Dumontier M, Aalbersberg IJJ, Appleton G, Axton M, Baak A, et al. The FAIR Guiding Principles for scientific data management and stewardship. *Sci Data*. 2016;3:1–9.
7. van der Walt S, Schönberger JL, Nunez-Iglesias J, Boulogne F, Warner JD, Yager N, et al. scikit-image: image processing in Python. *PeerJ*. 2014;2:e453.
8. Allan C, Burel J-M, Moore J, Blackburn C, Linkert M, Loynton S, et al. OMERO: flexible, model-driven data management for experimental biology. *Nat Methods*. 2012;9:245–53.
9. Bayer M. SQLAlchemy. In: Wilson G, Brown A, editors. The architecture of open source applications, volume II: structure, scale, and a few more fearless hacks. Mountain View: Aosabook.org; 2012.
10. Vendelin M, Laasmaa M, Kalda M, Branovets J, Karro N, Barsunova K, et al. IOCBIO Kinetics: an open-source software solution for analysis of data traces. *PLoS Comput Biol*. 2020;16:e1008475.
11. Laasmaa M, Karro N, Birkedal R, Vendelin M. IOCBIO sparks detection and analysis software. *PeerJ*. 2019;7:e6652.
12. Bauch A, Adamczyk I, Buczek P, Elmer FJ, Enimanev K, Glyzowski P, et al. openBIS: a flexible framework for managing and analyzing complex data in biology research. *BMC Bioinformatics*. 2011;12:468.
13. Wolstencroft K, Owen S, Krebs O, Nguyen Q, Stanford NJ, Golebiewski M, et al. SEEK: a systems biology data and model management platform. *BMC Syst Biol*. 2015;9:33.
14. Heinle CE, Gaultier NPE, Miller D, Purbojati RW, Lauro FM. MetaLIMS, a simple open-source laboratory information management system for small metagenomic labs. *Gigascience*. 2017;6:gix025.
15. Grand A, Geda E, Mignone A, Bertotti A, Fiori A. One tool to find them all: a case of data integration and querying in a distributed LIMS platform. *Database*. 2019;2019:baz004.
16. Laasmaa M, Branovets J, Barsunova K, Karro N, Lygate CA, Birkedal R, et al. Altered calcium handling in cardiomyocytes from arginine-glycine amidinotransferase-knockout mice is rescued by creatine. *Am J Physiol Heart Circ Physiol*. 2021;320:H805–25.
17. Stael S, Miller LP, Fernández-Fernández AD, Van Breusegem F. Detection of damage-activated metacaspase activity activities by western blot in plants. In: Klemenčič M, Stael S, Huesgen PF, editors. *Plant proteases and plant cell death: methods and protocols*. Springer US: New York; 2022. p. 127–37.
18. R Core Team. R: a language and environment for statistical computing. 2023.

## Publisher's Note

Springer Nature remains neutral with regard to jurisdictional claims in published maps and institutional affiliations.

**Ready to submit your research? Choose BMC and benefit from:**

- fast, convenient online submission
- thorough peer review by experienced researchers in your field
- rapid publication on acceptance
- support for research data, including large and complex data types
- gold Open Access which fosters wider collaboration and increased citations
- maximum visibility for your research: over 100M website views per year

**At BMC, research is always in progress.**

Learn more [biomedcentral.com/submissions](https://biomedcentral.com/submissions)



## Publication II

**Bernasconi, R**; Soodla, K; Sirp, A; Zovo, K; Kuhtinskaja, M; Lukk, T; Vendelin, M; Birkedal, R.  
**Higher AMPK activation in mouse oxidative compared to glycolytic muscle does not correlate with LKB1 or CaMKK $\beta$  expression.**

Am J Physiol - Endocrinology and Metabolism, Nov 2024, DOI: 10.1152/ajpendo.00261.2024.



## RESEARCH ARTICLE

Higher AMPK activation in mouse oxidative compared with glycolytic muscle does not correlate with LKB1 or CaMKK $\beta$  expression

Romain Bernasconi,<sup>1</sup> K arol Soodla,<sup>1</sup> Alex Sirp,<sup>2</sup> Kairit Zovo,<sup>3</sup> Maria Kuhtinskaja,<sup>4</sup> Tiit Lukk,<sup>3</sup>  
Marko Vendelin,<sup>1</sup> and Rikke Birkedal<sup>1</sup>

<sup>1</sup>Laboratory of Systems Biology, Department of Cybernetics, Tallinn University of Technology, Tallinn, Estonia; <sup>2</sup>Laboratory of Molecular Neurobiology, Department of Chemistry and Biotechnology, Tallinn University of Technology, Tallinn, Estonia; <sup>3</sup>Laboratory of Wood Chemistry, Department of Chemistry and Biotechnology, Tallinn University of Technology, Tallinn, Estonia; and <sup>4</sup>Laboratory of Analytical Chemistry, Department of Chemistry and Biotechnology, Tallinn University of Technology, Tallinn, Estonia

## Abstract

AMP-activated protein kinase (AMPK) is an energy-sensing serine/threonine kinase involved in metabolic regulation. It is phosphorylated by the upstream liver kinase B1 (LKB1) or calcium/calmodulin-dependent kinase kinase 2 (CaMKK $\beta$ ). In cultured cells, AMPK activation correlates with LKB1 activity. The phosphorylation activates AMPK, shifting metabolism toward catabolism and promoting mitogenesis. In muscles, inactivity reduces AMPK activation, shifting the phenotype of oxidative muscles toward a more glycolytic profile. Here, we compared the basal level of AMPK activation in glycolytic and oxidative muscles and analyzed whether this relates to LKB1 or CaMKK $\beta$ . Using Western blotting, we assessed AMPK expression and phosphorylation in soleus, gastrocnemius (GAST), extensor digitorum longus (EDL), and heart from C57BL6J mice. We also assessed LKB1 and CaMKK $\beta$  expression, and CaMKK $\beta$  activity in tissue homogenates. AMPK activation was higher in oxidative (soleus and heart) than in glycolytic muscles (gastrocnemius and EDL). This correlated with AMPK  $\alpha$ 1-isoform expression, but not LKB1 and CaMKK $\beta$ . LKB1 expression was sex dependent and lower in male than female muscles. CaMKK $\beta$  expression was very low in skeletal muscles and did not phosphorylate AMPK in muscle lysates. The higher AMPK activation in oxidative muscles is in line with the fact that activated AMPK maintains an oxidative phenotype. However, this could not be explained by LKB1 and CaMKK $\beta$ . These results suggest that the regulation of AMPK activation is more complex in muscle than in cultured cells. As AMPK has been proposed as a therapeutic target for several diseases, future research should consider AMPK isoform expression and localization, and energetic compartmentalization.

**NEW & NOTEWORTHY** It is important to understand how AMP-activated kinase, AMPK, is regulated, as it is a potential therapeutic target for several diseases. AMPK is activated by liver kinase B1, LKB1, and calcium/calmodulin-dependent kinase kinase 2, CaMKK $\beta$ . In cultured cells, AMPK activation correlates with LKB1 expression. In contrast, we show that AMPK-activation was higher in oxidative than glycolytic muscle, without correlating with LKB1 or CaMKK $\beta$  expression. Thus, AMPK regulation is more complex in highly compartmentalized muscle cells.

AMPK; CaMKK $\beta$ ; glycolytic muscle; LKB1; oxidative muscle

## INTRODUCTION

The AMP-activated protein kinase (AMPK) is a ubiquitous serine/threonine protein kinase known as the master regulator of metabolism (1). Due to its enhancement of catabolism and inhibition of anabolism, activation of AMPK has been suggested as a therapeutic target for several diseases such as some types of cancer, tissue inflammation, and cardiovascular and metabolic diseases (2–10).

The phosphorylation of AMPK is the main regulator of its kinase activity (11). Therefore, the extent to which AMPK is phosphorylated is often used as a measure of its activation, and this is also used throughout the present paper.

The main AMPK kinase is liver kinase B1 (LKB1), which phosphorylates AMPK on Thr<sup>172</sup>. This is promoted by an increase in the concentrations of AMP or ADP, whose binding to AMPK changes its allosteric conformation, allowing its phosphorylation by LKB1 (12, 13). Conversely, ATP binding can prevent AMPK activation by obstructing AMP attachment and promoting its dephosphorylation by phosphatases (11, 14, 15). AMPK can also be activated by glucose deprivation, independent of AMP/ADP-levels, as the associated decline in fructose-1,6-bisphosphate promotes the aldolase-dependent activation of AMPK by LKB1 (16). Although it has been suggested that transforming growth factor  $\beta$  activated kinase-1 (TAK1) can activate AMPK directly



Correspondence: R. Birkedal (rikke@sysbio.ioc.ee).

Submitted 11 July 2024 / Revised 14 October 2024 / Accepted 1 November 2024



(17, 18), others argue that TAK1 is required for the activation of AMPK by LKB1 (19). In cultured cells, the AMPK activity correlates with the LKB1 expression (13).

Alternatively, AMPK can be activated by an increase in  $\text{Ca}^{2+}$ , which leads to its phosphorylation on Thr<sup>172</sup> by calcium/calmodulin-dependent protein kinase 2 (CaMKK $\beta$ ) (20–22). CaMKK $\beta$  is mainly expressed in the brain (23), and its role in muscle tissue is controversial (21, 22, 24).

LKB1 and CaMKK $\beta$  differ in potency depending on the isoform composition (25). AMPK is heterotrimeric and composed of a catalytic  $\alpha$  subunit, a regulatory  $\beta$  subunit, and a  $\gamma$  subunit. Each of the subunits occurs as multiple isoforms ( $\alpha 1$ ,  $\alpha 2$ ,  $\beta 1$ ,  $\beta 2$ ,  $\gamma 1$ ,  $\gamma 2$ , and  $\gamma 3$ ), allowing the formation of 12 different  $\alpha\beta\gamma$  heterotrimer combinations. AMPK $\alpha 1$  seems to be more sensitive to  $\text{Ca}^{2+}$  signaling (21), whereas AMPK $\alpha 2$  is more likely to interact with LKB1 (26).

In muscle tissue, AMPK serves an important role in adjusting metabolism according to the needs, which in turn depends on mechanical performance. AMPK increases the cellular uptake of glucose and fatty acids by promoting the translocation of glucose transporter (GLUT)4 and CD36 transporters to the cell membrane (27–29). In addition, it enhances the oxidation of fatty acids through its inhibition of acetyl-CoA carboxylase (ACC) (30, 31). Finally, it stimulates mitogenesis through its phosphorylation of peroxisome proliferator-activated receptor- $\gamma$  coactivator-1 $\alpha$  (PGC-1 $\alpha$ ) (32). It is involved in the regulation of muscle phenotype, as demonstrated in unloading studies, where inactivity is associated with a decline in AMPK activity and a decrease in oxidative enzymes (33–37). Thus, inactivity leads to a shift from oxidative to glycolytic phenotype.

The basal AMPK activation in different muscle types has, to the best of our knowledge, never been directly compared. The present study aimed to address this by assessing the expression and activation of AMPK in oxidative and glycolytic muscles. We expected a greater AMPK activation in oxidative muscles to maintain the phenotype, but we were uncertain whether this was regulated energetically or through  $\text{Ca}^{2+}$ . Energetically, oxidative muscles are characterized by low and stable levels of ADP, whereas glycolytic muscles show greater fluctuations. The heart exhibits a stable ADP-concentration over a range of workloads when oxygen consumption increases (38). Among skeletal muscles, the oxidative soleus also demonstrates remarkable metabolic stability during increases in workload, whereas in glycolytic muscles such as the gastrocnemius (GAST), the levels of ADP and  $\text{P}_i$  increase significantly during exercise (39–41). In terms of  $\text{Ca}^{2+}$ , oxidative muscles receive more continuous daily electrical stimulation (42), triggering  $\text{Ca}^{2+}$ -efflux from the sarcoplasmic reticulum to the cytosol. Furthermore, although AMPK $\alpha 2$  is the most abundant isoform in skeletal muscle, the expression of the more  $\text{Ca}^{2+}$ -sensitive AMPK $\alpha 1$  is higher in oxidative skeletal muscle (25, 43). While AMPK $\alpha 2$  represents 90% and 60%, AMPK $\alpha 1$  represents 10% and 40% of the AMPK expression in glycolytic and oxidative muscles, respectively (43). Thus, we speculated whether the mechanisms of AMPK activation differed between muscle types with energetic activation through LKB1 perhaps being more important in glycolytic muscle and  $\text{Ca}^{2+}$  activation through CaMKK $\beta$  being more important in oxidative muscle.

Using Western blotting, we compared AMPK expression and activation in four different muscles: the oxidative heart and soleus (SOL) muscles, the glycolytic extensor digitorum longus (EDL), and gastrocnemius (GAST). When we found that the AMPK activation was significantly higher in oxidative than glycolytic muscles, we assessed the expression of the upstream regulators, LKB1 and CaMKK $\beta$ , and the ability of CaMKK $\beta$  in tissue lysates to phosphorylate AMPK.

## METHODS

### Ethics

All animal procedures were carried out according to directive 2010/63/EU of the European Parliament and had been approved by the Project Authorization Committee for Animal Experiments in the Estonian Ministry of Rural Affairs.

### Animals

Twenty-five C57BL6J mice, 11 males and 14 females, were kept and bred in the animal facility of Tallinn University of Technology, in a 12:12-h light-dark cycle, and an ambient temperature of 22–23°C with free access to food (V1534-000 rat/mouse maintenance from Ssniff Spezialdiäten GmbH, Germany) and water.

The mice were anesthetized with a ketamine/dexmedetomidine mixture (150 mg·kg<sup>-1</sup> and 0.5 mg·kg<sup>-1</sup>, respectively) and received an injection of 250 U of heparin to prevent blood coagulation. When the toe-pinch reflex was absent, the animal was euthanized by cervical dislocation. The brain, heart, gastrocnemius, soleus, and EDL were excised and immediately placed in an ice-cold wash solution consisting of the following (in mM): 117 NaCl, 5.7 KCl, 1.5 KH<sub>2</sub>PO<sub>4</sub>, 4.4 NaHCO<sub>3</sub>, 1.7 MgCl<sub>2</sub>, 21 HEPES, 20 taurine, 11.7 glucose, and 10 2,3-butanedione monoxime (pH was adjusted to 7.4 with NaOH). After cleaning and weighing, the tissues for Western blot were snap frozen in liquid nitrogen and stored at –80°C.

### Homogenization for Western Blotting

Frozen muscles were homogenized in a glass homogenizer at a concentration of 20 mg·mL<sup>-1</sup> of extraction buffer (50 mM Tris, 150 mM NaCl, 2% SDS, 1 mM DTT) with protease and phosphate inhibitor cocktails (cOmplete Mini and PhosSTOP, respectively, both from Roche, Merck). The protein concentration was determined spectrophotometrically. Ten microliters of tissue extract were diluted 1:5 and incubated at 80°C for 30 min. After heating, the protein content was determined in a NanoDrop 2000c spectrophotometer (Thermo Fisher Scientific). The protein content of each sample was measured at least three times, and the results were averaged. The absorption at 280 nm was background corrected by subtracting the absorption at 330 nm, and protein content was calculated using the molecular weight and extinction coefficient of BSA (66,400 g·mol<sup>-1</sup> and 43,824 M<sup>-1</sup>·cm<sup>-1</sup>, respectively). The protein content of the tissue extract was corrected by the protein content of the extraction buffer.

### Western Blotting

Twenty micrograms of protein (40  $\mu\text{g}$  for AMPK $\alpha 1$ ) were loaded in a polyacrylamide SDS-page gel (4% stacking gel,

12% separating gel) and separated using a PowerPac HC power supply (Bio-Rad Laboratories), run at 60 V for ~30 min and followed by 120 V for ~1 h. Proteins were transferred onto a nitrocellulose blotting membrane (0.45 μm) using the Bio-Rad Turbo Transfer System. Membranes were stained with 0.1% Ponceau solution to stain the proteins and imaged in an Image Quant LAS 400 Imager for normalization. Then, membranes were washed with 0.1% Tween-20 (Tris-buffered saline-Tween-20, TBST) three times for 10 min and blocked with 5% milk in TBS-T solution for an hour on a roller machine at room temperature. Primary antibodies in 5% BSA TBS-T solution were incubated overnight on a roller machine at 4°C followed by three washes with TBS-T and a 1-h incubation of secondary antibody in 5% milk TBS-T solution. Membranes were washed three times for 10 min with TBS-T and incubated with Bio-Rad Clarity Western ECL substrate for 5 min. Finally, membranes were imaged with an Image Quant LAS 400 imager.

### Phosphorylation of AMPK by CaMKKβ in Tissue Lysates

To assess the phosphorylation of AMPK by CaMKKβ in tissue lysates, we used a modification of the assay by Yurimoto et al. (44), where CaMKKβ was activated by CaCl<sub>2</sub> and calmodulin (CaM) to phosphorylate a downstream target, in our case the mutant AMPKα2 K45R protein, which is catalytically inactive (45, 46) and does not inhibit CaMKKβ autonomous activity (47). This phosphorylation was then inhibited by STO-609, which is a specific inhibitor of CaMKK that can be used as an inhibitor of AMPK phosphorylation by CaMKKβ (20, 48). CaMKKβ has a three times lower IC<sub>50</sub> than CaMKKα (49). This assay was first tested with recombinant CaMKKβ and brain lysate (see Supplemental Materials), before being performed with muscle lysate.

### Recombinant Proteins

Recombinant Calmodulin bovine (CaM) was obtained from Sigma-Aldrich (C4874-0.5 mg). Recombinant rat AMPKα2 K45R mutant and rat CaMKKβ gene sequence were expressed in *E. coli*, as described in the Supplemental Materials.

The expression of CaMKKβ and AMPKα2 K45R was verified with specific antibodies (see Supplemental Figs. S4 and S5, respectively). Both proteins exhibited truncated versions or unspecific signals. We also verified that AMPKα2 K45R was not phosphorylated in *E. coli* (Supplemental Fig. S5).

### Assay with Tissue Lysate

Frozen muscles and brain were lysed in nondenaturing extraction buffer [50 mM Tris, 150 mM NaCl, 1% Nonidet P40, 1 mM DTT, 1 mM EGTA, 1 mM EDTA, protease, and phosphate inhibitor cocktails (cOMpleteMini and PhosSTOP)]. Muscle and brain lysates were tested in 40 μL of kinase

activity buffer (50 mM HEPES, 10 mM magnesium acetate, 2 mM DTT, 1 mM ATP, pH = 7.5) under different conditions:

**Lysate:** 5 μL of tissue lysate was added to the kinase activity buffer.

**Lysate + AMPK:** 5 μL of tissue lysate with 2 μL of purified rat AMPKα2 K45R.

**Lysate + STO + AMPK:** 5 μL of tissue lysate was incubated 10 min before with 5 μM STO-609 acetic acid (diluted in DMSO). After 10 min, 2 μL of rat AMPKα2 K45R was added.

**Lysate + CaCl<sub>2</sub> + CaM + AMPK:** 5 μL of tissue lysate was incubated with 1 μM of CaM and 2 mM calcium chloride to stimulate CaMKKβ activity. This was followed by the addition of 2 μL of rat AMPKα2 K45R.

**Lysate + STO + CaCl<sub>2</sub> + CaM + AMPK:** 5 μL of tissue lysate was incubated 10 min before with 5 μM STO-609 acetic acid. This was followed by 1 μM of CaM and 2 mM calcium chloride, and 2 μL of rat AMPKα2 K45R recombinant protein.

All preparations were incubated for 30 min at 30°C, and the reaction was stopped by the addition of 2% SDS (3.33 μL of 30% SDS). A total of 17.5 μL of each preparation was immediately mixed with 10 μL of SDS page buffer (90% 4× Laemmli and 10% β-mercaptoethanol) and loaded on a polyacrylamide gel (4% stacking gel, 12% separating gel). The western blot procedure used is the same as described earlier, and the p-AMPK antibody was used as described in Table 1.

### Data Analysis

Western blot images were analyzed using IOC BIO GEL software (50). For each sample, the antibody (AB) signal intensity was normalized to the Ponceau (P) signal intensity ( $AB_{\text{sample}}/P_{\text{sample}}$ ), and this was normalized to the averaged  $AB_{\text{RF}}/P_{\text{RF}}$  of the reference samples called “RF” (two per gel). For Western blots of total AMPK, phosphorylated AMPK, AMPKα1, and LKB1, we used the same reference sample throughout. This was a mix of several muscle lysates (heart, gastrocnemius, EDL, and soleus) from both males and females. Using the same reference throughout allowed us to directly compare the results from different gels. The reference sample used to compare CaMKKβ gels was 10 μg of brain lysate from a single, male individual.

In Fig. 2, the total AMPK expression (T-AMPK) in each sample was related to that of the reference (RF) sample and was calculated as  $(T\text{-AMPK}_{\text{sample}}/P_{\text{sample}})/(T\text{-AMPK}_{\text{RF}}/P_{\text{RF}})$ .

In Fig. 3, the AMPK activation was calculated as the ratio of phosphorylated AMPK (p-AMPK) to total AMPK (T-AMPK). The AMPK activation in each sample was related to that of the reference sample (RF) and was calculated as  $[(p\text{-AMPK}_{\text{sample}}/P_{\text{sample}})/(p\text{-AMPK}_{\text{RF}}/P_{\text{RF}})]/[(T\text{-AMPK}_{\text{sample}}/P_{\text{sample}})/(T\text{-AMPK}_{\text{RF}}/P_{\text{RF}})]$ .

**Table 1.** Antibodies and their dilutions used in this study

Protein of Interest	Company	Catalogue Number	RR-ID	Dilution	Secondary Antibody	Dilution of Secondary
Total AMPK	Cell Signaling	2532	AB_330331	1:1,000	Anti-rabbit IgG	1:10,000
AMPKα1	Abcam	Ab32047	AB_722764	1:500	111-035-045 Jackson	1:10,000
p-AMPK Thr <sup>172</sup>	Cell Signaling	2535	AB_331250	1:1,000	ImmunoResearch	1:10,000
LKB1	Cell Signaling	3047	AB_2198327	1:1,000		1:10,000
CaMKKβ	GeneTex	GTX108305	AB_1949818	1:500		1:10,000

**Table 2.** Morphological characteristics of male and female mice used in this study

Sex	Age, days	Body Weight, g	Body Length, cm	Tibial Length, cm
Females, <i>n</i> = 14	232 ± 55	24.7 ± 4.2	8.9 ± 0.6	2.16 ± 0.06
Males, <i>n</i> = 11	226 ± 50	33.4 ± 3	9.2 ± 0.3	2.25 ± 0.1
Bayesian <i>T</i> test	NS	###	NS	NS

Values are shown in means ± SE. Males and females were compared using a Bayesian *T* test. ###BF ≥ 100, extremely strong evidence.

In Fig. 5, the ratio of AMPKα1 to total AMPK (T-AMPK) in each sample was related to that of the reference sample (RF) and was calculated as [(AMPKα1<sub>sample</sub>/P<sub>sample</sub>)/(AMPKα1<sub>RF</sub>/P<sub>RF</sub>)]/[(T-AMPK<sub>sample</sub>/P<sub>sample</sub>)/(T-AMPK<sub>RF</sub>/P<sub>RF</sub>)].

In Fig. 7, the LKB1 expression in each sample was related to that of the reference sample (RF) and was calculated as (LKB1<sub>sample</sub>/P<sub>sample</sub>)/(LKB1<sub>RF</sub>/P<sub>RF</sub>).

In Fig. 9, the CaMKKβ expression in each sample was related to that of the reference sample (RF) and was calculated as (CaMKKβ<sub>sample</sub>/P<sub>sample</sub>)/(CaMKKβ<sub>RF</sub>/P<sub>RF</sub>).

In Fig. 11, the amount of phosphorylated AMPK (p-AMPK) under different conditions was related to that in the lysate alone and was calculated as (p-AMPK<sub>condition</sub>/P<sub>condition</sub>)/(p-AMPK<sub>lysate</sub>/P<sub>lysate</sub>).

Moreover, each primary antibody had been previously calibrated with the reference sample “RF” and different muscle samples at different protein and antibody concentrations to ensure that the antibody responded in a linear fashion to an increase in protein. This allowed us to be certain that we were below the maximal binding threshold. Each Western blot sample was measured at least twice (except AMPKα1 and CaMKKβ) and the average is shown as a single data point. Outliers were measured a third time or deleted from the dataset.

Kinase activity images were analyzed using ImageJ software. For the experiments with tissue lysates, the results from each condition, AB<sub>condition</sub>/P<sub>condition</sub>, were further normalized to the result from the lysates alone, AB<sub>lysate</sub>/P<sub>lysate</sub>.

**Statistics**

The graphs are shown as box-and-whisker plots according to the Tukey notation and were made using R software.

Statistical analyses were performed in JASP software using Bayesian statistical tests (51). For the assessments of expression and phosphorylation, we first used Bayesian two-way ANOVA to test the effects of sex, muscle, and sex × muscle. Significance is shown using an asterisk, \*. Then, Bayesian post hoc single comparisons were performed to assess differences between muscles (significance shown using daggers, †) and differences between sexes (significance shown using hashtags, #). Kinase activity gels were statistically analyzed with single Bayesian independent *T* tests between the conditions for each tissue type (brain, soleus, gastrocnemius, and heart), and significance is shown using daggers, †.

For statistical significance, we considered BF < 10 not significant (NS), 10 ≤ BF < 30 strong evidence (\* or † or #), 30 ≤ BF < 100 very strong evidence (\*\* or †† or ##), and BF ≥ 100 extremely strong evidence (\*\*\*) or ††† or ###) as in Ref. 52.

**RESULTS**

**Morphological Data**

Table 2 shows the morphological characteristics of the mice used for the Western blot experiments. The body weight was significantly lower in females compared with males. Age, body length, and tibial length were not significantly different between males and females.

**AMPK Is More Activated in Oxidative Muscles**

To determine whether the basal activation of AMPK differed between the muscle types, we assessed the levels of total and phosphorylated (Thr<sup>172</sup>) AMPK. An illustrative blot is shown in Fig. 1, but for the experiments, the samples were loaded in random order. The total AMPK expression was normalized to the overall protein staining by Ponceau (Fig. 1C).

Total AMPK expression was similar in EDL, gastrocnemius, and heart, but it was lower in the soleus (Fig. 2).

AMPK activation was determined as the ratio of phosphorylated AMPK-Thr<sup>172</sup> to total AMPK for each sample. The overall results are shown in Fig. 3 and demonstrate that AMPK activation was significantly higher in oxidative (soleus and heart) than in glycolytic muscles (EDL and gastrocnemius).

**AMPKα1 Isoform Is More Expressed in Oxidative Muscles**

To evaluate the proportion of AMPKα1 within the different muscle types, we measured AMPKα1 expression and normalized the signal to the total AMPK expression. A representative picture is shown in Fig. 4, and the overall dataset is summarized in Fig. 5. The AMPKα1/total AMPK ratio was significantly higher in the oxidative than in the glycolytic muscles, in agreement with the findings of Treebak et al. (43). The relative expression of AMPKα2 was not assessed, but we expect the relative contributions of AMPKα1 and AMPKα2 to sum to unity, as also shown in Ref. 25.

**LKB1 Expression Differs between Sexes but Cannot Explain the Muscle-Specific Differences in AMPK Activation**

To explain the tissue-specific difference in AMPK activation, we looked into the expression of LKB1, which is considered the main activator of AMPK (12, 13). A representative picture of a Western blot for LKB1 is shown in Fig. 6, and the averaged results are shown in Fig. 7. Overall, the LKB1 expression was

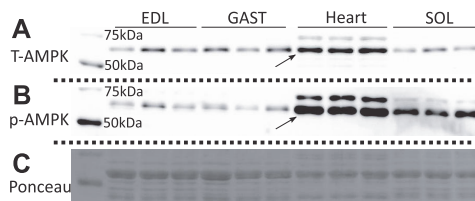


**Figure 1.** Total and phosphorylated AMP-activated protein kinase (AMPK) in extensor digitorum longus (EDL), gastrocnemius (GAST), heart, and soleus. Illustrative pictures showing the Western blots of total AMPK (A), p-AMPK Thr<sup>172</sup> (B), and Ponceau protein staining (C). 20 μg of protein from each sample was loaded into each well.

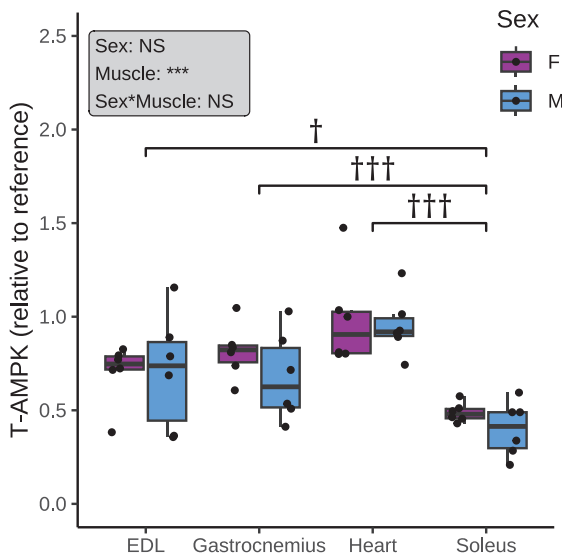


**Figure 2.** Total AMP-activated protein kinase (AMPK) expression in extensor digitorum longus (EDL), gastrocnemius, heart, and soleus. Soleus had a significantly lower AMPK expression than the other muscles. The total AMPK expression (T-AMPK) in each sample was normalized to that of the reference sample (mix of muscle lysates, calculation specified in MATERIALS AND METHODS, *Data Analysis*). A two-way Bayesian ANOVA tested the impact of sex, muscles, and sex  $\times$  muscles, and the results are shown in the gray box on the top left. The significant impact of muscle was followed up by *T* tests between muscle pairs, and these results are indicated with brackets. Significance notation: \*ANOVA, and †*T* tests between muscles (including both subgroups Male and Female). †10  $\leq$  BF < 30, strong evidence; \*\*\* or ††† BF  $\geq$  100, extremely strong evidence. Each dot represents an average of at least two measurements for the same sample. *n* = 6 for each sex subgroup and *n* = 12 for each muscle group.

higher in the muscles of female compared with male mice (Bayesian two-way ANOVA, 30  $\leq$  BF < 100, very strong evidence). There was a significant effect of muscle type (Bayesian two-way ANOVA, 30  $\leq$  BF < 100, very strong evidence), as LKB1 expression was higher in the heart compared with gastrocnemius. However, LKB1 expression did not correlate with the AMPK activation (Supplemental Fig. S3).

**CaMKK $\beta$  Is Present in the Heart but Poorly Expressed in Skeletal Muscle**

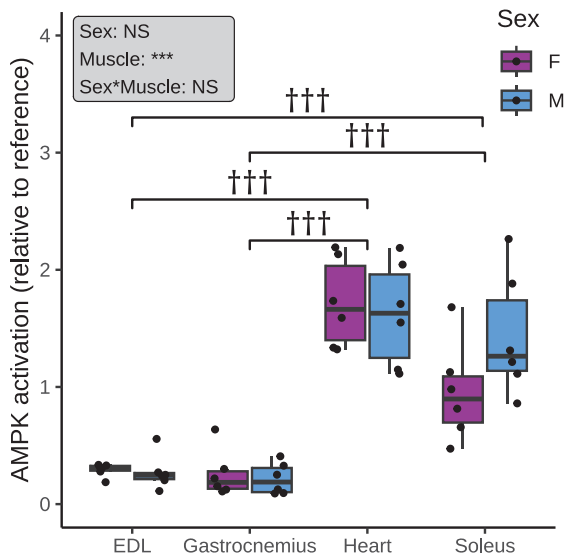
CaMKK $\beta$  is the second-most studied AMPK-kinase, activated by Ca<sup>2+</sup> and CaM. We assessed the overall CaMKK $\beta$  expression in the different muscles and used the brain as a positive control. The raw Western Blot pictures (Fig. 8) and the summarized data (Fig. 9) showed that the expression of CaMKK $\beta$  was very low in all skeletal muscle types, but higher in the heart.

**In Muscle Lysate, AMPK Phosphorylation Is Not Increased by CaMKK $\beta$  Stimulation, but by STO-609 Itself**

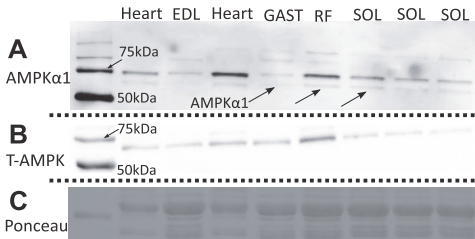
We assessed whether AMPK could be phosphorylated through the Ca<sup>2+</sup>/CaM/CaMKK $\beta$  signaling pathway in muscle lysate. This assay was tested with recombinant CaMKK $\beta$ ,

where CaCl<sub>2</sub> and CaM increased the amount of phosphorylated AMPK, and this was inhibited by STO-609, as expected (see Supplemental Figs. S6 and S7). The assay was also tested with brain lysate. In males, but not females, the addition of CaCl<sub>2</sub> and CaM to stimulate CaMKK $\beta$  led to a modest, but significant increase in AMPK phosphorylation and this was reduced by the addition of STO-609. However, the effect of STO-609 was diminished by the fact that STO-609 alone tended to increase the amount of phosphorylated AMPK (see Supplemental Figs. S8 and S9).

We performed the same assay with lysate of different muscles: gastrocnemius, soleus, and heart. EDL was not included in this assay, as the muscles from one animal are too small to provide enough homogenate for all conditions. Furthermore, we assumed that the results from gastrocnemius were representative of the situation in glycolytic muscles. Representative Western blots of p-AMPK are shown in Fig. 10, and the summarized data are shown in Fig. 11. It is important to note that the data from all three muscles show the same overall pattern. In gastrocnemius, none of the effects were significant, because of the large spread of the data, but the trend is the same as in soleus and heart, and we will describe the data overall. The addition of AMPK $\alpha$ 2 K45R to the lysate did not increase the amount of phosphorylated AMPK. As a control, we added STO to lysate and AMPK and

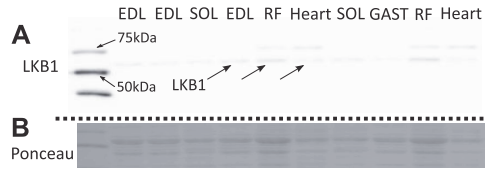


**Figure 3.** AMPK activation in extensor digitorum longus (EDL), gastrocnemius, heart, and soleus. AMPK is more activated in the oxidative heart and soleus than in the glycolytic gastrocnemius and EDL. The AMPK activation [phosphorylated AMP-activated protein kinase (AMPK)/total AMPK] in each sample was normalized to that of the reference sample (mix of muscle lysates, calculation specified in MATERIALS AND METHODS, *Data Analysis*). A two-way Bayesian ANOVA tested the impact of sex, muscles, and sex  $\times$  muscles, and the results are shown in the gray box on the top left. The significant impact of muscle was followed up by *T* tests between muscle pairs, and these results are indicated with brackets. Significance notation: \*ANOVA, and †*T* tests between muscles (including both subgroups Male and Female). \*\*\* or †††BF  $\geq$  100, extremely strong evidence. Each dot represents an average of at least two measurements for the same sample. *n* = 6 for each sex subgroup and *n* = 12 for each muscle group.



**Figure 4.** Representative picture of AMP-activated protein kinase (AMPK) $\alpha$ 1 expression in extensor digitorum longus (EDL), gastrocnemius (GAST), heart, and soleus (SOL). RF is the reference sample (mix of muscle lysates). 40  $\mu$ g of protein were loaded into each well. In these blots, there were nonspecific bands. We analyzed the band between the 50 and 75 kDa markers (shown with arrows), as AMPK $\alpha$ 1 has a predicted weight of  $\sim$ 63 kDa. In Supplemental Fig. S1, we show the same picture with enhanced contrast, where the analyzed bands are more visible. *A*: Western blot of AMPK $\alpha$ 1 in different tissues. *B*: total AMPK expression in the same samples. *C*: Ponceau staining of protein on the AMPK $\alpha$ 1 blot.

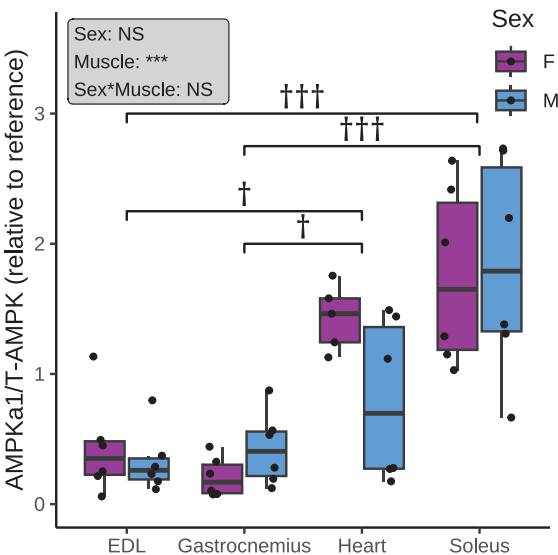
were surprised to see that the addition of STO-609 increased AMPK phosphorylation, but this only reached significance in soleus and heart (in the latter only relative to lysate alone). A similar trend was observed with brain lysate (Supplemental



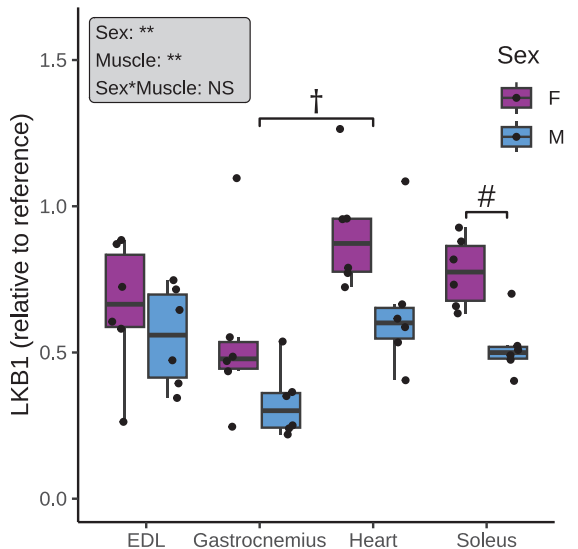
**Figure 6.** Representative picture of liver kinase B1 (LKB1) expression in extensor digitorum longus (EDL), gastrocnemius (GAST), heart, and soleus (SOL). RF is the reference sample (mix of muscle lysates). 20  $\mu$ g of protein were loaded into each well. We analyzed the band just above the 50 kDa markers (shown with arrows), as LKB1 has a predicted weight of  $\sim$ 55 kDa. In Supplemental Fig. S2, we show the same picture with enhanced contrast, where the analyzed bands are more visible. *A*: Western blot of LKB1 in different tissues. *B*: Ponceau protein staining from the same blot.

Fig. S9). In contrast, the addition of CaM and CaCl<sub>2</sub> to stimulate the CaMKK $\beta$  activity had no significant effect on AMPK phosphorylation relative to lysate alone or lysate and AMPK (Fig. 11).

As intracellular signaling in many cases depends on the colocalization of proteins involved in the signaling cascade, we speculated whether keeping the muscle structure and the



**Figure 5.** AMP-activated protein kinase (AMPK) $\alpha$ 1/total (T)-AMPK in extensor digitorum longus (EDL), gastrocnemius, heart, and soleus. AMPK $\alpha$ 1 is more abundant in oxidative than glycolytic muscles. The AMPK $\alpha$ 1 expression in each sample was normalized to that of the reference sample (mix of muscle lysates, calculation specified in MATERIALS AND METHODS, *Data Analysis*). A two-way Bayesian ANOVA tested the impact of sex, muscles, and sex  $\times$  muscles, and the results are shown in the gray box on the top left. The significant impact of muscle was followed up by *T* tests between muscle pairs, and these results are indicated with brackets. Significance notation: \*ANOVA, †*T* tests between muscles (including both subgroups Male and Female), ††0  $\leq$  BF < 30, strong evidence; \*\*\* or ††† BF  $\geq$  100, extremely strong evidence. Each dot represents a single measurement of one sample.  $n = 6$  for each sex subgroups and  $n = 12$  for each muscle groups.



**Figure 7.** Liver kinase B1 (LKB1) expression in extensor digitorum longus (EDL), gastrocnemius, heart, and soleus. LKB1 expression was higher in muscles from female mice, and it was higher in the heart compared with gastrocnemius. The LKB1 expression in each sample was normalized to that of the reference sample (mix of muscle lysates, calculation specified in MATERIALS AND METHODS, *Data Analysis*). A two-way Bayesian ANOVA tested the impact of sex, muscles, and sex  $\times$  muscles, and the results are shown in the gray box on the top left. The significant impact of muscles and sex was followed up by *T* tests between muscle pairs, and *T* tests between males and females for each muscle, and these results are indicated with brackets. Significance notation: \*ANOVA, †*T* tests between muscles (including both subgroups Male and Female), and †† tests of sex difference. † or ††0  $\leq$  BF < 30, strong evidence; \*\*30  $\leq$  BF < 100, very strong evidence. Each dot represents an average of at least two measurements for the same sample.  $n = 6$  for each sex subgroups and  $n = 12$  for each muscle groups.

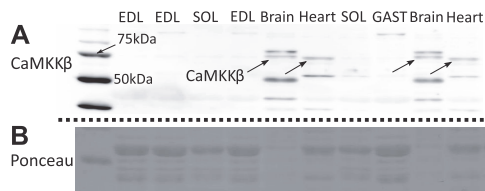


**Figure 8.** Representative picture of calcium/calmodulin-dependent protein kinase kinase 2 (CaMKKβ) expression in extensor digitorum longus (EDL), gastrocnemius (GAST), heart, and soleus (SOL), with brain as a reference and positive control. 20 μg of protein were loaded for muscles samples and 10 μg for brain. CaMKKβ was found just below 75 kDa (shown with arrows) as in previous works (20, 47). A: Western blot of CaMKKβ expression in different tissues. B: Ponceau protein staining.

relative position of CaMKKβ to AMPK would affect the results. To address that, we incubated intact soleus fibers with caffeine to stimulate Ca<sup>2+</sup> release in the absence and presence of STO-609 and assessed the AMPK phosphorylation (Supplemental Fig. S10). We did not observe any effect of caffeine or STO-609 on AMPK phosphorylation.

Overall, our results suggest that CaMKKβ did not phosphorylate AMPK in any of the muscle homogenates and

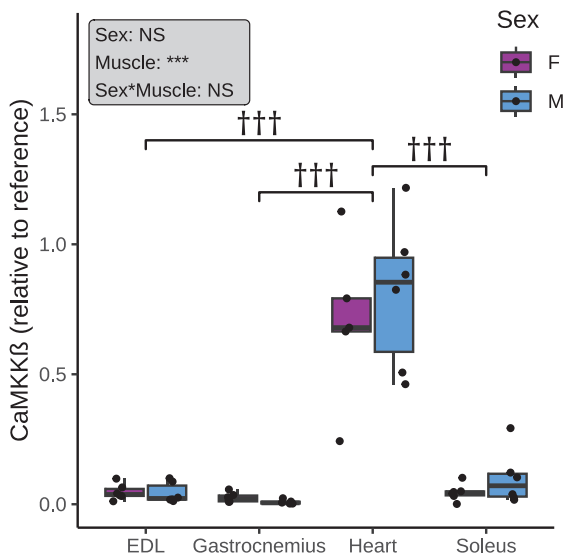


**Figure 9.** Calcium/calmodulin-dependent protein kinase kinase 2 (CaMKKβ) expression in extensor digitorum longus (EDL), gastrocnemius, heart, and soleus. CaMKKβ is poorly expressed in skeletal muscles compared with heart. The CaMKKβ expression in each sample was normalized to that of the reference sample (brain lysate, calculation specified in MATERIALS AND METHODS, Data Analysis). A two-way Bayesian ANOVA tested the impact of sex, muscles, and sex × muscles, and the results are shown in the gray box on the top left. The significant impact of muscle was followed up by 7 tests between muscle pairs, and these results are indicated with brackets. Significance notation: \*ANOVA, †T test between muscles (including both subgroups Male and Female). \*\*\* or ††† BF ≥ 100, extremely strong evidence. Each dot represents a single measurement for one sample. n = 6 for each sex subgroups and n = 12 for each muscle groups.

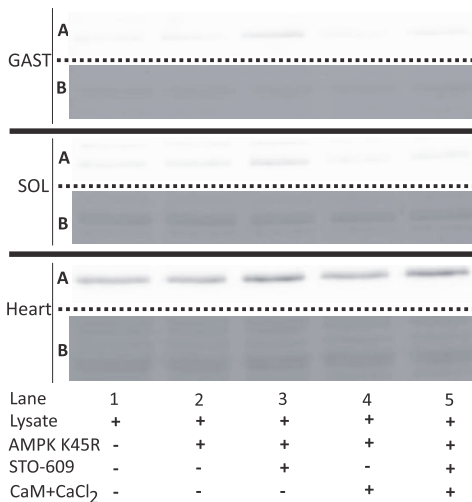


**Figure 10.** Phosphorylation of AMP-activated protein kinase (AMPK) in lysate of different muscles (gastrocnemius, soleus, and heart). A: representative Western blots of p-AMPK under the conditions shown below. B: Ponceau staining.

therefore cannot explain the differential AMPK activation in oxidative and glycolytic muscles (Figs. 1 and 3).

## DISCUSSION

To the best of our knowledge, we show for the first time that the basal level of AMPK activation is muscle dependent and that a larger fraction of AMPK is phosphorylated in oxidative compared with glycolytic muscles. In addition, we confirmed that there is more AMPKα1 in oxidative compared with glycolytic muscles. The AMPK activation did not correlate with the expression of LKB1 or CaMKKβ. Our results point to that in muscle tissue, the regulation of AMPK phosphorylation is more complex than depending merely on the expression of the upstream kinases.

### AMPK Activation Is Higher in Oxidative Than in Glycolytic Muscles

AMPK, at the basal state, was much more activated in oxidative (soleus and heart) compared with glycolytic muscles (gastrocnemius and EDL; Fig. 3). This is consistent with its role as a regulator of muscle phenotype. AMPK activation is well known to induce changes in muscle phenotype toward a more slow, oxidative profile. When AMPK is activated, it phosphorylates peroxisome proliferator-activated receptor-γ coactivator-1α (PGC-1α), which is a transcription factor regulating gene expression. The phosphorylation of PGC-1α is necessary for many of the effects of AMPK activation, including the upregulation of PGC-1α expression (32), which increases the activity of oxidative enzymes and modifies the myosin heavy chain (MHC) composition (53, 54). Studies on AMPK knockout (KO) or knockdown models also highlighted its involvement in fiber-type transition from fast glycolytic toward a slow, oxidative phenotype (55–59). Inactivity,

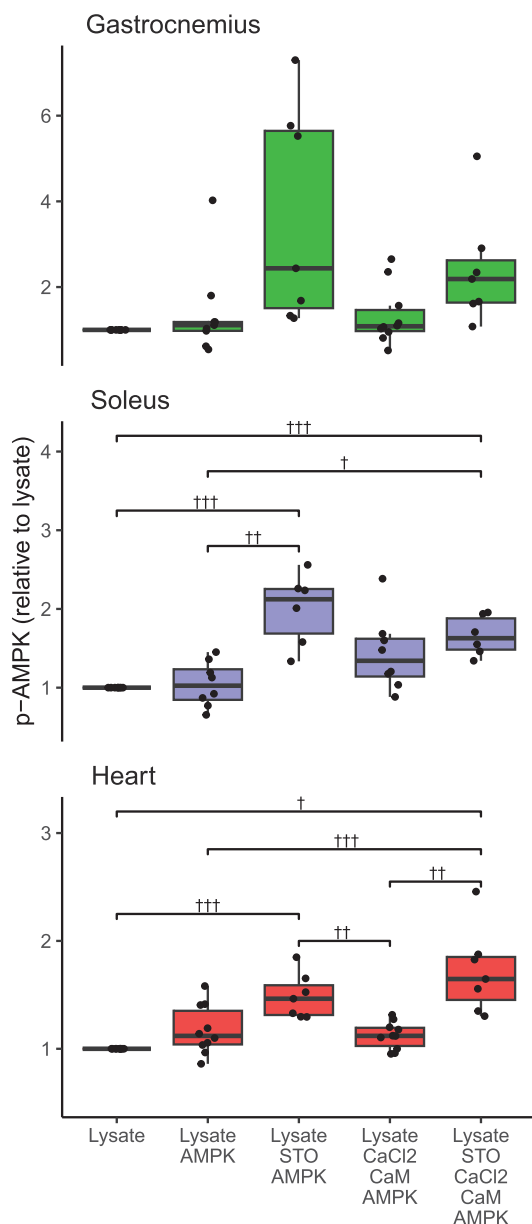


**Figure 11.** Phosphorylation of AMP-activated protein kinase (AMPK) under different conditions in lysate of gastrocnemius (A), soleus (B), and heart (C). Interestingly, AMPK phosphorylation was higher in the presence of 5  $\mu$ M STO-609, but this effect only reached significance in soleus and heart and not under all conditions. The phosphorylation of AMPK under each condition was normalized to that of the lysate alone (calculation specified in MATERIALS AND METHODS, *Data Analysis*). † $0 < BF < 30$ , strong evidence; †† $30 \leq BF < 100$ , very strong evidence; ††† $BF \geq 100$ , extremely strong evidence. In total, 6–10 measurements were performed with muscle lysate from  $n = 5$  animals (1 male and 4 females), and each dot represents a single measurement.

on the contrary, as studied by muscle unloading, greatly reduces electrical stimulation and ATP consumption (60). Overall, unloading leads to dephosphorylation of AMPK and a decrease in oxidative enzymes and PGC-1 $\alpha$  expression in skeletal muscle (33–37). The greater AMPK activation in oxidative muscles (Fig. 3) highlights that continuous AMPK activation is needed to maintain the oxidative phenotype.

### AMPK Activation Does Not Correlate with LKB1 Expression in Muscle Tissue

To elucidate the mechanism behind, we first measured the expression of LKB1, which is the main upstream kinase responsible for AMPK phosphorylation (13). Works carried out on LKB1-deficient mice show that disturbing LKB1 expression affects AMPK phosphorylation in all muscle types (26, 58, 61, 62).

Although LKB1 was significantly more expressed in the heart compared with gastrocnemius, there was no clear difference between the muscle types (oxidative vs. glycolytic) (Fig. 7), in agreement with another study (63). Thus, when comparing different muscle types, LKB1 expression did not correlate with AMPK activation (compare Figs. 3 and 7; Supplemental Fig. S3). This is different from the situation in cultured cells. When comparing different cell lines, Woods et al. (13) demonstrated a remarkable correlation between LKB1 and AMPK activity. Furthermore, in cultured adipocytes, the influence of sex hormones on the LKB1 expression translated into an effect on AMPK activation: dihydrotestosterone lowered the fraction of phosphorylated AMPK, and this effect was reversed by estrogen (64, 65). In contrast, the present results suggest that in muscle cells, the regulation of AMPK activation by LKB1 is more complex.

It is interesting that the LKB1 expression was higher in the muscles of female compared with male muscles (Fig. 7). It has been shown in adipocytes that LKB1 mRNA levels are increased by estrogen and decreased by testosterone and dihydrotestosterone (65). This effect is mediated by the androgen receptor and estrogen receptor  $\alpha$  (ER $\alpha$ ) (65). Androgen receptors are present in skeletal muscles (66), and although one study suggested that ER $\beta$  is the dominant ER in skeletal muscles (67), other studies have demonstrated that ER $\alpha$  is present in the nuclei of both mouse and human skeletal muscles (68, 69). This could explain the present results and suggest that sex hormones also influence LKB1 expression in muscle tissues (Fig. 7).

### CaMKK $\beta$ Is Poorly Expressed in Skeletal Muscle and Does Not Seem to Play Any Role in AMPK Activation in Muscle Tissue

Another upstream kinase of AMPK is CaMKK $\beta$ , which is activated by Ca<sup>2+</sup> and CaM. We speculated whether the AMPK activation in heart and soleus could be due to their tonic activity (42), leading to a chronic activation of the Ca<sup>2+</sup>/CaM/CaMKK $\beta$ /AMPK signaling pathway. As noted earlier, the AMPK $\alpha$ 1 isoform seems to be more sensitive to Ca<sup>2+</sup> signaling (21), and we found a higher expression of AMPK $\alpha$ 1 in oxidative muscles (Fig. 5).

We assessed the CaMKK $\beta$  expression in heart, soleus, gastrocnemius, and EDL using brain lysate as a positive control and reference (Fig. 8). We observed CaMKK $\beta$  expression in

the heart, albeit at lower levels than in the brain (Fig. 8). This is in contrast to some other studies showing that CaMKK $\beta$  is not significantly expressed in rat and mouse heart (70, 71). In the present study, the expression in the heart was higher than in any of the skeletal muscles, where only faint bands were detected (Figs. 8 and 9). The low CaMKK $\beta$  expression in skeletal muscles is in agreement with the literature (71).

To assess the function of CaMKK $\beta$ , we conducted a CaMKK $\beta$  activity assay in which we assessed its phosphorylation of recombinant AMPK $\alpha$ 2 K45R, which is catalytically inactive (45). This kinase activity assay worked with recombinant CaMKK $\beta$  (Supplemental Figs. S6 and S7), in agreement with the works of others (20, 72), and in brain lysate, although here, the effects were sex-dependent (Supplemental Figs. S8 and S9). In brain lysate, the addition of STO-609 alone also increased AMPK phosphorylation. This could explain why, in male brain lysates, STO-609 reduced, but did not abolish the effect of Ca<sup>2+</sup> and CaM (Supplemental Fig. S9).

In the skeletal muscle lysates, the addition of CaCl<sub>2</sub> and CaM had no effect on AMPK phosphorylation (Figs. 10 and 11), suggesting that CaMKK $\beta$  is not responsible for the basal tissue-specific AMPK activation. This is in agreement with the very low expression of CaMKK $\beta$  in soleus, gastrocnemius, and EDL (Figs. 8 and 9). The physiological importance of CaMKK $\beta$  as an activator of AMPK in skeletal muscle is controversial. A few studies have found that CaMKK $\beta$  can increase AMPK activity in skeletal muscle (21, 22, 73), although these studies did not find a direct effect on AMPK phosphorylation (in agreement with the present results), but observed significant effects on AMPK downstream targets such as acetyl-CoA carboxylase (ACC) or glucose uptake. However, a recent study demonstrated that contraction-induced AMPK phosphorylation and glucose uptake are similar in EDL and soleus from wild-type (WT) and CaMKK $\beta$  KO mice (24), and others have also been skeptical about the role of CaMKK $\beta$  in skeletal muscle (74). This is in agreement with the present results.

The heart differed from the skeletal muscles in having a greater expression of CaMKK $\beta$  (Figs. 8 and 9). However, CaMKK $\beta$  expression in the heart is controversial. As noted earlier, some have found only trace levels (70, 71). However, others have shown clearly visible CaMKK $\beta$  expression in the heart and suggested that its phosphorylation of AMPK is important during cardiac ischemia and pressure overload (75, 76). CaMKK $\beta$  is also the main activator of CaMKI and CaMKIV (77), which are involved in cardiac hypertrophy (78). Thus, CaMKK $\beta$  has the potential to play an important role in the heart in stressful situations. Despite the higher CaMKK $\beta$  expression in the heart, our results from the kinase activity assay suggested that CaMKK $\beta$  neither phosphorylated AMPK in heart nor in skeletal muscles (Figs. 10 and 11).

### STO-609 Moderately Increases Phosphorylated AMPK in Tissue Lysates

The addition of STO-609 led to a moderate increase in phosphorylated AMPK. This effect was only observed in the tissue lysates (Fig. 11 and Supplemental Fig. S9) and not with recombinant CaMKK $\beta$  (Supplemental Fig. S7). It was not significant in brain or gastrocnemius lysates (Supplemental

Fig. S9 and Fig. 11), and only under some conditions in soleus and heart lysates (Fig. 11). At present, we are unable to explain this. STO-609 is known to be a strong inhibitor of CaMKK $\beta$  (49), which is also confirmed by our experiments (Supplemental Fig. S7). Although some works have highlighted its potency to inhibit other kinases (24, 79, 80), it is unclear how STO-609 could lead to an increase in AMPK phosphorylation.

### Limitations of the Study

As the phosphorylation of AMPK by LKB1 depends on the concentrations of AMP and ADP, we speculated whether these varied between the muscles. We tried to measure the concentrations of ATP, ADP, and AMP in heart, soleus, and gastrocnemius muscles using perchloric acid extraction and HPLC/MS, which is widely used for these kinds of measurements (81–83). However, in our hands, there was a degradation of ATP even when extracting with high concentrations of acid. This degradation manifested itself as unphysiologically high concentrations of ADP. In muscle, the overall ATP and ADP concentrations are in the mM and  $\mu$ M range, respectively. However, in our experiments, the peaks of ATP and ADP were of similar magnitude (results not shown), indicating that ATP was broken down to ADP, or reflected the bound fraction of ADP that would not play a role in regulation of AMPK *in vivo*. Furthermore, assuming the equilibrium of adenylate kinase, the concentration of AMP is estimated to be 10–100 times lower than that of ADP (84). Considering that the samples are diluted upon perchloric acid extraction and neutralization, the AMP concentrations would be below the limit of quantification of the available equipment. Therefore, we did not proceed with these experiments.

The literature on AMP and ADP concentrations in different muscles is inconclusive. Knowing the concentrations of ATP, phosphocreatine, creatine, and pH from NMR measurements and assuming equilibrium of the creatine kinase reaction, the intracellular ADP concentration has been estimated to be around 50  $\mu$ M in the working heart (85) and to increase from 20  $\mu$ M at rest to peak at  $\sim$ 170  $\mu$ M during high-intensity exercise in gastrocnemius (86). However, these values are from separate studies. Another study calculated the overall concentrations of ADP and AMP from NMR and HPLC measurements and found no difference between mouse soleus and EDL (87).

The overall concentrations of AMP and ADP in different muscles may be inadequate to explain the muscle-specific AMPK activation because muscle cells are highly compartmentalized. Energetic compartmentalization has been demonstrated in cardiomyocytes, (88–92), and a recent study also pointed to energetic compartmentalization near cytosolic adenylate kinase, the main generator of AMP (93). This suggests that in some intracellular compartments, AMP and ADP concentrations are significantly different from the overall concentrations. Recent works by others have also highlighted the compartmentalization of AMPK activation at specific subcellular locations such as the mitochondria (94–97). Thus, it is conceivable that some AMPK is associated with compartments whose ADP and/or AMP concentrations are different from the overall cytosolic levels. In this respect, it is interesting that the higher AMPK activation coincides

with a larger fraction of the  $\alpha 1$  isoform in oxidative muscles (Fig. 5). However, further studies are needed to address whether the greater AMPK phosphorylation in oxidative muscles is specific to isoforms and/or intracellular localization.

### Conclusions

The present study demonstrates that AMPK is more activated in oxidative muscle (heart and soleus) compared with glycolytic muscle (gastrocnemius and EDL), highlighting that a high AMPK activity is required to maintain the oxidative phenotype. Oxidative muscles also had a greater expression of the AMPK  $\alpha 1$  isoform. In contrast to other cell types, AMPK activation did not correlate with the expression of the main AMPK upstream kinases, LKB1 and CaMKK $\beta$ , in muscle tissue. We hypothesize that the regulation of AMPK activation is more complex in muscle tissues because of their highly compartmentalized intracellular environment.

### DATA AVAILABILITY

All data supporting the results are included in the figures or as Supplemental Material. The datasets generated during the current study are available from the corresponding author upon reasonable request. The analysis tools used in this paper are referred to in the Methods.

### SUPPLEMENTAL MATERIAL

Supplemental Figs. S1–S10: <https://www.doi.org/10.6084/m9.figshare.27210642>.

### GRANTS

This work was supported by the Estonian Research Council under Grant No. PRG1127.

### DISCLOSURES

No conflicts of interest, financial or otherwise, are declared by the authors.

### AUTHOR CONTRIBUTIONS

R. Bernasconi and R. Birkedal conceived and designed research; R. Bernasconi, K.S., A.S., K.Z., and M.K. performed experiments; R. Bernasconi analyzed data; R. Bernasconi and R. Birkedal interpreted results of experiments; R. Bernasconi prepared figures; R. Bernasconi and R. Birkedal drafted manuscript; R. Bernasconi and R. Birkedal edited and revised manuscript; R. Bernasconi, K.S., A.S., K.Z., M.K., T.L., M.V., and R. Birkedal approved final version of manuscript.

### REFERENCES

- Garcia D, Shaw RJ. AMPK: mechanisms of cellular energy sensing and restoration of metabolic balance. *Mol Cell* 66: 789–800, 2017. doi:10.1016/j.molcel.2017.05.032.
- Wen Z, Jin K, Shen Y, Yang Z, Li Y, Wu B, Tian L, Shoor S, Roche NE, Goronzy JJ, Weyand CM. N-myristoyltransferase deficiency impairs activation of kinase AMPK and promotes synovial tissue inflammation. *Nat Immunol* 20: 313–325, 2019. doi:10.1038/s41590-018-0296-7.
- McHugh J. AMPK: a therapeutic target in RA? *Nat Rev Rheumatol* 15: 188–188, 2019. doi:10.1038/s41584-019-0192-z.
- Li X, Liu J, Lu Q, Ren D, Sun X, Rousselle T, Tan Y, Li J. AMPK: a therapeutic target of heart failure—not only metabolism regulation. *Biosci Rep* 39: BSR20181767, 2019. doi:10.1042/BSR20181767.

- Day EA, Ford RJ, Steinberg GR. AMPK as a therapeutic target for treating metabolic diseases. *Trends Endocrinol Metab* 28: 545–560, 2017. doi:10.1016/j.tem.2017.05.004.
- Lu Y, Yuan T, Min X, Yuan Z, Cai Z. AMPK: potential therapeutic target for vascular calcification. *Front Cardiovasc Med* 8: 670222, 2021. doi:10.3389/fcvm.2021.670222.
- Jiang S, Li T, Ji T, Yi W, Yang Z, Wang S, Yang Y, Gu C. AMPK: potential therapeutic target for ischemic stroke. *Theranostics* 8: 4535–4551, 2018. doi:10.7150/thno.25674.
- Coughlan KA, Valentine RJ, Ruderman NB, Saha AK. AMPK activation: a therapeutic target for type 2 diabetes? *Diabetes Metab Syndr Obes* 7: 241–253, 2014. doi:10.2147/DMSO.S43731.
- Woodard J, Joshi S, Viollet B, Hay N, Platanias LC. AMPK as a therapeutic target in renal cell carcinoma. *Cancer Biol Ther* 10: 1168–1177, 2010. doi:10.4161/cbt.10.11.13629.
- Beauloye C, Bertrand L, Horman S, Hue L. AMPK activation, a preventive therapeutic target in the transition from cardiac injury to heart failure. *Cardiovasc Res* 90: 224–233, 2011. doi:10.1093/cvr/cvr034.
- Gowans GJ, Hawley SA, Ross FA, Hardie DG. AMP is a true physiological regulator of AMP-activated protein kinase by both allosteric activation and enhancing net phosphorylation. *Cell Metab* 18: 556–566, 2013. doi:10.1016/j.cmet.2013.08.019.
- Suter M, Riek U, Tuerk R, Schlattner U, Wallimann T, Neumann D. Dissecting the role of 5'-AMP for allosteric stimulation, activation, and deactivation of AMP-activated protein kinase. *J Biol Chem* 281: 32207–32216, 2006. doi:10.1074/jbc.M606357200.
- Woods A, Johnstone SR, Dickerson K, Leiper FC, Fryer LGD, Neumann D, Schlattner U, Wallimann T, Carlson M, Carling D. LKB1 is the upstream kinase in the AMP-activated protein kinase cascade. *Curr Biol* 13: 2004–2008, 2003. doi:10.1016/j.cub.2003.10.031.
- Hardie DG, Ashford ML. AMPK: regulating energy balance at the cellular and whole body levels. *Physiology (Bethesda)* 29: 99–107, 2014. doi:10.1152/physiol.00050.2013.
- Pelosse M, Cottet-Rousselle C, Bidan CM, Dupont A, Gupta K, Berger I, Schlattner U. Synthetic energy sensor AMPfret deciphers adenylate-dependent AMPK activation mechanism. *Nat Commun* 10: 1038, 2019. doi:10.1038/s41467-019-08938-z.
- Zhang CS, Hawley SA, Zong Y, Li M, Wang Z, Gray A, Ma T, Cui J, Feng JW, Zhu M, Wu YQ, Li TY, Ye Z, Lin SY, Yin H, Piao HL, Hardie DG, Lin SC. Fructose-1,6-bisphosphate and aldolase mediate glucose sensing by AMPK. *Nature* 548: 112–116, 2017. doi:10.1038/nature23275.
- Momcilovic M, Hong SP, Carlson M. Mammalian TAK1 activates Snf1 protein kinase in yeast and phosphorylates AMP-activated protein kinase in vitro. *J Biol Chem* 281: 25336–25343, 2006. doi:10.1074/jbc.M604399200.
- Neumann D. Is TAK1 a direct upstream kinase of AMPK? *Int J Mol Sci* 19: 2412, 2018. doi:10.3390/ijms19082412.
- Xie M, Zhang D, Dyck JR, Li Y, Zhang H, Morishima M, Mann DL, Taffet GE, Baldini A, Khoury DS, Schneider MD. A pivotal role for endogenous TGF- $\beta$ -activated kinase-1 in the LKB1/AMP-activated protein kinase energy-sensor pathway. *Proc Natl Acad Sci USA* 103: 17378–17383, 2006. doi:10.1073/pnas.0604708103.
- Fujiwara Y, Kawaguchi Y, Fujimoto T, Kanayama N, Magari M, Tokumitsu H. Differential AMP-activated protein kinase (AMPK) recognition mechanism of Ca<sup>2+</sup>/calmodulin-dependent protein kinase kinase isoforms. *J Biol Chem* 291: 13802–13808, 2016. doi:10.1074/jbc.M116.727867.
- Jensen TE, Rose AJ, Hellsten Y, Wojtaszewski JFP, Richter EA. Caffeine-induced Ca<sup>2+</sup> release increases AMPK-dependent glucose uptake in rodent soleus muscle. *Am J Physiol Endocrinol Physiol* 293: E286–E292, 2007. doi:10.1152/ajpendo.00693.2006.
- Jensen TE, Rose AJ, Jørgensen SB, Brandt N, Schjerling P, Wojtaszewski JFP, Richter EA. Possible CaMKK-dependent regulation of AMPK phosphorylation and glucose uptake at the onset of mild tetanic skeletal muscle contraction. *Am J Physiol Endocrinol Physiol* 292: E1308–E1317, 2007. doi:10.1152/ajpendo.00456.2006.
- Fagerberg L, Hallström BM, Oksvold P, Kampf C, Djureinovic D, Odeberg J, Habuka M, Tahmasebpoor S, Danielsson A, Edlund K, Asplund A, Sjöstedt E, Lundberg E, Sztybel CA, Skogs M, Takanen JO, Berling H, Tegel H, Mulder J, Nilsson P, Schwenk JM, Lindskog C, Danielsson F, Mardinoglu A, Sivertsson A, von Felitzien K, Forsberg M, Zwaalen M, Olsson I, Navani S, Huss M, Nielsen J,

- Ponten F, Uhlén M. Analysis of the human tissue-specific expression by genome-wide integration of transcriptomics and antibody-based proteomics. *Mol Cell Proteomics* 13: 397–406, 2014. doi:10.1074/mcp.M113.035600.
24. Negoita F, Addinsall AB, Hellberg K, Bringas CF, Hafen PS, Sermersheim TJ, Agerholm M, Lewis CTA, Ahwazi D, Ling NXY, Larsen JK, Deshmukh AS, Hossain MA, Oakhill JS, Ochala J, Brault JJ, Sankar U, Drewry DH, Scott JW, Witzczak CA, Sakamoto K. CaMKK2 is not involved in contraction-stimulated AMPK activation and glucose uptake in skeletal muscle. *Mol Metab* 75: 101761, 2023. doi:10.1016/j.molmet.2023.101761.
  25. Kjøbsted R, Hingst JR, Fentz J, Foretz M, Sanz MN, Pehmøller C, Shum M, Marette A, Mounier R, Trebak JT, Wojtaszewski JFP, Viollet B, Lantier L. AMPK in skeletal muscle function and metabolism. *FASEB J* 32: 1741–1777, 2018. doi:10.1096/fj.201700442R.
  26. Sakamoto K, McCarthy A, Smith D, Green KA, Grahame Hardie D, Ashworth A, Alessi DR. Deficiency of LKB1 in skeletal muscle prevents AMPK activation and glucose uptake during contraction. *EMBO J* 24: 1810–1820, 2005. doi:10.1038/sj.emboj.7600667.
  27. Habets DD, Coumans WA, Voshol PJ, den Boer MA, Febbraio M, Bonen A, Glatz JF, Luiken JJ. AMPK-mediated increase in myocardial long-chain fatty acid uptake critically depends on sarcolemmal CD36. *Biochem Biophys Res Commun* 355: 204–210, 2007. doi:10.1016/j.bbrc.2007.01.141.
  28. Holmes BF, Kurth-Kraczek EJ, Winder WW. Chronic activation of 5'-AMP-activated protein kinase increases GLUT-4, hexokinase, and glycogen in muscle. *J Appl Physiol* (1985) 87: 1990–1995, 1999. doi:10.1152/jappl.1999.87.5.1990.
  29. Kurth-Kraczek EJ, Hirshman MF, Goodyear LJ, Winder WW. 5' AMP-activated protein kinase activation causes GLUT4 translocation in skeletal muscle. *Diabetes* 48: 1667–1671, 1999. doi:10.2337/diabetes.48.8.1667.
  30. Dzamko N, Schertzer JD, Ryall JG, Steel R, Macaulay SL, Wee S, Chen ZP, Michell BJ, Oakhill JS, Watt MJ, Jørgensen SB, Lynch GS, Kemp BE, Steinberg GR. AMPK-independent pathways regulate skeletal muscle fatty acid oxidation. *J Physiol* 586: 5819–5831, 2008. doi:10.1113/jphysiol.2008.159814.
  31. Park SH, Gammon SR, Knippers JD, Paulsen SR, Rubink DS, Winder WW. Phosphorylation-activity relationships of AMPK and acetyl-CoA carboxylase in muscle. *J Appl Physiol* (1985) 92: 2475–2482, 2002. doi:10.1152/japplphysiol.00071.2002.
  32. Jager S, Handschin C, St-Pierre J, Spiegelman BM. AMP-activated protein kinase (AMPK) action in skeletal muscle via direct phosphorylation of PGC-1. *Proc Natl Acad Sci USA* 104: 12017–12022, 2007. doi:10.1073/pnas.0705070104.
  33. Belova SP, Vilchinskaya NA, Mochalova EP, Mirzoev TM, Nemirovskaya TL, Shenkman BS. Elevated p70S6K phosphorylation in rat soleus muscle during the early stage of unloading: Causes and consequences. *Arch Biochem Biophys* 674: 108105, 2019. doi:10.1016/j.abb.2019.108105.
  34. Chibalin AV, Benziane B, Zakryjanova GF, Kravtsova VV, Krivoi II. Early endplate remodeling and skeletal muscle signaling events following rat hindlimb suspension. *J Cell Physiol* 233: 6329–6336, 2018. doi:10.1002/jcp.26594.
  35. Theilen NT, Jeremic N, Weber GJ, Tyagi SC. Exercise preconditioning diminishes skeletal muscle atrophy after hindlimb suspension in mice. *J Appl Physiol* (1985) 125: 999–1010, 2018. doi:10.1152/japplphysiol.00137.2018.
  36. Vilchinskaya NA, Mirzoev TM, Lomonosova YN, Kozlovskaya IB, Shenkman BS. Human muscle signaling responses to 3-day head-out dry immersion. *J Musculoskelet Neuronal Interact* 15: 286–293, 2015.
  37. Vilchinskaya NA, Mochalova EP, Nemirovskaya TL, Mirzoev TM, Turtikova OV, Shenkman BS. Rapid decline in MyHC I(β) mRNA expression in rat soleus during hindlimb unloading is associated with AMPK dephosphorylation. *J Physiol* 595: 7123–7134, 2017. doi:10.1113/JP275184.
  38. Katz LA, Swain JA, Portman MA, Balaban RS. Relation between phosphate metabolites and oxygen consumption of heart in vivo. *Am J Physiol Heart Circ Physiol* 256: H265–H274, 1989. doi:10.1152/ajpheart.1989.256.1.H265.
  39. Allen PS, Matheson GO, Zhu G, Gheorgiu D, Dunlop RS, Falconer T, Stanley C, Hochachka PW. Simultaneous 31P MRS of the soleus and gastrocnemius in Sherpas during graded calf muscle exercise. *Am J Physiol Regul Integr Comp Physiol* 273: R999–R1007, 1997. doi:10.1152/ajpregu.1997.273.3.R999.
  40. Hochachka PW, Mcclelland GB. Cellular metabolic homeostasis during large-scale change in ATP turnover rates in muscles. *J Exp Biol* 200: 381–386, 1997. doi:10.1242/jeb.200.2.381.
  41. Kushmerick MJ, Meyer RA, Brown TR. Regulation of oxygen consumption in fast- and slow-twitch muscle. *Am J Physiol Cell Physiol* 263: C598–C606, 1992. doi:10.1152/ajpcell.1992.263.3.C598.
  42. Hodgson JA, Roy RR, Higuchi N, Monti RJ, Zhong H, Grossman E, Edgerton VR. Does daily activity level determine muscle phenotype? *J Exp Biol* 208: 3761–3770, 2005. doi:10.1242/jeb.01825.
  43. Trebak JT, Birk JB, Hansen BF, Olsen GS, Wojtaszewski JFP. A-769662 activates AMPK β1-containing complexes but induces glucose uptake through a PI3-kinase-dependent pathway in mouse skeletal muscle. *Am J Physiol Cell Physiol* 297: C1041–C1052, 2009. doi:10.1152/ajpcell.00051.2009.
  44. Yurimoto S, Fujimoto T, Magari M, Kanayama N, Kobayashi R, Tokumitsu H. In vitro substrate phosphorylation by Ca<sup>2+</sup>/calmodulin-dependent protein kinase kinase using guanosine-5'-triphosphate as a phosphate donor. *BMC Biochem* 13: 27, 2012. doi:10.1186/1471-2091-13-27.
  45. Bobela W, Nazeeruddin S, Knott G, Aebischer P, Schneider BL. Modulating the catalytic activity of AMPK has neuroprotective effects against α-synuclein toxicity. *Mol Neurodegener* 12: 80, 2017. doi:10.1186/s13024-017-0220-x.
  46. Mu J, Brozinick JT Jr, Valladares O, Bucan M, Birnbaum MJ. A role for AMP-activated protein kinase in contraction- and hypoxia-regulated glucose transport in skeletal muscle. *Mol Cell* 7: 1085–1094, 2001. doi:10.1016/S1097-2765(01)00251-9.
  47. Nakanishi A, Hatano N, Fujiwara Y, Sha'ri A, Takabatake S, Akano H, Kanayama N, Magari M, Nozaki N, Tokumitsu H. AMP-activated protein kinase-mediated feedback phosphorylation controls the Ca<sup>2+</sup>/calmodulin (CaM) dependence of Ca<sup>2+</sup>/CaM-dependent protein kinase kinase β. *J Biol Chem* 292: 19804–19813, 2017. doi:10.1074/jbc.M117.805085.
  48. Fujiwara Y, Hiraoka Y, Fujimoto T, Kanayama N, Magari M, Tokumitsu H. Analysis of distinct roles of CaMK isoforms using STO-609-resistant mutants in living cells. *Biochemistry* 54: 3969–3977, 2015. doi:10.1021/acs.biochem.5b00149.
  49. Tokumitsu H, Inuzuka H, Ishikawa Y, Ikeda M, Saji I, Kobayashi R. STO-609, a Specific Inhibitor of the Ca<sup>2+</sup>/calmodulin-dependent protein kinase kinase. *J Biol Chem* 277: 15813–15818, 2002 [Erratum in *J Biol Chem* 278: 4368, 2003]. doi:10.1074/jbc.M201075200.
  50. Kütt J, Margus G, Kask L, Rätsepso T, Soodla K, Bernasconi R, Birkedal R, Järvi P, Laasmaa M, Vendelin M. Simple analysis of gel images with IOCBIO Gel. *BMC Biol* 21: 225, 2023. doi:10.1186/s12915-023-01734-8.
  51. Eddy SR. What is Bayesian statistics? *Nat Biotechnol* 22: 1177–1178, 2004. doi:10.1038/nbt0904-1177.
  52. Lee MD, Wagenmakers E-J. *Bayesian Cognitive Modeling: A Practical Course*. Cambridge, England: Cambridge University Press, 2014. doi:10.1017/CBO9781139087759.
  53. Hou Y, Su L, Zhao Y, Liu C, Yao D, Zhang M, Zhao L, Jin Y. Effect of chronic AICAR treatment on muscle fiber composition and enzyme activity in skeletal muscle of rats. *J Appl Anim Res* 49: 89–96, 2021. doi:10.1080/09712119.2021.1889563.
  54. Suwa M, Nakano H, Kumagai S. Effects of chronic AICAR treatment on fiber composition, enzyme activity, UCP3, and PGC-1 in rat muscles. *J Appl Physiol* (1985) 95: 960–968, 2003. doi:10.1152/japplphysiol.00349.2003.
  55. Fentz J, Kjøbsted R, Kristensen CM, Hingst JR, Birk JB, Gudiksen A, Foretz M, Schjerling P, Viollet B, Pilegaard H, Wojtaszewski JF. AMPKα is essential for acute exercise-induced gene responses but not for exercise training-induced adaptations in mouse skeletal muscle. *Am J Physiol Endocrinol Physiol* 309: E900–E914, 2015. doi:10.1152/ajpendo.00157.2015.
  56. Jørgensen SB, Trebak JT, Viollet B, Schjerling P, Vaulont S, Wojtaszewski JFP, Richter EA. Role of AMPKα2 in basal, training-, and AICAR-induced GLUT4, hexokinase II, and mitochondrial protein expression in mouse muscle. *Am J Physiol Endocrinol Physiol* 292: E331–E339, 2007. doi:10.1152/ajpendo.00243.2006.
  57. Lantier L, Fentz J, Mounier R, Leclerc J, Trebak JT, Pehmøller C, Sanz N, Sakakibara I, Saint-Amand E, Rimbaud S, Maire P, Marette A, Ventura-Clapier R, Ferry A, Wojtaszewski JFP, Foretz M, Viollet B.

- AMPK controls exercise endurance, mitochondrial oxidative capacity, and skeletal muscle integrity. *FASEB J* 28: 3211–3224, 2014. doi:10.1096/fj.14-250449.
58. Miura S, Kai Y, Tadaishi M, Tokutake Y, Sakamoto K, Bruce CR, Febbraio MA, Kita K, Cohnan S, Ezaki O. Marked phenotypic differences of endurance performance and exercise-induced oxygen consumption between AMPK and LKB1 deficiency in mouse skeletal muscle: changes occurring in the diaphragm. *Am J Physiol Endocrinol Physiol* 305: E213–E229, 2013. doi:10.1152/ajpendo.00114.2013.
  59. Röckl KSC, Hirshman MF, Brandauer J, Fujii N, Witters LA, Goodyear LJ. Skeletal muscle adaptation to exercise training: AMP-activated protein kinase mediates muscle fiber type shift. *Diabetes* 56: 2062–2069, 2007. doi:10.2337/db07-0255.
  60. Shenkan MS. How postural muscle senses disuse? Early signs and signals. *Int J Mol Sci* 21: 5037, 2020. doi:10.3390/ijms21145037.
  61. Sakamoto K, Zarrinpashneh E, Budas GR, Pouleur A-C, Dutta A, Prescott AR, Vanoverschelde J-L, Ashworth A, Jovanović A, Alessi DR, Bertrand L. Deficiency of LKB1 in heart prevents ischemia-mediated activation of AMPK $\alpha$ 2 but not AMPK $\alpha$ 1. *Am J Physiol Endocrinol Physiol* 290: E780–E788, 2006. doi:10.1152/ajpendo.00443.2005.
  62. Thomson DM, Porter BB, Tall JH, Kim HJ, Barrow JR, Winder WW. Skeletal muscle and heart LKB1 deficiency causes decreased voluntary running and reduced muscle mitochondrial marker enzyme expression in mice. *Am J Physiol Endocrinol Physiol* 292: E196–E202, 2007. doi:10.1152/ajpendo.00366.2006.
  63. Taylor EB, Hurst D, Greenwood LJ, Lamb JD, Cline TD, Sudweeks SN, Winder WW. Endurance training increases LKB1 and MO25 protein but not AMP-activated protein kinase activity in skeletal muscle. *Am J Physiol Endocrinol Physiol* 287: E1082–E1089, 2004. doi:10.1152/ajpendo.00179.2004.
  64. McInnes KJ, Corbould A, Simpson ER, Jones ME. Regulation of adenosine 5',monophosphate-activated protein kinase and lipogenesis by androgens contributes to visceral obesity in an estrogen-deficient state. *Endocrinology* 147: 5907–5913, 2006. doi:10.1210/en.2006-0879.
  65. McInnes KJ, Brown KA, Hunger NI, Simpson ER. Regulation of LKB1 expression by sex hormones in adipocytes. *Int J Obes (Lond)* 36: 982–985, 2012. doi:10.1038/ijo.2011.172.
  66. Snochowski M, Dahlberg E, Gustafsson J-Å. Characterization and quantification of the androgen and glucocorticoid receptors in cytosol from rat skeletal muscle. *Eur J Biochem* 111: 603–616, 1980. doi:10.1111/j.1432-1033.1980.tb04977.x.
  67. Barros RPA, Gabbi C, Morani A, Warner M, Gustafsson JÅ. Participation of ER $\alpha$  and ER $\beta$  in glucose homeostasis in skeletal muscle and white adipose tissue. *Am J Physiol Endocrinol Physiol* 297: E124–E133, 2009. doi:10.1152/ajpendo.00189.2009.
  68. Barros RPA, Machado UF, Warner M, Gustafsson J-Å. Muscle GLUT4 regulation by estrogen receptors ER $\beta$  and ER $\alpha$ . *Proc Natl Acad Sci USA* 103: 1605–1608, 2006 [Erratum in *Proc Natl Acad Sci USA* 103: 8298, 2006]. doi:10.1073/pnas.0510391103.
  69. Wiik A, Ekman M, Johansson O, Jansson E, Esbjörnsson M. Expression of both oestrogen receptor alpha and beta in human skeletal muscle tissue. *Histochem Cell Biol* 131: 181–189, 2009. doi:10.1007/s00418-008-0512-x.
  70. Anderson KA, Means RL, Huang Q-H, Kemp BE, Goldstein EG, Selbert MA, Edelman AM, Fremereau RT, Means AR. Components of a calmodulin-dependent protein kinase cascade: molecular cloning, functional characterization and cellular localization of Ca<sup>2+</sup>/calmodulin-dependent protein kinase kinase  $\beta$ . *J Biol Chem* 273: 31880–31889, 1998. doi:10.1074/jbc.273.48.31880.
  71. McGee SL, Mustard KJ, Hardie DG, Baar K. Normal hypertrophy accompanied by phosphorylation and activation of AMP-activated protein kinase  $\alpha$ 1 following overload in LKB1 knockout mice. *J Physiol* 586: 1731–1741, 2008. doi:10.1113/jphysiol.2007.143685.
  72. Woods A, Dickerson K, Heath R, Hong S-P, Momcilovic M, Johnstone SR, Carlson M, Carling D. Ca<sup>2+</sup>/calmodulin-dependent protein kinase kinase- $\beta$  acts upstream of AMP-activated protein kinase in mammalian cells. *Cell Metab* 2: 21–33, 2005. doi:10.1016/j.cmet.2005.06.005.
  73. Abbott MJ, Edelman AM, Turcotte LP. CaMKK is an upstream signal of AMP-activated protein kinase in regulation of substrate metabolism in contracting skeletal muscle. *Am J Physiol Regul Integr Comp Physiol* 297: R1724–R1732, 2009. doi:10.1152/ajpregu.00179.2009.
  74. Hawley SA, Pan DA, Mustard KJ, Ross L, Bain J, Edelman AM, Frenguelli BG, Hardie DG. Calmodulin-dependent protein kinase kinase- $\beta$  is an alternative upstream kinase for AMP-activated protein kinase. *Cell Metab* 2: 9–19, 2005. doi:10.1016/j.cmet.2005.05.009.
  75. Altarejos JY, Taniguchi M, Clanachan AS, Lopaschuk GD. Myocardial ischemia differentially regulates LKB1 and an alternate 5'-AMP-activated protein kinase kinase. *J Biol Chem* 280: 183–190, 2005. doi:10.1074/jbc.M411810200.
  76. Watanabe S, Horie T, Nagao K, Kuwabara Y, Baba O, Nishi H, Sowa N, Narazaki M, Matsuda T, Takemura G, Wada H, Hasegawa K, Kimura T, Ono K. Cardiac-specific inhibition of kinase activity in calcium/calmodulin-dependent protein kinase kinase- $\beta$  leads to accelerated left ventricular remodeling and heart failure after transverse aortic constriction in mice. *PLoS One* 9: e108201, 2014. doi:10.1371/journal.pone.0108201.
  77. Racioppi L, Means AR. Calcium/calmodulin-dependent protein kinase kinase 2: roles in signaling and pathophysiology. *J Biol Chem* 287: 31658–31665, 2012. doi:10.1074/jbc.R112.356485.
  78. Passier R, Zeng H, Frey N, Naya FJ, Nicol RL, McKinsey TA, Overbeek P, Richardson JA, Grant SR, Olson EN. CaM kinase signaling induces cardiac hypertrophy and activates the MEF2 transcription factor in vivo. *J Clin Invest* 105: 1395–1406, 2000. doi:10.1172/JCI8551.
  79. O'Byrne SN, Scott JW, Pilotte JR, Santiago A da S, Langendorf CG, Oakhill JS, Edfudul BJ, Couñago RM, Wells CI, Zuercher WJ, Wilson TM, Drewry DH. In depth analysis of kinase cross screening data to identify CAMKK2 inhibitory scaffolds. *Molecules* 25: 325, 2020. doi:10.3390/molecules25020325.
  80. Bain J, Plater L, Elliott M, Shpuro N, Hastie CJ, Mclauchlan H, Klevernic I, Arthur JS, Alessi DR, Cohen P. The selectivity of protein kinase inhibitors: a further update. *Biochem J* 408: 297–315, 2007. doi:10.1042/BJ20070797.
  81. Chida J, Kido H. Extraction and quantification of adenosine triphosphate in mammalian tissues and cells. *Methods Mol Biol Clifton Biol* 1098: 21–32, 2014. doi:10.1007/978-1-62703-718-1\_2.
  82. Law AS, Hafen PS, Brault JJ. Liquid chromatography method for simultaneous quantification of ATP and its degradation products compatible with both UV-Vis and mass spectrometry. *J Chromatogr B Analyt Technol Biomed Life Sci* 1206: 123351, 2022. doi:10.1016/j.jchromb.2022.123351.
  83. Rammouz RE, Létisse F, Durand S, Portais JC, Moussa ZW, Fernandez X. Analysis of skeletal muscle metabolome: evaluation of extraction methods for targeted metabolite quantification using liquid chromatography tandem mass spectrometry. *Anal Biochem* 398: 169–177, 2010. doi:10.1016/j.ab.2009.12.006.
  84. Hardie DG, Carling D, Gamblin SJ. AMP-activated protein kinase: also regulated by ADP? *Trends Biochem Sci* 36: 470–477, 2011. doi:10.1016/j.tibs.2011.06.004.
  85. Vendelin M, Kongas O, Saks V. Regulation of mitochondrial respiration in heart cells analyzed by reaction-diffusion model of energy transfer. *Am J Physiol Cell Physiol* 278: C747–C764, 2000. doi:10.1152/ajpcell.2000.278.4.C747.
  86. Liu M, Walter GA, Pathare NC, Forster RE, Vandeborn K. A quantitative study of bioenergetics in skeletal muscle lacking carbonic anhydrase III using 31P magnetic resonance spectroscopy. *Proc Natl Acad Sci USA* 104: 371–376, 2007. doi:10.1073/pnas.0609870104.
  87. Overton JD, Adams GS, McCall RD, Kinsey ST. High energy phosphate concentrations and AMPK phosphorylation in skeletal muscle from mice with inherited differences in hypoxic exercise tolerance. *Comp Biochem Physiol A Mol Integr Physiol* 152: 478–485, 2009. doi:10.1016/j.cbpa.2008.11.019.
  88. Illaste A, Laasma M, Peterson P, Vendelin M. Analysis of molecular movement reveals latticelike obstructions to diffusion in heart muscle cells. *Biophys J* 102: 739–748, 2012. doi:10.1016/j.bpj.2012.01.012.
  89. Jephthina N, Beraud N, Sepp M, Birkedal R, Vendelin M. Permeabilized rat cardiomyocyte response demonstrates intracellular origin of diffusion obstacles. *Biophys J* 101: 2112–2121, 2011. doi:10.1016/j.bpj.2011.09.025.
  90. Kaasik A, Veksler V, Boehm E, Novotova M, Minajeva A, Ventura-Clapier R. Energetic crosstalk between organelles: architectural integration of energy production and utilization. *Circ Res* 89: 153–159, 2001. doi:10.1161/hh1401.093440.

91. **Sepp M, Vendelin M, Vija H, Birkedal R.** ADP compartmentation analysis reveals coupling between pyruvate kinase and ATPases in heart muscle. *Biophys J* 98: 2785–2793, 2010. doi:10.1016/j.bpj.2010.03.025.
92. **Simson P, Jepihina N, Laasmaa M, Peterson P, Birkedal R, Vendelin M.** Restricted ADP movement in cardiomyocytes: cytosolic diffusion obstacles are complemented with a small number of open mitochondrial voltage-dependent anion channels. *J Mol Cell Cardiol* 97: 197–203, 2016. doi:10.1016/j.yjmcc.2016.04.012.
93. **Branovets J, Soodia K, Vendelin M, Birkedal R.** Rat and mouse cardiomyocytes show subtle differences in creatine kinase expression and compartmentalization. *PLoS One* 18: e0294718, 2023. doi:10.1371/journal.pone.0294718.
94. **Drake JC, Wilson RJ, Laker RC, Guan Y, Spaulding HR, Nichenko AS, Shen W, Shang H, Dorn MV, Huang K, Zhang M, Bandara AB, Brisendine MH, Kashatus JA, Sharma PR, Young A, Gautam J, Cao R, Wallrabe H, Chang PA, Wong M, Desjardins EM, Hawley SA, Christ GJ, Kashatus DF, Miller CL, Wolf MJ, Periasamy A, Steinberg GR, Hardie DG, Yan Z.** Mitochondria-localized AMPK responds to local energetics and contributes to exercise and energetic stress-induced mitophagy. *Proc Natl Acad Sci USA* 118: e2025932118, 2021. doi:10.1073/pnas.2025932118.
95. **Schmitt DL, Curtis SD, Lyons AC, Zhang J, Chen M, He CY, Mehta S, Shaw RJ, Zhang J.** Spatial regulation of AMPK signaling revealed by a sensitive kinase activity reporter. *Nat Commun* 13: 3856, 2022. doi:10.1038/s41467-022-31190-x.
96. **Trefts E, Shaw RJ.** AMPK: restoring metabolic homeostasis over space and time. *Mol Cell* 81: 3677–3690, 2021. doi:10.1016/j.molcel.2021.08.015.
97. **Zong Y, Zhang CS, Li M, Wang W, Wang Z, Hawley SA, Ma T, Feng JW, Tian X, Qi Q, Wu YQ, Zhang C, Ye Z, Lin SY, Piao HL, Hardie DG, Lin SC.** Hierarchical activation of compartmentalized pools of AMPK depends on severity of nutrient or energy stress. *Cell Res* 29: 460–473, 2019. doi:10.1038/s41422-019-0163-6.



## Publication III

**Bernasconi, R**; Soodla, K; Samuli, M; Rätsepso, T; Vendelin, M; Birkedal, R.

**Similar levels of phosphorylated AMPK in skeletal muscles from creatine deficient guanidino-acetate methyltransferase knockout (GAMT KO) and wildtype mice.**

(Manuscript)

The rules of the publisher prevent the publication of the manuscript of **Publication III** before acceptance. Official committee members and opponents will be given a copy of the manuscript to enable them to carry out a judicious review of the dissertation.



## Publication IV

**Bernasconi, R**; Soodla, K; Samuli, M; Rätsepso, T; Vendelin, M; Birkedal, R.

**Creatine deficient AGAT KO mice exhibit stronger remodeling of glycolytic than oxidative muscles through ER $\alpha$ -LKB1-AMPK-PGC1 $\alpha$  signaling.**

(Manuscript)

The rules of the publisher prevent the publication of the manuscript of **Publication IV** before acceptance. Official committee members and opponents will be given a copy of the manuscript to enable them to carry out a judicious review of the dissertation.



## Publication V

Branovets, J\*; Laasmaa, M\*; Stolova, J; Shen, X; Rätsepso, T; **Bernasconi, R**; Soodla, K; Balodis, MJ; Grahv, C; Hendrikson, E; Louch, W; Birkedal, R; Vendelin, M.

**Life-long creatine deficiency leads to augmented sarcoplasmic reticulum calcium release but not heart failure.**

Am J Physiol – Heart Circ Physiol, July 2025, DOI: 10.1152/ajpheart.00106.2025.

\*Equal contribution



RESEARCH ARTICLE

*Cardiac Excitation and Contraction*

## Lifelong creatine deficiency leads to augmented sarcoplasmic reticulum calcium release but not heart failure

 Jelena Branovets,<sup>1\*</sup>  Martin Laasmaa,<sup>1,2,3\*</sup>  Jekaterina Stolova,<sup>1</sup>  Xin Shen,<sup>2,3</sup> Triinu Rätsepso,<sup>1</sup>  
 Romain Bernasconi,<sup>1</sup> Kārol Soodla,<sup>1</sup> Mihkel Jaan Balodis,<sup>1</sup> Cärolin Grahv,<sup>1</sup> Eliise Hendrikson,<sup>1</sup>  
 William Edward Louch,<sup>2,3</sup>  Rikke Birkedal,<sup>1</sup> and  Marko Vendelin<sup>1</sup>

<sup>1</sup>Laboratory of Systems Biology, Department of Cybernetics, Tallinn University of Technology, Tallinn, Estonia; <sup>2</sup>University of Oslo, Institute for Experimental Medical Research, Oslo, Norway; and <sup>3</sup>K.G. Jebsen Centre for Cardiac Research, University of Oslo, Oslo, Norway

### Abstract

Creatine kinase (CK) is considered a crucial energy transfer system in cardiac muscle. Some studies have suggested that reduced CK energy transfer in the heart causes energy starvation, limits cardiac performance, and ultimately leads to heart failure. In agreement with this hypothesis, the hearts from creatine-deficient mice lacking arginine:glycine amidinotransferase (AGAT KO) have been shown, in some experiments, to resemble failing hearts. However, it is unclear if AGAT KO induces changes in cardiomyocyte substructure and Ca<sup>2+</sup> cycling that resemble heart failure, including impairment of sarcoplasmic reticulum (SR) Ca<sup>2+</sup> release and reuptake. To investigate this, we assessed functional and structural aspects of Ca<sup>2+</sup> handling in cardiomyocytes from KO and WT littermates. We found minor, sex-dependent differences in the organization of transverse tubules and ryanodine receptors (RyRs), no differences in the expression and relative phosphorylation of RyR and PLB, but higher S100A1 expression levels. AGAT KO cardiomyocytes exhibited larger and longer Ca<sup>2+</sup> transients with the same decay rate as WT. Ca<sup>2+</sup> spark frequency and SR Ca<sup>2+</sup> content were also increased in KO, while sodium-calcium exchanger activity was unchanged. Thus, our results strongly suggest that SR Ca<sup>2+</sup> cycling is augmented in AGAT KO hearts. Although AGAT KO hearts also exhibited increased AMPK activation, suggesting higher levels of AMP/ADP, this did not detectably impair sarcoendoplasmic reticulum Ca<sup>2+</sup>-ATPase activity. In conclusion, the changes in AGAT KO cardiomyocytes are opposite to those in failing cardiomyocytes, showing that lifelong absence of CK energy transfer does not lead to heart failure.

**NEW & NOTEWORTHY** Previous studies have suggested that reduced creatine kinase (CK) activity may lead to heart failure. Here, we studied calcium handling in the hearts of creatine-deficient arginine-glycine amidino-transferase knockout (AGAT KO) mice with lifelong inhibition of CK. In contrast to failing cardiomyocytes, AGAT KO cardiomyocytes exhibited larger calcium transients due to more readily firing RyR clusters releasing more calcium from the SR. Thus, lifelong creatine deficiency does not lead to the phenotype observed in heart failure.

*calcium dynamics; creatine kinase; energy transfer; excitation-contraction coupling; heart*

### INTRODUCTION

In the heart, excitation-contraction coupling (1) and mechanical work cost energy in the form of ATP, mainly generated by the mitochondria. Mitochondrial ATP generation is, among other factors, regulated by ADP feedback from the ATPases. Thus, an energy circuit is formed, where ATP diffuses from mitochondria to ATPases, and ADP diffuses from ATPases back to mitochondria. In addition to direct diffusion, the creatine kinase (CK) system can function as a spatial energy buffer, forming a parallel circuit to

facilitate energy transfer between cellular ATPases and mitochondria. CK catalyzes the reversible reaction: ADP + phosphocreatine ↔ ATP + creatine. It is mainly known as a temporal energy buffer using phosphocreatine when ATP demand exceeds its generation. In addition, a spatial energy buffering component is suggested due to CK binding near ATP generation and utilization sites (2–7).

The role of the CK system in muscle has been studied in transgenic mouse models lacking either the muscle-specific cytosolic and mitochondrial CK isoforms (CK KO) or one of the enzymes involved in creatine synthesis or uptake (8).



\*J. Branovets and M. Laasmaa contributed equally to this work.

Correspondence: M. Vendelin (markov@sysbio.ioc.ee).

Submitted 11 February 2025 / Revised 2 March 2025 / Accepted 4 July 2025



Creatine is synthesized by arginine:glycine amidinotransferase (AGAT) in the liver and guanidinoacetate methyl transferase (GAMT) in the kidney, and is taken up by the muscle tissue through the creatine transporter (CrT). Creatine deficiency syndrome is a human disease (9, 10), and there are transgenic knockout (KO) mouse models of both AGAT KO (11), GAMT KO (12) and CrT KO (13).

Despite decades of research, the role of the CK system in the heart is still controversial (14). In diseased hearts, the outcome relates to the CK activity. In general, myocardial infarction leads to diminished CK activity and less coupling to mitochondrial respiration (15), and this may be one of the reasons why failing hearts are energy starved (16–18). Although ischemia-reperfusion (IR) injury is aggravated in CK KO and GAMT KO mice that have lifelong inhibition of the CK system (19, 20), overexpression of CK has a protective effect (21–23). Taken together, we can conclude from these studies that the CK system is a valuable energy buffer in critical situations. If CK is inhibited at the time of IR, the outcome is aggravated, but if more CK is active at the time of IR, the outcome is ameliorated. The effect of the CK depends critically on the timing, as inhibition of the CK system after IR does not aggravate the outcome. This was recently demonstrated in a model of acute creatine deficiency, where AGAT KO mice had received creatine supplementation until 1 wk after the induction of myocardial infarction (24).

In healthy hearts, the role of the CK system is a different story. Some decades ago, it was hypothesized that, as the function of the CK system declines in heart failure, so can long-term inhibition of the CK system lead to heart failure. Indeed, initial studies on CK KO mice found significant hypertrophy (25) and changes in mitochondrial organization (26). However, in these earlier studies, CK KO mice on a mixed S129/C57Bl6 background were compared with C57Bl6 mice. In contrast, when CK KO mice were backcrossed to a pure C57Bl6 background, the CK KO and WT echocardiograms were similar, and there were no signs of hypertrophy (27). Thus, the initial perception that CK KO cardiomyocytes have a severely altered phenotype turned out to be incorrect. Among the creatine-deficient mice, GAMT KO cardiomyocytes have unaltered mitochondrial organization and energetics (28, 29), and normal cardiac performance until 1 yr of age (30). Only older GAMT KO (>18 mo) mice exhibit slightly lower intrinsic heart rate and systolic developed pressure, but their longevity is the same as that of WT mice (31). In contrast, AGAT KO mice, which have a more severe phenotype in terms of body weight reduction and skeletal muscle atrophy (32, 33), have been shown to exhibit characteristics reminiscent of heart failure. Although the cardiac phenotype is relatively mild, their left ventricular end systolic pressure is lower, and the rates of contraction and relaxation are slower (34), resembling heart failure.

If inhibition of the CK system does, in fact, promote heart failure development, one might expect that cardiomyocyte  $\text{Ca}^{2+}$  homeostasis is also similar in these two conditions. A study using whole cell patch clamp and fluorescence microscopy demonstrated that AGAT KO cardiomyocytes exhibit reduced voltage-sensitive L-type  $\text{Ca}^{2+}$  channel (LTCC) current and lower sarcoendoplasmic reticulum  $\text{Ca}^{2+}$  ATPase (SERCA) activity (35). Reduction of SERCA activity is characteristic of failing hearts with reduced ejection fraction

(HFrEF), and, through contribution to altered  $\text{Ca}^{2+}$  handling in HFrEF, promotes contractile dysfunction (36). SERCA activity is lowered in HFrEF due to a decrease in SERCA expression (37, 38) and increased inhibition by unphosphorylated phospholamban (PLB) (39–41). A resulting reduction in sarcoplasmic reticulum (SR) content decreases the magnitude of the  $\text{Ca}^{2+}$  transient, while lowered SERCA activity additionally slows the  $\text{Ca}^{2+}$  transient decline (42). Spark frequency is also reduced in HFrEF and, similar to the overall  $\text{Ca}^{2+}$  transient, the sparks have a smaller amplitude and slower dynamics (36). However, in HFrEF,  $\text{Ca}^{2+}$ -induced  $\text{Ca}^{2+}$  release (CICR) is further reduced and desynchronized as LTCCs and ryanodine receptors 2 (RyRs) in dyads are uncoupled due to the reduction and disorganization of the transverse tubular (t-tubular) network (43–45) and dispersion of RyR clusters (46, 47). It is unknown if these alterations in HFrEF are linked to inhibition of the CK system.

The aim of the present study was to assess whether AGAT KO cardiomyocytes exhibit traits characteristic of cardiomyocytes from failing hearts. In the previous study using patch clamp, the pipette contained phosphocreatine, which could have partially rescued energy transfer during the experiments (35). Therefore, in the present study, we focused on intact cardiomyocytes, expecting a more severe phenotype. We assessed overall Ca transients, Ca sparks, and the organization of t-tubules and RyRs that are known to be critical modulators of the excitation-contraction coupling. In addition, as the previous study showed no changes in LTCC and SERCA expression, we assessed the expression and phosphorylation of RyR and PLB. In contrast to our expectations, the AGAT KO cardiomyocytes exhibited larger  $\text{Ca}^{2+}$  transients and higher  $\text{Ca}^{2+}$  spark frequency than WT cardiomyocytes. This could be due to a higher SR  $\text{Ca}^{2+}$  content and/or higher gain of CICR. Thus, we also recorded the SR  $\text{Ca}^{2+}$  content and the expression of S100A1 and Bridging Integrator 1 (BIN1, also known as amphiphysin II), which are known modulators of CICR gain and dyadic space organization (48–50).

To comply with the 3Rs and reduce the number of experimental animals, many of these experiments were performed in parallel. To take into account the differences between sexes in  $\text{Ca}^{2+}$  handling (51–53), we studied male and female mice as separate groups. The original dataset obtained in KO animals is compared with the reference data from WT littermates, which were presented earlier, describing sex differences in calcium handling in the heart (51).

## METHODS

### Animals

All animal procedures were carried out according to the guidelines of Directive 2010/63/EU of the European Parliament on the protection of animals used for scientific purposes and had been approved by the Project Authorisation Committee for Animal Experiments in the Estonian Ministry of Rural Affairs.

For the experiments, arginine:glycine amidinotransferase (AGAT) KO and WT littermates were used (11). The animals were back-crossed for more than 10 generations with C57BL/6J0laHsd (Envigo). They were bred and kept at our local animal facility with free access to water and food at an ambient temperature of 22–23°C and a 12:12-h light-dark cycle. KO

mice were separated from WT to prevent creatine ingestion via coprophagia. Because the AGAT KO animals were skinny, but active, they were housed in groups whenever possible, given moistened food at the bottom of the cage, and had longer cages with a heating lamp at one end to allow for behavioral thermoregulation. All animals were fed the same creatine-free chow (V1534-000 R/M-H complete maintenance diet for rats and mice; Ssniff Spezialdiäten GmbH, Soest, Germany). As shown earlier (34), this housing and diet arrangement led to the absence of cardiac creatine in KO animals.

### Genotyping

AGAT mice were genotyped as in Refs. 28, 29, and 35.

### Cardiomyocyte Isolation

Mice were anaesthetized with a ketamine/dexmedetomidine mixture (150 mg·kg<sup>-1</sup> and 0.5 mg·kg<sup>-1</sup>, respectively) and received an injection of 250 U of heparin to prevent blood coagulation. When the toe-pinch reflex was absent, the animal was euthanized by cervical dislocation. The heart was immediately excised and transferred to ice-cold Krebs-Henseleit buffer. Cardiomyocytes were isolated as in Refs. 28, 29, and 35.

### Determination of Cardiomyocyte Sizes

Bright-field images of the isolated cardiomyocytes were taken using a Zeiss PrimoStar upright microscope with a Zeiss Plan/ACROMAT ×10/0.25 objective and equipped with an AxioCam ERc5s camera connected to a computer running the ZEN 3.4 Blue software (Zeiss, Inc). An image of a stage calibration slide with a length of 1 mm was used to determine the pixel size. The images were imported into ImageJ, and the length and width of 20 randomly selected cells from five animals from each group (5 female WT, 5 male WT, 5 female KO, and 5 male KO) was determined using the line tool.

### Detection and Analysis of Calcium Transients and Sparks

Ca<sup>2+</sup> sparks and transients were detected according to a previously described protocol (54). Freshly isolated cardiomyocytes were loaded in the presence of 5 μM fluo-4 AM (Invitrogen, Carlsbad, CA) for 20 min in Tyrode solution containing (in mM): 150 NaCl, 5.4 KCl, 0.33 NaH<sub>2</sub>PO<sub>4</sub>, 1 MgCl<sub>2</sub>, 1.13 CaCl<sub>2</sub>, 10 glucose, and 10 HEPES (pH was adjusted to 7.4 with NaOH). After loading cells with the Ca<sup>2+</sup>-sensitive dye, 100 μL of cell suspension was placed in a measuring chamber RC-21BRFS (Warner Instruments, Hamden), and 100 μL of Tyrode with or without 100 nM ISO was added, corresponding to β-adrenergic stimulated condition or control, respectively.

For experiments, rod-shaped cardiomyocytes with clear striations that responded to each stimulation pulse were chosen for imaging Ca<sup>2+</sup> transient and sparks. Before starting linescan imaging, the cardiomyocyte was field-stimulated for ~5 min at 21°C with square pulses (width 10 ms, height 10 V) at 1 Hz using Stimulator C Type 224 (Harvard Apparatus, Holliston, Massachusetts) connected to the imaging chamber with platinum wires. After starting the acquisition, transients were recorded for 5–15 s, after which sparks

were recorded for ~100 s. After each measurement, cells were replaced with freshly loaded cells.

Confocal images were acquired using a Zeiss LSM510 Duo confocal microscope with a ×63 water-immersion objective (1.2 NA). The signal was obtained via a single high-voltage PMT using 8-bit mode; the pinhole was set to one Airy disk. Fluo-4 was excited with a 488-nm Argon laser (0.8% of the power), and after passing 488-nm dichroic, the fluorescence was recorded through a long-pass 505-nm filter. Linescans were performed unidirectionally, and *xt* images were made to cover a line of ~70 μm (512 pixels, 0.14 μm pixel size) along the cell, avoiding nuclei. In total, 70,000 lines 1.53 ms apart were acquired. For background estimation, a single 2-D image of each cell with the surrounding background was recorded after linescans with the same imaging configuration.

Ca<sup>2+</sup> sparks were detected and analyzed using default parameters with IOCBIO Sparks open-source software (54). The background intensity from the separately recorded image was determined using ImageJ. Ca<sup>2+</sup> transients were analyzed by IOCBIO Kinetics open-source software after manually marking each Ca<sup>2+</sup> transient (55). In this analysis, transient signal was fitted by splines, and transient properties, such as amplitude, duration at half-maximum, and time-moments at which transient reached half-maximum values were determined. Corresponding analysis modules are incorporated into IOCBIO Kinetics and available.

For further statistical analysis of calcium sparks and transient amplitude, decay time, full width at half maximum and full duration at half maximum were used.

### Detection of Sarcoplasmic Reticulum Calcium Content

SR Ca<sup>2+</sup> content was determined using the same setup as for calcium transients and sparks measurements. The cardiomyocytes in the chamber were perfused with different solutions. After loading with 5 μM of Ca<sup>2+</sup>-sensitive fluo-4 AM, the cell suspension was placed in a measuring chamber and perfused with Tyrode solution (see composition in *Detection and Analysis of Calcium Transients and Sparks*) with or without 50 nM ISO.

Each cell was subjected to two protocols. First, calcium transients were recorded for 45 s, after which the perfusion was switched to Tyrode solution containing 10 mM caffeine and Ca<sup>2+</sup> release from SR was recorded for ~30 s by recording Ca<sup>2+</sup>-induced fluo-4 fluorescence signal. Next, the fluorescence was calibrated by assessing the fluorescence intensity of the fluo-4 in the absence of calcium (zero calcium) and under calcium-saturated conditions (maximal calcium). For calibrating zero calcium, each cell, after perfusion with caffeine, was perfused for 120 s with Tyrode solution with zero free calcium containing an additional 10 mM EGTA and 10 μM calcimycin. Then, for calibrating maximal calcium, the same cell was perfused with Tyrode solution containing: 10 mM CaCl<sub>2</sub>, 10 μM calcimycin, 10 μM FCCP, 2 μM Thapsigargin, 2 μM oligomycin, and 55 μg/mL eschin. In addition, solutions with caffeine, zero and maximal calcium contained 20 mM BDM.

Confocal images were acquired using Zeiss LSM 900 system (Carl Zeiss) with a ×63 water-immersion objective (1.2 NA). Fluo4 was excited with a 488-nm laser and the emission in the range of 490–700 nm was collected by a gallium arsenide phosphide photomultiplier tube using 8-bit mode.

Similarly to calcium transients and sparks measurements, linescans were performed unidirectionally, and *xt* images were made to cover a line of  $\sim 70$   $\mu\text{m}$  (512 pixels, 0.83- $\mu\text{m}$  pixel size) along the cell, avoiding nuclei. The background estimation and analysis of the data were performed as in *Detection and Analysis of Calcium Transients and Sparks* (see above).

### Dyssynchrony Index Calculation

The dyssynchrony index was calculated as in Ref. 51. In short, *xt* scan images acquired for  $\text{Ca}^{2+}$  transients and spark determination (see above) were split into smaller sections along the *x*-axis, 16 pixels per section. The signal in each section was averaged and analyzed as  $\text{Ca}^{2+}$  transient above. Time-moments at which local  $\text{Ca}^{2+}$  transient reached half-maximum at the beginning of the transient were found and stored in the central database. Dyssynchrony index was calculated as a logarithm of standard deviation of the time-moments for each transient separately. Next, the dyssynchrony index for an experiment was found as an average index of all transients measured in the experiment, usually 5–15.

### Detecting t-Tubular Network

Freshly isolated cells were loaded with CellMask Green Plasma Membrane Stain (Invitrogen, C37608) at 1:1,000 dilution in respiration solution containing (in mM): 110 sucrose, 60 K-lactobionic acid, 3  $\text{KH}_2\text{PO}_4$ ,  $\text{MgCl}_2$ , 20 HEPES, 20 taurine, 0.5 EGTA, and 0.5 dithiothreitol (pH was adjusted to 7.1 with KOH). After incubation for 20 min at room temperature and sedimentation of the cells, the supernatant was removed and replaced with the fresh respiration solution. Cell suspension (100–150  $\mu\text{L}$ ) was added into the chamber of a flexiPERM micro 12 reusable silicone cell culture chamber (Greiner Bio-One) attached to a coverslip. Imaging was performed using either Zeiss LSM 510 Duo or Zeiss LSM 900 system (Carl Zeiss) with a  $\times 63$  water-immersion objective (1.2 NA). CellMask was excited with a 488-nm laser. In the case of Zeiss LSM 900, the emission in the range of 495–700 nm was collected by a gallium arsenide phosphide photomultiplier tube using 16-bit mode. When Zeiss LSM 510 Duo was used, emission was recorded through a 505-nm long-pass filter by a high-voltage single photomultiplier tube using 12-bit mode.

The t-tubular network was detected and analyzed as in Ref. 51. In short, the confocal microscopy images were analyzed using Ilastik (56) and custom postprocessing scripts. All images were stored and processed using local OMERO server (57). The analysis was performed in the following stages. First, a neural network was trained in Ilastik to classify pixels belonging to the t-tubules or background. Care was taken to mark as t-tubules only the pixels close to the center of each t-tubule, thereby obtaining the thinnest possible representation of the t-tubular network. Second, in all analyzed images, a region corresponding to the intracellular space excluding nuclei and sarcolemma was marked in OMERO. Third, with the training ready and intracellular space marked in OMERO, we processed all images using the custom script to detect t-tubules and store corresponding skeleton in OMERO as a region of interest. For that, Ilastik classification was loaded, and pixels classified as belonging

to the t-tubule network were dilated by one pixel. After that, connected regions were evaluated for size and regions smaller than 16 pixels were excluded from further analysis. Remaining regions were skeletonized. Skeleton was analyzed to remove small edges (smaller than 5 pixels), with the remaining skeleton saved as region of interest in OMERO. These image manipulations were performed using packages scikit-image (58) and sknw of ImagePy (59).

With t-tubules detected and stored in OMERO, we determined the overall t-tubule network length per intracellular area. The network orientation was described by calculating the overall length of all network segments in that orientation (within given range of angles, see results) per intracellular area. To describe branching patterns of the network, Minkowski–Bouligand fractal dimension was determined.

Developed scripts are released open-source and available at <https://gitlab.com/iocbio/ttubules>.

### Superresolution Imaging and Image Analysis

Fixed cardiomyocytes were placed on poly-L-lysine (Sigma Aldrich, P8920)-coated coverslips (MatTek, P35G-0.170-14-C) and left to sediment for 30 min. Next, the supernatant was removed, and cells were permeabilized with the addition of 0.5% Triton X-100 in Dulbecco's PBS (Biowhittaker, No. 4387) for 10 min. After permeabilization, cells were washed three times with PBS (5 min between each wash) and blocked using Image-iT FX Signal Enhancer (Invitrogen, I36933) for 30 min at room temperature. Cells were immunolabeled with primary anti-RyR antibody (ThermoFisher Scientific, MA3-916) at 1:100 dilution in a low blocking buffer (2.5% normal goat serum in PBS) overnight at 4°C. The following day, cells were washed three times with PBS, after which secondary antibody (goat anti-mouse IgG Alexa Fluor Plus 647, Invitrogen, A32728) was added at 1:100 dilution in the low blocking buffer and incubated at room temperature for 1 h. Finally, cells were washed three times with PBS, and imaging buffer containing 20% VectaShield (Vector Laboratories, H-1000) diluted in TRIS-Glycerol (5% vol/vol TRIS 1 M pH 8 in Glycerol, Sigma Aldrich) was added before imaging. This composition has been previously shown to produce comparable, if not superior, quality dSTORM images compared with conventional oxygen scavenging-dependent systems (60).

Imaging was carried out using the Zeiss ELYRA/LSM 710 system (Carl Zeiss) equipped with a Zeiss  $\alpha$  Plan-Apochromat  $\times 63$  1.46 NA objective (420780-9970-000, Carl Zeiss). A 642-nm laser illumination at 300 W/mm<sup>2</sup> was used for excitation. For 3-D imaging, the excitation beam was configured in a highly inclined and laminated optical sheet (HiLo), utilizing Phase Ramp Imaging Localization Microscopy (PRILM) technology (61). Emission  $> 655$  nm was collected with an iXon 897 back-thinned EMCCD camera (Andor Technology, Belfast), where EMCCD gain was set to 100, the frame exposure time to 40 ms, and 15,000 frames were acquired per cell. Throughout image acquisition, a piezo-operated Definite Focus system was used to autocorrect for axial drift.

The "PALM Processing" module in the ZEN Black software (Carl Zeiss) was used to reconstruct dSTORM data. In short, an 11-pixel circular mask with a signal-to-background noise ratio of 6 was used to detect the individual single-fluorophore blinks. For mapping blinks to 3-D space, an experimental 3-D

point spread function with an axial range of 4  $\mu\text{m}$  was acquired using 100-nm fluorescent beads (Thermo Fisher Scientific, T7279). The drift correction was performed using a five-segment piece-wise linear function. Events from only the central 600 nm of the 4- $\mu\text{m}$  stack were included for further analysis to minimize the inclusion of clusters with larger localization error (61). The x, y, and z coordinates of each localization event were saved in a comma-separated value format.

Custom Python scripts were used to estimate RyR cluster and  $\text{Ca}^{2+}$  release unit (CRU) size, count, and density per imaging volume, the nearest neighbor distance between RyR clusters, and rendering point data. Briefly, on the basis of the point data, 3-D histogram was created with a bin size of 30 nm in the lateral and axial directions. The image was then convolved with a Gaussian filter whose width corresponded to single event lateral and axial precision values and thresholded image using the thresholding Otsu method. This resulted in a binary image where each voxel contained no more than a single RyR. From the binary image, RyR clusters were determined as areas where the non-zero pixels were side-by-side. RyR clusters with edges localized within 100 nm were assigned to the same CRU (62).

#### Western Blot Analysis

##### **PLB, pPLB Ser-16, pPLB Thr-17.**

Ten micrograms (8  $\mu\text{g}$  in case pPLB Thr-17) of protein was preheated at 95°C for 5 min and loaded onto SDS-PAGE gels (4% stacking gel, 15% separating gel), which were run at 60 V for 35 min, followed by 120 V for 50–55 min in a Mini-PROTEAN Tetra System using a PowerPac HC power supply (Bio-Rad Laboratories). The separated proteins were transferred onto a 0.2- $\mu\text{m}$  PVDF membrane for 5 min following Bio-Rad low MW protocol (2.5 A, up to 25 V) using a Trans-Blot Turbo Transfer System (Bio-Rad Laboratories).

##### **RyR, pRyR Ser-2808, pRyR Ser-2814.**

Thirty micrograms (RyR and pRyR Ser-2808) or 50  $\mu\text{g}$  (pRyR Ser-2814) of protein was preheated at 37°C for 10 min (RyR and pRyR Ser-2808) or 15 min (pRyR Ser-2814) and loaded onto SDS-PAGE Mini-PROTEAN TGX precast gels (4–15%, Bio-Rad Laboratories), which were run at 120 V for 1 h in a Mini-PROTEAN Tetra System using a PowerPac HC power supply (Bio-Rad Laboratories). The separated proteins were transferred onto a 0.45- $\mu\text{m}$  PVDF membrane for 1 h on ice at 0.35 A (RyR and pRyR Ser-2808) or using a Trans-Blot Turbo Transfer System (Bio-Rad Laboratories) for 10 min following Bio-Rad high MW protocol (1.3 A, up to 25 V; pRyR Ser-2814).

##### **AMPK, pAMPK Thr-172, LKB1, S100A1, BIN1.**

Twenty micrograms (AMPK, p-AMPK, and S100A1) or 30  $\mu\text{g}$  (BIN1) of protein was preheated at 90°C for 5 min and loaded onto SDS-PAGE gels, which were run at 60 V for 40 min, followed by 120 V for 60 min in a Mini-PROTEAN Tetra System using a PowerPac HC power supply (Bio-Rad Laboratories). All the gels had 4% stacking gel, and the resolving gels were 8% for BIN1, 12% for AMPK, p-AMPK, and LKB1, and 15% for S100A1. The separated proteins were transferred using a Trans-Blot Turbo Transfer System (Bio-Rad Laboratories). For S100A1, the proteins were transferred onto a 0.2- $\mu\text{m}$  nitrocellulose membrane for 5 min following the Bio-Rad

low MW protocol (2.5 A, up to 25 V). For AMPK, p-AMPK, LKB1, and BIN1, the proteins were transferred onto a 0.45- $\mu\text{m}$  nitrocellulose membrane for 7 min following the Bio-Rad mixed MW protocol (2.5 A, up to 25 V).

After transfer, the nitrocellulose membranes were treated with 0.1% Ponceau solution to stain the proteins and imaged in an Image Quant LAS 400 Imager for normalization, before the Ponceau was washed off by three washes in Tris-buffered saline with 0.1% Tween-20 (TBST) containing various reagents. All membranes were blocked for 1 h with 5% nonfat milk or 3% BSA (pRyR Ser-2814) and then incubated with primary antibody in TBST containing 5% BSA or no BSA (pRyR Ser-2814) overnight at 4°C. The next day, the membranes were incubated with secondary antibody in 5% BSA or 3% BSA (pRyR Ser-2814) for 1 h at room temperature. Between each step, the membranes were washed three times for 7–10 min in TBST. After the final wash, the antibodies were detected with the Bio-Rad Clarity Western ECL substrate, imaged in an Image Quant LAS 400 imager (GE Healthcare, Chicago, IL). The following primary antibodies were used: AMPK (Cell Signaling 2532, RRID AB\_330331, dilution 1:1,000), AMPK-phospho-Thr172 (Cell Signaling 2535, RRID AB\_331250, dilution 1:1,000), BIN1 (Santa Cruz sc-23918, RRID AB\_667901, dilution 1:500), LKB1 (Cell Signaling 3047, RRID AB\_2198327, dilution 1:1,000), PLB (Abcam ab86930, RRID AB\_1952347, dilution 1:1,000), PLB-phospho-Ser16 (Abcam ab15000, RRID AB\_301562, dilution 1:1,000), PLB-phospho-Thr17 (Badrilla A010-13AP, RRID AB\_2617048, dilution 1:1,000), RyR2 (Invitrogen PA5-87416, RRID AB\_2804131, dilution 1:2,000), RYR2-phospho-S2808 (Abcam ab59225, RRID AB\_946327, dilution 1:2,000), RYR2-phospho-S2814 (Badrilla A010-31, RRID:AB\_2617055, dilution 1:1,000), and S100A1 (GeneTex GTX11428, RRID: AB\_372948, dilution 1:5,000). For the Western blots on PVDF membranes, anti-GAPDH (Cell Signaling Technology 2118, RRID AB\_561053) was used to assess the expression of GAPDH, a commonly used house-keeping protein. When assessing PLB relative to GAPDH, the anti-GAPDH dilution was 1:6,000, when assessing RyR and pRyR Ser-2808 relative to GAPDH, the anti-GAPDH dilution was 1:8,000, and when assessing pRyR Ser-2814 relative to GAPDH, the anti-GAPDH dilution was 1:10,000. The secondary antibody was a horseradish peroxidase (HRP)-conjugated goat anti-rabbit IgG (H + L, Jackson ImmunoResearch Laboratories, Inc.), which was used at a dilution of 1:10,000 for detection of AMPK, p-AMPK, BIN1, LKB1, PLB, pPLB Ser-16, pPLB Thr-17, and pRyR Ser-2814, 1:20,000 for detection of RyR and pRyR Ser-2808, 1:50,000 for detection of S100A1, 1:60,000 for detection of GAPDH relative to PLB, pPLB Ser-16, pPLB Thr-17, 1:80,000 for detection of GAPDH relative to RyR and pRyR Ser-2808, and 1:100,000 for detection of GAPDH relative to pRyR Ser-2814.

##### **Expression analysis.**

Expression was analyzed as in Refs. 29 and 35, with the exception that the staining intensity was quantified using ImageJ or in IOC BIO Gel (63). In short, the samples were distributed in random order on a gel, with each gel having two lanes allocated to the reference samples consisting of a mix of all samples for normalization. Each sample was measured at least two or three times in different gels. Before the

measurements, dilutions of primary and secondary antibodies were calibrated to ensure proportionality of the measurement with the content of the protein of interest.

For the statistical analysis, the signal of the protein of interest was normalized to protein content or GAPDH intensity. For analysis of expression levels, all measurements were taken into account while linking all repeated measurements of each sample in the statistical software. When analyzing phosphorylated state relative to overall expression of the protein, repeated measurements from each sample for the overall and phosphorylated state expressions were averaged before finding the ratio.

### Statistics

If not stated otherwise, statistics are reported using means  $\pm$  SE. For experiments repeated on several cells from the same animal, we used linear mixed models to quantify the impact of the fixed factors. The models were composed with random intercepts. Where repeated measurements from the same cell were analyzed, the random intercepts were considered for nested random effects, taking into account animal-cell relationship. To determine significance of the fixed factor(s) and their interaction(s), we composed models with and without the corresponding factor or interaction, and *P* values were obtained by likelihood ratio test of the full and simplified models.

In addition, ANOVA was used to study the effects of factors when marked in the text.

The impact is calculated as the corresponding *P* value and indicates whether the factor is statistically significant (*P* value is low) or not. These calculations take into account the full dataset, not just two separate conditions. To reflect the results of the statistical analysis of such datasets, as a notation, the results are shown under the analyzed data if there were more than two factors considered in the figure. For example, in Fig. 1, we considered the impacts of genotype (WT vs. KO), sex (female vs. male), and solution (with and without ISO). For those unfamiliar with the use of linear mixed models for testing the significance of the factors, one could consider them as an analysis of pooled data. Thus, significance of the factor solution would correspond to the pooled data with and without ISO being statistically significantly different. Although not exactly the same, it gives a perception of the analysis to the reader not used to this approach.

Statistical analysis was performed in R (64) using lme4 (65) for linear mixed-model analysis. *P* < 0.05 was considered statistically significant and is marked in bold in the figures.

Data was fetched from the central database using scripts from IOCBIO Kinetics (55).

## RESULTS

### AGAT KO Mice Are Smaller than Their Wildtype Littermates and Have Smaller Cardiomyocytes

The characteristics of the animals used in the study are given in Table 1. Body weight, tibial length (TL), and heart weight (HW) were affected by genotype and sex, with AGAT KO and females being smaller than AGAT WT and males,

respectively. These data agree with earlier observations (28, 29, 35).

When heart weights were normalized to body weight, it was significantly higher in AGAT KO than in WT mice. This finding has been reported previously and is attributed to the severe skeletal muscle atrophy characteristic of AGAT KO mice (29, 32). However, when heart weights were normalized to tibial length, it was significantly higher in WT than in KO mice and in males compared with females. A similar conclusion was reached using dimensionally consistent indexing with tibial length cubed (66), as shown in Table 1. To put the reduction of heart weight in AGAT KO into perspective, the knockouts had 17–18% lower normalized heart weight (HW/TL<sup>3</sup>) compared with WT mice of the same sex, while the difference between male and female hearts was 10–12% within each genotype. Thus, the reduction induced by creatine deficiency was moderately larger than the sex-related differences observed within each genotype group.

The length and width of the isolated cardiomyocytes are shown in Table 2. The cardiomyocytes from AGAT KO mice were significantly smaller than the cardiomyocytes from WT mice.

Based on these results, we conclude that cardiac atrophy occurs in AGAT KO mice.

### AGAT KO Cardiomyocytes Have Larger and Longer Ca<sup>2+</sup> Transients than in WT

Cardiomyocytes from failing hearts (HFREF) exhibit reduced amplitude and slower relaxation of Ca<sup>2+</sup> transients (42). In AGAT KO, we similarly observed smaller Ca<sup>2+</sup> fluxes through LTCC and SERCA in patch-clamped cardiomyocytes stimulated with square pulses (33). However, the behavior of patch-clamped cells is strongly dependent on the pipette solution, and in that study, the solution contained phosphocreatine. To address this potential confounding factor, we presently assessed Ca transients in intact, field-stimulated AGAT KO cardiomyocytes. The Ca<sup>2+</sup> transients were recorded by measuring the fluorescence of the Ca<sup>2+</sup>-sensitive dye (Fura-2/AM). The data were analyzed using linear mixed models (for details, see MATERIALS AND METHODS, *Statistics*). Representative transients from AGAT KO and WT cells recorded in the presence of isoprenaline (ISO), stimulating the  $\beta$ -adrenergic signaling cascade, are shown in Fig. 1A.

According to our measurements (Fig. 1), the Ca<sup>2+</sup> transient amplitude was higher and the duration was longer in AGAT KO in both the absence (Control) and presence of ISO (Fig. 1, C and D). The larger Ca<sup>2+</sup> transient amplitude in AGAT KO was accompanied by a higher Ca<sup>2+</sup> rise rate (Fig. 1E), but the transient decay rate was similar in AGAT KO and WT (Fig. 1F). Thus, the longer Ca<sup>2+</sup> transient duration was related to the higher Ca<sup>2+</sup> transient amplitude and not due to a slower rate of Ca<sup>2+</sup> removal from the cytoplasm. We did not find any statistically significant impact of sex in these data.

When compared with control conditions, ISO led to larger Ca<sup>2+</sup> transients, with faster kinetics with increases in both the rates of Ca<sup>2+</sup> rise and decay (Fig. 1). Interestingly, ISO increased the Ca<sup>2+</sup> transient amplitude more in AGAT KO than in WT cardiomyocytes (*P* < 0.001 for interaction between genotype and solution). This suggests that AGAT

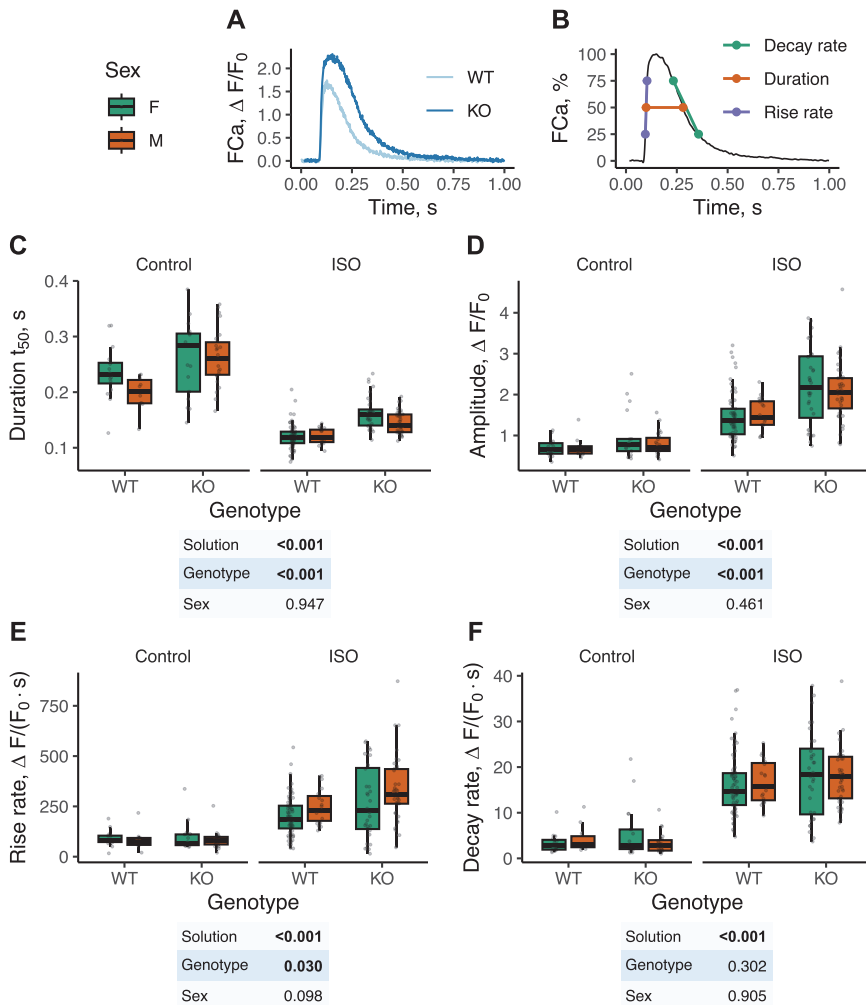


**Figure 1.** Larger  $Ca^{2+}$  transient amplitude with prolonged duration in AGAT KO cardiomyocytes when compared with WT littermates.  $Ca^{2+}$  concentration changes were visualized using Fluo-4 with its fluorescence FCa recorded by confocal line-scan along the cardiomyocytes. The figure key is on the top left. The summary of statistical analysis by linear mixed models is depicted below the graphs and shows the significance of the factors by *P* value. **A:** representative spatially averaged FCa changes recorded in AGAT KO and WT cardiomyocytes in the presence of ISO. Notice the larger amplitude and prolonged transient in AGAT KO. **B:** scheme visualizing the determination of duration and rates of rise and decay for a transient. **C:** transient duration. **D:** transient amplitude. **E:** transient rise rate. **F:** transient decay rate. All parameters were significantly affected by the solution, as in the presence of 50 nM isoprenaline (ISO), the transients were shorter (C), but with higher amplitudes (D) and faster rates of rise (E) and decay (F). In AGAT KO compared with WT cardiomyocytes, the transients were longer (C), with a higher amplitude (D) and faster rate of rise (E) and faster rate of decay (F). The number of animals and cells used in the experiments were as follows (reported in animals/cells notation): AGAT WT female (11/81), AGAT WT male (4/29), AGAT KO female (7/49), and AGAT KO male (8/61). As the contribution of solution was significant for all analyzed measurements, the contribution of the genotype and sex was determined by including solution into the null model. AGAT, arginine:glycine amidinotransferase; FCa, fluorescence of the  $Ca^{2+}$ -sensitive dye.

KO cardiomyocytes exhibit a stronger response to ISO than WT cardiomyocytes.

### Similar Dyssynchrony of $Ca^{2+}$ Transients and Only Modest Changes in the t-Tubular Network

As dyssynchrony of  $Ca^{2+}$  transients has been reported in heart failure (44), we studied the synchronicity of  $Ca^{2+}$  release

in AGAT KO cardiomyocytes. Cardiomyocytes with synchronous and dyssynchronous  $Ca^{2+}$  transients were found in all the groups studied, and each animal would have cells with different characteristics (Supplemental Fig. S1A). Overall,  $\beta$ -adrenergic stimulation with ISO led to more synchronous  $Ca^{2+}$  transients (Supplemental Fig. S1B), but there was no difference between AGAT KO and WT (Supplemental Fig. S1B).

**Table 1.** Body weight, tibial length, and the heart weight of the animals in the different groups

Genotype	Sex	n	Age, days	BW (n), g	TL (n), cm	HW (n), mg	HW/BW (n)	HW/TL (n), mg/cm	HW/TL <sup>3</sup> (n), mg/cm <sup>3</sup>
WT	Female	24	250 ± 8	25 ± 0.5 (24)	2.20 ± 0.01 (24)	109 ± 9 (6)	4.29 ± 0.25 (6)	49.8 ± 3.8 (6)	10.4 ± 0.7 (6)
	Male	17	262 ± 9	32 ± 0.7 (16)	2.24 ± 0.01 (17)	137 ± 2 (7)	4.26 ± 0.15 (6)	60.6 ± 1 (7)	11.8 ± 0.2 (7)
KO	Female	21	238 ± 10	15 ± 0.3 (21)	2.07 ± 0.01 (21)	79 ± 4 (5)	5.68 ± 0.11 (5)	37.7 ± 1.8 (5)	8.6 ± 0.4 (5)
	Male	22	240 ± 8	17 ± 0.3 (22)	2.10 ± 0.01 (22)	89 ± 4 (7)	5.54 ± 0.16 (7)	42.4 ± 1.7 (7)	9.7 ± 0.4 (7)
Effect of genotype				<i>P</i> < 0.001					
Effect of sex				<i>P</i> < 0.001	<i>P</i> < 0.001	<i>P</i> = 0.001		<i>P</i> = 0.002	<i>P</i> = 0.013

Data presented as means ± SD with *n* shown in brackets. BW, body weight; HW, heart weight; TL, tibial length.

Dyssynchrony of Ca<sup>2+</sup> transients in failing hearts is related to a disruption of the t-tubular network and, in particular, to a loss of transversal t-tubules (43–45). Therefore, we also assessed the t-tubular organization in AGAT KO and WT cardiomyocytes (Fig. 2). We found moderate differences between male AGAT KO and WT. In male AGAT KO cardiomyocytes, the t-tubular network was shorter (Fig. 2B) and with a reduced fractal dimension, a measure describing how well the network fills the space (Fig. 2C). This could be attributed to a reduction in longitudinal t-tubules (Fig. 2D). However, there were no differences in the transversal t-tubules between AGAT KO and WT. This is in agreement with the similar dyssynchrony indexes for AGAT KO and WT, as the transversal t-tubules play a main role in the excitation and Ca<sup>2+</sup> transients.

### Ca<sup>2+</sup> Sparks Are More Frequent and Prolonged in AGAT KO Cardiomyocytes

As we found that AGAT KO resulted in changes of Ca<sup>2+</sup> transients that were opposite to the impact of heart failure (Fig. 1), we looked into elementary Ca<sup>2+</sup> release events, Ca<sup>2+</sup> sparks (67), shown in Fig. 3A. We detected sparks with different amplitudes and plotted their frequency as a histogram (Fig. 3B). When analyzing the data from WT mice separately, we found that cardiomyocytes from female mice have a higher spark frequency in the presence of ISO (51). When analyzing the data from AGAT KO and WT together, we found no significant sex differences, probably due to the spread of the data. However, cardiomyocytes from AGAT KO had significantly higher spark frequency than WT (effect of genotype and its interaction with the amplitude; Fig. 3B). In addition, the spark duration was longer in AGAT KO than in WT (Fig. 3C), while the spark width was similar (Fig. 3D).

Spark pairs (example shown in the top half of Fig. 3A) can be used to analyze SR refilling by following the ratio between amplitudes of the second and first spark in a pair as a function of spark-to-spark delay time (68), as shown in Supplemental Fig. S2. However, the number of spark pairs in the AGAT WT group was too small to perform this analysis with high

precision, and we found no difference between AGAT KO and WT (*F* test, nested models comparison).

Interestingly, despite the significantly higher spark frequency in AGAT KO cardiomyocytes, their probability of exhibiting calcium waves after pacing was the same as in WT (results not shown).

### SR Ca<sup>2+</sup> Content is Larger in AGAT KO than in WT

As we observed higher Ca<sup>2+</sup> transient amplitude and Ca<sup>2+</sup> spark frequency in AGAT KO, we performed a separate set of experiments to estimate SR Ca<sup>2+</sup> content. For that, we recorded the Ca<sup>2+</sup> released from the SR by caffeine application (Fig. 4). We used the peak Ca<sup>2+</sup> concentration change ( $\Delta$ Ca<sup>2+</sup>) in the cell as a measure of SR load (see MATERIALS AND METHODS for details). As shown in Fig. 4B, when taking KO and WT together, the presence of ISO increased SR Ca<sup>2+</sup> content (effect of solution), and female cardiomyocytes responded more to ISO than males (effect of interaction between sex and solution). In line with the observed differences in Ca<sup>2+</sup> transients (Fig. 1) and spark frequencies (Fig. 3), we observed a significant effect of genotype in the statistical analysis, demonstrating that the SR Ca<sup>2+</sup> content is higher in AGAT KO cardiomyocytes.

During caffeine application, the Ca<sup>2+</sup> released from the SR is extruded from the cell by the NCX. Therefore, we estimated the NCX activity as the rate with which the intracellular Ca<sup>2+</sup> concentration declined after the peak ( $\Delta$ Ca<sup>2+</sup> decay rate). We found no differences between AGAT KO and WT cardiomyocytes (Fig. 4C), suggesting that their NCX activity was similar.

### The Spatial Arrangement of RyRs is Mainly Altered in Female WT but Not AGAT KO Cardiomyocytes

The Ca<sup>2+</sup> spark frequency can be affected by the organization of RyRs. Although a higher Ca<sup>2+</sup> spark frequency is frequently associated with larger clusters of RyRs (69), the lower spark frequency often observed in heart failure is accompanied by the dispersion of RyR clusters (46, 47). Therefore, we

**Table 2.** Length and width of cardiomyocytes from male and female AGAT KO and WT mice

Genotype	Sex	n	Cardiomyocyte Length, $\mu$ m	Cardiomyocyte Width, $\mu$ m	Width/Length, %
WT	Female	5	120.4 ± 3.7	25.5 ± 0.5	22.0 ± 0.6
	Male	5	129.6 ± 5.2	27.4 ± 0.7	22.2 ± 1.0
KO	Female	5	109.7 ± 1.6	20.4 ± 0.6	19.4 ± 0.5
	Male	5	107.3 ± 2.9	23.7 ± 1.3	23.2 ± 1.7
Effect of genotype			<i>P</i> < 0.001	<i>P</i> < 0.001	
Effect of sex				<i>P</i> < 0.01	

Data presented as means ± SD.

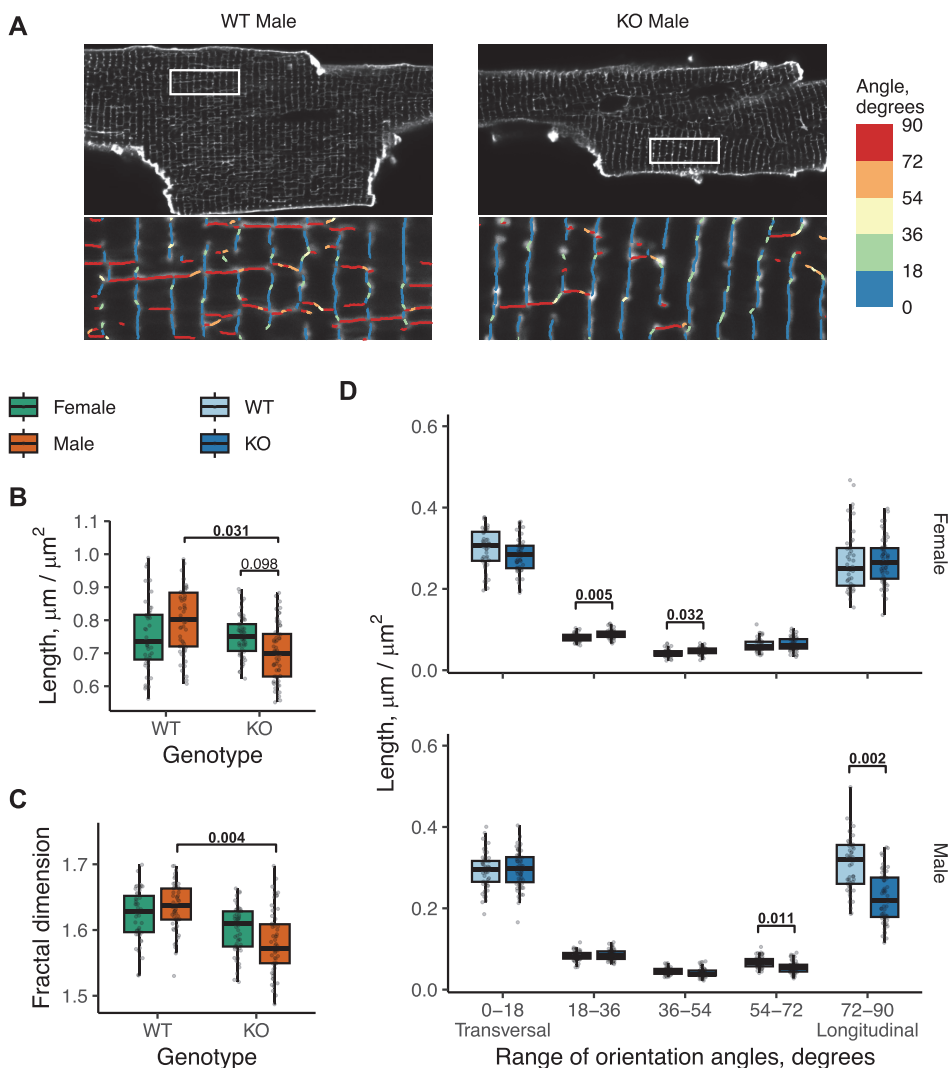


**Figure 2.** Male AGAT KO mice have fewer longitudinal t-tubules. The sarcolemma of live cardiomyocytes from AGAT KO and WT littermates was labeled with CellMask and imaged in a confocal microscope. Figure key is above *B*. *A*: representative images of the t-tubules (*top*) in cardiomyocytes isolated from male KO and WT mice. The automatic detection of the network in the small section of the image (section shown by white box  $20 \times 7 \mu\text{m}$  on the image in the *top*) is demonstrated at the *bottom*. The orientation of t-tubules was divided into five groups from  $0^\circ$ – $90^\circ$  and indicated in color, as shown on the *right*, with  $0^\circ$ – $90^\circ$  corresponding to the transversal and longitudinal orientation, respectively. *B*: the overall length of the t-tubules was significantly lower in male AGAT KO than in male WT littermates. There were no statistically significant sex differences. *C*: the fractal dimension of the t-tubules, a measure of the space-filling capacity, was significantly lower in AGAT KO males. *D*: the overall length of differently oriented segments of t-tubules clearly shows the reduction of longitudinally oriented t-tubules in male AGAT KO compared with male WT littermates. This difference was not observed in female AGAT KO and WT. The number of animals and cells used in the experiments were as follows (reported in animals/cells notation): AGAT WT female (5/47), AGAT WT male (5/53), AGAT KO female (5/54), and AGAT KO male (5/60). Statistical analysis was performed using linear mixed models to take into account the repeated measurements from the same animal. Comparisons were done for sex as a factor when comparing female and male parameters for WT or KO separately (*C* and *D*). For contribution of genotype, females WT and KO were compared and similar comparison was done for males (*B*, *C*, and *D*). In the figure, *P* value is shown only if smaller than 0.15. AGAT, arginine:glycine amidinotransferase.

studied the RyR distribution in cardiomyocytes using dSTORM super-resolution imaging. Representative images of RyRs from female AGAT KO and WT are shown in Fig. 5A with 3-D rotation of the region shown in Supplemental Video S1.

When analyzing the data from WT mice separately, we found that the higher spark frequency correlated with fewer, but larger, RyR clusters in female cardiomyocytes (49). In WT mice, female cardiomyocytes had 25% more RyRs in a

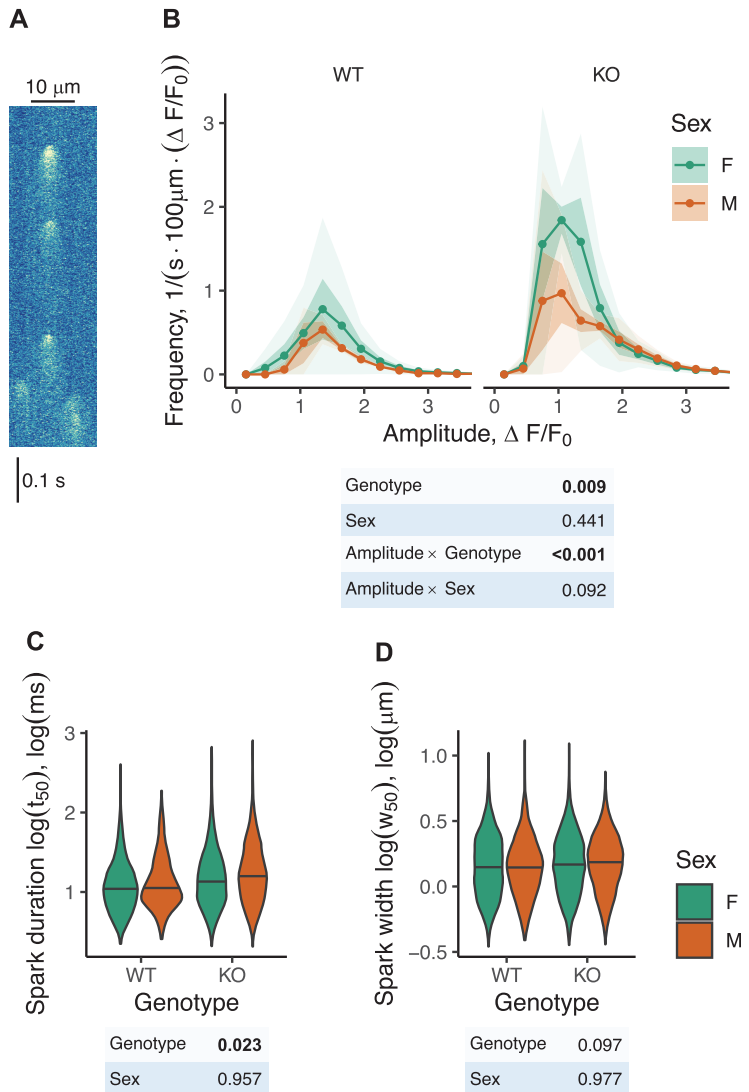


**Figure 3.** Impact of AGAT KO and sex on  $\text{Ca}^{2+}$  spark frequency and morphology. The summary of statistical analysis by linear mixed models is depicted below the graphs. **A:** representative sparks measured in a confocal microscope. **B:** mean spark frequency distribution ( $\pm$ SE shown by darker shaded area;  $\pm$ SD shown as lighter shaded area) as a function of spark amplitude in the different groups. The mean value was found by averaging data obtained on the animal first and then finding mean, SD, and SE from animal-averaged dataset. AGAT KO cardiomyocytes had a significantly higher frequency of sparks than WT littermates. Spark duration in AGAT KO was longer than in WT (C, log10 scale), while the width was not statistically significantly different between AGAT KO and WT (D, log scale). In some of the statistical tests, sex was found to be a significant factor. The number of animals and cells used in the experiments were as follows (reported in animals/cells notation): AGAT WT female (9/69), AGAT WT male (3/27), AGAT KO female (6/41), and AGAT KO male (7/54). AGAT, arginine:glycine amidinotransferase.

cluster than male cardiomyocytes (females  $19.0 \pm 0.6$  vs. males  $15.1 \pm 0.6$  RyRs per cluster,  $P = 0.028$ ). However, in AGAT KO cardiomyocytes, average RyR cluster size reduced in both sexes (KO females  $12.6 \pm 0.7$  vs. KO, males  $13.1 \pm 0.7$  RyRs per cluster, Fig. 5B), whereas in females (KO vs. WT), the decrease was statistically significant ( $P = 0.005$ ). Most of the differences between AGAT KO and WT were only found in females, where WT cardiomyocytes had more RyRs per cluster (Fig. 5B), more clusters per CRU (Fig. 5C), and smaller cluster density (Fig. 5D). However, the overall RyR densities did not differ between any groups (Fig. 5E). Thus, the main difference between genotypes came from the fact that female WT had fewer, larger clusters than male WT cardiomyocytes,

while there was no difference between the sexes in AGAT KO cardiomyocytes.

**Minor Changes in RyR, but no Changes in PLB Expression and Phosphorylation**

We used Western blotting to look further into the molecular mechanisms behind the increased spark frequency and higher SR  $\text{Ca}^{2+}$  load in AGAT KO cardiomyocytes. RyR assembly in the dyadic space and spark frequency are affected by phosphorylation at Ser2808 and Ser2814, which are the sites of PKA and CaMKII phosphorylation, respectively (49, 70). Spark frequency is also affected by SR  $\text{Ca}^{2+}$  load, which in turn depends on the rate with which SERCA

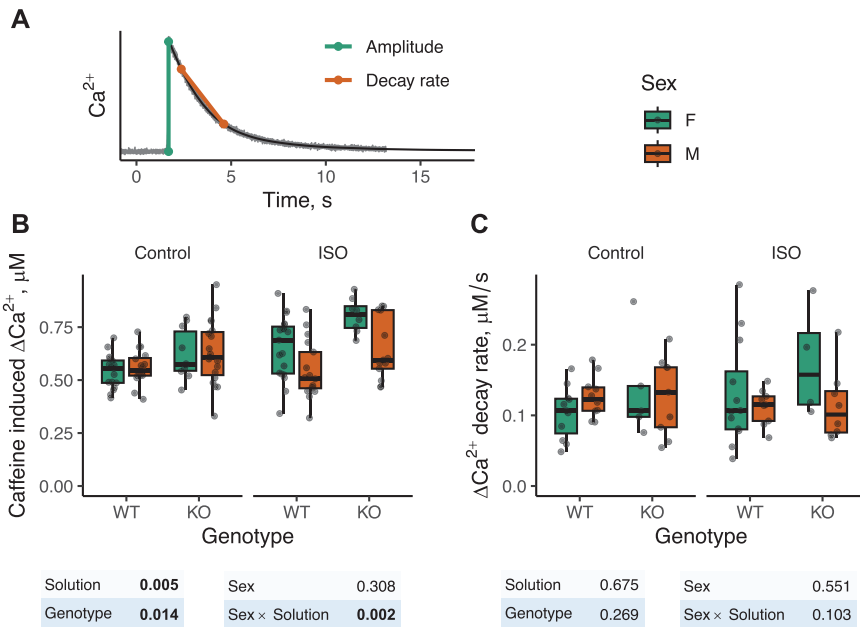


**Figure 4.** The SR  $\text{Ca}^{2+}$  content is larger in AGAT KO compared with WT cardiomyocytes. Caffeine-induced SR  $\text{Ca}^{2+}$  release led to a transient increase in the intracellular  $\text{Ca}^{2+}$  concentration, which was recorded using the  $\text{Ca}^{2+}$  indicator Fluo-4. *A*: representative trace showing the  $\text{Ca}^{2+}$  concentration as a function of time, and how the amplitude and decay rate are calculated. *B*: the amplitude of the  $\text{Ca}^{2+}$  concentration change,  $\Delta\text{Ca}^{2+}$ , was taken as a measure of SR  $\text{Ca}^{2+}$  content. It was recorded in female and male AGAT WT and KO cardiomyocytes under control conditions and in the presence of 50 nM isoprenaline (ISO) to stimulate the adrenergic signaling pathway. A summary of the statistical analysis by linear mixed models is depicted below the graph. Note that  $\Delta\text{Ca}^{2+}$  was significantly higher in AGAT KO than in WT (effect of genotype). It was also significantly higher in the presence of ISO (effect of solution), with females responding more than males to ISO (interaction between sex and solution). The number of animals and cells used in the experiments were as follows (reported in animals/cells notation): AGAT WT female (7/36), AGAT WT male (6/33), AGAT KO female (4/18), and AGAT KO male (6/32). *C*: during caffeine application, the  $\text{Ca}^{2+}$  released from the SR is extruded from the cell by the  $\text{Na}^{+}$ - $\text{Ca}^{2+}$  exchanger (NCX). The rate with which the intracellular  $\text{Ca}^{2+}$  concentration decays,  $\Delta\text{Ca}^{2+}$  decay rate, can be taken as a measure of the NCX activity. A summary of the statistical analysis by linear mixed models is depicted below the graph. The  $\Delta\text{Ca}^{2+}$  decay rate was the same in male and female AGAT WT and KO cardiomyocytes, and it was not affected by ISO. The number of animals and cells used in the experiments were as follows (reported in animals/cells notation): AGAT WT female (7/23), AGAT WT male (6/19), AGAT KO female (4/9), and AGAT KO male (6/17). AGAT, arginine:glycine amidinotransferase; SR, sarcoplasmic reticulum.

pumps  $\text{Ca}^{2+}$  back into the SR during excitation-contraction coupling. As we showed in our previous study that SERCA expression is similar in AGAT KO and WT hearts (35), we looked into PLB, which is the main regulator of SERCA activity. Increased phosphorylation of PLB at Ser16 and Thr17 by PKA and CaMKII, respectively, has been shown to increase SR  $\text{Ca}^{2+}$  load, which in turn may increase spark frequency (71, 72).

Representative photos of the gels are shown in Supplemental Fig. S3, and the statistical analyses are shown in Supplemental Figs. S4 and S5. We originally used GAPDH as a loading control, but we observed a slightly higher GAPDH expression in AGAT KO compared with WT ( $P < 0.001$ , linear mixed models comparison of the dataset with both sexes, data not shown). Therefore, we show the data without normalization to GAPDH in Supplemental Fig. S4, where we assumed that the amount of protein transferred during Western blotting was proportional to the amount of protein loaded onto the gel. In addition, we show the data with normalization to GAPDH in Supplemental Fig. S5. For simplicity, we focus the text on the data in Supplemental Fig. S4.

There was a large variation for each target separately (Supplemental Fig. S4), but this was due to variation between

individuals (data not shown). The total expression of RyR did not differ between AGAT KO and WT hearts (Supplemental Fig. S4A). This finding corroborates the RyR content estimated by dSTORM (Supplemental Fig. S4H). Although the data point toward a somewhat reduced phosphorylation of Ser2808 RyR site in female compared with male AGAT KO (Supplemental Fig. S4B), and a reduced phosphorylation in Ser2814 RyR in AGAT KO compared with WT (Supplemental Fig. S4C), the relative phosphorylation states did not differ significantly (Supplemental Fig. S4, D and E, respectively).

The total expression (Supplemental Fig. S4F) and phosphorylation of PLB (Supplemental Fig. S4, G–J) were similar in AGAT KO and WT hearts. We conclude that RyR, SERCA, and PLB could not explain the higher SR  $\text{Ca}^{2+}$  load, spark frequency, and  $\text{Ca}^{2+}$  transients in AGAT KO cardiomyocytes.

#### The Expression of S100A1, but Not BIN1, is Higher in AGAT KO Cardiomyocytes

In addition to the SR  $\text{Ca}^{2+}$  load, we looked into two well-known modulators of CICR. BIN1 is an anchoring protein involved in the folding of t-tubules and in recruiting LTCC and RyR to the dyadic space (49, 50). Failing hearts have a

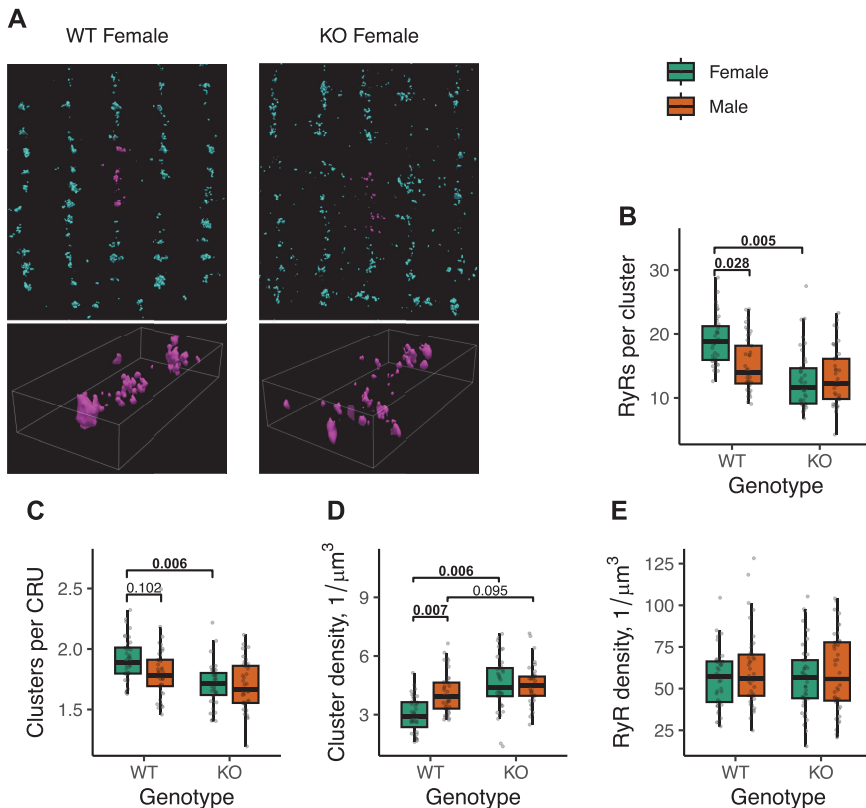


**Figure 5.** Analysis of super-resolution images of RyRs reveal multiple changes in RyR organization of female AGAT KO compared with WT littermates. Figure key is on the top right. *A*: representative images of RyRs in cardiomyocytes isolated from female KO and WT mice (image size  $10 \times 12 \mu\text{m}$ , top). Below, a 3-D rendering shows the RyRs marked in magenta on the top image (box size  $1.5 \times 2.55 \times 0.84 \mu\text{m}$ ). *B*: the number of RyRs in each cluster was significantly higher in female AGAT KO than in female KO or male WT littermates. *C*: female AGAT KO cardiomyocytes also had fewer RyR clusters per CRU when compared with female WT littermates. *D*: the overall RyR cluster density, i.e., the number of clusters per volume, was smaller for female AGAT WT than for female KO or male WT. *E*: the observed differences in RyR organization were not the result of the difference in the overall RyR content, estimated via the number of RyRs per unit volume, RyR density. All the studied groups had a similar RyR density, and no statistically significant differences were found between the groups. The number of animals and cells used in the experiments were as follows (reported in animals/cells notation): AGAT WT female (5/41), AGAT WT male (5/42), AGAT KO female (5/42), and AGAT KO male (5/40). Statistical analysis was performed using linear mixed models to take into account the repeated measurements from the same animal. Comparisons were done for sex as a factor when comparing female and male parameters for WT or KO separately. For contribution of genotype, females WT and KO were compared and similar comparison was done for males. In the figure, *P* value is shown only if smaller than 0.15. AGAT, arginine:glycine amidinotransferase; RyRs, ryanodine receptors.

lower expression of BIN1, and this is associated with severe disorganization of the t-tubules (43). Furthermore, overexpression of BIN1 partially rescues the function of failing hearts and improves survival (73, 74). However, in AGAT KO hearts, the expression of BIN1 did not differ from WT hearts (Fig. 6A, representative photos of the gels shown in Supplemental Fig. S6). This is in agreement with our finding that although AGAT KO males had fewer longitudinal t-tubules, there was no difference in the transversal t-tubules (Fig. 2), where BIN1 is localized (43).

S100A1 interacts with SERCA and RyR to increase SR  $\text{Ca}^{2+}$  load (75) and enhance CICR gain (48). Failing hearts have reduced S100A1 expression (76), and S100A1 overexpression rescues cardiac function after myocardial infarction

(77). Interestingly, the S100A1 expression was significantly higher in AGAT KO than in WT hearts (Fig. 6B, representative photos of the gels shown in Supplemental Fig. S6), suggesting that it may have a role in the AGAT KO phenotype.

#### Higher AMPK Activation in AGAT KO Hearts Suggest Higher Levels of AMP or ADP

We would expect that the larger  $\text{Ca}^{2+}$  transients in AGAT KO cardiomyocytes cost more ATP, as SERCA uses 0.5 ATP for each  $\text{Ca}^{2+}$  that is pumped back into the SR (78). Furthermore, as AGAT KO cardiomyocytes do not have an active CK system to buffer fluctuations in ADP, this could lead to elevated levels of ADP or AMP relative to ATP. As an indication of the energy levels, we used AMP-activated

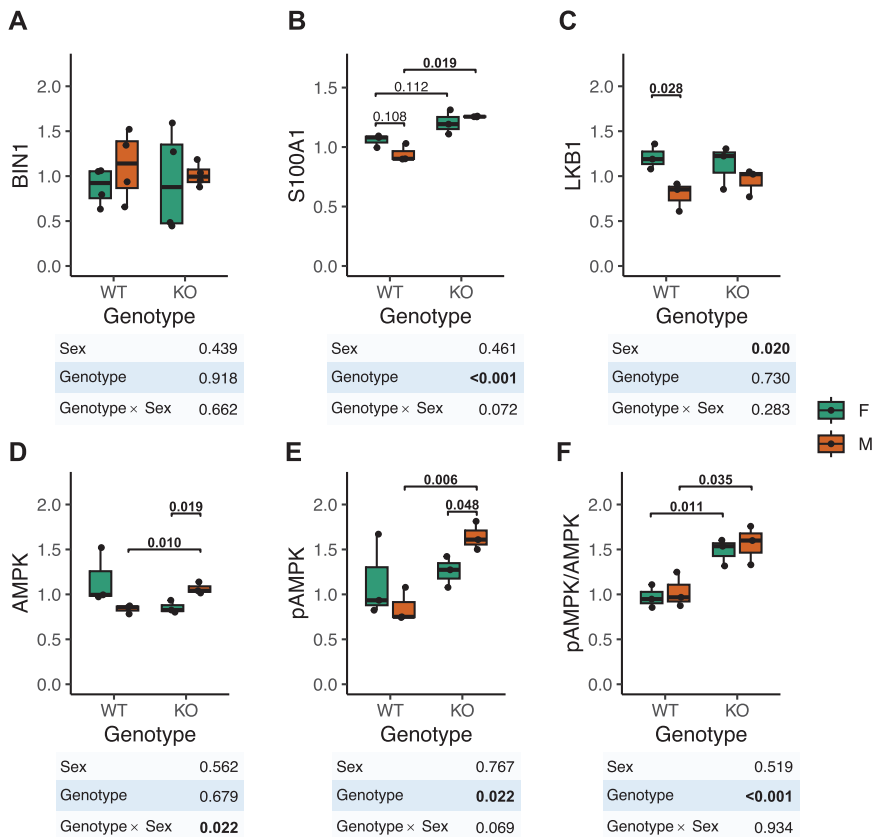


**Figure 6.** Expression of BIN1, S100A1, and LKB1, and expression and phosphorylation of AMPK in AGAT KO and WT mice. The expression and phosphorylation were determined by Western blotting, and representative images are shown in Supplemental Figs. S6 and S7. The legend is located in the right side of the figure. All data were normalized to the corresponding average values of WT littermates. **A:** BIN1 expression was similar in AGAT KO and WT. **B:** S100A1 expression was significantly higher in AGAT KO than WT mice. **C:** LKB1 expression did not differ between AGAT KO and WT, but was sex-dependent and higher in females than in males. However, LK did not differ showing no statistically significant difference in activation of AMPK phosphorylation between genotypes. AMPK activation was significantly elevated in AGAT KO mice compared with WT littermates. **D–F:** although the groups had some minor differences in AMPK expression (**D**), the phosphorylation was significantly affected by genotype and higher in AGAT KO than WT (**E**). As a result, the AMPK activation was significantly higher in AGAT KO compared with WT hearts. These measurements were performed on samples from 12 animals (6 WT and 6 KO), with equal distribution of males and females (3 each per genotype). Each sample was analyzed 3–5 times independently, with the mean value for each animal represented as individual dots on the plots. Statistical analysis was conducted using ANOVA, with the effects of contributing factors displayed below each measurement. In addition, *t* tests were performed to evaluate differences between groups, with *P* values indicated in the figure only when smaller than 0.15. AGAT, arginine:glycine amidinotransferase.

protein kinase (AMPK). When AMPK binds AMP or ADP, it is phosphorylated by liver kinase B1 (LKB1), and this triggers a signaling cascade that regulates metabolism according to the conditions (79–81).

Western blots of AMPK and pAMPK demonstrated that relative AMPK phosphorylation was significantly higher in AGAT KO animals of both sexes (Fig. 6, D–F, representative photos of the gels shown in Supplemental Fig. S7). The expression of LKB1 (Fig. 6C) was sex-dependent and higher in females than in males. This sex-dependency was also found in skeletal muscles (82). However, LKB1 expression did not differ between AGAT KO and WT. This suggests that elevated AMP and ADP concentrations lead to higher AMPK activation in AGAT KO hearts.

## DISCUSSION

In this work, we tested whether the lifelong absence of energy transfer through CK in AGAT KO hearts would result in Ca<sup>2+</sup>-handling abnormalities similar to those observed in failing hearts, where CK activity is reduced. At the whole heart level, the contractility of AGAT KO hearts is reduced (34), as in failing hearts. But the present study demonstrated that intact AGAT KO cardiomyocytes had more frequent Ca<sup>2+</sup> sparks and larger Ca<sup>2+</sup> transients, suggesting that, in contrast to failing cardiomyocytes, they had larger Ca<sup>2+</sup> fluxes. This augmented Ca<sup>2+</sup> release was linked to higher SR Ca<sup>2+</sup> content and was particularly prominent in the presence of ISO. These changes were accompanied by higher

expression levels of S100A1 in AGAT KO, which is known to increase the SR  $\text{Ca}^{2+}$  content and the gain of excitation-contraction coupling. Our results emphasize that the phenotype of AGAT KO cardiomyocytes is very different from that described for HFrEF failing hearts. This demonstrates that the absence of CK energy transfer alone is insufficient to trigger heart failure.

### Intact AGAT KO Cardiomyocytes Have Larger $\text{Ca}^{2+}$ Transients Due to Enhanced SR $\text{Ca}^{2+}$ Cycling

One of the most striking findings in the present study was the larger  $\text{Ca}^{2+}$  transients with a faster  $\text{Ca}^{2+}$  rise rate in AGAT KO compared with WT cardiomyocytes (Fig. 1). In addition, AGAT KO cardiomyocytes exhibited a higher  $\text{Ca}^{2+}$  spark frequency (Fig. 3) and larger SR  $\text{Ca}^{2+}$  content (Fig. 4B), while NCX activity was the same as in WT cardiomyocytes (Fig. 4C). This strongly suggests that the larger  $\text{Ca}^{2+}$  transients were due to more readily firing RyR clusters releasing more  $\text{Ca}^{2+}$  from the SR.

In addition to elevated SR  $\text{Ca}^{2+}$  content, AGAT KO hearts exhibited a higher expression of S100A1 (Fig. 6B), which is known to increase cytosolic  $\text{Ca}^{2+}$  turnover. S100A1 binds to SERCA and RyR in a  $\text{Ca}^{2+}$ -dependent manner. It stimulates SERCA  $\text{Ca}^{2+}$  uptake and lowers the RyR  $\text{Ca}^{2+}$  spark frequency, which may lead to a modest increase in SR  $\text{Ca}^{2+}$  content (48, 75). However, its effects on RyR are complex. Although S100A1 decreases the  $\text{Ca}^{2+}$  spark frequency at resting  $\text{Ca}^{2+}$  concentrations, it increases the gain of excitation-contraction coupling (48, 75). This increase in gain is in agreement with our data showing larger  $\text{Ca}^{2+}$  transients in AGAT KO.

The larger  $\text{Ca}^{2+}$  transients in intact AGAT KO cardiomyocytes were surprising, because we found in our previous study on whole cell patch-clamped cardiomyocytes that LTCC maximal current, exchange constant between the dyadic subspace and cytosol, and SERCA activity were reduced in AGAT KO (35). Furthermore, in contrast to the present study, AGAT KO cardiomyocytes tended to have a lower SR  $\text{Ca}^{2+}$  content, although the difference was not significant (35). We hypothesize that this difference between studies is because the patch-clamp study focused on LTCC and the associated CICR using square pulses, while TTX-sensitive  $\text{Na}^+$  channels were inhibited, and the remaining  $\text{Na}^+$  current was separated in time from the  $\text{Ca}^{2+}$  current. In contrast, in the present study, the membrane potential would have followed the action potential of the cells, and the  $\text{Na}^+$  current was intact. The shape of the membrane potential changes (square pulse vs. action potential) has been previously demonstrated to affect both LTCC  $\text{Ca}^{2+}$  influx (83), SR  $\text{Ca}^{2+}$  load (84), and CICR (85). Studies have suggested that the  $\text{Na}^+$  current can influence NCX  $\text{Ca}^{2+}$  influx (86, 87), but its role in mouse cardiomyocyte excitation-contraction coupling is controversial (1). Thus, future studies should address the  $\text{Ca}^{2+}$  fluxes during action potential clamp as in Ref. 88. Another important factor to take into account is that in whole cell patch clamp, the cytosol is dialyzed by the pipette solution. As S100A1 is readily lost upon permeabilization of cardiac fibers (89), the effect of S100A1 could also be negated in patch-clamped cells. The discrepancy between the previous and present study highlights that when studying only a part of a complex system, the results should be interpreted with caution.

### Sex-Dependent Changes in t-Tubular and RyR Organization Did Not Translate into Changes in the $\text{Ca}^{2+}$ -Transient

The disorganization of t-tubules leading to systolic dyssynchrony is one of the hallmarks of failing cardiomyocytes (44, 45), and it is accompanied by a decrease in BIN 1 expression (43). In failing hearts, the lower t-tubule density is reflected in the density of the transversal tubules, while there is an increased fraction of longitudinal t-tubules (90). Here, however, we found that BIN1 expression was similar in AGAT KO and WT (Fig. 6A), and while the t-tubular network did change in male AGAT KO cardiomyocytes, there was only a lower density of longitudinal t-tubules, but no difference in the transversal t-tubules (Fig. 4). This did not affect systolic dyssynchrony (Supplemental Fig. S1) or the overall  $\text{Ca}^{2+}$  dynamics.

Previous studies have demonstrated that RyR cluster organization influences calcium release dynamics in failing hearts, where RyR dispersion into smaller clusters typically results in slower and more dyssynchronous  $\text{Ca}^{2+}$  release (46). In the present study, female AGAT KO mice exhibited smaller RyR clusters than female WT mice (Fig. 5), with changes in cluster size similar to those reported in failing hearts (46, 91, 92). However, this was mainly due to female WT cardiomyocytes having relatively large RyR clusters, so that female AGAT KO mice actually just had RyR cluster sizes comparable to those found in both WT and KO males. This did not affect the synchrony of  $\text{Ca}^{2+}$  release (Supplemental Fig. S1), suggesting that the relationship between RyR cluster organization and  $\text{Ca}^{2+}$  transient synchrony is not strictly causal, or that the changes were below the threshold necessary to detect functional consequences in our experiments.

The precise mechanism that causes RyR cluster rearrangement is not clear. It has been reported that phosphorylation of RyRs promotes the dispersion of the channels' arrangement (92). Thus, we looked into expression levels of phosphorylated RyR (Ser2808 and Ser2814) and total RyR (Supplemental Fig. S4). Interestingly, we found only a modest decline in phosphorylated RyR by CAMKII (Ser2814, Supplemental Fig. S4C) in female AGAT KO mice compared with WT, but the relative phosphorylation was similar in KO and WT. Furthermore, there was no difference between males and females (Supplemental Fig. S4). Thus, in the present study, RyR phosphorylation cannot explain the differences in RyR cluster sizes and dispersion (Fig. 5).

### Higher AMPK Activation Implies Higher ADP/AMP Concentrations in AGAT KO Hearts

It is intriguing that  $\text{Ca}^{2+}$  dynamics are increased in AGAT KO cardiomyocytes, because this increases the cost of excitation-contraction coupling. In steady state, augmented CICR requires a matching pumping of  $\text{Ca}^{2+}$  back to the SR by SERCA, which costs 0.5 ATP per  $\text{Ca}^{2+}$  (93). In the heart, ATPases can be supplied with ATP through direct ATP diffusion and the CK "shuttle" with their relative contributions changing depending on the conditions (94). As this latter mechanism is inhibited in AGAT KO mice, we would expect AGAT KO cardiomyocytes to struggle with higher levels of ADP and/or AMP, which both activate AMPK (80).

Our results show that AMPK activation was indeed elevated in AGAT KO hearts (Fig. 6, D–F). Although SERCA is highly sensitive to the intracellular ADP/ATP ratio (95), the  $\text{Ca}^{2+}$  decay rate was similar in KO and WT (Fig. 1F). This is in agreement with that SERCA expression (35), as well as PLB expression and phosphorylation (Fig. S4) were similar in AGAT KO and WT hearts. Thus, based on our data, SERCA activity was not limited under the present conditions.

The higher AMPK activation in AGAT KO should be interpreted with caution. Indeed, recent studies have suggested that AMPK activation is compartmentalized and thus does not necessarily correlate with the overall cellular ADP/ATP ratio (82, 96, 97). Therefore, it is unclear whether the higher AMPK activation is near SERCA or in a different intracellular compartment. Although sensors to assess the intracellular energy state are being developed (98), it is not yet possible to assess the intracellular ADP/ATP ratio near specific ATPases, such as SERCA, in isolated cardiomyocytes. Taken together, our results suggest that in intact, field-stimulated AGAT KO cardiomyocytes, i.e., under physiological conditions, direct ATP diffusion from mitochondria was sufficient to sustain the required SERCA rate.

### Creatine-Deficient AGAT KO Hearts Have Very Different Adaptations than Failing Hearts

The changes in AGAT KO  $\text{Ca}^{2+}$  handling are interesting because they are very different from the pattern observed in failing cardiomyocytes, pointing to a novel adaptation mechanism to the absence of energy transfer through CK. Heart failure is a clinical syndrome that can manifest itself as heart failure with reduced ejection fraction (HFrEF) and heart failure with preserved ejection fraction (HFpEF) (99). Impairment of  $\text{Ca}^{2+}$  handling in heart failure is different between HFrEF and HFpEF (100), and below we will focus on comparing AGAT KO  $\text{Ca}^{2+}$  handling to changes in cardiomyocytes from HFrEF (“classical” failing heart).

In HFrEF, it is believed that the reduced contractility is largely related to changes in the  $\text{Ca}^{2+}$  dynamics. As noted in INTRODUCTION, these cardiomyocytes are characterized by  $\text{Ca}^{2+}$  transients with reduced amplitude and slower relaxation (42). They have higher levels of intracellular  $\text{Na}^+$  and more  $\text{Ca}^{2+}$  cycles across the sarcolemma through NCX (36, 101), whereas the SR  $\text{Ca}^{2+}$  content is lower, and less  $\text{Ca}^{2+}$  cycles through the SR (42). The RyR-LTCC cross talk in the dyads is compromised as the t-tubules become disorganized (43, 44), RyR expression is lowered (47), and RyR clusters are “orphaned,” i.e., not associated with the t-tubules (102). As much of the t-tubular connection and dyadic structure is lost, the  $\text{Ca}^{2+}$  transients become dyssynchronous (44, 103).

In the present study, the AGAT KO cardiomyocytes exhibited almost opposite adaptations, as the  $\text{Ca}^{2+}$  transients were larger (Fig. 1) and exhibited the same dyssynchrony index (Supplemental Fig. S1) as WT cardiomyocytes. In addition, AGAT KO cardiomyocytes had higher spark frequency (Fig. 3) and SR  $\text{Ca}^{2+}$  content (Fig. 4). These alterations in  $\text{Ca}^{2+}$  handling were accompanied by minor, sex-specific differences in the t-tubular network (Fig. 2) and RyR organization (Fig. 5), aligning with previously documented sex differences in cardiac  $\text{Ca}^{2+}$  handling (51). In addition, we observed no differences in RyR and PLB expression and phosphorylation (Supplemental

Fig. S4), and the expression of BIN1 and S100A1, which usually declines in HFrEF, were either the same or even up-regulated in AGAT KO, respectively (Fig. 6, A and B).

Our results demonstrate that lifelong creatine deficiency in AGAT mice does not lead to a phenotype similar to that of failing hearts. The etiologies of failing and AGAT KO hearts are also very different. Failing hearts struggle to produce adequate pressure to circulate the blood and typically respond by developing hypertrophy, leading to increased heart stiffness. They are energy-starved, as the mechanical work becomes more costly, while ATP supply and energy transfer are compromised (16, 17). In AGAT KO hearts, the energy transfer may be compromised, but the cardiomyocytes show no signs of hypertrophy (34) and are even smaller than WT cardiomyocytes (Table 2), suggesting that their mechanical performance is adequate.

### Study Limitations

One of the study limitations is that creatine deficiency can only be induced by whole body knockouts. As noted in INTRODUCTION, creatine is synthesized in the kidney and liver and circulated with the bloodstream to be taken up by the heart and other tissues through the creatine transporter (SLC6A8) (104). Thus, other organs, such as the brain and skeletal muscles, are also affected by creatine deficiency.

AGAT KO mice have constitutively active AMP-activated kinase (AMPK) in the brain, liver, skeletal muscle, and fat (11). This shifts the overall metabolism of AGAT KO mice toward catabolism. As a result, although AGAT KO mice are protected against metabolic syndrome (11), they are also very small and fragile with a severely reduced body and muscle weight, and large shifts in the metabolism of glycolytic muscles in particular (32, 33, 105). This is rescued by supplementation with creatine (33, 105).

In the present study, we used AGAT KO mice as a model to study the correlation between heart failure and inhibited CK energy transfer. We expected that during lifelong absence of CK energy transfer,  $\text{Ca}^{2+}$  handling would change toward the heart failure phenotype. However, this was not the case, and any changes recorded were opposite to what we expected. Interestingly, many of the adaptations were not directly linked to energy-consuming processes. We cannot say whether the recorded  $\text{Ca}^{2+}$ -handling adaptations in AGAT KO mice were induced by the absence of CK energy transfer, systemic effects, or a combination thereof. But we can conclude that the absence of CK energy transfer does not lead to the development of the heart failure phenotype.

### Conclusions

Taken together, we conclude that AGAT KO cardiomyocytes exhibit larger  $\text{Ca}^{2+}$  transients due to a larger CICR from the SR, which has higher  $\text{Ca}^{2+}$  content and more readily firing RyR clusters. Furthermore, the higher S100A1 expression could be involved in enhancing the gain of excitation-contraction coupling in AGAT KO.

This phenotype of AGAT KO cardiomyocytes is distinct from the phenotype of cardiomyocytes from failing hearts. The larger  $\text{Ca}^{2+}$  transients in AGAT KO cardiomyocytes, which were even more prominent during  $\beta$ -adrenergic stimulation, are opposite to observations on failing cardiomyocytes.

Thus, although the contraction of the whole heart is slowed down and reduced in both AGAT KO and failing hearts, the present study demonstrates that different etiologies have led to different adaptations at the cellular and molecular levels.

## DATA AVAILABILITY

The datasets generated during and/or analyzed during the current study are available from the corresponding author upon reasonable request. Used analysis tools are referred to in the methods either through references or, in the newly developed code, through open access software repository link.

## SUPPLEMENTAL MATERIAL

Supplemental Figs. S1–S7 and Supplemental Video S1: <https://www.doi.org/10.5281/zenodo.15658358>.

## GRANTS

This work was supported by the Estonian Research Council grants PRG1127 and PSG832 (the latter to M.L.).

## DISCLOSURES

No conflicts of interest, financial or otherwise, are declared by the authors.

## AUTHOR CONTRIBUTIONS

M.L., R.B., and M.V. conceived and designed research; J.B., M.L., J.S., X.S., T.R., R.B., K.S., M.J.B., and M.V. performed experiments; J.B., M.L., J.S., T.R., R.B., K.S., M.J.B., C.G., E.H., and M.V. analyzed data; M.L., W.E.L., R.B., and M.V. interpreted results of experiments; J.B., M.L., J.S., and M.V. prepared figures; R.B. and M.V. drafted manuscript; J.B., M.L., W.E.L., R.B., and M.V. edited and revised manuscript; J.B., M.L., J.S., X.S., T.R., R.B., K.S., M.J.B., C.G., E.H., W.E.L., R.B., and M.V. approved final version of manuscript.

## REFERENCES

- Bers DM. Cardiac excitation-contraction coupling. *Nature* 415: 198–205, 2002. doi:10.1038/415198a.
- Meyer RA, Sweeney HL, Kushmerick MJ. A simple analysis of the "phosphocreatine shuttle. *Am J Physiol Cell Mol Physiol* 246C3: C365–C377, 1984.
- Ventura-Clapier R, Kuznetsov A, Veksler V, Boehm E, Anfous K. Functional coupling of creatine kinases in muscles: species and tissue specificity. *Mol Cell Biochem* 184: 231–247, 1998.
- Wallimann T, Wyss M, Brdiczka D, Nicolay K, Eppenberger HM. Intracellular compartmentation, structure and function of creatine kinase isoenzymes in tissues with high and fluctuating energy demands: the "phosphocreatine circuit" for cellular energy homeostasis. *Biochem J* 281: 21–40, 1992. doi:10.1042/bj2810021.
- Vendelin M, Lemba M, Saks VA. Analysis of functional coupling: mitochondrial creatine kinase and adenine nucleotide translocase. *Biophys J* 87: 696–713, 2004. doi:10.1529/biophysj.103.036210.
- Wallimann T, Schlosser T, Eppenberger HM. Function of M-line-bound creatine kinase as intramyofibrillar ATP regenerator at the receiving end of the phosphorylcreatine shuttle in muscle. *J Biol Chem* 259: 5238–5246, 1984.
- Minajeva A, Ventura-Clapier R, Veksler V. Ca<sup>2+</sup> uptake by cardiac sarcoplasmic reticulum ATPase in situ strongly depends on bound creatine kinase. *Pflugers Arch* 432: 904–912, 1996. doi:10.1007/s004240050214.
- Lygate CA. The pitfalls of in vivo cardiac physiology in genetically modified mice – lessons learnt the hard way in the creatine kinase system. *Front Physiol* 12: 685064, 2021. doi:10.3389/fphys.2021.685064.
- Braissant O, Henry H, Béard E, Uldry J. Creatine deficiency syndromes and the importance of creatine synthesis in the brain. *Amino Acids* 40: 1315–1324, 2011. doi:10.1007/s00726-011-0852-z.
- Nasrallah F, Feki M, Kaabachi N. Creatine and creatine deficiency syndromes: biochemical and clinical aspects. *Pediatr Neurol* 42: 163–171, 2010. doi:10.1016/j.pediatrneurol.2009.07.015.
- Choe C, Nabuurs C, Stockebrand MC, Neu A, Nunes P, Morellini F, Sauter K, Schillemeit S, Hermans-Borgmeyer I, Marescau B, Heerschap A, Isbrandt D. L-arginine:glycine amidinotransferase deficiency protects from metabolic syndrome. *Hum Mol Genet* 22: 110–123, 2013 [Erratum in *Hum Mol Genet* 22: 4030, 2013]. doi:10.1093/hmg/ddt407.
- Schmidt A, Marescau B, Boehm EA, Renema WK, Peco R, Das A, Steinfeld R, Chan S, Wallis J, Davidoff M, Ullrich K, Waldschutz R, Heerschap A, De Deyn PP, Neubauer S, Isbrandt D. Severely altered guanidino compound levels, disturbed body weight homeostasis and impaired fertility in a mouse model of guanidinoacetate N-methyltransferase (GAMT) deficiency. *Hum Mol Genet* 13: 905–921, 2004. doi:10.1093/hmg/ddh112.
- Stockebrand M, Sasani A, Das D, Hornig S, Hermans-Borgmeyer I, Lake HA, Isbrandt D, Lygate CA, Heerschap A, Neu A, Choe C-U. A mouse model of creatine transporter deficiency reveals impaired motor function and muscle energy metabolism. *Front Physiol* 9: 773, 2018. doi:10.3389/fphys.2018.00773.
- Lygate CA, Neubauer S. The myocardial creatine kinase system in the normal, ischaemic and failing heart. In: *Cardiac Energy Metabolism in Health and Disease*, edited by Lopaschuk GD, Dhalla NS. Springer, 2014, p. 155–168.
- De Sousa E, Veksler V, Minajeva A, Kaasik A, Mateo P, Mayoux E, Hoerter J, Bigard X, Serrurier B, Ventura-Clapier R. Subcellular creatine kinase alterations. Implications in heart failure. *Circ Res* 85: 68–76, 1999. doi:10.1161/01.res.85.1.68.
- Ingwall JS, Weiss RG. Is the failing heart energy starved?: On using chemical energy to support cardiac function. *Circ Res* 95: 135–145, 2004. doi:10.1161/01.RES.0000137170.41939.d9.
- Ingwall JS. Energy metabolism in heart failure and remodelling. *Cardiovasc Res* 81: 412–419, 2009. doi:10.1093/cvr/cvn301.
- Neubauer S. The failing heart—an engine out of fuel. *N Engl J Med* 356: 1140–1151, 2007. doi:10.1056/NEJMra063052.
- Spindler M, Meyer K, Strömer H, Leupold A, Boehm E, Wagner H, Neubauer S. Creatine kinase-deficient hearts exhibit increased susceptibility to ischemia-reperfusion injury and impaired calcium homeostasis. *Am J Physiol Heart Circ Physiol* 287: H1039–H1045, 2004. doi:10.1152/ajpheart.01016.2003.
- Ten Hove M, Lygate CA, Fischer A, Schneider JE, Sang AE, Hulbert K, Sebag-Montefiore L, Watkins H, Clarke K, Isbrandt D, Wallis J, Neubauer S. Reduced inotropic reserve and increased susceptibility to cardiac ischemia/reperfusion injury in phosphocreatine-deficient guanidinoacetate-N-methyltransferase-knockout mice. *Circulation* 111: 2477–2485, 2005. doi:10.1161/01.CIR.0000165147.99592.01.
- Akki A, Su J, Yano T, Gupta A, Wang Y, Leppo MK, Chacko VP, Steenbergen C, Weiss RG. Creatine kinase overexpression improves ATP kinetics and contractile function in postschemic myocardium. *Am J Physiol Heart Circ Physiol* 303: H844–H852, 2012. doi:10.1152/ajpheart.00268.2012.
- Gupta A, Akki A, Wang Y, Leppo MK, Chacko VP, Foster DB, Caceres V, Shi S, Kirk JA, Su J, Lai S, Paolucci N, Steenbergen C, Gerstenblith G, Weiss RG. Creatine kinase-mediated improvement of function in failing mouse hearts provides causal evidence the failing heart is energy starved. *J Clin Invest* 122: 291–302, 2012. doi:10.1172/JCI57426.
- Whittington HJ, Ostrowski PJ, McAndrew DJ, Cao F, Shaw A, Ekyun TR, Lake HA, Tyler J, Schneider JE, Neubauer S, Zervou S, Lygate CA. Over-expression of mitochondrial creatine kinase in the murine heart improves functional recovery and protects against injury following ischaemia-reperfusion. *Cardiovasc Res* 114: 858–869, 2018. doi:10.1093/cvr/cvy054.
- McAndrew DJ, Lake HA, Zervou S, Schwedhelm E, Schneider JE, Neubauer S, Lygate CA. Homocysteine and creatine deficiency do not exacerbate murine ischaemic heart failure. *ESC Heart Fail* 10: 189–199, 2023. doi:10.1002/ehf2.14183.

25. Nahrendorf M, Spindler M, Hu K, Bauer L, Ritter O, Nordbeck P, Quaschnig T, Hiller K-H, Wallis J, Ertl G, Bauer WR, Neubauer S. Creatine kinase knockout mice show left ventricular hypertrophy and dilatation, but unaltered remodeling post-myocardial infarction. *Cardiovasc Res* 65: 419–427, 2005. doi:10.1016/j.cardiores.2004.10.006.
26. Kaasik A, Veksler V, Boehm E, Novotova M, Minajeva A, Ventura-Clapier R. Energetic crosstalk between organelles: architectural integration of energy production and utilization. *Circ Res* 89: 153–159, 2001. doi:10.1161/hh1401.093440.
27. Lygate CA, Medway DJ, Ostrowski PJ, Aksentijevic D, Sebag-Montefiore L, Hunyor I, Zervou S, Schneider JE, Neubauer S. Chronic creatine kinase deficiency eventually leads to congestive heart failure, but severity is dependent on genetic background, gender and age. *Basic Res Cardiol* 107: 276–286, 2012. doi:10.1007/s00395-012-0276-2.
28. Branovets J, Sepp M, Kotlyarova S, Jephthina N, Sokolova N, Aksentijevic D, Lygate CA, Neubauer S, Vendelin M, Birkedal R. Unchanged mitochondrial organization and compartmentation of high-energy phosphates in creatine-deficient *GAMT*<sup>-/-</sup> mouse hearts. *Am J Physiol Heart Circ Physiol* 305: H506–H520, 2013. doi:10.1152/ajpheart.00919.2012.
29. Branovets J, Karro N, Barsunova K, Laasmaa M, Lygate CA, Vendelin M, Birkedal R. Cardiac expression and location of hexokinase changes in a mouse model of pure creatine deficiency. *Am J Physiol Heart Circ Physiol* 320: H613–H629, 2021. doi:10.1152/ajpheart.00188.2020.
30. Schneider JE, Stork LA, Bell JT, ten Hove M, Isbrandt D, Clarke K, Watkins H, Lygate CA, Neubauer S. Cardiac structure and function during ageing in energetically compromised Guanidinoacetate N-methyltransferase (*GAMT*)-knockout mice - a one year longitudinal MRI study. *J Cardiovasc Magn Reson* 10: 9, 2008. doi:10.1186/1532-429X-10-9.
31. Aksentijevic D, Zervou S, Eykyn TR, McAndrew DJ, Wallis J, Schneider JE, Neubauer S, Lygate CA. Age-dependent decline in cardiac function in guanidinoacetate-N-methyltransferase knockout mice. *Front Physiol* 10: 1535, 2019. doi:10.3389/fphys.2019.01535.
32. Barsunova K, Vendelin M, Birkedal R. Marker enzyme activities in hindleg from creatine-deficient *AGAT* and *GAMT* KO mice – differences between models, muscles, and sexes. *Sci Rep* 10: 7956, 2020. doi:10.1038/s41598-020-64740-8.
33. Sasani A, Hornig S, Grzybowski R, Cordts K, Hanff E, Tsikas D, Böger R, Gerloff C, Isbrandt D, Neu A, Schwedhelm E, Choe C. Muscle phenotype of *AGAT*- and *GAMT*-deficient mice after simvastatin exposure. *Amino Acids* 52: 73–85, 2020. doi:10.1007/s00726-019-02812-4.
34. Faller KNE, Atzler D, McAndrew DJ, Zervou S, Whittington HJ, Simon JM, Aksentijevic D, ten Hove M, Choe C, Isbrandt D, Casadei B, Schneider JE, Neubauer S, Lygate CA. Impaired cardiac contractile function in arginine:glycine amidinotransferase knockout mice devoid of creatine is rescued by homoarginine but not creatine. *Cardiovasc Res* 114: 417–430, 2018. doi:10.1093/cvr/cvx242.
35. Laasmaa M, Branovets J, Barsunova K, Karro N, Lygate CA, Birkedal R, Vendelin M. Altered calcium handling in cardiomyocytes from arginine-glycine amidinotransferase-knockout mice is rescued by creatine. *Am J Physiol Heart Circ Physiol* 320: H805–H825, 2021. doi:10.1152/ajpheart.00300.2020.
36. Bers DM, Despa S. Cardiac myocytes  $Ca^{2+}$  and  $Na^{+}$  regulation in normal and failing hearts. *J Pharmacol Sci* 100: 315–322, 2006. doi:10.1254/jphs.cpj06001x.
37. Lipskaia L, Chemaly ER, Hadri L, Lompre A-M, Hajjar RJ. Sarcoplasmic reticulum  $Ca^{2+}$  ATPase as a therapeutic target for heart failure. *Expert Opin Biol Ther* 10: 29–41, 2010. doi:10.1517/14715290903321462.
38. Eisner D, Caldwell J, Trafford A. Sarcoplasmic reticulum Ca-ATPase and heart failure 20 years later. *Circ Res* 113: 958–961, 2013. doi:10.1161/CIRCRESAHA.113.302187.
39. Schmidt U, Hajjar RJ, Kim CS, Lebeche D, Doye AA, Gwathmey JK. Human heart failure: cAMP stimulation of SR  $Ca^{2+}$ -ATPase activity and phosphorylation level of phospholamban. *Am J Physiol* 277: H474–H480, 1999. doi:10.1152/ajpheart.1999.277.2.H474.
40. Kranias EG, Hajjar RJ. Modulation of cardiac contractility by the phospholamban/SERCA2a regulatome. *Circ Res* 110: 1646–1660, 2012. doi:10.1161/CIRCRESAHA.111.259754.
41. del Monte F, Harding SE, William Dec G, Gwathmey JK, Hajjar RJ. Targeting phospholamban by gene transfer in human heart failure. *Circulation* 105: 904–907, 2002. doi:10.1161/hc0802.105564.
42. Piacentino V, Weber CR, Chen X, Weisser-Thomas J, Margulies KB, Bers DM, Houser SR. Cellular basis of abnormal calcium transients of failing human ventricular myocytes. *Circ Res* 92: 651–658, 2003. doi:10.1161/01.RES.0000062469.83985.9B.
43. Caldwell JL, Smith CER, Taylor RF, Kitmitto A, Eisner DA, Dibb KM, Trafford AW. Dependence of cardiac transverse tubules on the BAR domain protein amphiphysin II (BIN-1). *Circ Res* 115: 986–996, 2014. doi:10.1161/CIRCRESAHA.116.303448.
44. Louch WE, Mørk HK, Sexton J, Strømme TA, Laake P, Sjaastad I, Sejersted OM. T-tubule disorganization and reduced synchrony of  $Ca^{2+}$  release in murine cardiomyocytes following myocardial infarction. *J Physiol* 574: 519–533, 2006. doi:10.1113/jphysiol.2006.107227.
45. Louch WE, Sejersted OM, Swift F. There goes the neighborhood: pathological alterations in t-tubule morphology and consequences for cardiomyocyte  $Ca^{2+}$  handling. *J Biomed Biotechnol* 2010: 503906–503918, 2010. doi:10.1155/2010/503906.
46. Kolstad TR, van den Brink J, MacQuaide N, Lunde PK, Frisk M, Aronsen JM, Norden ES, Cataliotti A, Sjaastad I, Sejersted OM, Edwards AG, Lines GT, Louch WE. Ryanodine receptor dispersion disrupts  $Ca^{2+}$  release in failing cardiac myocytes. *eLife* 7: e39427, 2018. doi:10.7554/eLife.39427.
47. Hou Y, Bai J, Shen X, de Langen O, Li A, Lal S, dos Remedios CG, Baddeley D, Ruygrok PN, Soeller C, Crossman DJ. Nanoscale organisation of ryanodine receptors and junctophilin-2 in the failing human heart. *Front Physiol* 12: 724372, 2021. doi:10.3389/fphys.2021.724372.
48. Kettlewell S, Most P, Currie S, Koch WJ, Smith GL. S100A1 increases the gain of excitation–contraction coupling in isolated rabbit ventricular cardiomyocytes. *J Mol Cell Cardiol* 39: 900–910, 2005. doi:10.1016/j.yjmcc.2005.06.018.
49. Fu Y, Shaw SA, Naami R, Vuong CL, Basheer WA, Guo X, Hong T. Isoproterenol promotes rapid ryanodine receptor movement to bridging integrator 1 (BIN1)-organized dyads. *Circulation* 133: 388–397, 2016. doi:10.1161/CIRCULATIONAHA.115.018535.
50. Fu Y, Hong T. BIN1 regulates dynamic t-tubule membrane. *Biochim Biophys Acta* 1863: 1839–1847, 2016. doi:10.1016/j.bbamcr.2015.11.004.
51. Laasmaa M, Branovets J, Stolova J, Shen X, Rätsepõ T, Balodis MJ, Grahv C, Hendrikson E, Louch WE, Birkedal R, Vendelin M. Cardiomyocytes from female compared to male mice have larger ryanodine receptor clusters and higher calcium spark frequency. *J Physiol* 601: 4033–4052, 2023. doi:10.1113/JP284515.
52. Parks RJ, Howlett SE. Sex differences in mechanisms of cardiac excitation–contraction coupling. *Pflugers Arch* 465: 747–763, 2013. doi:10.1007/s00424-013-1233-0.
53. Prajapati C, Koivumäki J, Pekkanen-Mattila M, Aalto-Setälä K. Sex differences in heart: from basics to clinics. *Eur J Med Res* 27: 241, 2022. doi:10.1186/s40001-022-00880-z.
54. Laasmaa M, Karro N, Birkedal R, Vendelin M. IOCBIO Sparks detection and analysis software. *PeerJ* 7: e6652, 2019. doi:10.7717/peerj.6652.
55. Vendelin M, Laasmaa M, Kalda M, Branovets J, Karro N, Barsunova K, Birkedal R. IOCBIO Kinetics: an open-source software solution for analysis of data traces. *PLoS Comput Biol* 16: e1008475, 2020. doi:10.1371/journal.pcbi.1008475.
56. Berg S, Kutra D, Kroeger T, Straehle CN, Kausler BX, Haubold C, Schiegg M, Ales J, Beier T, Rudy M, Eren K, Cervantes JI, Xu B, Beuttenmueller F, Wolny A, Zhang C, Koethe U, Hamprecht FA, Kreshuk A. Ilastik: interactive machine learning for (bio)image analysis. *Nat Methods* 16: 1226–1232, 2019. doi:10.1038/s41592-019-0582-9.
57. Allan C, Burel J-M, Moore J, Blackburn C, Linkert M, Lyontson S, MacDonald D, Moore WJ, Neves C, Patterson A, Porter M, Tarkowska A, Loranger B, Avondo J, Lagerstedt I, Lianas L, Leo S, Hands K, Hay RT, Patwardhan A, Best C, Kleywegt GJ, Zanetti G, Swedlow JR. OMERO: flexible, model-driven data management for experimental biology. *Nat Methods* 9: 245–253, 2012. doi:10.1038/nmeth.1896.
58. S van der W, Schönberger JL, Nunez-Iglesias J, Boulogne F, Warner JD, Yager N, Guillier E, Yu T; scikit-image contributors.

- scikit-image: image processing in Python. *PeerJ* 2: e453, 2014. doi:10.7717/peerj.453.
59. Wang A, Yan X, Wei Z. ImagePy: an open-source, Python-based and platform-independent software package for bioimage analysis. *Bioinformatics* 34: 3238–3240, 2018. doi:10.1093/bioinformatics/bty313.
  60. Olivier N, Keller D, Rajan VS, Gónczy P, Manley S. Simple buffers for 3D STORM microscopy. *Biomed Opt Express* 4: 885–899, 2013. doi:10.1364/BOE.4.000885.
  61. Baddeley D, Cannell MB, Soeller C. Three-dimensional sub-100 nm super-resolution imaging of biological samples using a phase ramp in the objective pupil. *Nano Res* 4: 589–598, 2011. doi:10.1007/s12274-011-0115-z.
  62. Sobie EA, Guatimosim S, Gómez-Viquez L, Song L-S, Hartmann H, Saleet Jafri M, Lederer WJ. The Ca<sup>2+</sup> leak paradox and “rogue ryanodine receptors”: SR Ca<sup>2+</sup> efflux theory and practice. *Prog Biophys Mol Biol* 90: 172–185, 2006. doi:10.1016/j.pbiomolbio.2005.06.010.
  63. Kütt J, Margus G, Kask L, Rätsepso T, Soodla K, Bernasconi R, Birkedal R, Järv P, Laasmaa M, Vendelin M. Simple analysis of gel images with IOCBIO Gel. *BMC Biol* 21: 225, 2023. doi:10.1186/s12915-023-01734-8.
  64. R Core Team. R: A Language and Environment for Statistical Computing (Online). R Foundation for Statistical Computing, Vienna, Austria: 2023. <https://www.R-project.org>.
  65. Bates D, Mächler M, Bolker B, Walker S. Fitting linear mixed-effects models using lme4. *J Stat Soft* 67: 1–48, 2015. doi:10.18637/jss.v067.i01.
  66. Hagdorn QAJ, Bossers GPL, Koop A-MC, Piek A, Eijgenraam TR, van der Feen DE, Silljé HHW, de Boer RA, Berger RMF. A novel method optimizing the normalization of cardiac parameters in small animal models: the importance of dimensional indexing. *Am J Physiol Heart Circ Physiol* 316: H1552–H1557, 2019. doi:10.1152/ajpheart.00182.2019.
  67. Cheng H, Lederer W, Cannell M. Calcium sparks: elementary events underlying excitation-contraction coupling in heart muscle. *Science* 262: 740–744, 1993. doi:10.1126/science.8235594.
  68. Ramay HR, Liu OZ, Sobie EA. Recovery of cardiac calcium release is controlled by sarcoplasmic reticulum refilling and ryanodine receptor sensitivity. *Cardiovasc Res* 91: 598–605, 2011. doi:10.1093/cvr/cvr143.
  69. Galice S, Xie Y, Yang Y, Sato D, Bers DM. Size matters: ryanodine receptor cluster size affects arrhythmogenic sarcoplasmic reticulum calcium release. *J Am Heart Assoc* 7: e008724, 2018. doi:10.1161/JAHA.118.008724.
  70. Bovo E, Huke S, Blatter LA, Zima AV. The effect of PKA-mediated phosphorylation of ryanodine receptor on SR Ca<sup>2+</sup> leak in ventricular myocytes. *J Mol Cell Cardiol* 104: 9–16, 2017. doi:10.1016/j.yjmcc.2017.01.015.
  71. Guo T, Zhang T, Mestrlil R, Bers DM. Ca<sup>2+</sup>/calmodulin-dependent protein kinase II phosphorylation of ryanodine receptor does affect calcium sparks in mouse ventricular myocytes. *Circ Res* 99: 398–406, 2006. doi:10.1161/01.RES.0000236756.06252.13.
  72. Li Y, Kranias EG, Mignery GA, Bers DM. Protein kinase A phosphorylation of the ryanodine receptor does not affect calcium sparks in mouse ventricular myocytes. *Circ Res* 90: 309–316, 2002. doi:10.1161/hh0302.105660.
  73. Li J, Agvanyan S, Zhou K, Shaw RM, Hong T. Exogenous cardiac bridging integrator 1 benefits mouse hearts with pre-existing pressure overload-induced heart failure. *Front Physiol* 11: 708, 2020. doi:10.3389/fphys.2020.00708.
  74. Li J, Balmaceda P, Ha T, Visker JR, Maalouf N, Kwan E, Hoareau GL, Accad M, Ranjan R, Selzman CH, Drakos SG, Shaw RM, Hong T. Cardiac bridging integrator 1 gene therapy rescues chronic non-ischemic heart failure in minipigs. *NPJ Regen Med* 9: 36–44, 2024. doi:10.1038/s41536-024-00380-0.
  75. Völkers M, Loughrey CM, MacQuaide N, Remppis A, DeGeorge BR, Wegner FV, Friedrich O, Fink RHA, Koch WJ, Smith GL, Most P. S100A1 decreases calcium spark frequency and alters their spatial characteristics in permeabilized adult ventricular cardiomyocytes. *Cell Calcium* 41: 135–143, 2007. doi:10.1016/j.ceca.2006.06.001.
  76. Remppis A, Gretten T, Schäfer BW, Hunziker P, Erne P, Katus HA, Heizmann CW. Altered expression of the Ca<sup>2+</sup>-binding protein S100A1 in human cardiomyopathy. *Biochim Biophys Acta* 1313: 253–257, 1996. doi:10.1016/0167-4889(96)00097-3.
  77. Most P, Seifert H, Gao E, Funakoshi H, Völkers M, Heierhorst J, Remppis A, Plegler ST, DeGeorge BR, Eckhart AD, Feldman AM, Koch WJ. Cardiac S100A1 protein levels determine contractile performance and propensity toward heart failure after myocardial infarction. *Circulation* 114: 1258–1268, 2006. doi:10.1161/CIRCULATIONAHA.106.622415.
  78. Inesi G, Kurzmack M, Coan C, Lewis DE. Cooperative calcium binding and ATPase activation in sarcoplasmic reticulum vesicles. *J Biol Chem* 255: 3025–3031, 1980. doi:10.1016/S0021-9258(19)85846-5.
  79. Woods A, Johnstone SR, Dickerson K, Leiper FC, Fryer LGD, Neumann D, Schlattner U, Wallimann T, Carlson M, Carling D. LKB1 is the upstream kinase in the AMP-activated protein kinase cascade. *Curr Biol* 13: 2004–2008, 2003. doi:10.1016/j.cub.2003.10.031.
  80. Hardie DG, Carling D, Gamblin SJ. AMP-activated protein kinase: also regulated by ADP? *Trends Biochem Sci* 36: 470–477, 2011. doi:10.1016/j.tibs.2011.06.004.
  81. Herzig S, Shaw RJ. AMPK: guardian of metabolism and mitochondrial homeostasis. *Nat Rev Mol Cell Biol* 19: 121–135, 2018. doi:10.1038/nrm.2017.95.
  82. Bernasconi R, Soodla K, Sirp A, Zovo K, Kuhtinskaja M, Lukk T, Vendelin M, Birkedal R. Higher AMPK activation in mouse oxidative compared with glycolytic muscle does not correlate with LKB1 or CaMKKβ expression. *Am J Physiol Endocrinol Metab* 328: E21–E33, 2025. doi:10.1152/ajpendo.00261.2024.
  83. Yuan W, Ginsburg KS, Bers DM. Comparison of sarcolemmal calcium channel current in rabbit and rat ventricular myocytes. *J Physiol* 493: 733–746, 1996. doi:10.1113/jphysiol.1996.sp021418.
  84. Shiels HA, Vornanen M, Farrell AP. Temperature dependence of cardiac sarcoplasmic reticulum function in rainbow trout myocytes. *J Exp Biol* 205: 3631–3639, 2002. doi:10.1242/jeb.205.23.3631.
  85. Beuckelmann DJ, Wier WG. Mechanism of release of calcium from sarcoplasmic reticulum of guinea-pig cardiac cells. *J Physiol* 405: 233–255, 1988. doi:10.1113/jphysiol.1988.sp017331.
  86. Lines GT, Sande JB, Louch WE, Mork HK, Grottum P, Sejersted OM. Contribution of the Na<sup>+</sup>/Ca<sup>2+</sup> exchanger to rapid Ca<sup>2+</sup> release in cardiomyocytes. *Biophys J* 91: 779–792, 2006. doi:10.1529/biophysj.105.072447.
  87. Larbig R, Torres N, Bridge JHB, Goldhaber JJ, Philipson KD. Activation of reverse Na<sup>+</sup>-Ca<sup>2+</sup> exchange by the Na<sup>+</sup> current augments the cardiac Ca<sup>2+</sup> transient: evidence from NCX knock-out mice. *J Physiol* 588: 3267–3276, 2010. doi:10.1113/jphysiol.2010.187708.
  88. Laasmaa M, Birkedal R, Vendelin M. Revealing calcium fluxes by analyzing inhibition dynamics in action potential clamp. *J Mol Cell Cardiol* 100: 93–108, 2016. doi:10.1016/j.yjmcc.2016.08.015.
  89. Most P, Remppis A, Weber C, Bernotat J, Ehlermann P, Plegler ST, Kirsch W, Weber M, Uttenweiler D, Smith GL, Katus HA, Fink RHA. The C terminus (amino acids 75–94) and the linker region (amino acids 42–54) of the Ca<sup>2+</sup>-binding protein S100A1 differentially enhance sarcoplasmic Ca<sup>2+</sup> release in murine skinned skeletal muscle fibers. *J Biol Chem* 278: 26356–26364, 2003. doi:10.1074/jbc.M303338200.
  90. Setterberg IE, Le C, Frisk M, Perdreau-Dahl H, Li J, Louch WE. The physiology and pathophysiology of t-tubules in the heart. *Front Physiol* 12: 790227, 2021. doi:10.3389/fphys.2021.718404.
  91. Hou Y, Laasmaa M, Li J, Shen X, Manfra O, Nórdén ES, Le C, Zhang L, Sjaastad I, Jones PP, Soeller C, Louch WE. Live-cell photo-activated localization microscopy correlates nanoscale ryanodine receptor configuration to calcium sparks in cardiomyocytes. *Nat Cardiovasc Res* 2: 251–267, 2023. doi:10.1038/s44161-022-00199-2.
  92. Shen X, van den Brink J, Bergan-Dahl A, Kolstad TR, Norden ES, Hou Y, Laasmaa M, Aguilar-Sanchez Y, Quick AP, Espe EK, Sjaastad I, Wehrens XH, Edwards AG, Soeller C, Louch WE. Prolonged β-adrenergic stimulation disperses ryanodine receptor clusters in cardiomyocytes and has implications for heart failure. *eLife* 11: e77725, 2022. doi:10.7554/eLife.77725.
  93. Boardman N, Hafstad AD, Larsen TS, Severson DL, Aasum E. Increased O<sub>2</sub> cost of basal metabolism and excitation-contraction coupling in hearts from type 2 diabetic mice. *Am J Physiol Heart Circ Physiol* 296: H1373–H1379, 2009. doi:10.1152/ajpheart.01264.2008.
  94. Vendelin M, Hoerter JA, Mateo P, Soboll S, Gillet B, Mazet J-L. Modulation of energy transfer pathways between mitochondria and

- myofibrils by changes in performance of perfused heart. *J Biol Chem* 285: 37240–37250, 2010. doi:10.1074/jbc.M110.147116.
95. **Tian R, Ingwall JS.** Energetic basis for reduced contractile reserve in isolated rat hearts. *Am J Physiol Heart Circ Physiol* 270: H1207–H1216, 1996. doi:10.1152/ajpheart.1996.270.4.H1207.
  96. **Zong Y, Zhang C-S, Li M, Wang W, Wang Z, Hawley SA, Ma T, Feng J-W, Tian X, Qi Q, Wu Y-Q, Zhang C, Ye Z, Lin S-Y, Piao H-L, Hardie DG, Lin S-C.** Hierarchical activation of compartmentalized pools of AMPK depends on severity of nutrient or energy stress. *Cell Res* 29: 460–473, 2019. doi:10.1038/s41422-019-0163-6.
  97. **Drake JC, Wilson RJ, Laker RC, Guan Y, Spaulding HR, Nichenko AS, et al.** Mitochondria-localized AMPK responds to local energetics and contributes to exercise and energetic stress-induced mitophagy. *Proc Natl Acad Sci USA* 118: e2025932118, 2021. doi:10.1073/pnas.2025932118.
  98. **Pelosse M, Cottet-Rousselle C, Bidan CM, Dupont A, Gupta K, Berger I, Schlattner U.** Synthetic energy sensor AMPfret deciphers adenylate-dependent AMPK activation mechanism. *Nat Commun* 10: 1038, 2019. doi:10.1038/s41467-019-08938-z.
  99. **Ponikowski P, Voors AA, Anker SD, Bueno H, Cleland JGF, Coats AJS, Falk V, González-Juanatey JR, Harjola V-P, Jankowska EA, Jessup M, Linde C, Nihoyannopoulos P, Parissis JT, Pieske B, Riley JP, Rosano GMC, Ruilope LM, Ruschitzka F, Rutten FH, van der Meer P; ESC Scientific Document Group.** 2016 ESC Guidelines for the diagnosis and treatment of acute and chronic heart failure: The Task Force for the diagnosis and treatment of acute and chronic heart failure of the European Society of Cardiology (ESC) Developed with the special contribution of the Heart Failure Association (HFA) of the ESC. *Eur Heart J* 37: 2129–2200, 2016 [Erratum in *Eur Heart J* 39: 860, 2018]. doi:10.1093/eurheartj/ehw128.
  100. **Frisk M, Le C, Shen X, Røe ÅT, Hou Y, Manfra O, Silva GJJ, van Hout I, Norden ES, Aronsen JM, Laasmaa M, Espe EKS, Zouein FA, Lambert RR, Dahl CP, Sjaastad I, Lunde IG, Coffey S, Cataliotti A, Gullestad L, Tønnessen T, Jones PP, Altara R, Louch WE.** Etiology-dependent impairment of diastolic cardiomyocyte calcium homeostasis in heart failure with preserved ejection fraction. *J Am Coll Cardiol* 77: 405–419, 2021. doi:10.1016/j.jacc.2020.11.044.
  101. **Despa S, Bers DM.** Na<sup>+</sup> transport in the normal and failing heart — remember the balance. *J Mol Cell Cardiol* 61: 2–10, 2013. doi:10.1016/j.yjmcc.2013.04.011.
  102. **Lipsett DB, Frisk M, Aronsen JM, Nordén ES, Buonarati OR, Cataliotti A, Hell JW, Sjaastad I, Christensen G, Louch WE.** Cardiomyocyte substructure reverts to an immature phenotype during heart failure. *J Physiol* 597: 1833–1853, 2019. doi:10.1113/JP277273.
  103. **Øyehaug L, Loose KØ, Jølle GF, Røe ÅT, Sjaastad I, Christensen G, Sejersted OM, Louch WE.** Synchrony of cardiomyocyte Ca<sup>2+</sup> release is controlled by t-tubule organization, SR Ca<sup>2+</sup> content, and ryanodine receptor Ca<sup>2+</sup> sensitivity. *Biophys J* 104: 1685–1697, 2013. doi:10.1016/j.bpj.2013.03.022.
  104. **Brosnan ME, Edison EE, da Silva R, Brosnan JT.** New insights into creatine function and synthesis. *Adv Enzyme Regul* 47: 252–260, 2007. doi:10.1016/j.advenzreg.2006.12.005.
  105. **Nabuurs CI, Choe CU, Veltien A, Kan HE, van Loon LJC, Rodenburg RJT, Matschke J, Wieringa B, Kemp GJ, Isbrandt D, Heerschap A.** Disturbed energy metabolism and muscular dystrophy caused by pure creatine deficiency are reversible by creatine intake. *J Physiol* 591: 571–592, 2013. doi:10.1113/jphysiol.2012.241760.



## Publication VI

Di Gallo, M; Delivry, L; Pereira, D; Jauliac, E; Macaux, G; Guilbert, T; Denis, RGP; Backer, S; Saintpierre, M; Adoux, L; **Bernasconi, R**; Laasmaa, M; Birkedal, R; Vendelin, M; Dos Santos, M; Wojtaszewski, JFP; Foretz, M; Viollet, B; Maire, P; Sotiropoulos, A; Launay, T\*; Britto, FA\*.

**SIX1-dependent myofiber typology and metabolism controls muscle hypertrophy.**

(Manuscript)

\*Equal contribution

The rules of the publisher prevent the publication of the manuscript of **Publication VI** before acceptance. Official committee members and opponents will be given a copy of the manuscript to enable them to carry out a judicious review of the dissertation.



# Curriculum vitae

## Personal data

Name: **Romain Bernasconi**  
Date of birth: 12.10.1995  
Place of birth: Montpellier, France  
Citizenship: French

## Contact data

E-mail: bernasconiromain34000@gmail.com

## Education

2021–2025 Tallinn University of Technology, PhD.  
2019–2021 MSC Kinesiology, MS thesis “Carnosol treatment on sarcopenia” (Laboratory “DMeM”, INRAE, Montpellier).  
2018–2019 BSC Kinesiology, physiopathology, handicap & physical activity.  
2013–2016 BSC Kinesiology, physical performance & training.  
2010–2013 High school “Paul Valéry”, Sète, France, Baccalaureate Sciences and laboratory techniques.

## Language competence

French Native  
English Fluent

## Awards

2024 Best oral presentation, “TalTech, Department of Chemistry and Biotechnology Symposium 2024, Tallinn, Estonia”.  
2023 Best poster presentation, “Conference Physiology in focus SPS-2023, Tallinn, Estonia”.

## Conferences

September 2025 IUPS 2025, Poster presentation: “Higher AMPK activation in mouse oxidative compared with glycolytic muscle does not correlate with LKB1 or CaMKK $\beta$  expression”.  
December 2024 FLASH presentation, Department of Chemistry and Biotechnology Symposium, TalTech, Oral presentation: “AMPK activation is higher in endurant muscles”.  
November 2023 School of Science conference 2023, TalTech, Oral presentation: “Creatine deficiency causes muscle-specific atrophy and shift in fiber composition”.  
November 2023 PhD conference, Department of Chemistry and Biotechnology, TalTech, Oral presentation: “AMPK: Chick or Egg of the muscle phenotype?”.  
September 2023 Physiology in Focus, SPS-2023, Oral and Poster presentation: “Pure creatine deficiency is associated with muscle-specific upregulation of LKB1/AMPK pathway and shift in myosin heavy chain composition”.

- September 2023 European Muscle Conference 50<sup>th</sup>, Poster presentation: “Pure creatine deficiency is associated with muscle-specific upregulation of LKB1/AMPK pathway and shift in myosin heavy chain composition”.
- August 2023 Association of Creatine Deficiency conference (Online), Oral presentation: “Creatine-deficiency in AGAT KO but not GAMT KO causes muscle-specific shift in myosin heavy chain composition”.
- September 2022 European Muscle Conference 49<sup>th</sup>, Attendance.

### Supervised dissertation

- 2025 K rol Soodla, Master’s thesis, “The expression and phosphorylation of AMP-activated protein kinase varies between intracellular compartments in a muscle specific manner”.
- 2023 K rol Soodla, Bachelor’s thesis, “Links between energetics and muscle phenotype: Pure creatine deficiency leads to skeletal muscle atrophy and shift in myosin heavy chain composition”.

### Publications

K tt, J; Margus, G; Kask, L; R tsepso, T; Soodla, K; **Bernasconi, R**; Birkedal, R; J rv, P; Laasmaa, M; Vendelin, M (2023). Simple analysis of gel images with IOC BIO Gel. BMC Biology, DOI: 10.1186/s12915-023-01734-8.

**Bernasconi, R**; Soodla, K; Sirp, A; Zovo, K; Kuhtinskaja, M; Lukk, T; Vendelin, M; Birkedal, R (2024). Higher AMPK activation in mouse oxidative compared to glycolytic muscle does not correlate with LKB1 or CaMKK  expression. Am J Physiol - Endocrinology and Metabolism, DOI: 10.1152/ajpendo.00261.2024.

Branovets, J\*; Laasmaa, M\*; Stolova, J; Shen, X; R tsepso, T; **Bernasconi, R**; Soodla, K; Balodis, M; Grahv, C; Hendrikson, E; Louch, W; Birkedal, R; Vendelin, M (2025). Life-long creatine deficiency leads to augmented sarcoplasmic reticulum calcium release but not heart failure. Am J Physiol – Heart, DOI: 10.1152/ajpheart.00106.2025.

## Elulookirjeldus

### Isikuandmed

Nimi: **Romain Bernasconi**  
Sünniaeg: 12.10.1995  
Sünnikoht: Montpellier, Prantsusmaa  
Kodakondsus: Prantsuse

### Kontaktandmed

E-post: bernasconiromain34000@gmail.com

### Hariduskäik

2021–2025 Tallinna Tehnikaülikool, PhD.  
2019–2021 MSC kinesioloogia, magistritöö “Karnosooliga ravi sarkopeenia korral” (labor “DMeM”, INRAE, Montpellier).  
2018–2019 BSC kinesioloogia, füsiopatoloogia, puue ja füüsiline aktiivsus.  
2013–2016 BSC kinesioloogia, füüsiline sooritusvõime ja treening.  
2010–2013 “Paul Valéry” Gümnaasium, Sète, Prantsusmaa, bakalaureusekraad teadused ja laboritehnikad.

### Keelteoskus

Inglise keel kõrgtase  
Prantsuse keel emakeel

### Auhinnad ja tunnustused

2024 Parim suuline ettekanne, “TalTech, Keemia ja Biotehnoloogia Instituudi Sümpoosium 2024, Tallinn, Eesti”.  
2023 Parim posterettekanne, “Konverents “Physiology in focus SPS-2023”, Tallinn, Eesti”.

### Konverentsid

September 2025 IUPS 2025, Posterettekanne: “Higher AMPK activation in mouse oxidative compared with glycolytic muscle does not correlate with LKB1 or CaMKK $\beta$  expression”.  
Detsember 2024 FLASH ettekanne, Keemia ja biotehnoloogia instituudi sümpoosium, TalTech, Suuline ettekanne: “AMPK activation is higher in endurant muscles”.  
November 2023 Teaduskooli konverents 2023, TalTech, Suuline ettekanne: “Creatine deficiency causes muscle-specific atrophy and shift in fiber composition”.  
November 2023 Doktorikraadi konverents, Keemia ja biotehnoloogia instituut, TalTech, Suuline ettekanne: “AMPK: Chick or Egg of the muscle phenotype?”.  
September 2023 Physiology in Focus, SPS-2023, Suuline ja posterettekanne: “Pure creatine deficiency is associated with muscle-specific upregulation of LKB1/AMPK pathway and shift in myosin heavy chain composition”.

- September 2023 European Muscle Conference 50<sup>th</sup>, Posterettekanne: “Pure creatine deficiency is associated with muscle-specific upregulation of LKB1/AMPK pathway and shift in myosin heavy chain composition”.
- August 2023 Association of Creatine Deficiency conference (virtuaalne), Suuline ettekanne: “Creatine-deficiency in AGAT KO but not GAMT KO causes muscle-specific shift in myosin heavy chain composition”.
- September 2022 European Muscle Conference 49<sup>th</sup>, Osavõtt.

#### Juhendatud dissertatsioon

- 2025 Kärol Soodla, Magistritöö, “The expression and phosphorylation of AMP-activated protein kinase varies between intracellular compartments in a muscle specific manner”.
- 2023 Kärol Soodla, Bakalaureusetöö, “Links between energetics and muscle phenotype: Pure creatine deficiency leads to skeletal muscle atrophy and shift in myosin heavy chain composition”.

#### Publikatsioonid

Kütt, J; Margus, G; Kask, L; Rätsepso, T; Soodla, K; **Bernasconi, R**; Birkedal, R; Järv, P; Laasmaa, M; Vendelin, M (2023). Simple analysis of gel images with IOC BIO Gel. BMC Biology, DOI: 10.1186/s12915-023-01734-8.

**Bernasconi, R**; Soodla, K; Sirp, A; Zovo, K; Kuhtinskaja, M; Lukk, T; Vendelin, M; Birkedal, R (2024). Higher AMPK activation in mouse oxidative compared to glycolytic muscle does not correlate with LKB1 or CaMKK $\beta$  expression. Am J Physiol - Endocrinology and Metabolism, DOI: 10.1152/ajpendo.00261.2024.

Branovets, J\*; Laasmaa, M\*; Stolova, J; Shen, X; Rätsepso, T; **Bernasconi, R**; Soodla, K; Balodis, M; Grahv, C; Hendrikson, E; Louch, W; Birkedal, R; Vendelin, M (2025). Life-long creatine deficiency leads to augmented sarcoplasmic reticulum calcium release but not heart failure. Am J Physiol – Heart, DOI: 10.1152/ajpheart.00106.2025.

ISSN 2585-6901 (PDF)  
ISBN 978-9916-80-412-4 (PDF)